COMMUNICATIONS PROTOCOLS FOR WIRELESS SENSOR NETWORKS IN PERTURBED ENVIRONMENT

by

Ndeye Bineta SARR

THESIS PRESENTED TO ÉCOLE DE TECHNOLOGIE SUPÉRIEURE
AND UNIVERSITY OF POITIERS (CO-TUTORSHIP)
IN PARTIAL FULFILLMENT FOR THE DEGREE OF
DOCTOR OF PHILOSOPHY
Ph.D.

MONTREAL, MARCH, 25, 2019

ÉCOLE DE TECHNOLOGIE SUPÉRIEURE
UNIVERSITÉ DU QUÉBEC

Université de Poitiers
Faculté des Sciences Fondamentales et Appliquées
(Diplôme National - Arrêté du 25 mai 2016)
École doctorale ED no 610 : Sciences et Ingénierie des Systèmes, Mathématiques, Informatique

Co-tutelle avec l'École de Technologie Supérieure de Montréal (ETS), Canada

THÈSE

Pour l'obtention du Grade de Docteur délivré par
l'Université de Poitiers
et Ph. D. de l'École de Technologie Supérieure de Montréal (ETS)

Secteur de Recherche : Électronique, microélectronique, nanoélectronique et micro-ondes

Présentée et soutenue par

Ndéye Bineta SARR

31 Janvier 2019

PROTOCOLES DE COMMUNICATIONS POUR RESEAUX DE CAPTEURS EN MILIEU FORTEMENT PERTURBÉ

COMMUNICATIONS PROTOCOLS FOR WIRELESS SENSOR NETWORKS IN PERTURBED ENVIRONMENT

Directeurs de Thèse : **Rodolphe Vauzelle, François Gagnon**
Co-directeurs de Thèse : **Hervé Boeglen, Basile L. Agba**

Jury

Basile L. AGBA, Chercheur, Institut de Recherche d'Hydro-Québec…..……Examinateur
Hervé BOEGLEN, Maître de Conférences, Université de Poitiers …….....Examinateur
Jean-François DIOURIS, Professeur, École Polytechnique de l'Université de Nantes……...Rapporteur
Ghais EL ZEIN, Professeur, INSA de Rennes…….Rapporteur
François GAGNON, Professeur, École de Technologie Supérieure de Montréal….....Examinateur
Georges KADDOUM, Professeur, École de Technologie Supérieure de Montréal...……....Examnateur
Kosai RAOOF, Professeur, Université Le Mans……...Examinateur
Rodolphe VAUZELLE, Professeur, Université de Poitiers……...Examinateur

To my husband and my parents.

Acknowledgments

First and foremost, I wish to express my deepest gratitude to all my supervisors for their availability, their wise advice, and the constant support they have shown during these four years of the thesis. In this sense, my first thanks to Pr. Rodolphe Vauzelle and Dr. Basile L. Agba for the implementation of the thesis, and for their great availability, their help, advice for writing and enriching discussions both from a scientific point of view than human. I would also like to thank Pr. François Gagnon for agreeing to co-supervise this thesis. His advice, ongoing support, and enriching discussions allowed me to reach my goals. My thanks also go to Herve Boeglen who joined us during the thesis and showed his real support both at the scientific level and in terms of writing.
I also thank a mother mine, Ms. Anne-Marie Poussard);
I thank Labex $\Sigma - Lim$, the research institute of Hydro-Quebec (IREQ), the Richard J. Marceau Research Chair, and MITACS for funding this thesis.
My warm thanks also go to the members of the jury: Georges Kaddoum, Jean-François Diouris, Ghais El Zein, Kosai Raoof. It is a great honor for me to have accepted to evaluate my thesis project.
It would be difficult to name all the people who contributed to the success of this thesis.
Thanks to my colleagues at the XLIM laboratory: Taha, Albekaye, Samir, Lidia, Romain.
I had an uneven experience in Canada thanks to the wonderful people I met at the Ecole de Technologie Superieure: Minh, Fabien, Omar, Koffi, Marwan. Thank you.
I thank also James Oyedapo for his help and his contribution to the realization of my last thesis chapter.
I also have an excellent memory of my visit to IREQ, and I particularly want to thank Stephane Gingras for his availability and his help during the experiments.
I wish to thank my family and friends (Diouwel, Amina, Fatou) for their presence and their unconditional support during this thesis.
Finally, I express my sincere gratitude to all members of the XLIM laboratory in Poitiers and the LACIME members of the Ecole de Technologie Superieure of Montreal.

Résumé

Cette thèse s'inscrit dans le domaine des réseaux intelligents (RI). Les RIs améliorent la sécurité des réseaux électriques et permettent une utilisation adaptée de l'énergie disponible de manière limitée. Ils augmentent également l'efficacité énergétique globale en réduisant la consommation. L'utilisation de cette technologie est la solution la plus appropriée car elle permet une gestion plus efficace de l'énergie. Dans ce contexte, des compagnies comme Hydro-Québec déploient des réseaux de capteurs pour contrôler les principaux équipements. Pour réduire les coûts de déploiement et la complexité du câblage, un réseau de capteurs semble être une solution optimale. Cependant, son déploiement nécessite une connaissance approfondie de l'environnement. Les postes à haute tension sont des points stratégiques du réseau électrique et génèrent un bruit impulsif qui dégrade les performances des communications sans fil. Les travaux dans cette thèse sont centrés sur le développement de protocoles de communication performants dans ces milieux fortement perturbés. Nous avons proposé une première approche basée sur la concaténation du code à métrique de rang et le code convolutif avec la modulation OFDM. C'est une technique très efficace pour réduire l'effet du bruit impulsif tout en ayant un niveau de complexité assez faible. Une autre solution basée sur un système multi-antennaire est développée. Nous avons aussi proposé un système MIMO coopératif codé en boucle fermée basée sur le code à métrique de rang et le précodeur $\max - d_{min}$. La deuxième technique est également une solution optimale pour améliorer la fiabilité du système et réduire la consommation énergétique dans les réseaux de capteurs.

Mots clés: Réaux intelligents, Réseaux de capteurs, Postes à Hautes Tensions, Bruit Impulsif, Codage à métrique de rang, OFDM, MIMO à boucle fermée.

Abstract

This thesis is mainly in the Smart Grid (SG) domain. SGs improve the safety of electrical networks and allow a more adapted use of electricity storage, available in a limited way. SGs also increase overall energy efficiency by reducing peak consumption. The use of this technology is the most appropriate solution because it allows more efficient energy management. In this context, manufacturers such as Hydro-Quebec deploy sensor networks in the nerve centers to control major equipment. To reduce deployment costs and cabling complexity, the option of a wireless sensor network seems the most obvious solution. However, deploying a sensor network requires in-depth knowledge of the environment. High voltages substations are strategic points in the power grid and generate impulse noise that can degrade the performance of wireless communications. The works in this thesis are focused on the development of high performance communication protocols for the profoundly disturbed environments. For this purpose, we have proposed an approach based on the concatenation of rank metric and convolutional coding with orthogonal frequency division multiplexing. This technique is very efficient in reducing the bursty nature of impulsive noise while having a quite low level of complexity. Another solution based on a multi-antenna system is also designed. We have proposed a cooperative closed-loop coded MIMO system based on rank metric code and max $-d_{min}$ precoder. The second technique is also an optimal solution for both improving the reliability of the system and energy saving in wireless sensor networks.

Keywords: Smart Grids, WSN, High Voltage, Impulsive Noise, Rank Metric coding, OFDM, Closed-loop MIMO.

Contents

List of Figures

List of Tables

Acronyms

6LoWPAN IPv6 over Wireless Personal Area Network

ANR Agence Nationale de la Recherche

ASK Amplitude Shift Keying

BER Bit Error Rate

BPSK Binary Phase Shift Keying

CSI Channel State Information

CSMA/CA Carrier Sense Multiple Access with Collision Avoidance

DQPSK Dual-polarization Quadrature Phase Shift Keying

DSSS Direct Sequence Spread Spectrum

EOLSR Energy-aware Optimized Link State Routing

FEC Forward Error Correction

FHSS Frequency Hopping Spread Spectrum

FSK Frequency Shift Keying

GFSK Gaussian Frequency Shift Keying

HART Hideway Addressable Remote Transducer

HV High Voltage

IEC International Electrotechnical Commission

IEEE Institute of Electrical and Electronics Engineers

IETF Internet Engineering Task Force

IP Internet Protocol

ISM Industrial Scientific and Medical

LAN Local Area Network

LLC Logical Link Control

LOS Line Of Sight

LRWPAN Low Rate Wireless Personal Area Network

MAC Medium Access Control

MIMO Multiple Input Multiple Output

ML Maximum Likelihood

MRC Maximal Ratio Combining

NIST National Institute of Standards and Technology

OCARI Optimization of Communications for Ad hoc Reliable Industrial network

OFDM Orthogonal Frequency Division Multiplexing

OQPSK Orthogonal Quadrature Phase Shift Keying

OSTBC Orthogonal Space-Time Block Coding

PER Packet Error Rate

PHY Physical Layer

QoS Quality Of Service

RFID Radio Frequency IDentification

SERENA SchEdule RoutEr Nodes Activity

SG Smart Grid

SISO Single Input Single Output

SNR Signal to Noise Ratio

WAN Wide Area Network

WF Waterfilling

WPAN Wireless Personal Access Network

WSN Wireless Sensor Network

Chapter 1

Introduction

Contents

1.1 Motivation

Modernization of electricity grids is underway in many countries around the world. Motivated by such essential factors as national security, economic development, the environment, and the incorporation of renewable energies, the provinces, states, and countries are prioritizing technological innovations to be deployed in order to make the electricity grid smarter. In Canada, the development of Smart Grids (SG) is recent (2009) and has grown in recent years. Although new technologies are present in many areas such as military, health, transport, it is not the same in the field of electricity networks. SGs improve the safety of electricity grids. By balancing supply and demand, they avoid the over-equipment of the means of production and allow a more adapted for the use of the means of storage of electricity, available in a limited way. SGs also increase overall energy efficiency by reducing peak consumption, which mitigates the risk of widespread failure. The use of this new technology is the most appropriate solution because it allows more efficient management of energy.
For Hydro-Quebec, which operates one of the largest electricity grids in the world, the economic benefits are obvious. Indeed, there are today more than 500 substations in the network. Indeed, the technical staff, from the information collected by the sensor network, can intervene remotely with the equipment of the station. The main objection is linked to the complexity of installing new shielded cables which requires to reverify security. Furthermore, adding new systems as they become available is of interest. The main SG applications targeted by Hydro-Quebec are described as follows:

- Teleprotection and network control automation, which serve to maintain the electrical stability of the network;
- Telecontrol applications that are used to operate the network;
- Remote maintenance used to analyze the behavior of the network and its automation systems, as well as for the configuration and maintenance of equipment.

The major equipment considered are among others transformers with and without on-load-tap-changers (OLTCs), online inductance, circuit breakers, switchers, and compressors. The operational functions of remote sensing, remote diagnostics, and downloading of intelligent electronic devices (IED) are part of remote maintenance applications. Depending on the context, the telemetry function performed by an IED may fall under the category of telecontrol and remote maintenance applications.
The main characteristics regarding the throughput needed to satisfy these applications are presented in Tables 1.1, 1.2, 1.3, and 1.4.

Consequently one of the most suitable solutions is to adopt a wireless sensor network (WSN) to these stations: it is easier to install and presents a cost-effective solution for these applications. Nevertheless, the transmission of information in wireless is done through electromagnetic waves emitted into the environment. As a result, the information transmitted can quickly be degraded, due to electromagnetic disturbances specific to the environment

Table 1.1: Requirements for Telemetry applications based on the major equipment and functions.

	Telemetry			
	Max		**Mean**	
Major Equipment	**kbps**	**pps**	**kbps**	**pps**
Transformers with OLTCs	17	28	9	19
Transformers without OLTCs	17	28	7	14
Online Inductance	10	14	2	5
Circuit breakers	10	14	0.2	0.2
Switches	6	14	0.1	0.2
Compressors	6	14	0.1	0.2

Table 1.2: Best Effort application requirements based on the major equipment and functions.

	Remote sensing, Remote diagnostic, and Downloading			
	Max		**Mean**	
Major Equipment	**kbps**	**pps**	**kbps**	**pps**
Transformers with OLTCs	910	210	150	35
Transformers without OLTCs	910	210	150	35
Online Inductance	910	210	150	35
Circuit breakers	910	210	150	35
Switches	20	15	20	15
Compressors	20	15	20	15

under consideration. As part of the thesis work, we will conduct a study of the physical layers and data link. We will be interested in everything related to the propagation aspect of electromagnetic waves, electromagnetic disturbances in high voltage substations. Digital transmission, signal processing, and coding strategies will also be used to protect the information exchanged and thereby improved the quality of service in such an environment. We will also focus on the data link layer more specifically the medium access (MAC) sub-layer to optimize transmission and energy consumption. Overall, we will propose a communication protocol that takes into account the electromagnetic disturbances resulting from

Table 1.3: Applications requirements based on the substation category and functions.

		Telemetry		**Remote sensing, Remote diagnostic, and downloading**	
		Max	**Mean**	**Max**	**Mean**
Category		kbps	kpbs	kbps	kpbs
Others		17	9	910	150
Primary	$< 100\ mW$	278	108	910	300
	$> 100\ mW$	824	325	910	300
Satellite	< 16 primary	160	67	910	300
	> 16 primary	201	83	910	300
Sources		317	157	910	450
Strategic		663	298	910	600

the operation of high-voltage (HV) equipment, the propagation of electromagnetic waves emitted by communicating wireless devices in the industrial environment.

1.2 Thesis Organization

This thesis is divided into four chapters:

- Chapter 2 presents the basic concepts of SG, WSN, and wireless communication channel. It gives an introduction to the SG system and wireless communication. The purpose is to provide a background of some characteristics of WSN and the propagation channel.

- Chapter 3 will present and analyze the communication protocols for WSN and the impulsive noise in substations. This chapter is fundamental since it gives the first ideas of how the existing communication protocols work in the presence of impulsive noise. The methods for modeling and measuring the impulsive noise are also overviewed in this chapter. Through a performance study of the few communication protocols, we will show how these systems are unsuitable for high voltage substations. These first results will allow us, however, to think of a suitable solution that will meet the requirements of the applications.

- Chapter 4 will present our approach for mitigating the impulsive noise in substation environments. Before, the existing methods for reducing the effect of impulsive noise are highlighted and analyzed. Our method is based on the concatenation of rank

metric (RC) and convolutional coding (CC) schemes with orthogonal frequency division multiplexing (OFDM). Based on the proposed approach and the performance results, we have implemented this solution on devices to compare the results for a future deployment.

- Chapter 5 also present another solution for deploying SG applications in substations. However, the existing cooperative techniques have been first reviewed and analyzed. Since the previously proposed technique concerns single input single output (SISO) communication, this second method is based on multiple antenna communications. In this chapter, we propose a closed-loop coded-multiple input multiple output (MIMO) transmission system. The approach combines the RC coding scheme with CC and $\max -d_{min}$ precoder to reduce both errors of transmission and save energy. The results presented in this chapter will help to understand how the optimized criterion affects the performance of MIMO systems.

1.3 Contributions

The field of sensor networks is a very dynamic research sector at national and international level. The application fields are incredibly varied regarding operating environments, measured physical quantities, robustness and latency constraints, and energy constraints. This research topic is mainly in the field of SG. Its principal objective is to develop a communication protocol for high-performance sensor networks adapted to highly disturbed environments for diagnostic and maintenance purposes to know the state of the electrical network and interact with essential equipment in HV substations or their neighborhoods.
In this thesis, a comparison between the existing models of impulsive noise such as Middleton Class A, Symmetric α Stable, and a recent model (Au model) is made to validate the model for use in our test of efficiency. The performance of existing communication protocol for WSN such as ZigBee is analyzed when the channel is impaired by impulsive noise.
Given the poor results obtained, we proposed a first robust technique to reduce the effects of impulse noise while meeting the requirements of smart grid applications. This approach is based on the concatenation of two error-correcting codes: the RC and the CC combined with the OFDM modulation technique. The benefits of OFDM are very well known in the field of digital communications and its robustness against frequency-selective channels. The RC scheme is a particular coding technique that is widely used in the field of cryptography but has proven recently in the field of digital communications. It allows us to correct burst errors while having low complexity.
The importance of synergy with the industry lies in the possibility of experimental validation of the work research results. With software defined radio (SDR) platforms, it is possible to implement a physical layer and to have tests with hardware in a real environment. We have investigated the validation of the proposed approach. We fully design and implement a new block namely $RC\ Encoder + Wifi\ Mapper$ in GNU Radio which acts as

a forward error correcting code to mitigate impulsive noise occurring in substations. After showing that using this coding scheme is very efficient in mitigating the bursty nature of impulsive noise by simulations, we now confirm that the same performance are maintained even with various impulsive voltages and experimental scenarios, which confirms the high performance of the proposed approach.
Given the extent of certain Hydro-Quebec HV substations, the first solution may be difficult to exploit. The energy constraints linked to the sensors must always be taken into account. For this purpose, we propose a second solution based on multi-antenna techniques (MIMO). MIMO systems achieve both very high spectral efficiency and effectively combat signal fading. The general idea is to take advantage of the spatial dimension of the channel and exploit multiple paths rather than deleting them. MIMO systems are very efficient because they can use all the techniques of SISO transmissions, in addition to their techniques. MIMO systems have several advantages that can be employed to reduce the transmission energy in the sensor networks for the same transmission reliability and rate. However, because of the limited size of the sensor, the direct application of MIMO is difficult. Given the constraint above, the solution is to consider the principle of sensors cooperation (or cooperative MIMO) to achieve MIMO transmission. The principle is to form virtual antennas in order to transmit using a MIMO technique. This solution is particularly attractive when very simple nodes are spatially distributed in a multi-path environment. Our contribution is the proposal of a closed-loop coded cooperative MIMO system based on the concatenation of rank metric and convolutional code with $\max - dmin$ precoder. The results obtained show not only that the performance concerning BER are improved but also the energy consumption has been reduced.

This work has led to the following publications:

Peer Reviewed Conference Papers

1. N. B. Sarr, H. Boeglen, B. L. Agba, F. Gagnon, R. Vauzelle, "Partial Discharge Impulsive Noise in 735 kV Electricity Substations and its Impacts on 2.4 GHz ZigBee Communications," *International Conference on Selected Topics in Mobile & Wireless Networking (MoWNeT)*, Cairo, Egypt, pp. 1-7, April 2016.

2. N. B. Sarr, A. K. Yazbek, H. Boeglen, J. P. Cances, R. Vauzelle, F. Gagnon, "An impulsive noise resistant physical layer for smart grid communications," *IEEE International Conference on Communications (ICC)*, Paris, pp. 1-7, May 2017.

List of Journal Articles

1. A. K. Yazbek, N. B. Sarr, I. El-Qachchach, J. P. Cances, V. Meghdadi, H. Boeglen, R. Vauzelle, "Performance of rank metric codes for interference constrained wireless sensor networks," *IET Wireless Sensor Systems*, May 2018.

2. N. B. Sarr, B. L. Agba, F. Gagnon, H. Boeglen, R. Vauzelle, "Analysis and Experimental Validation of Efficient Coded OFDM for an Impulsive Noise Environment," *Sensors*, Vol. 18, Issue 11, Nov. 2018.

3. N. B. Sarr, Olufemi J. Oyedapo, B. L. Agba, F. Gagnon, H. Boeglen, R. Vauzelle, "Cooperative Closed-Loop Coded-MIMO Transmissions for Smart Grid Wireless Applications," *Submitted to Wireless Communications and Mobile Computing Journal*

Chapter 2

Smart Grid (SG) and Wireless Sensors Networks (WSN)

Contents

2.1 Introduction

Power grids are facing new energy needs, including the development of air conditioning, audio, and video appliances or electric heating. Consumer uses, such as electric cars or heat pumps should amplify this increase, and energy demand is also rising putting pressure on global energy systems. To avoid the constraints mentioned above, energy companies resorted to the use of SG. SG improves the safety of electrical networks. By balancing supply and demand, it avoids over-equipment of the means of production and allows the more appropriate use of electricity storage facilities, available in a limited way. The SG also increases the overall energy efficiency: it reduces consumption peaks, which mitigates the risk of blackouts. The use of this new technology is the best solution because it allows more efficient energy management. To reduce deployment costs and complexity of wiring, the option of WSN seems the most obvious solution. Wireless technologies represent a convenient means of achieving the necessary communication connectivity in substations with significant flexibility and cost advantages over fiber and copper cabling. However, deploying a WSN requires a thorough knowledge of the environment. This chapter aims at reviewing the background of the SG concept, WSNs, and the propagation channel. Section 2 details the SG definition and characteristics. The conceptual model as defined by NIST (National Institute of Standards and Technology) is then overviewed. Section 3 describes the WSNs. It first gives a general definition of the WSN. The characteristics are then detailed. Finally, the parameters which are meaningful for the design of a WSN are reviewed. The principle of a digital transmission system is reviewed in section 4. Section 5 deals with the propagation channel aspects. It first details the physical phenomena. Secondly, a comparison is made between selectivity and coherence aspects. After that, we review the diversity techniques before studying the wireless channel modeling. Section 6 concludes this chapter.

2.2 The Smart Grid

Modernization of electricity grids is underway in many countries around the world. Induced by essential aspects such as national security, economic development, the environment, and the integration of renewable energies, the states are prioritizing technological innovations to be deployed to make the electricity network smarter.

2.2.1 Smart Grid Concept and Characteristics

A SG is an electrical network system which optimizes production, distribution, and consumption to better match electricity supply and demand acutely. It consists of the integration of communication and information technologies into the networks enabling a coordination which takes into account the actions of the players in the electricity system while ensuring a more efficient, economically viable and secure electricity supply. This communication between the various points of the networks makes it possible to efficiently

use the actions of the different actors of the electrical system, and in particular consumers. The aim is to provide equity between supply and demand at all times with increased responsiveness, reliability and to optimize network operations. IEEE standard [1], defines the SG as the combination of communication, information, and power technologies for an advanced electric power organization serving loads while bringing evolved end-user applications. The electrical system moves from a linearly functioning chain to a system where all the actors interact. For this purpose, SGs include transmission lines, substations, transformers, interface with generation, energy storage, and end-users as depicted in Fig. 2.1. Although many countries have already begun making their electrical systems smarter.

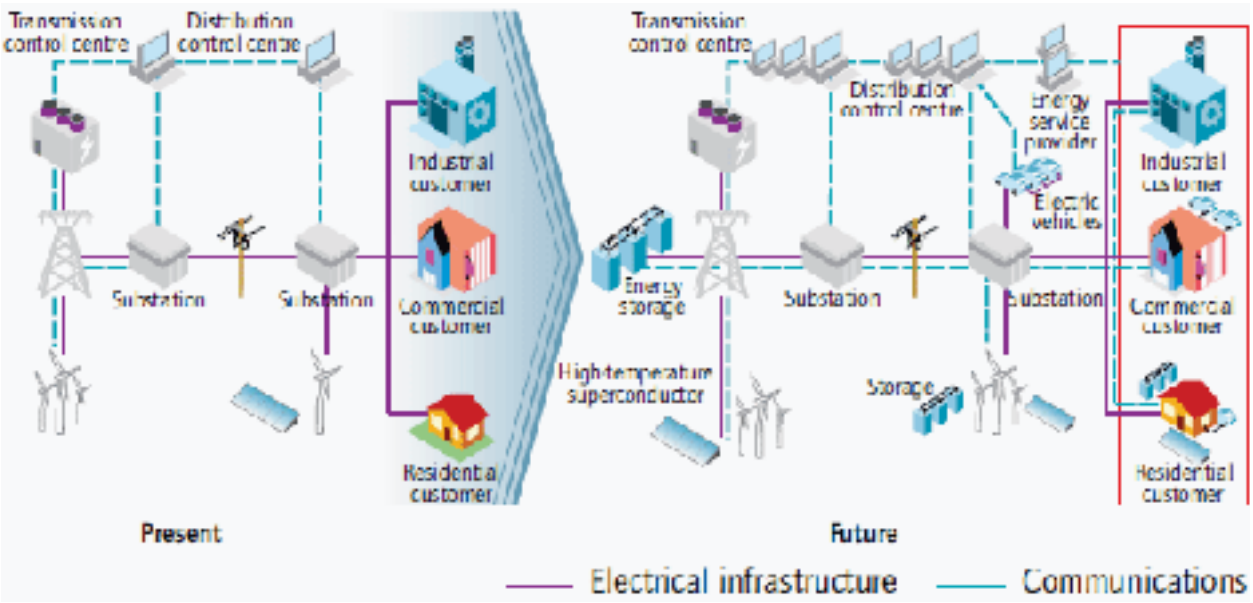

Figure 2.1: The evolutionary character of Smart Grid [2].

This development will require important investment and planning to perform the SG goals. SGs are an evolutionary group of technologies which will be spread in different rhythms in diverse worldwide contexts, according to the local commercial attractiveness, the adaptability with the actual technologies, the legal developments and the frames of the asset. However, the NIST was designated as "*primary responsibility to coordinate development of a framework that includes protocols and model standards for information management to achieve interoperability of Smart Grid devices and systems ...*". For the Department of Energy (DOE), the peculiar technologies of the SG are regrouped into the following five domains:

- Integrated Communications allow the interaction between users and intelligent electronic devices in an embedded system. It includes the acquisition of data, protection, and control.

- Advanced Sensing and Measurement technologies facilitate data acquisition to estimate the integrity and reliability of the network and enhance several aspects of

power grid management such as the elimination of invoicing estimates, automatic meter reading and avoid energy theft.

- Advanced Components play the role of determining the electrical operations of the grid and can be used in standalone or interconnected applications to create involved systems such as micro-grids.

- Advanced Control Methods refer to the devices and algorithms that will analyze, diagnose, and predict conditions in the grid. They are also responsible for determining and taking appropriate remedial actions autonomously to mitigate and prevent quality disturbances and power outage.

- Improved Interfaces and Decision Support assist grid operators and managers making decisions rapidly by converting complex system data into information that can be understood.

While the contribution of this section of our work is neither to provide the frameworks for integrated communications nor sensing and measurements in SG, it is worthy of being mentioned that the confinement of our contribution is limited to these two areas concerning the power substation of the electrical grid system.

2.2.2 Description of the NIST Conceptual Model

SG communication networks establish interactions between entities (systems, users, and applications) within the locations of the utility and various organizations. These entities can be organized into broad domains as shown in Fig. 2.2 which depicts the NIST model for the SG. It shows the link between the fields via secure communications flows. A more detailed model can be found in [3]. However, we are mostly interested in domains which substations are present, through this thesis considers the substation environment. For that purpose, we define the three main areas such as the bulk generation, the transmission, and the distribution domain. It is just a brief description of these domains. A more exhaustive description of substations is provided in the next chapter.

2.2.2.1 The Bulk Generation Domain

The bulk generation produces electricity in large capacities by utilizing supplies such as oil, wind, coal, flowing water, sunlight, nuclear fission, and tide. Furthermore, it also has the role of electricity storage with the management of renewable resources, electricity excesses and redistribution when during times of scarcity.

2.2.2.2 The Transmission Domain

It provides electricity from the bulk generation systems to the distribution field by several substations and transmission lines. Besides, this domain can also support small-scale en-

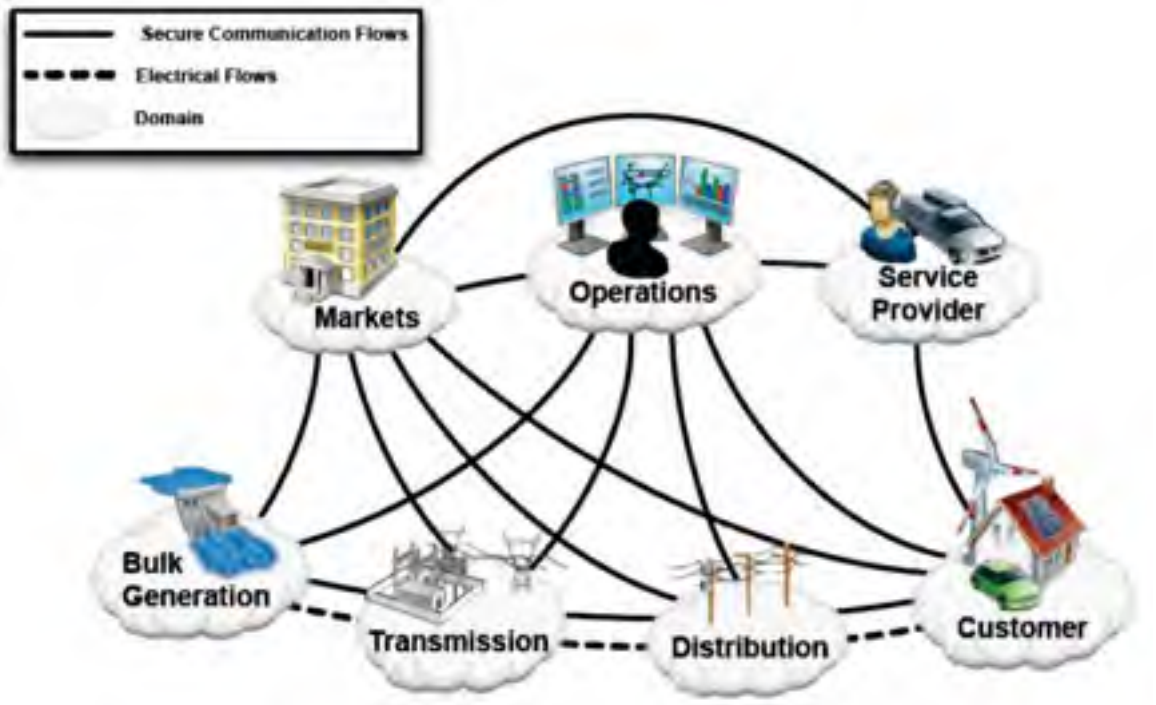

Figure 2.2: The NIST Conceptual model: Domains representation and interaction through Secure Communication [3].

ergy production and storage. These systems are typically designed to operate at very high voltage levels to minimize power losses.

2.2.2.3 The Distribution Domain

This domain is responsible for electricity distribution to energy consumers based on the energy availability and user demands. It can also store and generate electricity.

2.2.3 Conclusion

Smart Grid is a universal concept adopted by several organizations such as NIST, International Electrotechnical Commission (IEC), Electric Power Research Institute (EPRI), IEEE, European Technology Platform (ETP), etc. It consists of integrating electrical as well as information and communication technologies to ensure more reliability, flexibility, efficiency, and robustness to the power grid. To meet several demands of a modern grid, SGs utilize smarts meters, renewable energy generation, advanced sensing and communication technologies for efficient and reliable power grid system management. Recently, wireless sensor networks (WSNs) have been identified as a promising technology to perform energy efficient, seamless, secure, remote monitoring, and low-cost control in SG applications. For this purpose, we define the characteristics of WSN in the next section.

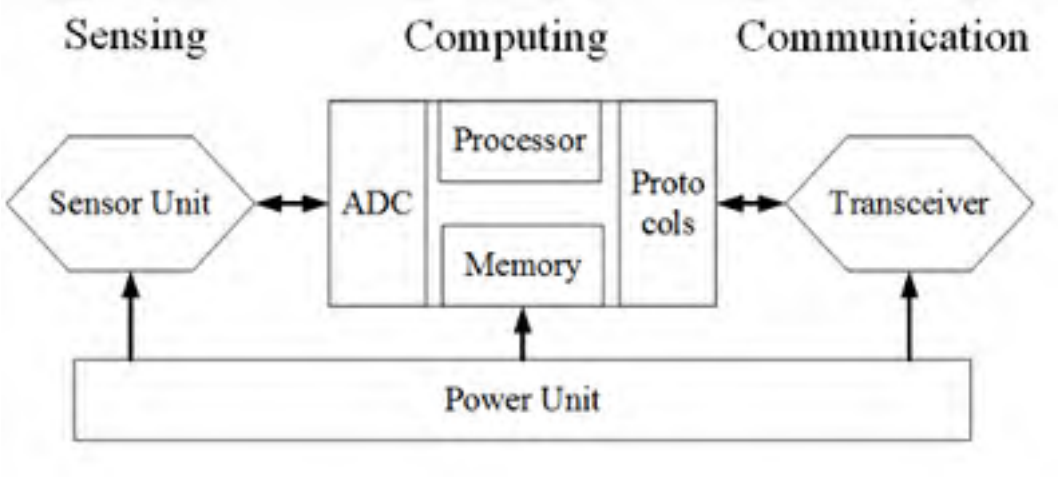

Figure 2.3: Sensor Node Components.

2.3 Wireless Sensor Networks

Numerous technical and technological advances in the fields of microelectronics, micromechanics, and wireless communication technologies have made possible to create small communicating objects equipped with sensors at a reasonable cost. These objects, called "sensor nodes" or commonly "sensors," are fitted with capture, calculation, storage, and communication units. For their power supply, the nodes are equipped with batteries or a method of energy recovery from the environment. As a result, the sensor nodes are real embedded entities. A wireless sensor network (WSN) is a set of these entities deployed for the collection and transmission of data to gathering points autonomously. This network offers various applications prospects in several fields, such as industrial surveillance, military operations, monitoring, and management of natural phenomena.

2.3.1 Description

WSN is a physical component, small, capable of performing three parallel tasks: measuring a physical quantity, processing information, and communication with other sensor nodes. Accomplishing the functions, a sensor node has four main components [4]: the sensing or acquisition unit, the processing or computing unit, the wireless communication unit, and the power as depicted in Fig. 2.3.

- The power unit: a battery usually provides the power of the sensors. It must present a large capacity with minimum weight and small size. Its carrying capacity must resist different uses because a node can consume different levels of power and need a different current according to its mode of operation. The self-discharge must, of course, be as slow as possible to hope for a longer lifespan possible. Also, energy recovery systems can be used to extend the state of the charge of the battery [5-6].

These systems are generally based on photovoltaic cells, pressure variation systems or gradients of temperature.

- The computing unit: It is also composed of a processor, and a specific operating system, receives data from the acquisition unit, processes them if necessary, and sends them to the communication unit.
  - The processor: the controller of a wireless sensor is at the heart of the hardware architecture. It manages the acquisition parts and radio, and thus allows the implementation of the communication protocols. It gathers data from the sensor, processes it, and decides when and to whom to transmit them. It also transforms the data received by the other nodes and puts the algorithms of the MAC layer.
  - Memory: several types of memory are needed to operate a node. RAM (Random Access Memory) is required to store temporary data acquired by sensors, but also the packets from the other nodes. Despite its speed, this type of memory has the disadvantage of losing its content if the power supply is interrupted. Read Only Memory (ROM) type memory is required to store program code. FLASH memory can also be used to temporarily store data from the RAM in case of insufficient space of the latter or case of power failure. Despite their great interest, FLASH memories are sources of power consumption quite important due to their write or read access times [7].
- The communication unit: it allows us to transmit the acquired data by the sensor to other communicating entities. Their performance are conditioned by the physical layer implemented. Therefore, they depend on the frequency band used, the transmission power level, the transmission range, the type of modulation, the presence or absence of errors correcting codes, and finally the level of consumption.

2.3.2 Characteristics

Some of the fundamental elements that the requirements or design constraints which WSNs need to take into consideration include the following [8-10]:

- The number of sensor nodes can reach several hundred.
- For reasons of reliability and observing the way in which WSN is deployed, there is generally a high density of sensor nodes.
- Because of the mass production model and the industrial type, it is not possible to check the correct operation of each sensor node. Moreover, among the sensor nodes with limited electrical energy, some will fail after a certain period of operation. This characteristic is to be considered in the design of the network.
- The topology of the WSN frequently changes because of node failures. Also, it is possible that we add new sensor nodes to the system already deployed, either to

extend the network or more safely to compensate for the failure of a large number of nodes, after a particular network operation time.

- The resources of the sensor nodes regarding electrical energy, heat capacity, and storage capacity are minimal. The main concern of the system will be to limit energy consumption for the extension of the network's existence while providing an acceptable quality of service. At the time of deployment, the user can choose between increasing the duration of the service networks life and the performance requirement to be provided by the network.

- Sensor nodes do not generally have an universal identifier because of their considerable number in the WSN and the overhead this entails. In WSN, importance is given to the captured information and the capture area rather than to the identity of the node capturing that information.

2.3.3 Design of WSN: Influencing Parameters

The design of WSN is influenced by several parameters that, once considered, generate a design guide. This guide can also be used to compare between two WSNs. Among these parameters, we mention the following: [8], [9], [11].

- Fault Tolerance: The collapse of one or several nodes should not cause the failure of the entire system. The WSN must be able to work partially and with reduced performance instead of breaking down completely.

- Scale factors: Most sensor networks are composed of a few dozen nodes, but some applications may require the use of sensor networks made up of hundreds or thousands of nodes. The zone, which the system must cover, is also decisive in its dimensioning.

- Low cost: Sensor networks can contain a large number of nodes. It is, therefore, necessary to have a unit cost per lowest node possible.

- Transmission medium: The node transmission medium must be universal. One possibility is to choose, for radio transmissions, bands of frequencies from industry, science and health fields, which do not require licenses and are available in all countries.

- Energy consumption: The sensor nodes usually carry a minimal amount of energy. Data transmissions between nodes consume a lot of power, especially if nodes fail and the WSN needs to be reorganized. For this purpose, algorithms and protocols have been developed with the primary concern of saving energy, sometimes to the detriment of the quality of service provided by WSN.

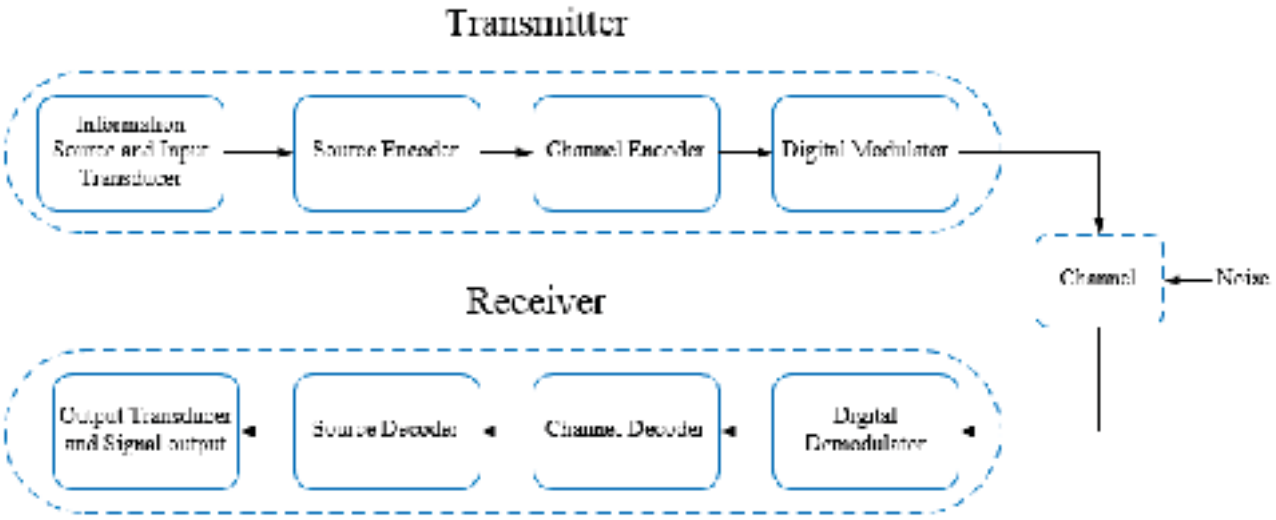

Figure 2.4: Principle of a digital transmission system.

2.3.4 Conclusion

In this section, a brief description of a WSN concept, characteristics and a sample of possible WSN applications are provided. It should be possible to imagine many other promising applications, as they seem limitless. Mostly, WSNs can be used to observe phenomena in an environment, react to events. WSN is constituted by a group of scattered sensors that have the liability of covering a surface according to specific measured parameters. Sensor nodes have some capacities for topology management, signal processing, and transmission management (coding, error correction) and wireless communication capabilities. The details about the wireless technologies linked to the WSNs are provided in chapter 3.

2.4 The Principle of Transmission System

Digital transmission systems convey information between a source and a sink using a physical medium like the cable, optical fiber or, yet, propagation on a radio channel. The transported signals can be either directly of digital origin as in data networks, or analog origin (speech, image) but converted into a digital form. The task of the transmission system consists of routing the signal from the source to the sink with the most reliability possible. The synoptic diagram and the essential components of a digital transmission system are given in Fig. 2.4.

2.4.1 The Transmitter

The source can send a message in a form a digital signal or audio and video signal. In a digital communication system, the source messages are generally adapted into a suite of

binary digits. The message from the encoder called information sequence is sent to the channel encoder. The principle of the channel encoder is the introduction of a conducted manner, redundancy in the information sequence. The aim of this is to subjugate the events of interference and noise encountered during the transmission of the signal through the channel. The output of the channel encoder is then sent to the modulator. The digital modulator maps the information sequence into signal waveforms ready to pass through the channel. It also serves as the interface to the channel communication.

2.4.2 The Channel

The communication channel is the physical medium which is utilized to transmit signals from the transmitter to the receiver. Several types of channels exit. A wired channel is generally used for traditional telephony. They are underwater acoustic, optical channels. In wireless systems, this channel consists of atmosphere and will be discussed in the next section. Regardless of the physical medium for signal transmission, the fundamental point is that a variety of possible phenomenon randomly alters the emitted signal. The additive noise also called thermal noise is the most common noise produced at the receiver front end. In wireless transmission, additional additive perturbations are atmospheric noise from a receiving antenna and human-made noise. An example of human-made noise is automobile ignition while electrical lightning discharges are a form of atmospheric noise. Interference from other channel users is other element of additive noise that often occurs in wireless and wired communication networks. However, another type of noise which is called impulsive noise from industrial environments like substations exists. It can also disrupt the communication. More details about this kind of noise are discussed in the next chapter.

2.4.3 The Receiver

At the receiver side, the digital demodulator converted the transmitted waveform altered by the channel and reduced it to a suite of numbers that represents the estimates of the transmitted data symbols. This sequence of numbers then goes through the channel decoder. With the redundancy in the received data and the knowledge of the code, the channel decoder tries to regenerate the initial information. In the end, the source decoder is used if an analog signal is desired. It tries to decode the information with the knowledge of the encoding algorithm.

2.5 Wireless Propagation Channel

The wireless channel environment conducts the performance of a communication system primarily. In contrast to the conventional constant and predictable proprieties of a wired channel, the wireless channel is relatively unpredictable and dynamic, that makes an accurate evaluation of a wireless communication system generally complicated. In wireless

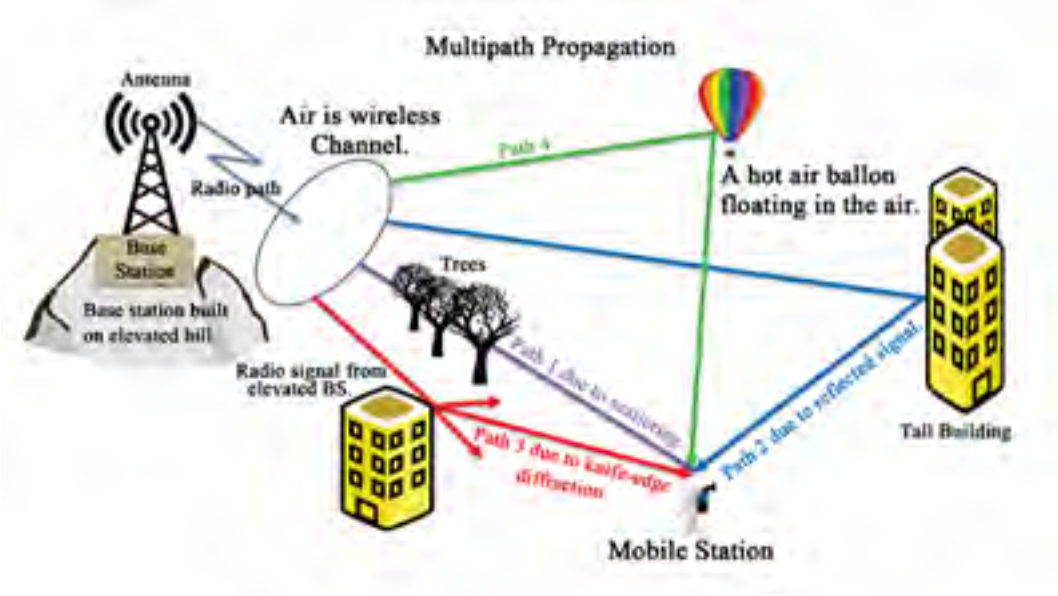

Figure 2.5: Illustration of the multi-path phenomenon in an environment [14].

communication, radio propagation refers to the behavior of the waves when they are transmitted. During this transmission, the signals are affected by various impairments such as noise issued from the electronic components and those from the environment and fading. In this section, we will discuss the phenomena that disrupt signal communication.

2.5.1 Physical Phenomena

In a homogeneous medium, the emitted wave propagates in the form of rectilinear rays. But most of the time, the stream will encounter obstacles (constructions, relief) that will cause a change in the path of the emitted wave. Depending on the nature of the impact, the wave will be altered by physical phenomena such as reflection/refraction, diffraction, and scattering [12-13] as depicted in Fig. 2.5.

Diffraction happens when the direct path between the transmitter and the receiver is obstructed by an opaque obstacle whose dimensions are more significant than the wavelength of the emitted signal.

Reflection / Refraction occurs when the wave interacts with an obstacle whose sizes are large and the irregularities small compared to the wavelength of these obstacles. When the object is perfectly conductive, all the incident energy is reflected. In the opposite case, a part of the power enters the purpose, according to the phenomenon of refraction. The amount of energy transported by the refracted wave depends on the absorption capacity of the materials. For a plane surface, the angles of incidence, reflection and refraction are connected by the Snell-Descartes law and, in particular, the edges of incidence and reflection are equal. Since the surface has a certain roughness relative to the wavelength, the incident wave is reflected in several directions and is referred to as diffuse reflection.

Figure 2.6: Fading phenomenon.

Scattering occurs in the same case as diffraction but when the dimensions of obstacles are comparable to the wavelength. Furthermore, the propagation of a radio wave is led by a phenomenon such as diffraction, reflection, and scattering which make it less predictable and complicated. In different instances, their intensity fluctuates with different environments. The variation of the signal amplitude over frequency and time, called "fading," is another characteristic of a wireless channel. Unlike the additive noise, fading is a source of signal disturbance that is identified as a non-additive signal perturbation. The different types of fading are described below.

Different scales of attenuation

The fading phenomena can be mainly divided into three different classes: large-scale fading, shadowing, and small-scale fading as depicted in Fig. 2.6.

Large-scale fading corresponds to the attenuation related to a great distance between the transmitter and the receiver [12]. An average path loss and shadowing represent large-scale fading.
Shadowing represents slow variations in the signal due to different interactions with obstacles in the environment. A Log-normal law generally models it.
Small-scale fading represents rapid signal fluctuations related to constructive and destructive interferences between different paths. The received signal can then vary by several tens

of decibels around the average signal. This type of phenomenon is the direct consequence of the multi-path event and the spatio-temporal variability of the channel.

2.5.2 Coherence vs. Selectivity

Channel coherence is the most critical parameter to describe a wireless channel [15]. When a channel is affected by some selectivity, the general term used to describe is fading. Selectivity is the contrary of coherence. A channel has a coherence time (T_c) and a coherence bandwidth (B_c).
The propagation phenomena cause several copies of the signal to arrive with different delays to the receiver. Measuring the time dispersion, the maximum exceeded delay τ_m may be used. It is described as the delay between the first incoming signal and the final signal having an energy level above a certain threshold. (B_c) is inversely proportional to this delay. It represents the frequency band in which all frequency elements of the signal undergo similar attenuation. A channel having a (B_c) much higher than the signal bandwidth is a flat fading channel. In the opposite case, the channel is frequency selective. The coherence time (T_c) when it represents the duration during which the impulse response of the channel can be considered constant. It depends directly on the Doppler spread. The latter represents the width of the spectral range of the signal after its passage through the channel. It is a function of the mobile speed. The coherence time (T_c) is inversely proportional to the Doppler spread. If the transmitted symbols have duration much less than (T_c) the channel is a slow-fading channel. If the symbols have a length much more significant than (T_c), the channel is a fast-fading channel. A wireless channel has *spatial coherence* if the magnitude of the carrier wave is static over a spatial shifting of the receiver. The coherence distance (D_c) is the relative distance that a wireless receiver can move with the channel attending to be invariant.

2.5.3 Diversity Techniques

Diversity techniques can be used in wireless transmission systems to combat small-scale fading caused by multi-paths. Indeed, if several replicas of the information are received by links whose respective fades are independent of each other, the probability that all the signal paths will fade at the same time decreases significantly. Diversity is proving to be very powerful for combating fading and improving performance, and in particular to increase capacity and coverage radio systems. Several methods of diversity techniques exist. We can cite among others frequency diversity, time diversity, spatial diversity. MIMO systems which are discussed in chapter 5 can create a significant spatial diversity.
Other diversity techniques exist in the literature but are not primarily used as those studied above. We can cite among additional polarization diversity, angle-arrival diversity.

2.5.4 Wireless Channel Modeling

2.5.4.1 Statistical Modeling

For the study of communications systems, the channel is represented mathematically by statistical distributions. As described above, the signals crossing the wireless channels are subject to different physical phenomena. Statistical models have been developed to predict the behavior of the signal towards these phenomena and to model the gain of the channel. Several statistical models exist, but in this manuscript, we only define the two widely used models, e.g., Rayleigh and Rician distributions.

Rayleigh Distribution

The Rayleigh distribution is a probability distribution popularly employed in communication theory, to define the rapid variations of the multi-path components. This model assumes a highly dispersive environment rich in uniformly distributed reflections. Several copies of the emitted signal appear to the receiver with different gains and delays on each of the paths. Each of the multi-paths arrives with a different phase representing the delays. These phases are assumed to be uniformly distributed over the interval $[0, 2\pi]$.The amplitude contribution of each path is distributed as a Gaussian. The probability density function (PDF) of a Rayleigh distribution is provided by

$$P(z) = \frac{z}{\sigma^2} e^{\left(-\frac{z^2}{2\sigma^2}\right)}, (0 \leq z \leq \infty) \tag{2.1}$$

where σ is the root mean square (RMS) value of the received signal and σ^2 represents the average power of the received signal.

Rician Distribution

Rician distribution considers a predominant non-fading signal in addition to the multi-path components. Thus, the amplitude and phase statistics no longer correspond to the previous case. This distribution can also be considered as the distribution of the length of a vector which would be the sum of a fixed vector and another one whose length has a Rayleigh distribution. The Rician distribution is given by

$$P(z) = \frac{z^{e^{-k}}}{\sigma^2} e^{\left(-\frac{z^2}{2\sigma^2}\right)} I_0\left(\frac{z\sqrt{(2k\sigma^2)}}{\sigma^2}\right) \tag{2.2}$$

where k is the parameter of Rice indicating the power ratio between the dominant path and the other paths, and $I_0(\cdot)$ is the modified Bessel function. When $k = 0$, PDF becomes a Rayleigh distribution. These two models can be used to model the complex gain relative to narrow band transmission channel. Besides these two models, there are others like the log-normal shadowing model [16] and the Nakagami model [17].

2.5.4.2 Deterministic Modeling

Also called physical models, they rely on the fundamental laws of physics with adequate approximations and models of the environment (position, geometry, material composition, and surface properties). They translate into complex mathematical relationships. They serve as reference models. These models employ ray optical techniques (ray tracing, rays launching combined with Uniform Theory of Diffraction method (UTD)) to compute the delay spread function using some more or less extensive geographical information (building layout, electric properties of walls and floors, etc.) about the propagation environment under consideration.

Free-Space Model

In telecommunications, the free-space propagation model is the ideal propagation of a signal inside a space where there would be only two transmitting and receiving antennas in the situation of direct visibility. Microwave radio links and satellite communications systems are associated with free space propagation. Like several large-scale models, the free-space is based on the separation distance between the transmitter and the receiver increased to absolute power. At a distance d from the transmitter, the receiver power by an antenna is given by the Friis equation [18]

$$P_r(d) = P_x G_x G_r \left(\frac{\lambda}{4\pi d}\right)^2 \tag{2.3}$$

where P_x is the transmitted power, G_x and G_r are the gains of the transmitter and receiver respectively, d is the distance, and finally, λ is the wavelength.
From this formula, we can see that the received power depends only on the wavelength and the distance between the transmitter and the receiver. However, in the case of mobile radio transmissions, where the various obstacles of the environment attenuate the wave, this relationship is no longer verified.
Another model which is based on the free-space is called Log-Distance Path Loss [19]. However, additional attenuation is introduced related to the nature of the propagation environment.

Ray Tracing

Ray tracing [20], [21] is a technique which determines without any approximation rays that can propagate from a transmitter to a receiver. The objective is to trace radio waves in the same way from a transmitter to a receiver. Once all combinations of the paths have been recognized, electromagnetic techniques are applied to the rays to determine essential parameters, such as signal strength. During the propagation, the signals are affected by some obstacles creating reflection, diffraction, and scattering. Those effects are also taken into account in the ray tracing calculation. By using site-specific information such as building databases and antenna characteristic ray models can deterministically describe

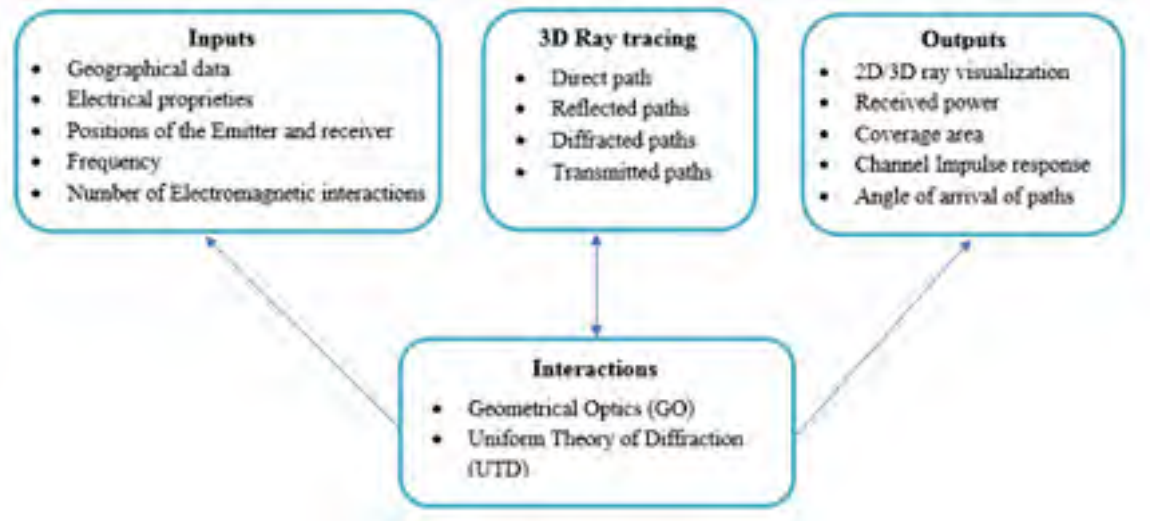

Figure 2.7: Synoptic of the 3D ray tracing channel simulator

a whole propagation scenario. Ray tracing model can be implemented in two or three dimensions. However, a three-dimensional model is better since other parameters such as floor and ceiling can also be taken into consideration, leading to more realistic models. We present now a channel simulator based on the ray tracing and allowing us to model the propagation of the wave in many environments.

RapSor

RaPSor for Ray Propagation Simulator is a radio propagation simulating tool fully developed by the XLIM laboratory [22]. This simulator is constructed on a 2D/3D ray tracing associated Uniform Theory of Diffraction (UTD) and to the Geometrical Optics laws (GO) for the calculation of several paths between a transmitter and a receiver. For a transceiver link, this simulator can identify and characterize the existing combination of multi-paths [23]. Moreover, we have access to the characteristics of each of these paths (attenuation, phase, delay). Hence, we can achieve the channel impulse response (CIR) noted h(τ) for the chosen point as

$$h(t,\tau) = \sum_{i=0}^{N_p} \tilde{a}_i(t)\delta(t-\tau_i(t)), \quad \tilde{a}_i(t) = a_i e^{-j\theta_i} \tag{2.4}$$

where a_i is the attenuation of the multi-path delayed by τ_i and the phase of θ_i depending on the electromagnetic interaction considered, δ is the Dirac impulse and N_p is the number of paths followed by the wave. Fig. 2.7 illustrates the principle of this simulator, while Fig. 2.8 depicts the user interface. It is also possible to support the evolution of this CIR by considering a path between the transmitter and the receiver. This propagation simulator also allows the calculation of the coverage area of a terminal positioned in the environment. This tool integrates all the specificities (geometrical and electrical) related to the situation,

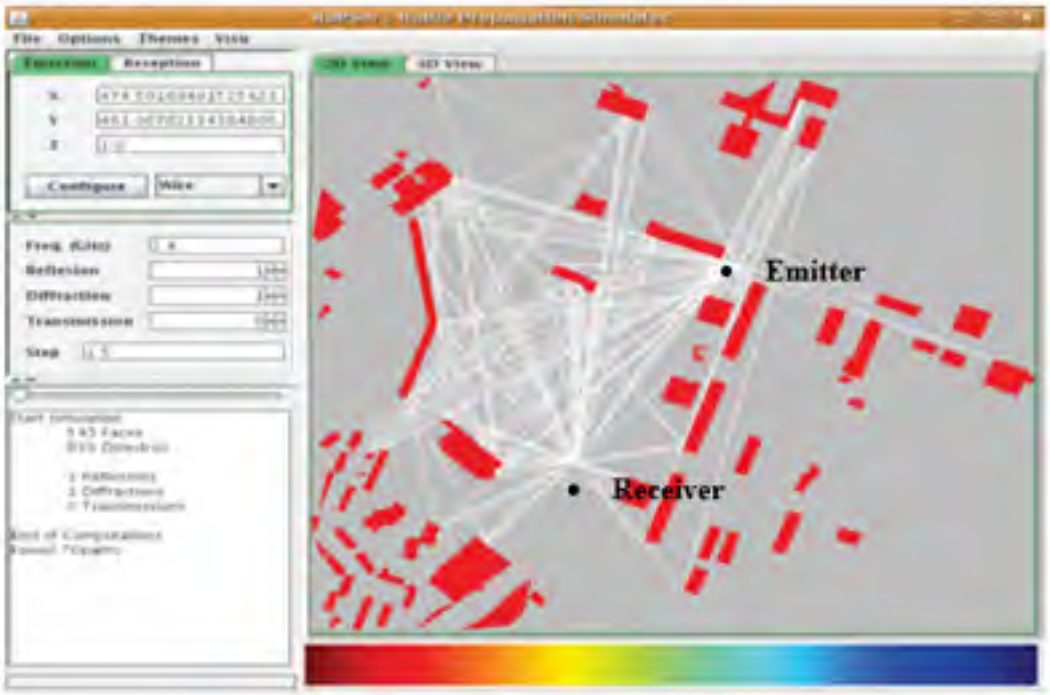

Figure 2.8: RapSor User interface [24]

and model all variations on a mobile radio channel: small, medium and on a large scale. Finally, this software offers the possibility of working indoors or outdoors. This simulator is used in chapter 4 of our work to obtain a realistic model of the transmission channel.

2.6 Conclusion

In this chapter, we introduced the concept and characteristics of SGs. Then, we have overviewed wireless sensor networks. The aspects of the channel propagation are also shown. WSN require a communication protocol to enable applications and their transmissions depend on the environment in which they operate. For this purpose, we study in the next chapter the wireless technologies for WSN and our environment which are the substations. Traditional wireless communication devices have been designed for rural or urban areas, but not for substations. As a result, the development of communication and detection networks in substations is an ambitious project with many challenges. The installation of copper or fiber-optic cabling in an electrical substation often entails prohibitive costs; wireless technologies, on the other hand, should be able to interact with substations from the outside and avoid costly changes.
However, the selection of the physical layer of the communication system is not inconsequential, and the advantages and disadvantages of the various communication protocols need to be carefully evaluated.

Chapter 3

Wireless technologies and High Voltage substations

Contents

3.1 Introduction

Integrating communication technologies with sensing and measurements at Smart Grid is expected to bring efficiency to the grid system at a lower cost. However, deploying a wireless sensor network requires a thorough knowledge of the environment. In particular, high voltage environments are subject to electromagnetic interference (EMI) known as impulsive noise that can degrade the quality of wireless communication. Noise environment may be intensely impulsive due to partial discharge, power electronic switching and other transient processes [25]. In substations, two kinds of noises must be distinguished: the ambient or thermal noise commonly considered as Gaussian noise and the impulsive noise. Impulsive noise has a highly structured form characterized by a short duration and significant probabilities of massive interference levels [26]. The impulsiveness of the interference can drastically degrade the performance and the reliability of wireless communication systems. To take account of the characteristics of the noise in the wireless network, an accurate model needs to be used to define such parameters. This chapter aims to analyze the wireless technologies and high voltage substations. For this purpose, section 2 reviews the existing techniques related to wireless sensors networks. It allows us to investigate the advantages and drawbacks of such technologies. Section 3 is about the power substation environment. It first details the functions. Secondly, the equipment and operations of substations are studied. Section 4 reviews the impulsive noise in high voltage substations while section 5 gives an overview of the noise models. An analysis of one of the technologies studied in section 2 is provided in section 6. It allows us to have the first ideas about the performance of a communication system in the presence of impulsive noise and in this case to see which approaches to putting in place to meet our needs. Section 7 concludes this chapter.

3.2 Communication Protocols for WSNs

Sensor networks become more and more essential in a world where resources are scarce and where optimization is still the only way to cope with the constant demands of using these resources. Sensor networks provide support for this optimization by identifying the necessary information, making the right decisions and activating the appropriate actions. It is to meet these needs that IEEE created the 802.15 group. This group aims to define standards that allow the connection between systems that are not very distant (a few meters away) with low transmission power and that constitutes personal wireless networks. It is in this context that in 2001, IEEE began work to propose a physical layer and data link layer adapted to low-speed, low-distance, and low-energy applications. This standard is known under IEEE 802.15.4 standard ratified in 2003 [27]. Communications protocols for sensor networks can be separated into two groups: those based on IEEE 802.15.4 standard, and those which define their own physical and medium access layers.

3.2.1 IEEE 802.15.4 Standard

At the beginning of 2003, IEEE 802.15.4 standard was approved after many years of study. This standard is designed to replace the high-speed protocols that IEEE 802 used to elaborate [28]. IEEE 802.15.4 is a communication standard which is intended for wireless networks of LR-WPAN (Low Rate Wireless Personal Area Network) family because of their low power consumption, the short range, and the low rate of devices using this protocol [29]. The characteristics of LR-WPAN are:

- Allocation of a 16-bit or 64-bit addresses,
- Operations with Star or Peer to peer networks,
- CSMA-CA channel access,
- Energy Detection (ED),
- Low energy consumption,
- Link Quality Indication (LQI),
- The use of 3 frequency bands such as : 868 MHz (1 channel), 915 MHz (10 channels), and 2.4 GHz (16 channels).

3.2.1.1 Protocol Architecture

IEEE 802.15.4 is a standard which designates the lowest layers of LR-WPANs such as the physical and medium access layers. The devices in this standard can communicate with others utilizing a simple wireless network architecture. Even though the lowest layers are specified in the standard, the highest layers are built on the OSI model (Open System Interconnection), and their interaction is provided utilizing an IEEE 802.2 standard as a possibility.

3.2.1.2 Physical Layer

IEEE 802.15.4 standard provides many advantages for inexpensive low power wireless application developers. It provides a reliable physical radio interface and has defined frequencies and frequency bands that it uses. It illustrates two physical layers with Direct Sequence Spread Spectrum (DSSS) which have the following features:

- Activation and deactivation of the radio transceiver: The radio module has three operating states: a transmission state, a reception state, and a sleep state. The state changes time between transmission and reception must not exceed 192 μs. The MAC layer controls this state. It is essential to save energy to put the module in sleep mode.

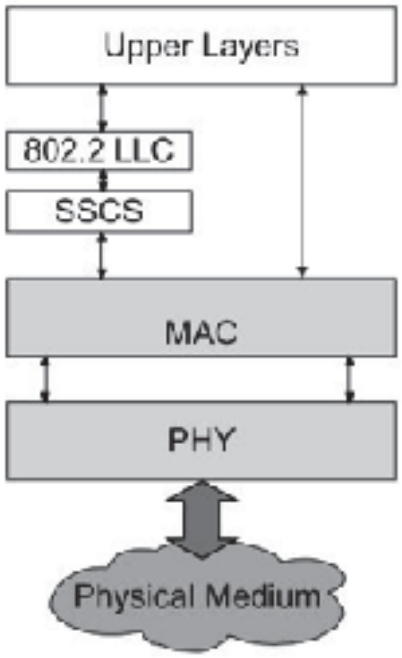

Figure 3.1: IEEE 802.15.4 Architecture [27]

- Reassign the state of the link to the upper layer: the LQI characterizes the quality of a relationship at a given moment following reception of a frame. This setting is essential for network and application layer protocols.
- Clear Channel Assessment (CCA) allows us to know the status of the radio channel. It is essential for the operation of the CSMA / CA algorithm of the MAC layer.
- Choose the transmission channel: as the physical layer offers several transmission channels, it is necessary to select a specific channel; this at the request of the upper layers. The channel change is also made implicitly by the physical layer following a scan request on all the frequency ranges each constituting a transmission channel. This action is called a scan.

The radio module is usually provided by the IEEE 802.15.4 physical layer. It offers three frequency bands each associated with modulations and bit rate (Table 3.1).
However, in 2006, the standard was updated, adding two more physical aspects [30]. The MAC layer offered new frames with new security features, an incremented version number, and a diversity of MAC enhancements, as well as:

- Beacon scheduling support,
- A shared time base with a data time stamping mechanism,
- Synchronization of broadcast messages in beacon-enabled PANs.

Table 3.1: Physical Layer specifications

Specifications	868 MHz	915 MHz	2450 MHz
Data Rate	20 kbps	40 kbps	250 kbps
No. of channel	1	10	16
Modulation	BPSK	BPSK	OQPSK
Chip pseudo-noise sequence	15	15	32

Two new physical layers were included as a reform in 2007, one of which supported proper ranging [31]. As a part of this amendment, MAC capability to support ranging was appended. In 2009, two new improvements were mandated. The first amendment concerns a new frequency band specific to China, while the second provides physical layer operations in Japan with a specific frequency band [32]. In 2012 and 2013, other amendments were made leading to other versions. More information are available at [33], [34].

3.2.2 Protocols based on IEEE 802.15.4

3.2.2.1 ZigBee

ZigBee is a low-rate wireless personal area network standard, builds on IEEE 802.15.4-2003 PHY standard as depicted in Fig. 3.2. It uses the physical layer of the latter and can transmit on three frequency bands: 868 MHz, 915 MHz, or 2.4 GHz with rates ranging from 20 to 250 kbps relied upon the band used and a direct sequence spread spectrum technique (DSSS). For each of these allowed bands, the protocol defines, according to the width of the band, a certain amount of communication channels. In the 2007 version of the protocol, there is a single communication channel between 868 MHz and 868.6 MHz, 30 channels between 902 and 928 MHz, and finally 16 channels between 2400 MHz and 2483.5 MHz. The modulation is always a phase modulation whose order depends on the frequency band. Thus, for 868 MHz and 915 MHz low bands, the standard carrier modulation is BPSK (Binary Phase-Shift Keying). It uses two-phase states, each associated with a bit to be transmitted. This modulation achieves a rate of 20 kbps at 868 MHz and 40 kbps at 915 MHz, while at 2.4 GHz, the modulation is OQPSK. To provide some robustness to interference caused by the simultaneous sending of information from several different users, ZigBee uses two techniques: an uncoordinated mode called CSMA/ CA (Carrier Sense Multiple Access with Collision Avoidance) and a coordinated mode or beacon mode. ZigBee technology provides two types of entities:

- Full entities, or FFDs (Full-Function Device);
- Reduced entities, or RFD (Reduce Function Device).

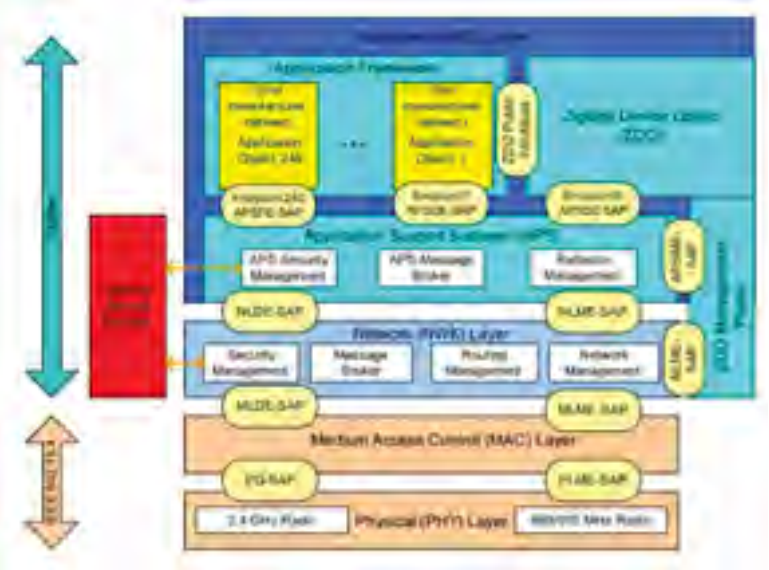

Figure 3.2: ZigBee Protocol Architecture [35]

FFDs implement the entire ZigBee specification whereas RFDs are lightened entities with the objective of reducing energy consumption and memory usage for the associated microcontroller. The RFD entities are necessarily ended nodes of the network; such a node can not route a packet on the network. In the network layer, ZigBee employs a mixed system based on the conventional AODV (ad-hoc on-Demand Distance Vector). More details about the network and application layers may be found in [38].

3.2.2.2 WirelessHart

WirelessHart is a scalable communication technology based on the HART Communication protocol. It is the first international standard for wireless communication or wireless in the process industry (IEC 62591, EN 62591) [39]. The Highway Addressable Remote Transducer (HART) is designed for data acquisition and control in industrial processes [40]. WirelessHart is a HART option at the physical, data link, and network levels as shown in Fig. 3.3. It uses a starless mesh network in which all radio stations, including mobile terrain nodes, from the mesh of the system. Each station involved can simultaneously serve as a transmission source for its data, but also as a repeater for data from other nodes. It uses the same frequency band (2.4 GHz) and the same channels as ZigBee but implements a jump mechanism between the channels, each packet being sent on a different channel to gain reliability.
At the MAC layer, the WirelessHart protocol uses a TDMA principle (Time Division Multiple Access) according to which a time slot (10 ms) is allocated individually to each node during a transmission. This principle, unlike the ZigBee CSMA / CA, ensures the determinism of communications.

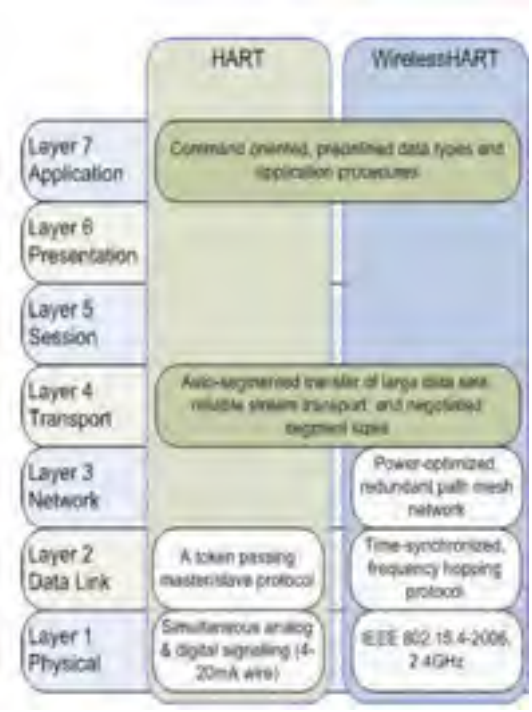

Figure 3.3: WirelessHart Protocol Architecture [35]

3.2.2.3 ISA100.11a

ISA100.11a standard is a sub-entity of the global ISA100 standard, a family of wireless system standards dedicated to industrial automation. This standard results from the convergence of efforts to define industry standards applicable to these systems, from different organizations and alliances such as NCCR-MICS, WINA, NSF-program. The purpose of ISA100.11a working group is to define all the specifications (with management and security) for wireless devices dedicated to five applications classes such as[41]:

- Control
  - Closed-loop industrial control,
  - Closed-loop supervision.
- Monitoring
  - Open-loop control,
  - Warnings,
  - Backups and downloads.

The features of ISA100.11a are intended to meet the following requirements:

- The ability to meet the demands of various industrial applications, including automation,
- Indoor and outdoor use,
- The same application layer providing both interoperability with pre-existing native protocols and broader use towards new protocols,
- Radio interoperability with IEEE 802.11 standard using frequency hopping,
- The use of the 2.4 GHz IEEE 802.15.4-2006 physical layer,
- Mesh and Star network operations.

As for WirelessHart technology, ISA100.11a proposes a TDMA access method. Besides, this standard also offers the possibility of using the CSMA as in ZigBee. ISA100.11a standard provides two types of topologies namely star and mesh.

3.2.2.4 OCARI

OCARI for Optimization of Communication for Ad-hoc Reliable Industrial networks is a protocol for industrial wireless sensor networks. This protocol was developed within the framework of the ANR (National Research Agency) project by the following consortium: EDF (Project Coordinator), DCNS (Directorate of Shipbuilding), INRIA (National Institute for Research in Computing and Automation)), LATTIS (Toulouse Laboratory of Technology and Systems Engineering), Telit, LIMOS (Laboratory of Computer Science, Modeling and Optimization of Systems), LRI (Research Laboratory in Computer Science) [42], [43].
The OCARI project aims to participate in the development of a new generation of networks based on the use of ad hoc wireless infrastructure in industrial environments. The aim is to provide a robust network infrastructure that takes into account highly constrained environments and favor the emergence of new industrial applications [44].
The OCARI infrastructure must meet criteria such as:

- Low energy consumption by implementing optimal protocol protocols for standby mode and route discovery on demand,
- Immunity to certain electromagnetic disturbances in the frequency bands used,
- Little degradation of radio transmission by physical obstacles.

OCARI is a wireless technology for sensor networks meeting the requirements of industrial applications. Indeed, OCARI differs from other techniques based at 802.15.4 by the following characteristics [45]:

- The determinism of access to the medium with the MaCARI protocol,

- A proactive routing strategy that considers the residual energy of the nodes and supports the nomadism, called EOLSR (Energy-aware Optimized Link State Routing),
- A mechanism for scheduling activities by coloring with three jumps to reduce interference and thus optimize the energy of the nodes, called SERENA (SchEdule RoutEr Nodes Activity).

3.2.2.5 6LoWPAN

In December 1998, IETF defined IPv6 as the successor to v4 by issuing RFC 2460. IPv6 has a larger address space, and it is based on a 128-bit address definition (vs. 32 for the v4). 6LoWPAN (IPv6 over Low Power Wireless Personal Area Network) is born from the desire to use IP in LR-WPAN networks. It is the result of a working group emanating from IETF which proposes an adaptation of the IPv6 protocol to the world of personal wireless networks, more precisely on the physical and link layers defined by IEEE 802.15.4 standard. The ultimate goal is to be able to take advantage of the possibilities offered by large networks such as the internet at 802.15.4 hardware. The main principles of 6LoWPAN are defined by RFC 4919; mechanisms are explicitly addressing 6LoWPAN / IEEE 802.15.4 interoperability are defined in RFC 4944 [46]. A 6LoWPAN protocol establishes the encapsulation and compression mechanisms of IPv6 protocol headers [47] so that it can be sent over a physical ZigBee layer. Indeed, the IP protocol is hugely used for the Internet connection of various devices, but its headers have a size of 40 bytes to which should be added the headers of the transport layer, or 20 bytes for TCP (Transmission Control Protocol) or 8 bytes for UDP (User Datagram Protocol). Thus, since the length of the 802.15.4 frame is 127 bytes, the space available for the data is only 33 bytes in the context of the UDP protocol and by 21 bytes for the TCP protocol. To ensure the transmission of an IPv6 frame, the available length for the data field must be at least 1280 bytes. The 6LoWPAN protocol provides fragmentation/reassembly, header compression, and IP auto-configuration mechanisms to allow the transmission of IPv6 frames over a ZigBee type radio layer [48].

3.2.3 Other Technologies

3.2.3.1 Bluetooth

Bluetooth is a wireless communication system that allows a personal network to exchange data between devices in a certain proximity. Bluetooth can be considered as the first WPAN to have been specified and developed [49]. The first version of Bluetooth was released in 1999 [50] and uses GFSK modulation (Gaussian Frequency Shift Keying) with a bit rate of 1 Mbps. It is frequency modulation of the FSK type (Frequency Shift Keying) with two states, whose modulating signal is filtered by a Gaussian. Version 2.0 [51] of the standard introduces a mode called EDR (Enhanced Data Rate) which uses a phase modulation in two variants: 4-DQPSK modulation to achieve a bit rate of 2 Mbps, and modulation 8-DQPSK for a bit rate of 3 Mbps. This increase in flow is, of course, at the cost of increased

complexity of the modulation and therefore slight over-consumption. On the other hand, with constant network traffic, an EDR module transmits the data more quickly and is, therefore, shorter in operation, which allows the designers of the standard to announce a reduced consumption in half. The Bluetooth radio layer uses a 2.4 GHz frequency band. This frequency band from 2.4 GHz to 2.4835 GHz is divided into 79 channels of 1 MHz.
Three power classes were defined: 100 mW (20 dBm) for class 1, 2.5 mW (4 dBm) for class 2, and 1 mW (0 dBm) for class 3. The power classes correspond to the maximum powers of the equipment. It is possible to implement a control algorithm to reduce the power used. To avoid the phenomenon of frequency fading and to minimize the interference with other systems coexisting in this popular band, Bluetooth uses the technique of frequency hopping which is based on the use of different carriers used one after the other in a pseudo-random sequence.

3.2.3.2 WiFi

IEEE 802.11 is an international standard specifying the features of a wireless local area network (WLAN). In the beginning, WiFi stands for Wireless Fidelity and corresponds to the name of the certification issued by the WiFi Alliance, previously WECA (Wireless Ethernet Compatibility Alliance), the organization responsible for providing the interoperability between 802.11 compliant equipment. The first version of the 802.11 standard was ratified in 1997. Two improvements were made in 1999, leading to 802.11a and 802.11b versions.
The initial standard specifies three physical layers and a Medium Access Control layer. One of the PHY layers uses IR (Infra Red) waves for rates up to 2 Mbps, and the other two layers use 2.4 GHz radio waves, one with DSSS and the other with frequency hopping spreading spectrum allowing both to achieve data rates of up to 2 Mbps. Extensions a and b respectively define an orthogonal frequency division multiplexing (OFDM) PHY layer at 5 GHz allowing rates up to 54 Mbps and a PHY layer at 2.4 GHz enabling speeds up to 11 Mbps.
The 802.11 is a rapidly evolving standard. Significant efforts have been made regarding interoperability. Security is also a weakness of the standard. To overcome the security problems, each manufacturer has proposed its solution. To maintain an open standard and interoperability, IEEE created the subgroup i to study these issues and provide answers. Another critical point to ensure the sustainability of the standard is the contribution of the quality of service (QoS). Increasing data rates is also a logical evolution of the standard. A subgroup has also been created. It is the subgroup g that is responsible for proposing a new physical layer that is compatible with the layer specified in extension b. Table 3.2 presents a summary of the different physical specifications presently in use.

3.2.3.3 WiMax

WiMAX for Worldwide Interoperability for Microwave Access (AXess) was designed with the goal of defining broadband technology based on the IP protocol replacing the wired

Table 3.2: IEEE 802.11 Physical Layer specifications

PHY types	802.11a	802.11b	802.11g	802.11n
Approval date	1999	1999	2003	2009
Operating Frequency	5 GHz	2.4 GHz	2.4 GHz	2.4 / 5 GHz
Modulation	OFDM	DSSS	OFDM	OFDM / MIMO
Typical Throughput	25-14 Mbps	5-7 Mbps	14 Mbps	100 Mbps
Bit Rate	54 Mbps	11 Mbps	54 Mbps	150 Mbps

network. It has features similar to WiFi while covering larger areas, similar to network cells. Its first version, 802.16-2001, offered a point-to-multipoint system with the throughput of about 70 Mbps, an operating frequency between 10 and 60 GHz for LOS situation and a single carrier transmission. In 2003, some modifications were made namely:

- Non-Line of sight transmission,
- The definition of the number profiles,
- The predefinition of interoperability parameters,
- New operating frequencies from 2 to 11 GHz.

Amendments were also made in 2004, to adopt multi-carrier modulation and to adopt the following modulation to the state of the channel. These allowed the introduction of OFDM and OFDMA. In 2005, the new version combined fixed and mobile systems in the regulatory band. It also integrates security, multi-carrier systems, and MIMO systems. The last release in 2011, introduced a speed of 100 Mbps for the mobile network and 1 Gbps for a fixed interface. The physical layer was based primarily on IEEE 802.16-2004 Single Carrier Standards for Fixed and IEEE 802.16-2005 Systems multi-carrier for mobile systems. However, during its development, the WiMax standard defines two additional physical layers that can work with existing MAC layers.

3.2.3.4 Sigfox [56]

Sigfox is a French company, headquartered in Lab‘ege, near Toulouse. It was born in 2009 on the initiative of two engineers. Sigfox has few limitations. It works in most areas of possible activities and all sectors imaginable. Sigfox defines a standardized way to collect data from sensors and objects with a single, standardized set of applications programming interfaces (API). Besides, Sigfox technology complements the traditional cellular machine-to-machine thanks to the implementation of global solutions and offering great energy autonomy at a low cost. Sigfox is, as secondary connectivity, a very promising solution

for achieving a very low energy consumption and improve the experience of users. Sigfox uses 192 KHz of the unlicensed ISM band to exchange messages over the air. The emission technique is what is called the ultra-low band (UNB - Ultra Narrow Band). Each message occupies 100 Hz (ETSI zones) or 600 Hz (FCC zones) and is transferred at a rate of 100 or 600 bits per second depending on the region. Sending a message over a 12-byte payload over a radio requires 2.08 seconds at a speed of 100 bps. This technology allows Sigfox base stations to communicate over long distances without being affected by noise. The band used varies according to the geographical zones:

- in countries according to ETSI standards, the band used is between 868 and 868.2 MHz;
- the band used in the rest of the world is between 902 and 928 MHz. Some restrictions can be applied to depend on to the local regulations.

3.2.3.5 LoRa

LoRa is a long-range network technology for low-speed communication of connected objects. Like 3G / 4G, LoRa protocol allows both outdoor and indoor transmission over longer distances. Promoted by the LoRa alliance, LoRa networks enable related objects to exchange small data packets. LoRa, for Long Range, is the name given to the radio frequency physical layer, while LoRaWan, for Lora-Wide Area Network, refers to the deficient protocol layer. Semtech's LoRa chips operate on 434 and 868 MHz frequency bands in Europe and 915 MHz for the rest of the world. The theoretical range in the suburban area is greater than 15 km with flows between 0.3 and 22 kbps. The transmit power is adaptive. It is also possible to implement on a Lora-radio-frequency chip various protocols such as LoRaWan but also 6LowPAN or ZigBee. The LoRaWan network defines three types of components:

- Class A: end-of-network nodes like sensors,
- Class B: Gateway,
- Class C: Data server.

LoRaWan is based on the LoRaMAC protocol that defines the interaction between nodes and gateways. The LoRaMAC protocol offers several interesting mechanisms such as the temporal synchronization of the nodes, the adaptation management of the transmission power of the node through an exchange with the gateway, as well as a set of identification keys of the node, network and application.

3.2.4 Communication Protocol Synthesis

Wireless technologies offer new opportunities in telecommunications and computer networks. Thanks to the progress made, a new type of ad-hoc network has emerged, which is

the Wireless Sensor Networks. These networks without fixed infrastructure can be deployed quickly in sensitive areas and difficult to access. Many standards provide a communication protocol to the sensor network. We distinguish among other Bluetooth, ZigBee, WirelessHart, OCARI, 6LoWPAN, LoRa, SigFox,...
In our review, we notice that many of these protocols are based on the IEEE 802.15.4 standard and therefore most often share the same physical layer. Standards like ZigBee, WirelessHart, ISA100.11a are the most popular and used. In the industrial sector, WirelessHart and ISA100.11a are the most recommended [62]. The 6LoWPAN allows us to use IP at low cost and low-speed standards. It makes it possible to use all the advantages of the Internet on a network with low energy consumption. OCARI although based on IEEE 802.15.4 offers the determinism of the access to the medium thanks to MaCARI, thus providing a little use and the advantage of testing a new protocol of access to the medium. However, the disadvantage of this protocol is that it is a proprietary protocol. Other standards such as LoRa, Bluetooth, WiMAX are also impressive. The use of a low frequency for LoRa, SigFox, and the frequency hopping of Bluetooth are advantageous. However, Bluetooth can be used to connect to phones as well, though this is less common in an industrial setting. ZigBee, WirelessHart and ISA100.11a are protocols that offer benefits that we can leverage. For this purpose, we compare these technologies.
WSN standards based on IEEE 802.15.4 standard and with 2.4 GHz frequency, offer some similitudes and dissimilarities. ZigBee, which is the first standard developed, supports three topologies such as a tree, star and mesh while WirelessHart and ISA100 propose star, mesh and hybrid topology based on the combination of the two. The key features of these standards are the same, and can be summarized as follows:

- Embedded communications systems,
- Favor industrial applications,
- Interoperability with other communications systems,
- Compatibility with existing industrial devices,
- Energy saving and security,
- Communication reliability and efficiency.

In industrial applications, ZigBee is not compatible with wired protocols while ISA100 can offer a simultaneous communication with the most common protocols and supports a smooth integration with other wired protocols. Moreover, ISA100 and WirelessHart standards integrate different approaches that are used to optimize coexistence with other users of the 2.4 GHz radio spectrum. Although ISA100 and WirelessHart are based on the physical layer defined IEEE 802.15.4, they specify their data link, network, transport, and application layers, while ZigBee specifies only the higher layers. Table 3.4 emphasizes the summary of the properties of these three standards.

Table 3.3: Comparative of ZigBee, WirelessHart and ISA100.11a

Features Set	ZigBee	WirelessHart	ISA100.11a
Approval date	2004	2007	2009
Operating Frequency	868, 915, 2400 MHz	2400 MHz	2400 MHz
Modulation	BPSK, OQPSK	OQPSK	OQPSK
Bit Rate	20, 40, 250 kbps	250 kbps	250 kbps
Spreading	DSSS	FHSS	DSSS
Multiple Access	CSMA/CA	TDMA	CSMA/CA, TDMA
Energy Consumption	Low	Low	Low
Implementation	Easy	Challenging	Challenging

3.2.5 Conclusion

Through this literature review, we find that there are several technologies proposed for the deployment of sensor networks. Numerous are built on IEEE 802.15.4 physical layer. Indeed, industrial environments are not taken into consideration in the design of these standards. Specific requirements are needed because such environments have particular characteristics such as reliability, interference with actual equipment, low power consumption, multi-path propagation, real-time reconfiguration, security) [63]. However, through our review, it could be concluded that protocols based on IEEE 802.15.4 physical layer network with the characteristics mentioned above, could be the most appropriate for implementing and testing the performance in the presence of impulsive noise introduced by substation environment.

3.3 Power Substation Environments

An electrical grid is a system whose position is a significant piece as it is the node from which the network is organized (configuration of the topology), monitored (monitoring function), and protected (action of protections). The power station can be considered as a bar (or bars) of which are connected feeders regarding electricity networks. An electrical substation is an element of the electricity grid serving transmission of electricity. It is possible to raise the dynamic tension for its transfer, then lower it for consumption by the users (private or industrial). The substations are therefore at the ends of the transmission lines or distribution.

3.3.1 Functions

The substations are located at the nodes of the mesh or the tree of the conductors. The features of these positions are as follows:

- The routing of the lines of the same tension between them,
- Evacuation of energy from generation sources to the grid,
- The link between networks of different voltages.

These different functions are provided by the apparatus which makes it possible to:

- Check the electrical quantities,
- Establish or interrupt the flow of current through the circuit breakers,
- Ensure continuity or isolation of a circuit through breeders,
- Change the voltage of the electrical energy, thanks to the power transformers.

Therefore, power substations are sensitive points in the organization of the network. Failure of a unit can cause many lines to become out of service, which becomes useless. In general, the constituent elements of a position are bus bars, circuit breakers, disconnectors, etc.
A power substation is an essential piece of work in the network, which you cannot afford to decommission in its entirety. However, for maintenance reasons, at least two bus bars can be installed in most substations of the transmission system. We will now describe the main elements of a power substation.

3.3.2 Equipment and Operations

A conventional substation will be constituted of transformers, switchgear, line termination structures, controls, circuit breakers, etc. Fig. 3.4 depicts the essential elements of a substation. Let us define some of these elements.

- Power lines also called “primary feeder,” allow to connect distribution substations to a sub-transmission system.
- Current transformers are devices that lower the value of current to enable measurement by protection and control equipment. The current is comparable to the flow.
- Circuit breakers are used to open or close a circuit. They are operated by a manual control during the performance of the interviews and are triggered automatically in case of a short circuit. Their function in the network is similar to that of the fuse or circuit breaker in the home switchboard.
- Disconnectors are located at several points in the station. These play a vital role in electrically isolating and two circuits to secure workers and equipment during maintenance work.

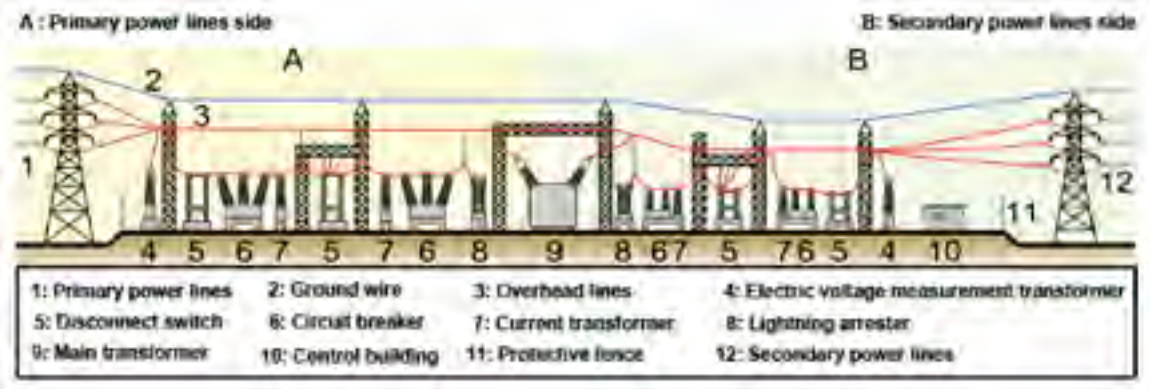

Figure 3.4: Elements of a substation [55].

- Bus bars are large conductors, usually rigid aluminum, which connects circuits. They can be compared to the home switchboard, which serves as the point of arrival and distributes it among the various circuits to be powered. The difference, necessarily, is that the bars distribute high currents.

3.3.3 Conclusion

Electricity networks are infrastructure that moves energy from production facilities to consumer facilities. There are several types of systems for transport, distribution, and distribution. Nodes called electrical stations provide these different functions. These stations contain equipment to ensure the various operations related to the network. It is in these positions that Hydro-Quebec wishes to modernize its system by using new information and communication technologies. The purpose is to monitor and control the electrical networks using Smart Grid. However, with the study done on the power grid, we have seen that these stations are equipped with many devices. So it is a challenging environment because of special effects of the equipment creating a pulse noise. This noise, also known as electromagnetic noise, affects wireless communication systems. They can degrade performance. In the next section, we will study the disturbances that may exist in the HV stations. There are several in the field of electrical engineering and are well known because they can generate energy losses and electromagnetic pollution.

3.4 Impulsive Noise in High Voltage Substations

In this section, we present the different types of impulsive noise. However, before introducing the impulsive noise, we first review the additive white Gaussian noise (AWGN) which is always considered as the background noise in the substation.

3.4.1 Additive White Gaussian Noise (AWGN)

Noise is generally being the source of disturbance in a communication system. The noise is expressed by a stochastic value such that neither the transmitter nor the receiver can control it. In a telecommunication system, a noise analysis is based on an ideal noise process named white noise. Besides, the background noise found in industrial environments such as substation is considered as Gaussian noise. White noise is a realization of a random process in which the power spectral density is the same for all frequencies. The widely used model to describe noise in a channel is Additive White Gaussian Noise, and it allows us to represent both internal and external noise [56]. Its probability density function follows a normal distribution and is given by [57]

$$P(y|\mu,\sigma) = \frac{1}{\sigma\sqrt{2\pi}}e - \frac{(y-\mu)^2}{2\sigma^2} \tag{3.1}$$

The normal distribution defines two parameters. μ is the first parameter and corresponds to the mean. σ, with its variance σ^2 is the second and corresponds to the standard deviation.

3.4.2 Partial Discharges

Partial discharges (PD) are an electrical burst which appears across a localized area of the insulation between two conducting electrodes, without entirely bridging the gap. Imperfections or discontinuities in the insulation system can be the causes of partial discharges. PD appears whenever there is a stressed region caused by some cavity inside the insulation or when there is a protrusion outside it. Sharp edges or protrusions around the conductor can form the stressed area. Under the effect of HV, the insulation between two conductors can be ineffective for a minimal period. The degradation of the dielectric or a fault of one of the conductors can be the cause of the discharges [58]. If the insulation is to be perforated (in the case of a solid), or if a piece of conductors protrudes and comes close to a neighboring conductor, there is the phenomenon of PD. Transformers that use oil or gas as an insulator, like most equipment, emit radiation caused by partial discharges. There are two types of discharges: internal and external discharges. The internal discharge occurs at the dielectric degradation between two live conductors while the external discharge occurs at the dielectric-conductive interface. Fig. 3.5 shows the different types of PDs.

3.4.3 Corona Effects and Gap Noise

The corona effect is manifested in the form of air conductivity in the vicinity of the conductor and can often be observed in the way of light discharges all along a voltage line. From the physical and electrical point of view, this phenomenon is due to the ionization of the air, as soon as the electric field prevailing near the conductor becomes sufficient. When using larger diameter conductors, such as those that equip the airlines, it is found that the light sheath evolves into discrete discharges that specialists usually call “egrets” or “emanations.” Disturbances mainly cause corona effect due to the presence of water droplets or insects

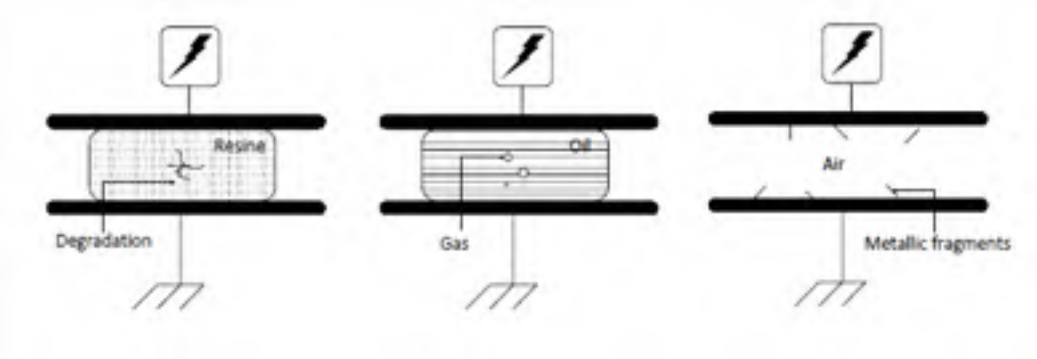

Figure 3.5: Different types of partial discharges [59]

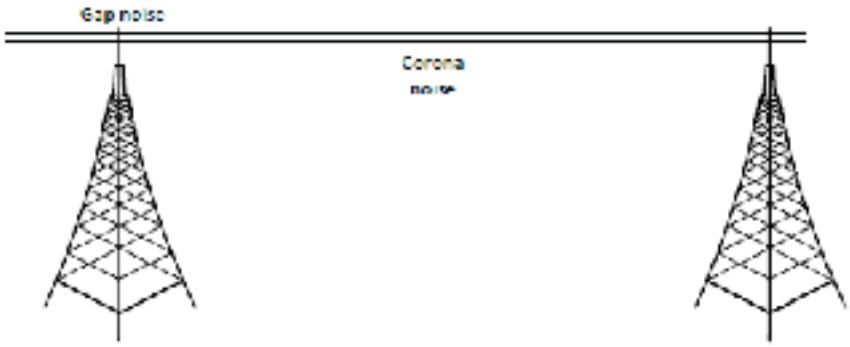

Figure 3.6: Corona and Gap noises [59]

on the conductors or contact with the turrets holding the wires. These disturbances cause at the local level an increase in the electric field thus creating an electrical short circuit. HV lines are not subject to the corona effect. For a voltage below 75 kV, the noise Gap seems to have much more influence, and its amplitude is much higher towards the very high frequencies, that the noise crowns. Gap noise can occur in places where very small separations develop between the mechanically connected metal parts [58]. Unlike corona effect, which manifests itself in the form of partial discharges, the Gap noise is characterized by complete discharges, whose direct radiated field is no longer negligible and is, on the contrary, the initial disturbance. These two types of noise coexist on HV lines, but on some frequency ranges, one predominates depending on line voltage or weather conditions. Corona noise is detectable accurately in a band of up to 1 GHz, while the Gap noise band is detectable up to 8 GHz.

3.4.4 Conclusion

In summary, in the substation environment, impulse noise occurs as PDs caused by material failures, such as transformer insulation, or HV line conductors and tie insulators. In the following, we will see how to model the impulse noise present in this environment.

3.5 Noise model in High Voltage Substations

Generally, in the signal processing domain, there are at least two kinds of noise: the white Gaussian noise and impulsive noise [61]. Currently, the statistical behavior of Gaussian noise is well-known. In contrast, impulse noise is a non-Gaussian random process that has a strongly structured form due to its impulsive nature. It often has non-stationary characteristics such as the appearance of random pulses over time with high levels of interference [62]. In this section, we present the impulsive noise measurement and statistical modeling.

3.5.1 Partial Discharge Measurements

Noise present at different levels in all environments can cause transmission errors and may also disturb the communication link. Over long transmissions, the impulsive noise is considered to be a significant source of interference. In power substations, the principal sources of impulsive noise are partial discharges. They are mainly caused by imperfect air insulation and spherical radiation. Partial discharges are characterized by strong amplitude with short duration [25], [63]. This interference characteristic can degrade the performance and reliability of any wireless communication systems severely. To avoid an unacceptable level of system performance, the right attributes of impulsive noise must be considered. For measuring the electromagnetic pulses radiated by PDs, several experiments have been conducted with antennas [60], [64]. For example, in [65], Chartier presented electromagnetic measurements of the 900 MHz range using a high gain parabolic antenna and a low noise pre-amplifier. In [61], the authors studied impulsive noise measurements acquired near overhead power lines from 2.4 to 345 kV in a frequency range from 60 Hz to 1 GHz. However, the frequency range of standard wireless communications is more extensive than those used in several experimentations. Therefore, the modeling and characterization of the impulsive noise are often insufficient. In the next section, we present a complete setup design for impulsive noise measurement.

3.5.1.1 Setup Design

Measuring impulsive noise in a wideband system becomes essential for evaluating the characteristics. F. Sacuto in [59] performed the setup below. For more information, readers can refer to it. The main components are an antenna and an oscilloscope as depicted in Fig. 3.7. The other elements of this setup are among other RF equipment to confirm that the measurements are achieved in the frequency band of interest. The list of the setup components is described below:

- A unidirectional and polarized antenna (Rhode and Schwartz (R&S)) with a linear gain on the band 780 MHz - 26.5 GHz;
- A high-pass filter from 780 MHz to 3 GHz with the attenuation of -100 dB and a pass-band gain of -0.5 dB;

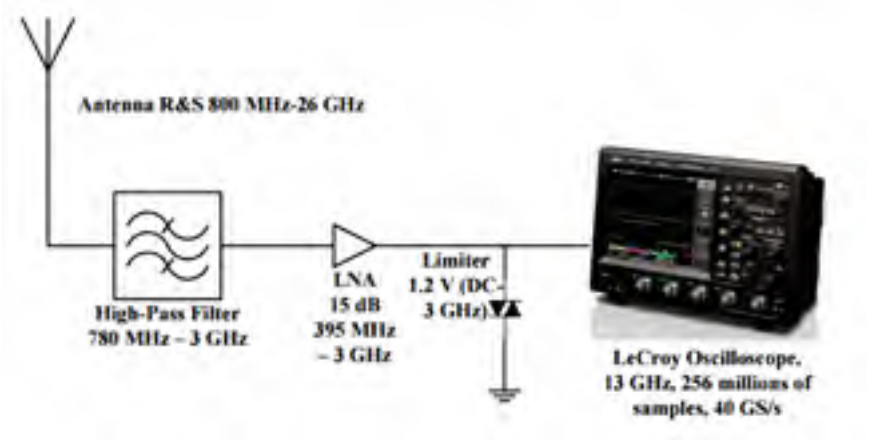

Figure 3.7: Measurement setup of Impulsive Noise [59]

- Low Noise Amplifier (LNA) with a gain of 15 dB on the 395 MHz - 3 GHz band;
- Limiter that clips the signal to 1.1 V on the DC -3 GHz band;
- Leroy 13 GHz digital oscilloscope with a maximum sampling rate of 40 GigaSamples per second and a memory of 256 million samples.

3.5.1.2 Measurement Campaign

3.5.1.2.1 Measurements in HV Substations

The substation where the measurements were carried out is situated in Quebec. It is an air-insulated power station where transformers, circuit-breakers, bus bars, disconnectors can be located there. It also offers several high voltages such as 230, 315, and 735 kV. During the measurements, a vehicle placed at 20 - 30 m from the nearest equipment was used for the shifting around the equipment. The antenna was oriented to the direction of power lines and other equipment situated in the different voltage localities with the possibility of a rotation of 360 and 180 degrees horizontally and vertically, respectively. The noise was registered during a 51.2 ms time window (chosen for having enough samples). To confirm the diversity in the collected samples, the procedure was repeated on different days.

3.5.1.2.2 Tests in Laboratory

As an alternative to the measurement campaign, other specimens can be employed to reproduce precisely the impulsive noise occurring in a substation. It is the Tesla Coil and the bar generator. Two specimens are used generally in electrotechnical and controlled laboratories to generate electrical discharges in the air. In this chapter, we only define the bar generator (Fig. 3.8) which will be used in chapter 4.

Figure 3.8: Setup for impulsive noise measurement in the laboratory.

Table 3.4: Characteristics of the air cavity

Dimensions	**Air cavity**	**Dielectric**
Height (mm)	0.25	3.6
Width (mm)	2.5	55
Depth (mm)	2	58
Relative permittivity (ϵ_r)	1	4
Conductivity (σ_i)	0	$2.8.10^{-9}$

Description of the Setup

Measuring impulsive noise becomes essential for evaluating the characteristics to be considered in a design of a communication system. For the measurements in the laboratory, we design the setup below. We use a model built in GNU Radio using USRP. The main components are the generator bar and an antenna as illustrated in Fig. 3.8(a). The list of the setup components is described below:

- The generator bar is utilized in controlled laboratory conditions through several voltages. Hydro-Quebec researchers employ this instrument to estimate the partial discharges localization on the voltage phase. In the middle of the bar, the insulation is covered by a conductor made with epoxy-mica insulated by a shield. The principal characteristics of the dimensions are summarized in Table 3.4. When a HV generator (1-18 kV) is connected, an electromagnetic field is emitted radially by the conductor that the isolator tries to isolate. The generator bar is an excellent possibility for the PD generation, and it controls the power supply accurately.

- USRP N10 is used as an antenna for recovering the signal from the generator bar. Indeed, we implement some blocks to save the measures issued by the impulsive noise generator as depicted in Fig. 3.8(b). More information on the functioning of the USRP is given in section 4.

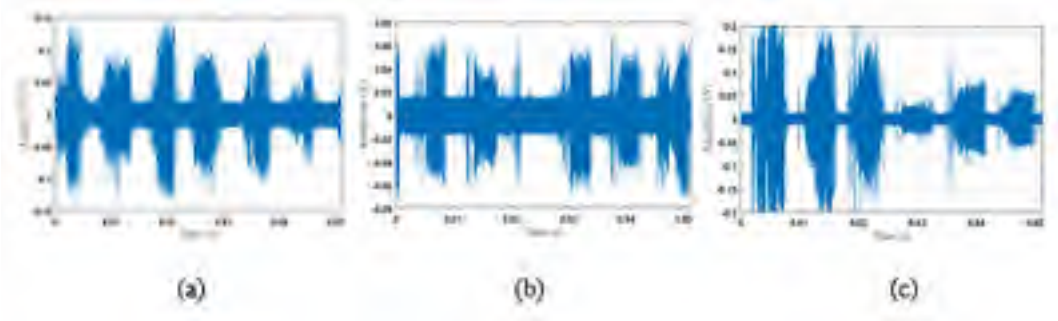

Figure 3.9: Impulsive noise measurements for 230 kV (a), 315 kV (b), and 735 kV (c) areas, respectively.

3.5.1.3 Results

In this section, we present the results regarding the amplitude versus time of the impulsive noise from the campaign measurements described above. As can be seen in these figures, the noise from 735 kV is more potent concerning amplitude than those measured from the other voltages. Its magnitude can reach 0.2 V while for the tensions of 230 and 315 kV, the maximum amplitudes revolve around 0.1 V. It can be explained by the fact that in 735 kV area, we note the presence of several metallic structures that cause great impulsive noises. The other remark is that we have approximately the same amplitude level and variation of the impulsive noise for the 230 and 315 kV areas.

Fig. 3.10 represents an example of measurements made with the generator bar at 16 kV. It corresponds to the plot of the noise level (amplitude) versus the time in milliseconds. In this figure, we notice that a short duration and high amplitude characterize the impulsive event, which is highlighted by the red-dashed contour. As can be seen, the alternative method for measuring partial discharges is also accurate. It represents the impulse event well and the background noise compared to the results from measurements obtained in a power substation [59].

3.5.2 Statistical Description of Impulsive Noise

3.5.2.1 Middleton Classes (A, B, and C)

- Class Class A model refers to the narrow-band noise in which the interference spectrum is narrower than the receiver bandwidth and includes all pulses which do not produce transients in the receiver front end [66]. Its probability density function (PDF), derived from [67], is Its probability density function (PDF), derived from [67], is

$$f(x) = e^{-A} \sum_{m=0}^{\infty} \frac{A^m}{m!\sqrt{2\pi\sigma_m^2}} e \frac{x^2}{2\sigma_m^2} \tag{3.2}$$

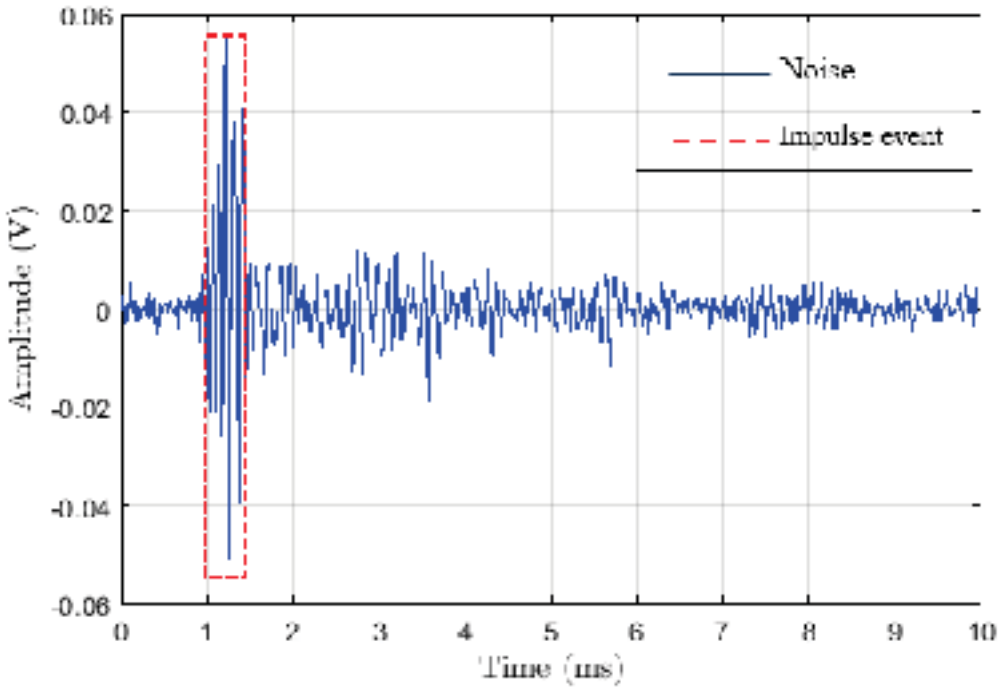

Figure 3.10: Impulsive noise measurements from the bar generator.

where $\sigma_m^2 = \frac{\frac{m}{A}+\gamma}{1+\gamma}$ is the noise variance, $A = \varphi T_m$ is the overlap or impulse index, T_m is the mean impulse duration, and γ is the Gaussian factor.
Equation (3.1) is a weighted sum of Gaussian distributions and is given by

$$X(t) = X_P(t) + X_G(t) \tag{3.3}$$

By increasing overlap index A, the noise can be made arbitrarily close to Gaussian, and by decreasing A, it can be made close to a conventional Poisson process. The Gaussian factor γ is the ratio of power in the Gaussian and Poisson components e.g.,

$$\gamma = \frac{X_P^2}{X_G^2} \tag{3.4}$$

- Class B model is used to represent impulsive broadband noise in which the noise spectrum is full than the receiver bandwidth [68]. Class B noise impulses produce transients in the receiver. It models an impulsive broadband noise with accuracy. However, it is complicated to implement in practice because of its complicated form of power density function which has five parameters to identify [68].

- Class C model is considered as a sum of Class B and Class A. In practice, Class C noise can often be approximated by Class B [68].

To estimate parameters, Middleton proposed two estimators: the first is based on empirical observations and the second method is based on the moments derived from the observed samples by using the following equations [60].

$$A_{est} = \frac{9(s_4 - 2s_2^2)^3}{2(s_6 + 12s_2^3 - 9s_2e_4)^2} \tag{3.5}$$

$$\gamma_{est} = \frac{2s_2(s_6 + 12s_2^3 - 9s_2s_4)}{3(s_4 - 2s_2^2)^3} \tag{3.6}$$

where s_6, s_4, and s_2 are the sixth, fourth, and second order moments of the envelope data, respectively.

3.5.2.2 Symmetric Alpha Stable

Symmetric Alpha-Stable (SαS) process, with $0 < \alpha < 2$, is commonly employed to model non-Gaussian signals. Generally, the probability density function has not a closed-form expression. However, the characteristic function is often used to define it [66].

$$\varphi(\omega) = e^{j\delta\omega - \gamma|\omega|^\alpha} \tag{3.7}$$

where

- α with value $0 < \alpha \leq 2$, corresponds to the characteristic exponent. It is an essential parameter and defines the shape of the distribution. The Gaussian behavior is obtained when $\alpha = 2$, whereas a value of $\alpha = 1$ determines the Cauchy distribution.
- γ is the dispersion parameter ($\gamma > 0$), that defines the density spread around δ.
- δ is the location parameter ($-\infty < \delta < +\infty$).

Only Gaussian and Cauchy distributions exist for closed-form expressions in general SαS distributions. However, power series expansions can be obtained in some cases. Symmetric Alpha-Stable model is also called the S(α, δ, γ) model. The authors in [68] have studied a convenient mean for evaluating the parameters of Symmetric Alpha-Stable model. The mathematical and the proof of the expressions have been developed in [68]. For more information, readers can refer to it.

3.5.2.3 Markov Chain Models

3.5.2.3.1 Markov-Middleton Model

The Markov-Middleton model employs the Middleton PDF in equation (3.2) reduced to the first four terms to describe the amplitude of noise [69]. Using a Markov chain description, the history of past events is considered on the current event, and bursty pulses are modeled more accurate. The proposed Markov chain model is depicted in Fig. 3.11 (a). This model represents four states the first four terms of the Middleton Class-A model in equation

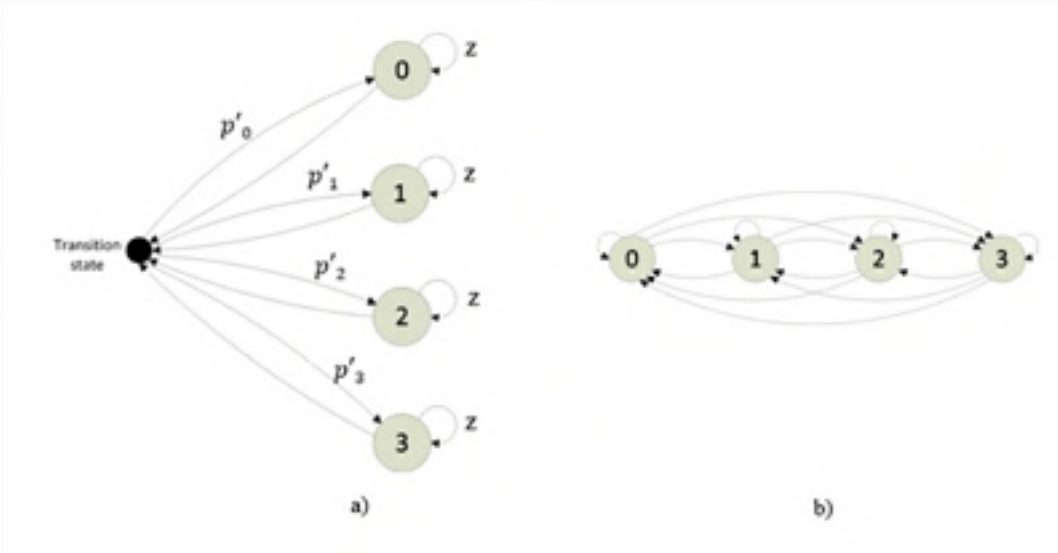

Figure 3.11: a) Markov-Middleton model. b) Equivalent representation of the Markov-Middleton model.

(3.2). Additionally, there is a transition state of duration null to connect the states. The probabilities p'_i describe the probability of arrival to the state i from the transition state. The value of x considers the correlation between the noisy samples and is independent of the canonical parameters of the Middleton model Γ, and σ^2. The equivalent representation of the model in Fig. 3.11 (a) is depicted at 3.11 (b).

The associated matrix $P = [p_{ij}]_{4\times 4}$ of transition probabilities is given by

$$P = \begin{bmatrix} z+(1-z)p'_0 & (1-z)p'_1 & (1-z)p'_2 & (1-z)p'_3 \\ (1-z)p'_0 & z+(1-z)p'_1 & (1-z)p'_2 & (1-z)p'_3 \\ (1-z)p'_0 & (1-z)p'_1 & z+(1-z)p'_2 & (1-z)p'_3 \\ (1-z)p'_0 & (1-z)p'_1 & (1-z)p'_2 & z+(1-z)p'_3 \end{bmatrix} \tag{3.8}$$

The parameters of this model are the same of the Middleton Class-A parameters A, γ, and σ^2 plus the correlation parameter z. Besides, the case $z = 0$ reduces the current model of the Middleton Class-A model. In this case, the transition probabilities $p_{ij} = p_j$ does not depend on the previous state, hence the states are independent and identically distributed and the model is identical to the Middleton Class-A model.

By means of this model, the total of samples $\bar{n}_i$ on each state (duration) is given by

$$\bar{n}_i = \frac{1}{1-P_{ii}} = \frac{1}{(1-z)(1-p'_i)}, \quad i = 0, 1, 2, 3. \tag{3.9}$$

3.5.2.3.2 Partitioned Markov Chain (PMC) Model

The Partitioned Markov Chain (PMC) model was introduced by Zimmerman [70]. It is a generalization of Bernouilli-Gaussian model. Zimmerman improves the Markov chain by

considering that impulsive noise is set up by M Gaussian noise sources and N impulsive noise sources. Each state of the PMC model generates its noise which duration relies on the probability to stay in the state. The transition from AWGN and impulsive states are made with the two transient states. They also organize the backward operation. However, the existing models for impulsive noise cannot reproduce the distributions of some of the substation impulsive noise characteristics performed through experiments.
In [59] the Author proposed a model utilizing a PMC to reproduce correlated samples which generates impulses with a damped oscillating waveform. The concept of this model is combining to each state a Gaussian distribution accurately parameterized, that produces a more authentic allocation of the samples, comprising the time correlation. The model consists of 19 states: one state describing the Gaussian noise and 18 states to illustrate the impulsive waveforms. The Markov chain is set up to reproduce correlated samples which can make accurate probability density functions of impulsive noise attributes which are closest to measurements. For the impulse generation, the oscillations are performed by employing four or even six states in each impulsive system (Fig. 3.12). This model is established on experience only and can be described as follows:

- The impulsive noise is considered as a transient process shifting from Gaussian noise to impulse state and ensure that the Gaussian variance is inferior to the variance of the impulse samples.
- Next, the pulses occur independently, which denotes that the appearance times are independent and identically distributed. Also, a damped oscillation waveform is produced by the correlated samples contained in an impulse.
- Finally, it is assumed that three types of impulses are formed that convene the long, the average, and the short pulses that are the large, the average and the small impulses regarding amplitude respectively [71].

3.5.2.4 Au Model

Au noise model is obtained from the physical aspect of the mechanism generating EMI in substations due to PD. Its model is considered as the first model that links the PD evolution and the induced far-field oscillation propagation [72]. To characterize the PD, they proposed a process in which main components are the impulse detection composed of a denoising process, a short-time analysis, peak detection, and statistical analysis. The first step is the conversion of the signal values from Volt to the electric field using the following relation

$$u_m(t) = V_m(t)\sqrt{\frac{Z_0 4\pi}{L_r G_{rf} \lambda^2}} \tag{3.10}$$

where L_r represents the load resistance, G_{rf} the RF system gain, while λ corresponds to the wideband antenna wavelength. After that, the denoising process consists of extracting the pulses from the noise. This operation is done using a wavelet transformation. The data

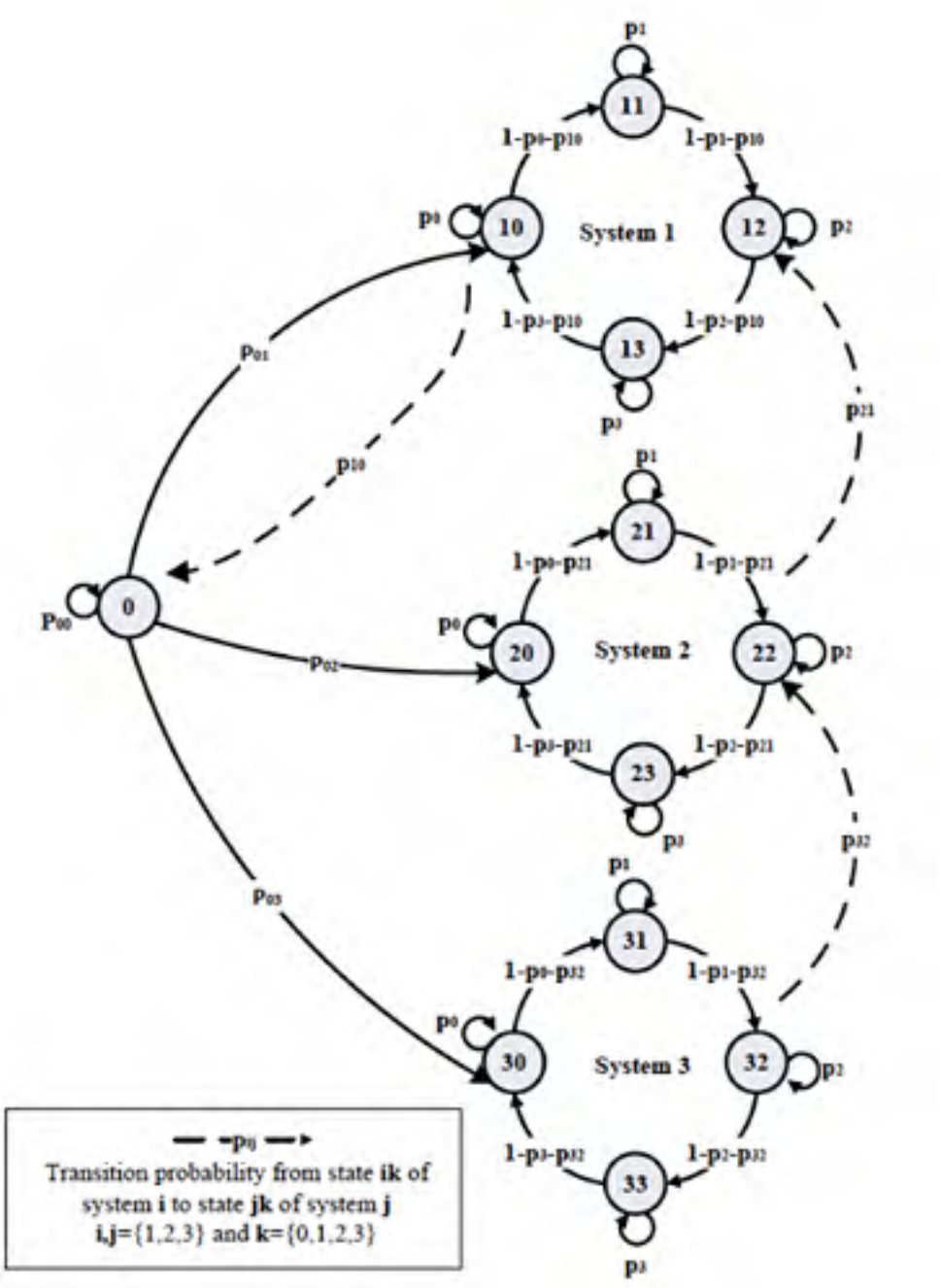

Figure 3.12: Partitioned Markov chain with 4 states for the impulse samples generation with an oscillating waveform [59].

obtained from measures are made up of a sequence of pulses located arbitrarily in time.

PDscan be identified by applying a temporal interpretation of the waveform spectrogram $U_m(l_x, f)$ given by

$$U_m(l_x, f) = \int_{\mathcal{R}} u_m(t)x(t - l_x)e^{-j2\pi ft}dt \tag{3.11}$$

where x_t is the window time and l_x is the length parameter.
This model also considers a Poisson spatial distribution of interference sources. A source represents a certain region where partial discharge may occur. At the receiver, the resulting waveform is a superposition of interferences created by each source. To represent the damped oscillations observed in measurements, a discrete time series model is proposed. The mathematical description of the model is detailed in [64], and it is summarized as follows. Let U_t denote the interference waveform generated by a single source at the t^{th} sample time. Since there is a correlation between successive noise samples, U_t depends on the previous samples U_{t-i} ,$i > 0$. It has been shown in [64] that using the two previous samples, gives transient impulsive waveform which is a good representation of the real measurements. Thus, U_t is represented by the following expression

$$U_t = \theta_1 U_{t-1} + \theta_2 U_{t-2} + \xi_t \tag{3.12}$$

The weights θ_1 and θ_1 are coefficients of a second order autoregressive process (AR). They represent the pulse amplitude decay over time. ξ_t is the disturbance term which is modeled as a heteroscedastic white noise process, i.e., the variance is not constant over time [73]. A single source can generate multiple pulses during the observation time. The total interference generated by this source is the superposition of all pulses. At t, the generated interference by this source is denoted by $I_{1,t}$, and can be written as a convolution product as follows

$$I_{1,t} = U_t * \sum\nolimits_{i=1}^{N_{imp}} d_i \delta(t - t_i) \tag{3.13}$$

where N_{imp} is the random number of discharge pulses following a Poisson distribution. The term d_i represents a random amplitude weighting factor and $\delta(t - t_i)$ is the Dirac function at t_i. If there are multiple sources at observation time, the total observed interference at the receiver, y_t, is the superposition of all of them

$$\mathrm{y}_t = \sum\nolimits_{k=1}^{Ns} I_{k,t} \tag{3.14}$$

3.5.2.5 Models Comparison

Statistical models of impulsive noise can be broadly divided into two groups: memoryless models (Middleton, Au, $\alpha - Stable$) and models with memory (Markov chains). Several experiments demonstrate that these models can reproduce electromagnetic interference in various impulsive noise environments. However, the challenge in the Markov chain remains on defining a suitable number of states and its procedure of estimation which is complicated. Thus, using models based on Markov chains can drastically increase computational complexity [74]. For this purpose, in our comparison, we only take into account memoryless models such as Middleton Class A, $\alpha - Stable$, and Au models.
The noise models are evaluated by using statistical methods such as

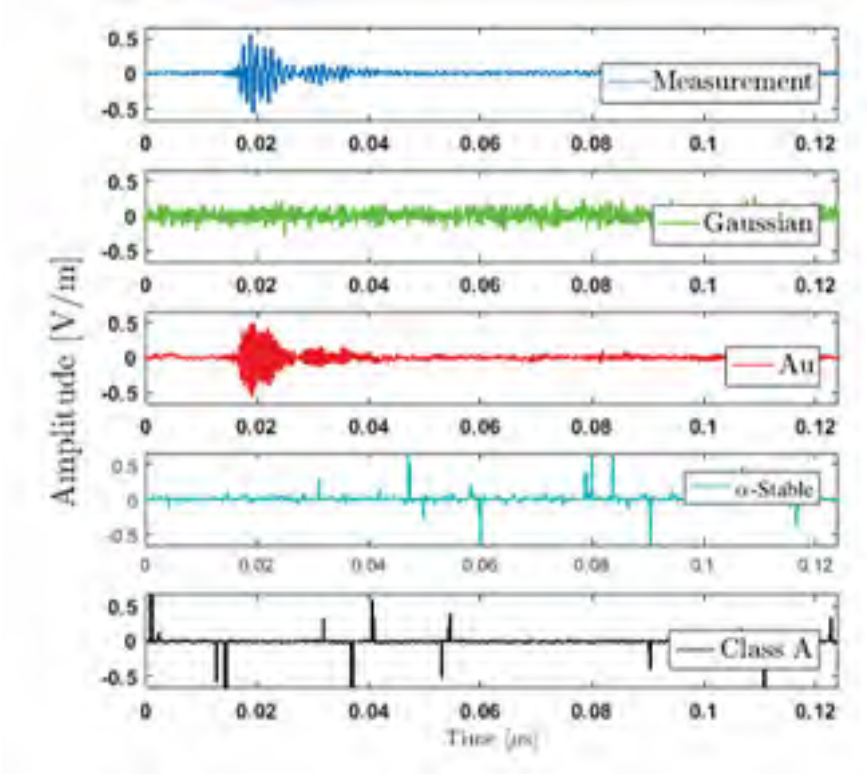

Figure 3.13: Gaussian and Impulsive noises compared to measurements.

Table 3.5: Measurement vs models.

Statistic Test	**Gaussian**	**Au**	$\alpha - Stable$	**Middleton Class A**
K-L	1.1800	0.025	0.07	0.5961

- Probability density function (PDF)

$$F_X(x) = P(X \leq x) \tag{3.15}$$

- Complementary cumulative distribution function (CCDF) defined as

$$\overline{F}_X(x) = P(X > x) = 1 - CDF(x) \tag{3.16}$$

  where CDF is the cumulative density function.

In order to have an objective test, Kullback-Liebler (K-L) divergence is used. This test measures the dissimilarity between two probabilities.

The PDFs and CCDFs of measurement, Gaussian, Au, $\alpha - Stable$, and Middleton Class A noise are shown in Figs. 3.14 and 3.15. The estimated parameters for Middleton Class A are $A_{est} = 0.0161$, and $\Gamma_{est} = 0.0015$. For $\alpha - Stable$, the characteristic exponent $\alpha =$

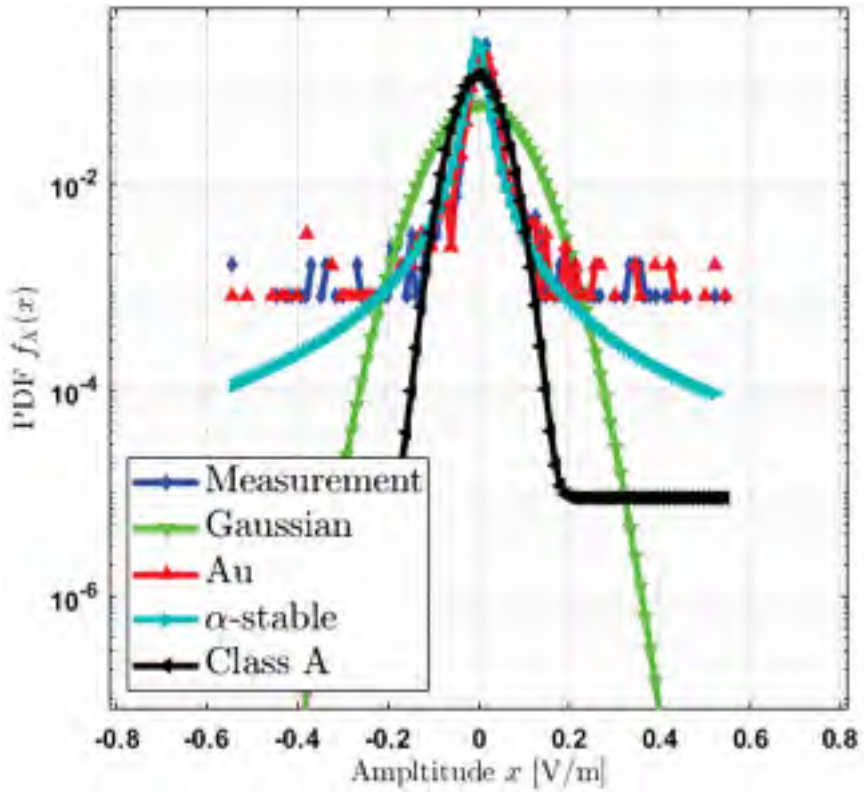

Figure 3.14: Probability density function (PDF) of noise models.

1.0901, the dispersion $\gamma = 0.0080$, and the location parameter $\delta = 0.0936$.
Presence of impulsive noise influences regarding amplitude distribution and density. By comparing the PDFs, Au model is more accurate than Middleton Class A and Gaussian models. Table 3.5 confirms these observations by presenting Kullback Liebler (K-L) divergences of the measured noise and the four models of noise (Gaussian, $\alpha - Stable$, Middleton Class A, and Au). So the K-L divergence of measured noise density is 0.025 from Au density, 1.1800 from the Gaussian density, 0.5961 from the Middleton Class A density, and 0.07 from the Symmetric Alpha-Stable density
We can note symmetry on probability densities, i.e., $f_X(x) = f_X(-x)$. The behaviors of the PDFs in the presence of impulsive noise are heavy-tailed, i.e., the tail is heavier compared to an exponential. The probability of getting substantial value is wide. It appears especially when amplitude distributions are asymptotically power laws. Besides, by comparing the CCDFs, the tail of the Au model gets closer to the measurement. One other point is that CCDFs decay slower than for the Gaussian case. Second order statistics are also used to evaluate the accuracy of the noise models:

- Level-crossing rate (LCR): how often the noise fades below a threshold
- Average duration of fades (ADF): the average interval of time the noise spends below this threshold.

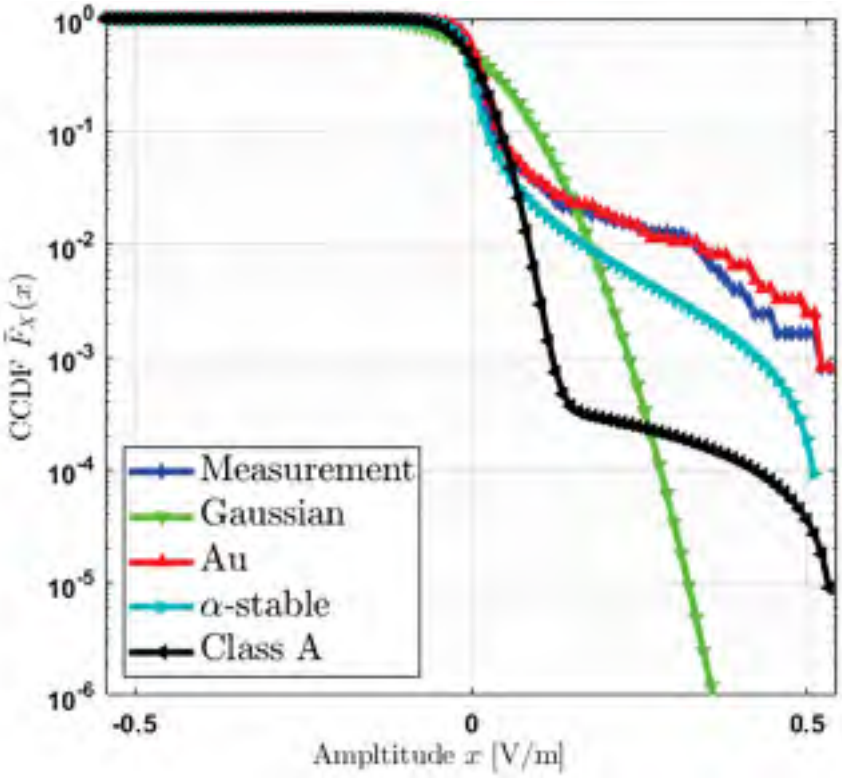

Figure 3.15: Tail distribution (CCDF) (b) of noise models.

Figs. 3.16 and 3.17 show the plot of the LCR envelope and the ADF as a function of the amplitude level r for the measurements. The obtained results were superimposed with those obtained using Gaussian, Au, $\alpha - Stable$, and Middleton Class A models. It can be easily seen that the Au model provides an excellent fit to the measurements. We can also note globally an amplitude offset between measurements, Middleton Class A, and $\alpha - Stable$ results. In Fig. 3.16, we observe an increase of the LCR with the rise in amplitude r until it reaches its maximum, and then decreases. At the maximum, the LCR is reduced when the system is exposed to a less severe fading channel (i.e., signal envelopes fluctuate less rapidly around their means). In Fig. 3.17, the average duration of fades of measured noise, Gaussian, Au, Middleton Class A, and $\alpha - Stable$ are represented. As expected, the ADF is an increasing function of r. This is because the signal is more likely to be below the target as the level target increases relative to the average.

3.5.3 Conclusion

In this section, we have studied the impulsive noise occurring in HV substations. The sources of this particular noise have been identified. After that, the methods of measuring the PD are described, and the existing models are presented. By using several statistical tests, we evaluated the four models. First, the results show that Middleton Class A and

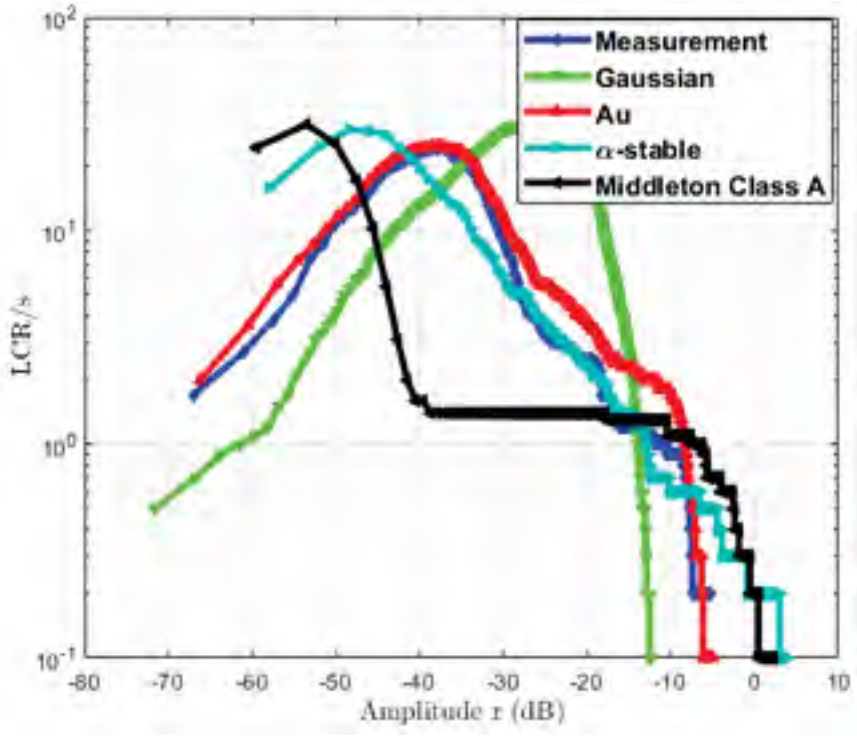

Figure 3.16: Level Crossing Rate (LCR) of noise models.

Symmetric $\alpha - Stable$ are not accurate for modeling partial discharges at 735 kV electricity substations. Au model is more accurate to model impulsive noise in HV substations. For this purpose, it will be used in the rest of this manuscript to model impulsive noise during performance evaluation.

3.6 Performance Analysis of ZigBee System in the Presence of Impulsive Noise

For the implementation of a physical layer, it is necessary to understand the operations of a radio communication system. This will improve performance through the associated signal processing techniques. As mentioned in the previous chapter, the original signal is processed separately by the different blocks of the communication chain to restore it as accurately as possible to the destination. However, at the communication channel level, harmful effects such as interference, multi-path, and impulsive noise are present and severely degrade the quality of the signal. For this purpose, it is essential to study the physical layer, see the influence of the parameters, and try to implement the appropriate techniques to have a good quality of transmission. In the literature review made in the previous section, we see

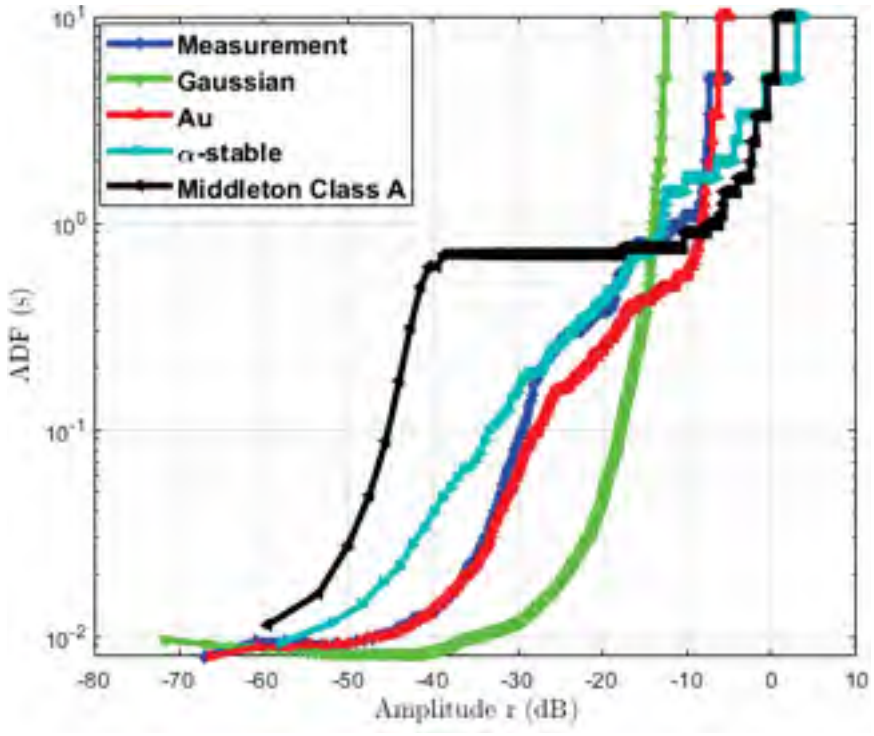

Figure 3.17: Average Duration of Fades (ADF) of noise models.

that ZigBee is an obvious candidate. For this purpose, we study this technology in the presence of Au impulsive noise.

3.6.1 ZigBee Narrowband System

3.6.1.1 System Model

The simulation diagram of ZigBee 2.4 GHz narrow-band system is depicted in Fig. 3.18 and the simulation settings are as follows: the binary source generates 50000 bits. Then, data are modulated using OQPSK with four symbols in which there are two bits per symbol. The modulated data (Tx_{Data}) pass through the channel (AWGN, Rayleigh or Rice). At the receiver side, the data denoted Rx_{Data} which is the sum of Tx_{Data} and Au impulsive noise are then demodulated. The Rayleigh and Rice channels used in our simulation are based on the Rayleigh and Rician multi-path fading channel simulators in Communications System Toolbox of Matlab. The simulation process is validated by comparing theoretical and simulated channels. To this end, BER vs. EbNo for AWGN, Rayleigh, and Rician channels are presented in Fig. 3.19. The agreement between simulated results and the theory is right. So, the simulation process is validated. The analytical aspects to produce the curves obtained for the theoretical results can be obtained by consulting [13], [16] or by using Bertool of Simulink in MatLab. However, from the considerable computation time,

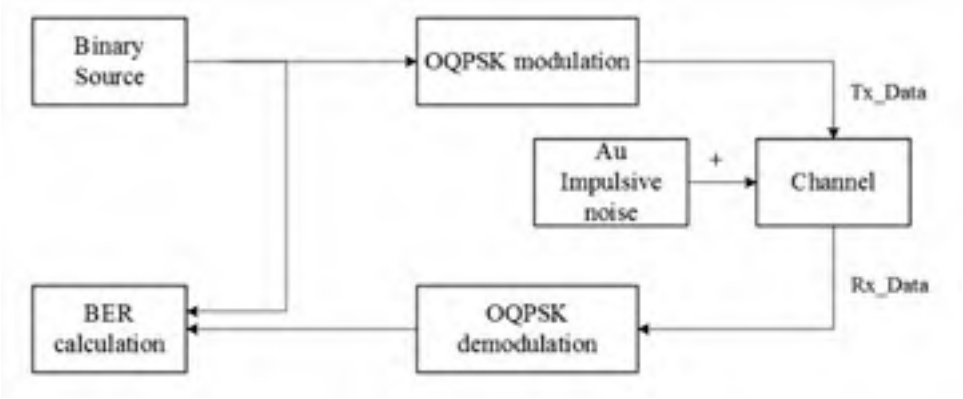

Figure 3.18: Diagram of ZigBee narrowband system simulation.

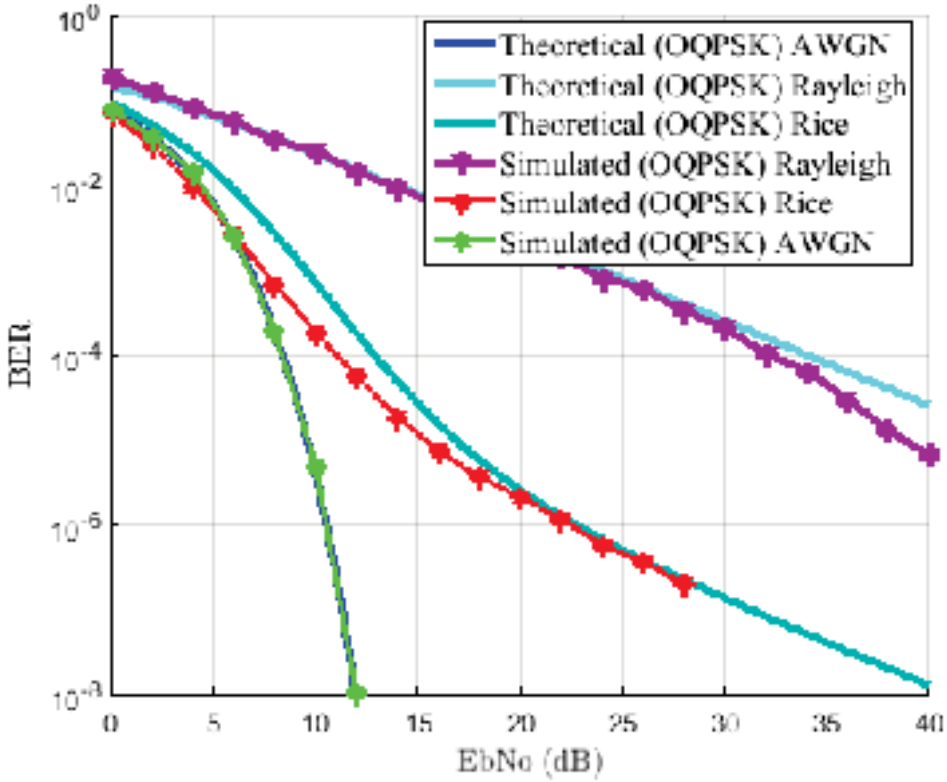

Figure 3.19: Validation of ZigBee (IEEE 802.15.4) physical layer simulation over AWGN, Rayleigh, and Rice channels.

we are afterward going to consider the theoretical result curves for comparing the results of simulation in the presence of impulsive noise.

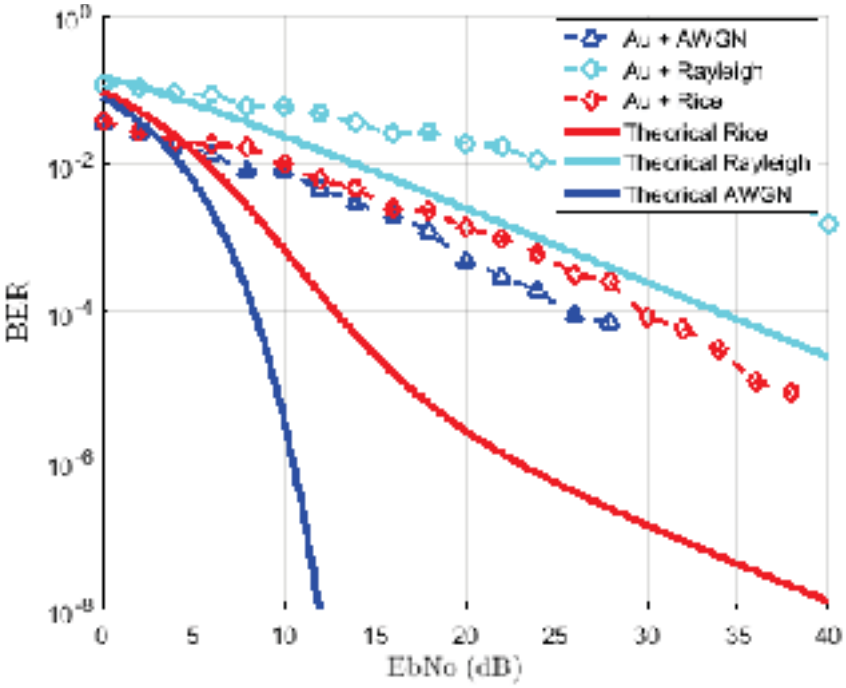

Figure 3.20: BER performance of Zigbee Narrowband in the presence of Au Impulsive noise in AWGN, Rayleigh, and Rician channels.

3.6.1.2 Performance Analysis

Fig. 3.20 shows results of ZigBee transceiver (IEEE 802.15.4 2.4 GHz) in a substation environment modeled using Au model. It compares the BER as a function of EbNo in three channels AWGN, Rayleigh, and Rice. In the presence of impulsive noise, we can note that the curves get closer to the theoretical Rayleigh curve. The interference generated by Au model is the sum of two components: impulsive and Gaussian. At low SNRs, we can notice that performance degradation is negligible and the curves fit approximately to the Gaussian one. It is because the impulsive noise power is smaller than standard Gaussian noise. On the contrary, at high SNRs, the performance degradation is more considerable. It is because the impulsive noise level is essential. This is due to the presence of more pulses in the signal. Indeed, for EbNo $>$ 10 dB, we note a significant degradation of the performance of the three channels. The BER target of 10^{-4} is achieved at EbNo of 20 dB for AWGN and 22 dB for the Rician channel. For the Rayleigh channel, we reach the target of more than 40 dB. It is evident from the results that the performance of ZigBee receiver is degraded by approximately 13 dB for target BER of 10^{-4} for AWGN channel, and 12 dB for the Rician channel.

3.6.2 ZigBee Wideband System

In the previous section, we performed simulations by considering only the modulation in the communication system. Indeed, we have seen that the performance are degraded. In this part, we now consider the spreading as defined in the protocol. We evaluate the three bands in the presence of Au impulsive noise.

3.6.2.1 System Model

3.6.2.1.1 Common specifications for 868/915 MHz and 2450 MHz PHY layers

The two frequency bands are different by their transmission parameters such as frequency bands, modulations, and pseudo-random sequence of a DSSS, etc. However, after analyzing specifications of each frequency band in [27], we find that common parameters of both 868/915 MHz and 2450 MHz PHY layers can be aggregated on the packet structure and the spread spectrum. A number of fields are packed to construct an IEEE 802.15.4 packet. Each field represents useful information for synchronization, error control and network signalization (packet type data or acknowledgment packet). Since the PHY layer is the last step before the radio front end, we need to present phy protocol data unit (PPDU) format, which contains the following fields depicted in Fig. 3.21.

- Preamble is a part of synchronization header (SHR) of a packet. Its length is 8 symbols (i.e., 4 bytes), and the bits in the preamble field shall be binary zeros.
- Start of Frame Delimiter (SFD) is a field indicating the end of SHR and the start of the packet data. SFD is formatted as illustrated in hexadecimal by $0 \times A7$.
- PHY header (PHR) is Frame Length Field which specifies the total number of bytes contained in the physical service data unit (PSDU), i.e., PHY payload. It is a value between 0 and 127 bytes.
- PSDU field carries the data of the PPDU with a maximum size of 127 bytes. It contains a number of fields such as:
  - Frame Control Field (FCF) that contains information defining the frame type, addressing fields, and other control flags.
  - Sequence Number Field specifies the sequence identifier for the frame. It specifies if the frame is a data, acknowledgment, or MAC command frame.
  - Address information can contain source/destination address and information for security protocols. The payload of a data frame shall contain the sequence of bytes that the next higher layer has requested the MAC PHY layer for transmission.
  - Frame Check Sequence (FCS) field contains a 16-bit cyclic redundancy check (CRC). FCS is computed from the MAC header and payload parts, i.e., from FCF to data payload passing through Sequence Number and Address information of the frame.

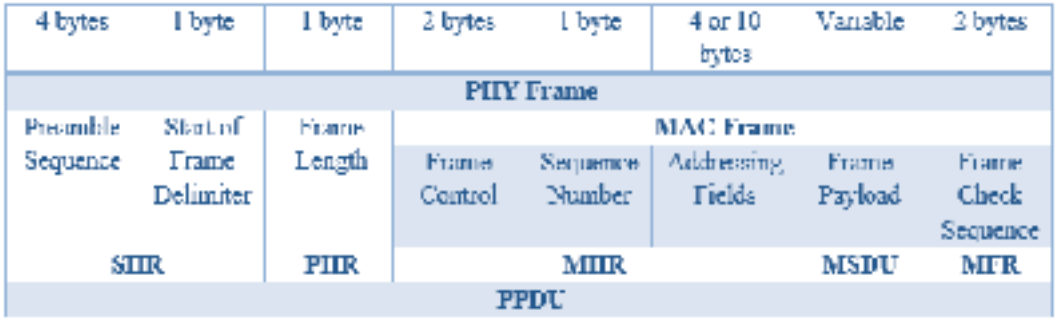

Figure 3.21: IEEE 802.15.4 packet structure and size [27].

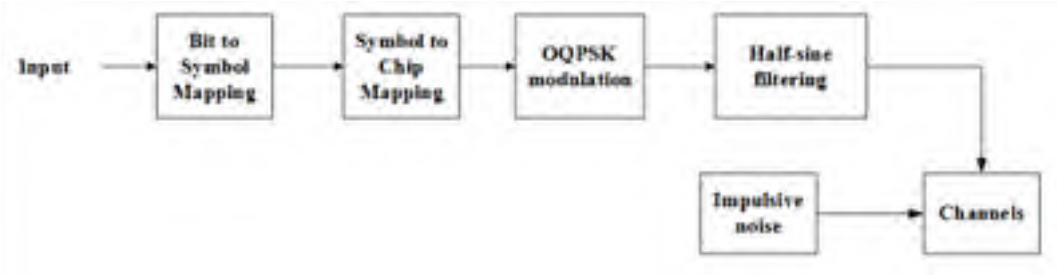

Figure 3.22: Diagram of OQPSK PHY simulation.

3.6.2.1.2 OQPSK 2450 MHz PHY

The 2.4 GHz ZigBee physical layer uses a 16-ary quasi-orthogonal modulation technique. The binary data are mapped into symbols (four bits per symbol).The data symbols obtained are also mapped into chips using 32 PN sequence as presented in Table 3.6 [27]. The chip sequences are modulated onto the carrier employing OQPSK with half-sine shaping as represented in equation 3.17.

$$f(t) = \begin{cases} sin(\pi \frac{t}{2T_c}), & 0 \leq t \leq 2T_c \\ 0, & otherwise \end{cases} \tag{3.17}$$

where T_c is the inverse of the chip rate.
Since each data symbol is expressed by a 32-chip sequence, the chip rate (2 Mchips/s) is 32 times the symbol rate. With this chip rate, the sampling frequency is about 2 MHz leading to a resolution of 500 ns. This spreading technique allows being robust face to interferers and jamming.

3.6.2.1.3 BPSK 865/915 MHz PHY

As for the frequency band of 2450 MHz, the name of these specifications is BPSK PHY since the signal is BPSK modulated. For the chip modulation, a direct sequence spread spectrum is used. Each input bit is mapped into 15-chip pseudo-noise (PN) sequence as described in Table 3.7 [27]. The data symbol are then assigned using a differential encoding.

Table 3.6: Symbol-to-chip mapping for the 2.4 GHz band.

Data symbols (dec)	**Chip values** $(c_0, c_1, \ldots, c_{31})$
0	1 1 0 1 1 0 0 1 1 1 0 0 0 0 1 1 0 1 0 1 0 0 1 0 0 0 1 0 1 1 1 0
1	1 1 1 0 1 1 0 1 1 0 0 1 1 1 0 0 0 0 1 1 0 1 0 1 0 0 1 0 0 0 1 0
2	0 0 1 0 1 1 1 0 1 1 0 1 1 0 0 1 1 1 0 0 0 0 1 1 0 1 0 1 0 0 1 0
3	0 0 1 0 0 0 1 0 1 1 1 0 1 1 0 1 1 0 0 1 1 1 0 0 0 0 1 1 0 1 0 1
4	0 1 0 1 0 0 1 0 0 0 1 0 1 1 1 0 1 1 0 1 1 0 0 1 1 1 0 0 0 0 1 1
5	0 0 1 1 0 1 0 1 0 0 1 0 0 0 1 0 1 1 1 0 1 1 0 1 1 0 0 1 1 1 0 0
6	1 1 0 0 0 0 1 1 0 1 0 1 0 0 1 0 0 0 1 0 1 1 1 0 1 1 0 1 1 0 0 1
7	1 0 0 1 1 1 0 0 0 0 1 1 0 1 0 1 0 0 1 0 0 0 1 0 1 1 1 0 1 1 0 1
8	1 0 0 0 1 1 0 0 1 0 0 1 0 1 1 0 0 0 0 0 0 1 1 1 0 1 1 1 1 0 1 1
9	1 0 1 1 1 0 0 0 1 1 0 0 1 0 0 1 0 1 1 0 0 0 0 0 0 1 1 1 0 1 1 1
10	0 1 1 1 1 0 1 1 1 0 0 0 1 1 0 0 1 0 0 1 0 1 1 0 0 0 0 0 0 1 1 1
11	0 1 1 1 0 1 1 1 1 0 1 1 1 0 0 0 1 1 0 0 1 0 0 1 0 1 1 0 0 0 0 0
12	0 0 0 0 0 1 1 1 0 1 1 1 1 0 1 1 1 0 0 0 1 1 0 0 1 0 0 1 0 1 1 0
13	0 1 1 0 0 0 0 0 0 1 1 1 0 1 1 1 1 0 1 1 1 0 0 0 1 1 0 0 1 0 0 1
14	1 0 0 1 0 1 1 0 0 0 0 0 0 1 1 1 0 1 1 1 1 0 1 1 1 0 0 0 1 1 0 0
15	1 1 0 0 1 0 0 1 0 1 1 0 0 0 0 0 0 1 1 1 0 1 1 1 1 0 1 1 1 0 0 0

Table 3.7: Symbol-to-chip mapping for the 865/915 MHz band.

Input bits	**Chip values** $(c_0, c_1, \ldots, c_{14})$
1	1 1 1 1 0 1 0 1 1 0 0 1 0 0 0
2	0 0 0 0 1 0 1 0 0 1 1 0 1 1 1

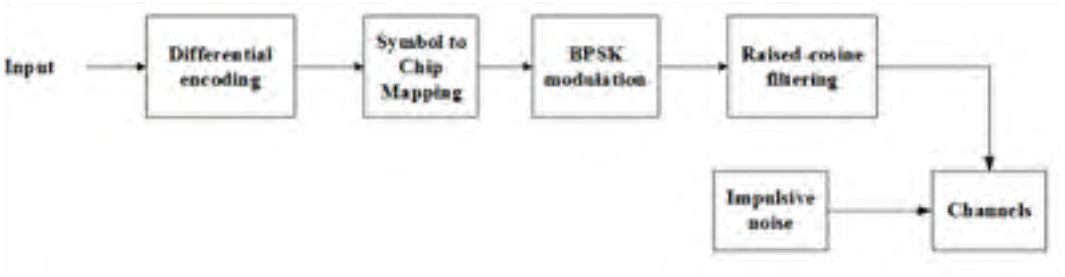

Figure 3.23: Diagram of BPSK PHY simulation.

It performs an or exclusive or addition modulo 2 of a raw data bit with its prior encoded bit. A raised-cosine pulse shape filter with a roll-off factor equal to 1 is used. It is represented by equation 3.18.

$$f(t) = \frac{sin(\pi t/T_c)}{\pi t/T_c} \frac{cos(\pi t/T_c)}{1-(4t^2/T_c^2)} \tag{3.18}$$

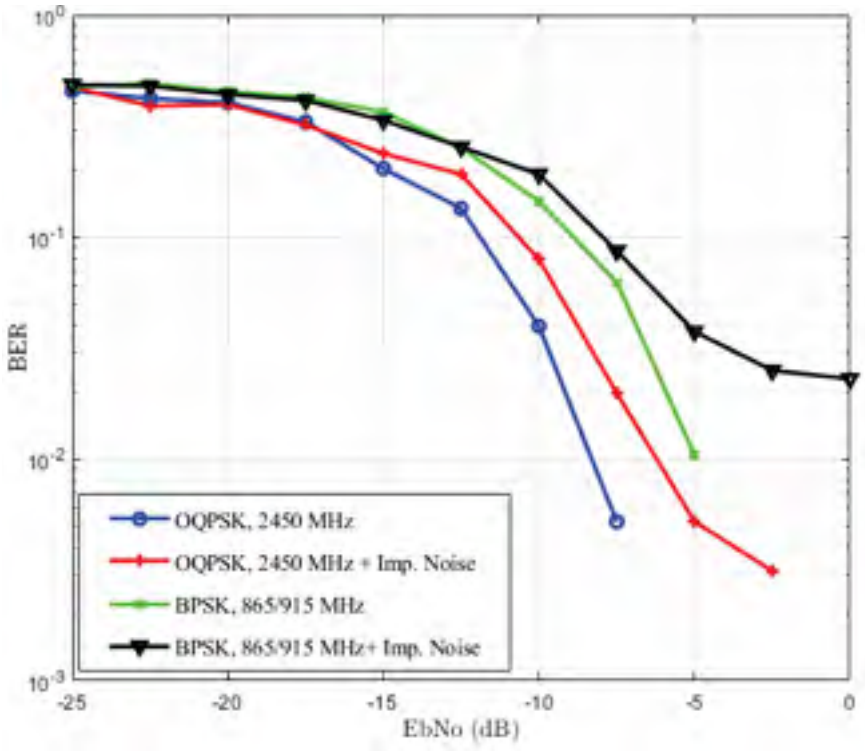

Figure 3.24: Performance of ZigBee in AWGN channel impaired by impulsive noise.

3.6.2.2 Performance Analysis

Considering the simulation diagrams depicted in Figs. 3.22 and 3.23, we evaluate the BER as a function of EbNo for the three bands in AWGN and Rayleigh's channel impaired by Au impulsive noise. The results are depicted in Figs. 3.24 and 3.24, respectively. As can be seen in these figures, the performance are improved compared to the narrowband system. We note a gain of approximately 14 dB in AWGN channel and 8 dB for Rayleigh channel. For the BPSK PHY, the degradation is also noticeable in both AWGN and Rayleigh channel. Despite these gains, the performance are not globally satisfactory since they do not allow us to meet the requirements in HV substations.

3.7 Conclusion

In this chapter, different technologies for wireless sensor networks have been presented. The substation environment and impulsive noise sources are also studied. The methods for measuring and representing the partial discharges occurring in the substations have also been introduced. We have also examined the impact of impulsive noise on a ZigBee narrowband receiver for AWGN, Rayleigh, and Rician channels. The results showed that the impulsive noise influence is close to a Gaussian noise or a Rayleigh noise according to the SNR. After that, the spreading as defined by the protocol is implemented. We

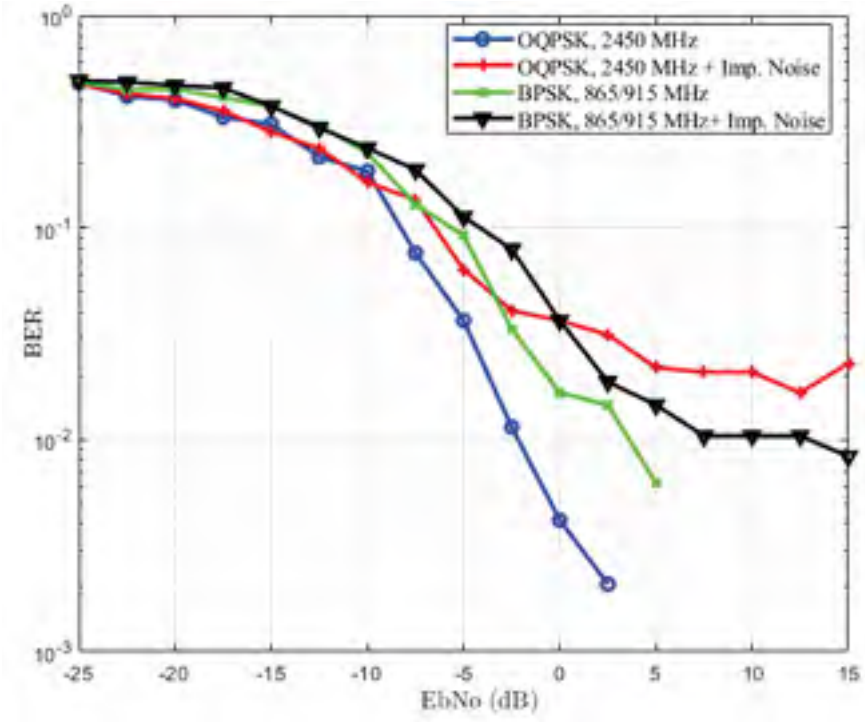

Figure 3.25: Performance of ZigBee in Rayleigh channel impaired by impulsive noise.

evaluate the performance of the three bands, i.e., the OQPSK PHY and BPSK PHY in AWGN and Rayleigh's channels impaired by Au impulsive noise. The results show that the performance are improved compared to the narrowband system. However, the obtained results are not satisfactory and do not allow us to meet the requirements for the deployment of SG applications in HV substations. Then, when considering a fading environment as the substation, the entire multi-path cannot be exploited by ZigBee due to the constraints of the distance (200 m). Indeed, several SG applications require a high data rate and a broad bandwidth. Standard wireless communication protocols as ZigBee cannot answer those needs. For this purpose, a reliable and efficient physical layer needs to be proposed leading to significant improvements. Next chapter will discuss solutions for mitigating the impulsive noise in power grid environment.

Chapter 4

Impulsive noise mitigation with coded-OFDM system

Contents

4.1 Introduction

Wireless communication systems continue to draw a symbolic role in the modernization grid. The deployment of WSNs in HV substations is becoming essential for the development of a smart electrical network. WSNs have several characteristics that make them an interesting solution for a harsh environment such as a power station. Such systems are used to increase communications in the electric power system for improving reliability and efficiency. Sensors are installed in substations for monitoring, diagnostics, and maintenance of the system. Because of their ease of deployment, cost saving, and flexibility, wireless systems are potential candidates compared to wireline deployments [75]. However, the wireless communication channel is dynamic and unpredictable. The behavior of radio waves is affected by phenomena such as interference or jamming, reflection, and diffraction. Besides, the deployment of WSNs in substations necessitates considering their specificities: metallic structures and devices may produce a specific and robust radio noise which is impulsive.

In HV environments, the ambient or thermal noise commonly considered as Gaussian noise are insufficient; the impulsive noise needs to be taken into account. Because of transient processes, electronic switching, and PD, the noise environment may be highly impulsive [76], [25]. Impulsive noises are characterized by short duration, and their interference levels are vast [67]. The performance and the efficiency of a wireless system can be degraded due to the impulsiveness of the interference. To enable smart grid applications, the design of a robust wireless communication system is growing in interest. Several types of research have been done in this domain. Recent publications show that impulsive noise appearing in electricity substations can degrade the performance of ZigBee systems [77-80]. In Bhatti's work, an impulsive noise model based on the Symmetric Alpha-Stable distribution was proposed to evaluate the performance of ZigBee. It also compared WLAN technology and ZigBee systems. Simulation results showed that the degradation performance of WLAN is more severe compared to the Gaussian noise environment whereas, for ZigBee systems, the degradation is modest [77], [78]. Ali presented several results in [79]. He showed that the performance of the communication system is degraded when the receiver is altered by impulsive noise. In our previous chapter, we studied the impact of impulsive noise on a ZigBee receiver for AWGN, Rayleigh, and Rician channels. The results showed that the impulsive noise influence is close to a Gaussian noise or a Rayleigh noise according to the SNR. Also, many smart grid applications require a high data rate and a broad bandwidth. In [81], the authors addressed the feasibility of wireless technologies deployment in power stations. Their analysis underlined that some requirements such as the interoperability and the bandwidth are inadequate. For solving the problems linked to wireless sensor protocols proposed in the literature and to enable smart grid applications, we propose a joint solution by combining forward error correction codes (FEC codes) and OFDM. OFDM is a well-known technique employed in wireless communications. It has several advantages over single carrier systems. OFDM's main advantage is its resistance to frequency selectivity. Moreover, coded OFDM allows the exploitation of frequency diversity and provides a total resistance to impulse noise and fast fades. Reed-Solomon (RS)

code, CC scheme, Turbo code, and Low Density Parity Check codes (LDPC) are common FEC codes associated with the coded OFDM systems [82].
This chapter aims to provide a proposal for a physical layer suitable for electricity substations to enable SG operations. The rest of this chapter is organized as follows. Section 2 reviews the impulsive noise reduction techniques, while section 3 concerns its synthesis. The method that we propose for impulsive noise cancellation is presented in section 4. Section 5 is about the implementation of the coded-OFDM system in GNU Radio. The comparison between simulation and measurements is provided in section 6. A conclusion is made in section 7.

4.2 Impulsive Noise Reduction Approaches

In this section, we describe a brief literature review of the impulsive noise mitigation techniques. Indeed, for the impulsive noise cancellation, several approaches have been developed. They can be divided into three categories. The first solution is the FEC schemes which consist of adapting the conventional channel coding to the impulsive environment. The second category concerns the modulation schemes, particularly Multi-Carrier Modulation (MCM) schemes. The last family of impulsive noise cancellation strategies consists of signal processing solutions.

4.2.1 Modulations Schemes for Impulsive Noise Systems

4.2.1.1 Single-Carrier Modulation

In order to transport information from one point to another in single carrier modulation, a high frequency sinusoidal carrier wave is used. This wave is characterized by its amplitude A, its pulsation ω_0 with ($\omega_0 = 2\pi f_0$) and its instantaneous phase $\omega_0 t + j_0$. By varying one of its three parameters as a function of the amplitude variations of the signal to be transmitted, also called "modulating signal", an amplitude, frequency or phase modulation is carried out. In digital, it is possible to realize three categories of modulation: amplitude shift keying (ASK), frequency shift keying (FSK), and phase shift keying (PSK).
In ASK, the message signal modulates the amplitude of the carrier signal without altering its phase and frequency. In PSK, at each of the binary states of the modulating signal, a phase state of the carrier is associated. PSKs considered as very robust modulations are used in the case of very disturbed transmission channels, or in systems introducing amplitude distortions. Mainly employed are Binary Phase Shift Keying (BPSK) and Quaternary Phase Shift Keying (QPSK). QAM (Quadrature Amplitude Modulation) is a mixed modulation: for each group of k bits (binary symbol) of the modulating binary signal, a state of phase and amplitude of the carrier is associated. QAM is the sum of two amplitude-modulated quadrature RF carriers represented by a two-axis state constellation in quadrature.
Due to their implementation simplicity, single -carrier modulation seems to be interesting candidates for systems affected by impulsive noise. For narrowband systems, single-carrier

modulation is an appropriate alternative and has been assumed in various practical applications [83], [84]. However, for broadband system, these strategies have been discovered to be inadequate for high-speed communications for these kinds of channels [85]. This is due to different aspects linked to the transmission attributes. The multi-path effects are the first causes, which introduce inter-symbol interference (ISI) and create wide alterations in the frequency domain illustrating frequency-selective fading. When this random frequency-selective fading is present, the reliability of a single-carrier modulation can be degraded [85]. To improve the performance and reduce the influence of ISI, some techniques such as detection and equalization can be applied, which introduce the complexity contrary to the feature associated with single-carrier schemes. Secondly, for high-data rate communications, widebands cannot be supposed to be enough flat since the channel attenuation mostly augments with frequency. Finally, in a perturbed environment, broadband approaches require to acquire high spectral efficiency. Unfortunately, primary single-carrier modulation approaches can just accomplish a spectral efficiency limited to 1 bps/Hz [86].

4.2.1.2 Spread Spectrum Techniques

Spread spectrum techniques (SS) have been used for many years, particularly in radiocommunications and the military, for its reliability and confidentiality. For such purposes, the concern in SS is because of its capability to resist to frequency-selective fading established by the multi-path phenomenon as well as its efficiency against several types of narrowband interference [85], [86]. In SS, before modulating the signal carrier, the symbols are multiplied by a determined spreading sequence, consisting of binary elements called chips of duration T. As a result of this spreading operation, the transmitted signal is a broadband signal having the characteristics of a pseudo-random noise whose power spectral density is invariant in the signal band. These features are achieved thanks to an appropriate choice of the spreading sequence that is is best qualified as pseudo random since it is deterministic but appears random to an unknowing observer. Indeed, a spreading sequence adapted to SS must have a proper correlation function, as close as possible to a Dirac pulse. There are different variants of SS including time-hopping, frequency hopping, hybrid approaches, and direct-sequence spread spectrum (DSSS). The media access in SS can be completed by code division multiple access technique (CDMA) [86]. A principal aspect of SS that allows it to reduce narrowband interference, is the substantial bandwidth. For a disposed transmission bandwidth, the elevated redundancy required for SS includes meaningful restraint the data rate through the transmission channel. Spectral efficiency in a wideband system can be accomplished by using multi-carrier modulation approaches such as orthogonal frequency division multiplexing (OFDM) which will be reviewed in the following section.

is best qualified as pseudo random since it is deterministic but appears random to an unknowing observer

4.2.1.3 Orthogonal Frequency Division Multiplexing

As seen before, in single-carrier modulation techniques such as ASK, PSK, and FSK, the input signal is mapped over a single carrier. However, Orthogonal Frequency Division Multiplexing (OFDM) is a combined approach consisting of modulation and multiplexing. In this technique, the bandwidth is divided into separate modulated data. It is a multi-carrier modulation procedure in which multiple carriers are utilized, to transmit the information from the source to the destination. Each sub-carrier may use one of the different digital modulation techniques. OFDM is a very efficient technique for communication over frequency selective fading channels. At the receiver side, it is very complicated to control frequency selective fading, in which, the model is hugely involved. Rather than trying to diminish frequency selective fading as an entirety (which appears if a large bandwidth is assigned for the data transmission over a frequency selective fading channel), OFDM moderates the problem by transposing the whole fading channel into limited flat fading channels. Contrary to frequency selective fading, flat fading is not difficult to cancel by utilizing error correction and equalization methods. Commonly, an OFDM signal can be denoted as

$$c(t) = \sum_{n=0}^{N-1} s_n(t) sin(2\pi f_n t) \tag{4.1}$$

Here, $s(t)$ represents the mapped symbols regarding the modulation (BPSK/QPSK/QAM) and f_n represents the orthogonal frequencies. This representation can be considered as an IFFT (Inverse Fast Fourier Transform) process. The Fourier transform parallels a signal into several frequency intervals by mapping the signal with a set of sinusoids. It is the translation of the signal from the time domain to the frequency domain. However, an IFFT is always seen as a transformation from the frequency domain to the time domain. FFT is expressed by

$$X(k) = \sum_{n=0}^{N-1} x(n) sin(\frac{2\pi kn}{N}) + j \sum_{n=0}^{N-1} x(n) cos(\frac{2\pi kn}{N}) \tag{4.2}$$

whereas its dual, IFFT is represented by

$$x(n) = \sum_{n=0}^{N-1} X(k) sin(\frac{2\pi kn}{N}) - j \sum_{n=0}^{N-1} X(k) cos(\frac{2\pi kn}{N}) \tag{4.3}$$

The equations for IFFT and FFT differ by the sign minus and the coefficients they take. Both equations do the same thing. They spread the incoming signal with a set of sinusoids and divide them into bins. Indeed, FFT and IFFT are dual operations and operate in the same way. IFFT and FFT operations are commutable. The complete structure of a simple OFDM system with the transmitter and receiver is depicted in Fig. 4.1.

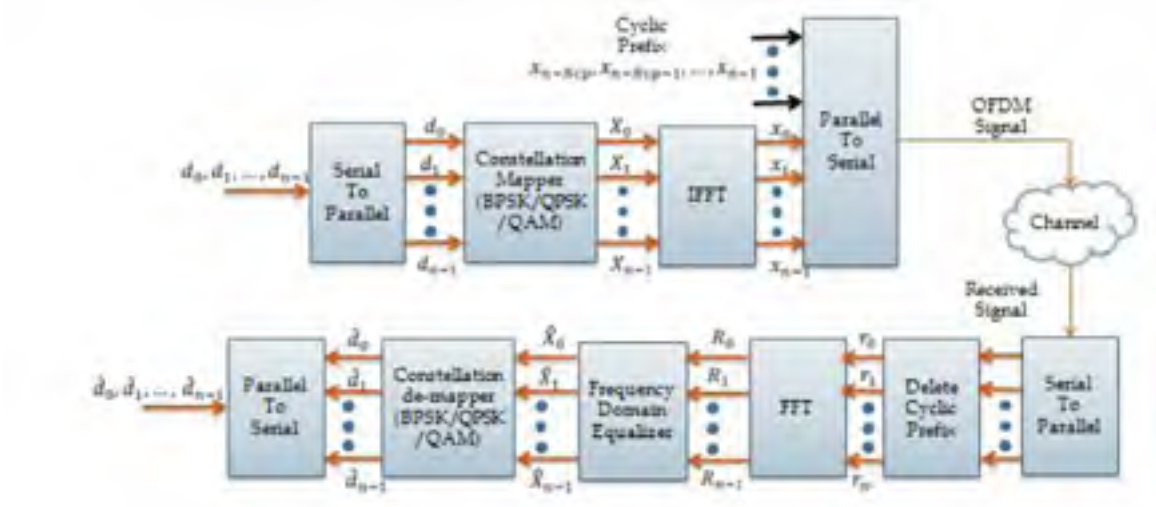

Figure 4.1: Architecture of a primary OFDM system [87].

4.2.2 Signal Processing Strategies

Several signal processing methods have been evolved in the literature to cope with the harmful effects of impulse noise on communications. They can be mainly separated into three categories: the time-based approaches [88-92] that act on the received signal envelope which has been polluted by impulses, the frequency-based methods [93] where the impulsive noise is seen and processed in the frequency domain, and finally both the time and frequency-based techniques [94] that combine the two previous methods. Although many solutions have been proposed, only a few are of reasonable complexity.

4.2.2.1 Time-Domain Methods

Non-linearity techniques such as clipping and blanking methods have been widely used for impulsive noise reduction because of their implementation simplicity. Their performance have been investigated in [95, 96].
The influence of impulsive noise in multi-carrier signals can be decreased by pre-processing time-domain signal at the front end of the receiver employing a memoryless non-linearity [97 - 99]. Because of their simplicity, nonlinear methods comprising blanking, blanking, and clipping/blanking are often employed in functional purposes [97], [98]. In this kind of technique, it is assumed that the amplitudes of the impulsive samples are generally much larger than the signal amplitudes [100]. Consequently, a threshold is expressed and the signal samples that have amplitudes wider than the threshold are supposed to be altered by impulsive noise and thus adapted following the used non-linearity. The three non-linearity methods are represented by the following:

1. Clipping: the signal amplitudes whose absolute value is larger than a given threshold γ_c are replaced by the threshold value.

$$y_i = \begin{cases} r_i, & if \quad |r_i| \leq \gamma_{cl} \\ \gamma_{cl} e^{jarg(ri)}, & otherwise \end{cases} \qquad i = 0, 1, \ldots, N-1 \tag{4.4}$$

   such as γ_{cl} is the threshold of clipping.

2. Blanking: the signal amplitudes whose absolute value is larger than a given threshold γ_{bl} are erased, i.e., replaced by zero.

$$y_i = \begin{cases} r_i, & if \quad |r_i| \leq \gamma_{bl} \\ 0, & otherwise \end{cases} \qquad i = 0, 1, \ldots, N-1 \tag{4.5}$$

   such as γ_{bl} corresponds to the blanking threshold.

3. Clipping/Blanking: very large amplitudes are erased while average amplitudes are clipped. Two thresholds values γ_{bl} and γ_{cl} are needed.

$$y_i = \begin{cases} r_i, & if \quad |r_i| \leq \gamma_{cl} \\ \gamma_{cl} e^{jarg(ri)}, & if \quad \gamma_{cl} < |r_i| \leq \gamma_{bl} \\ 0, & otherwise \end{cases} \qquad i = 0, 1, \ldots, N-1 \tag{4.6}$$

4.2.2.2 Frequency-Domain Methods

Frequency domain approaches are also a different method to reduce the effect of impulsive noise [101], [100], [102]. Contrary to the first approach, these methods are used at the OFDM receiver after the signal demodulation. The most widely used is the Zhidkov algorithm [101]. He introduced a frequency-domain technique to cancel impulsive noise after demodulating and equalizing the received signal derived on initial evaluation of the emitted signal which are employed to evaluate the noise in the received signal. If an OFDM signal S_k is sent through a channel which is altered by impulsive noise, the received signal that is achieved after equalizing the channel and DFT can be expressed by the succeeding relation

$$R_i^{(eq)} = R_i \hat{H}_i^{-1} = S_i + W_i \hat{H}_i^{-1} + U_i \hat{H}_i^{-1}, i = 0, 1, \ldots, N-1 \tag{4.7}$$

such as H is the transfer function of the channel, I and W are the impulsive noise and discrete Fourier transform forms of the additive noise, respectively. Depending on the algorithm in [101], if an evaluated of the emitted signal s_i is obtainable, subsequently the whole noise expression can be evaluated utilizing equation (4.7). Consequently, the received and equalized signal $R_i^{(eq)}$ is unmapped in conformity with the employed constellation after substituting any sub-carrier pilot with its associated value. Silent sub-carriers should be null. This determines an estimate $\hat{s}_i$ and its discrete Fourier transform $\hat{S}_i$ of the transmitted signal s_i. Applying this value of $\hat{S}_i$, the total noise expression $D_i = W_i + C_i$ can be evaluated depending to the equation below

$$\hat{D}_i = \hat{H}_i (R_i^{(eq)} - \hat{S}_i), i = 0, 1, \ldots, N-1 \tag{4.8}$$

D_i which corresponds to the total noise expression is translated into the time domain using the inverse DFT and a peak detector is employed to acquire the approximated impulsive noise component $\hat{c}_i$. Finally, the DFT of $\hat{c}_i$ is estimated and separated by the channel transfer function. Succeeding the impulsive noise decrease, obtained signal depends on the equation below

$$R_i^{(comp)} = R_i^{(eq)} - \hat{U}_i \hat{H}_i^{-1}, i = 0, 1, \ldots, N-1 \tag{4.9}$$

4.2.3 Error Correcting Codes

Forward error correction (FEC) mechanisms are of utter importance for reliable transmission over noisy channels. The two different kinds of codes commonly used today are block codes and convolutional codes. The block codes [103] constitute the historical FEC codes family. The encoder divides the information bits into groups of k bits and adds r redundant parity bits to each group. The second FEC family is composed of the well-known convolutional codes [103]. Unlike block encoding in which the data stream is processed in blocks independent of each other, a convolutional encoder continuously processes the information.

4.2.3.1 Convolutional Codes

Convolutional codes (CC) also called convolution codes were invented in 1954 by Elias [104]. The principle of convolution codes is to consider the message to be transmitted as a semi-infinite sequence of symbols. Convolutional encoding of data is achieved using a shift register and linked to the combinatorial logic which completes modulo-two addition. The combinatorial logic is often in the cascaded or-exclusive gates form.
Referred to as trellis codes, the CC present the twofold advantage to be very simple to implement thanks to shift registers. The encoder for a convolutional code adopts k bit blocks of the information sequence and generates an encoded sequence of $n - bits$ blocks. The encoding procedure is given as follows [104]. At each time index k, the coder outputs the sequence of N_C binary symbols $s_k = (s_{k,1}, s_{k,2}, \ldots, s_{k,N_C})$ depending on the input sequence i_k =$(i_{k,1}, i_{k,2}, \ldots, i_{k,K})$ and of the m preceding sequences $i_{(k-1)}, \ldots, d_{(k-m)}$. The coder therefore introduces a memory effect of order m.
The constraint length is defined as $u = m + 1$ and the coding rate is given by $R = \frac{K}{N_C}$. The coding is said to be systematic when the K information bits explicitly issued in the codeword s_k as follows

$$s_k = (i_{k,1}, i_{k,2}, \ldots, i_{k,K}, i_{k,K+1}, \ldots, s_{k,N_C}) \tag{4.10}$$

otherwise, the code is non-systematic. The code sequence is obtained by

$$s_{k,i} = \sum_{l=1}^{K} \sum_{j=0}^{m} g_{(l,j)}^{i} i_{k-j,l} \tag{4.11}$$

where $g^{i}_{(l,j)}$ are binary coefficients, and where the addition and the multiplication are defined modulo 2. Convolutional codes can be divided into two families: Recursive Systematic Convolutional (RSC) codes and the Non-Systematic Convolutional (NSC) codes which are also non-recursive [105]. An RSC can simply be derived from NSC by using a feedback loop to form the redundancy.
Several algorithms exist to decode convolutional codes: trellis decoders, sequential (Fano) decoders, stack decoders. Nevertheless, two algorithms are usually employed for the decoding of convolutional codes. The first one denoted the Viterbi algorithm [106-107], relies on the trellis code representation. Its principle is to find form in the noisy sequence of symbols received, the initial state of the encoder, the transitions permitted the most likely state sequences in the trellis. While the second decoding scheme, referred to as the BCJR (from the names of its inventors) or equivalently the maximum a posteriori (MAP) algorithm [108], operates the error probability minimization over the information block sequence.

4.2.3.2 Reed-Solomon

Reed-Solomon (RS) codes are a special case of BCH (Bose, Ray-Chaudhuri, Hocquenghem) codes. These are codes defined on a large alphabet over a non-binary finite field F_q, and which are of length $n \leq q$. RS codes are a subset of block error correction codes employed for a diversity of applications. They are employed to reduce the effect of errors occurring in many systems including mobile or wireless, satellite communications, digital television/DVB, etc. RS encoder considers a set of digital data and includes additional"redundant" bits. The RS decoder treats each block and essays to tackle errors and restore the authentic data. The characteristics of RS code determine the number and the types of errors that can be rectified. They are constituted of $x - bit$ sequences, where x is a positive integer with a value wider than 2. RS (n, k) codes occur for all n and k for which

$$1 \leq k \leq n \leq 2^x + 2 \tag{4.12}$$

where n corresponds to the total number of code symbols in the encoded block and k is the amount of data symbols being encoded. In the most common RS (n, k) code,

$$(n, k) = (2^x - 1, 2^x - 1 - 2t) \tag{4.13}$$

such as $2t = n - k$ corresponds to the parity symbols number and t is the capacity of correction of the code.
The minimum distance code in Reed Solomon codes is defined by

$$d_x = n - k - 1 \tag{4.14}$$

The code is able to correct up to

$$t = \lfloor \frac{d_x - 1}{2} \rfloor = \lfloor \frac{n - k}{2} \rfloor \tag{4.15}$$

where $\lfloor j \rfloor$ corresponds to the largest integer not to surpass j. Reed Solomon codes are specially effective for correcting burst-error [109]; that is, they are suitable for channels with memories.

4.2.3.3 Low-Density Parity Check Codes

Low-density-Parity Check (LDPC) was proposed by Gallager in 1962 [110]. However, due to its complexity of the decoding algorithm, regarding implementation, LDPC was forgotten for a long time. In 1997, MacKay and Neal [111] first showed that LDPC could also exhibit BERs that are very close to the Shannon limit over Gaussian channels when applying iterative decoding. Because of their exceptional performances that are comparable to those obtained with the turbo codes, LDPC is now utilized by some standards such as the DVB-S2 and the 10-Gigabit Ethernet. LDPC is defined as a class of block codes having the particularity to be sparse, i.e., the corresponding parity-check matrix only shows a minimal number of non-zero entries compared to the matrix size. For such reason, the matrix is said to have a low density. The weight of a row or a column is specified as the total number of one within the row or the column. Low-density parity check codes can be split into two families: the regular and the irregular LDPC. LDPC code is said to be regular when every column has the same weight wc, and every row has the same weight w_r [112]. When this condition is not verified, the LDPC code is irregular. The Tanner graph [113] is widely used to represent the LDPC parity-check matrix.

4.2.3.4 Polar Codes

Recently developed by E. Arikan [114], Polar coding is a method of error correction based on channel polarization, to design code sequences achieving the symmetric capacity $I(W)$ of binary input channels.

Definition 1 *Channel polarization method is constructed by channel combining and channel splitting.*

- *The channel combining is a recursive approach based on the combination of* $C = 2^c$ *copies of independent channels* W *with*

$$W_C : \mathcal{X}^{\mathcal{C}} \rightarrow \mathcal{Y}^{\mathcal{C}} \tag{4.16}$$

- *After that, the final step is to split* W_C *back into a set of* C *binary input channels as* $W_C^{(i)} : \mathcal{X} \rightarrow \mathcal{Y}^C \times \mathcal{X}^{i-1}$, $1 \leq i \leq C$

Definition 2 *A polar code is referred to as a* (C, K) *code, where* N *is the block length,* K *is the code dimension. Its matrix generator* G_C *which construction is defined below is a* $K \times C$ *sub-matrix of* $F^{\otimes c}$ *(c-fold tensor) [115].*

- *Computation of the vector* U_C *through the recursion*

$$U_{2k,j} = \begin{cases} 2u_{k,j} - u_{k,j}^2 & \text{if } 1 \leq j \leq k \\ u_{k,j-k}^2 & \text{if } k+1 \leq j \leq 2k \end{cases}$$

- *Permutation of* $\tilde{\Pi}_C$ $=(i_1, \ldots, i_C)$ *which corresponds to the bit reversal operation.*

The matrix generator is finally given by

$$G_C = F^{\otimes c}\tilde{\Pi}_C = \tilde{\Pi}_C F^{\otimes n} \tag{4.17}$$

Apart from its main characteristic, the polar codes allow having:

- The complexity of coding and decoding close to $(C \log C)$.
- The frame error probability $P_e(C, R)$=o$(2^{-\sqrt{N}+o(\sqrt{C})})$.

4.2.3.5 Rank Metric Codes

Introduced by Delsarte in coding theory [116] and developed by E. Gabidulin [117], RC or Gabidulin codes are widely employed in cryptography. However, recently it has been introduced in communication systems to improve the performance degraded by noise such as impulsive noise represented as a matrix in a row or column. For this purpose, we start with the definition of some meaningful parameters of this coding scheme.
Let q be a power of a prime and $\mathbb{F}_q$ designate Galois Field with q elements. Let $\mathbb{F}_q^{v\times u}$ express the $v \times u$ matrices over $\mathbb{F}_q$, and set $\mathbb{F}_q^v = \mathbb{F}_q^{v\times 1}$. Let $\mathbb{F}_q^u$ be an extension of $\mathbb{F}_q$. Every extension field can be considered as a vector space over the finite field. Let $\mathcal{B} = \beta_0, \beta_1, \ldots, \beta_{u-1}$ be a basis for $\mathbb{F}_q^u$ over $\mathbb{F}_q$. Since $\mathbb{F}_q^u$ is also a field, we may consider a vector $x \in \mathbb{F}_q^u$. Whenever $x \in \mathbb{F}_{q^u}^v$, we denote by x_i the i^{th} entry of x; that is $x = [x_0, x_1, \ldots, x_{v-1}]^T$. It is natural to extend the map [.] to a bijection from $\mathbb{F}_{q^u}^v$ to $\mathbb{F}_q^{v\times u}$, such as the i^{th} row of $[x]_{\mathcal{B}}$ is expressed by $[x_i]_{\mathcal{B}}$.
Rank codes are described as a non-empty subset $\mathcal{X} \subseteq \mathbb{F}_q^{v\times u}$. The rank weight of x, defined as $\mathcal{R}\mathrm{k}(x)$, is denoted to be the maximum number of coordinates in x that are linearly independent over $\mathbb{F}_q$.
The *rank distance* between two vectors $\mathbf{x_1}$ and $\mathbf{x_2}$ is the column rank of their difference $\mathcal{R}\mathrm{k}\ (\mathbf{x_1} - \mathbf{x_2}|\mathbb{F}_\mathbf{q})$. The *rank distance* of a vector rank code $\mathcal{X} \subset \mathbb{F}_{q^u}^v$ is expressed as the minimal rank distance

$$d(\mathcal{X}) = d = \min(\mathcal{R}\mathrm{k}(\mathbf{x_i} - \mathbf{x_j}) : \mathbf{x_i}, \mathbf{x_j} \in \mathcal{X}, \mathbf{i} \neq \mathbf{j}) \tag{4.18}$$

For $u \geq v$, an important class of rank metric codes was proposed by Gabidulin [118]. Gabidulin code is a linear (v, k, d) block code over $\mathbb{F}_{q^u}$ defined by the parity-check matrix $P = [p_j^{[i]}]$, $0 \leq i \leq v-k-1$, $0 \leq j \leq v-1$, where the elements $(p_0, p_1, \ldots, p_{v-1}) \in \mathbb{F}_{q^u}$ are linearly independent over $\mathbb{F}_q$, and $k = v - d - 1$ is the dimension of the code. P is expressed as follows

$$P = \begin{pmatrix} p_0 & p_1 & \cdots & p_{v-1} \\ p_0^q & p_1^q & \cdots & p_{v-1}^q \\ p_0^{q^2} & p_1^{q^2} & \cdots & p_{v-1}^{q^2} \\ \vdots & \vdots & \ddots & \vdots \\ p_0^{q^{d-2}} & p_1^{q^{d-2}} & \cdots & p_{v-1}^{q^{d-2}} \end{pmatrix} \tag{4.19}$$

The parity matrix defines a maximum rank distance (MRD) code with length $v \leq u$ and $d = v - k + 1$. Another method for MRD construction can be obtained using generator matrices [21] define as follows

$$G = \begin{pmatrix} g_0 & g_1 & \cdots & g_{v-1} \\ g_0^q & g_1^q & \cdots & g_{v-1}^q \\ g_0^{q^2} & g_1^{q^2} & \cdots & g_{v-1}^{q^2} \\ \vdots & \vdots & \ddots & \vdots \\ g_0^{q^{k-1}} & g_1^{q^{k-1}} & \cdots & g_{v-1}^{q^{k-1}} \end{pmatrix} \tag{4.20}$$

Rank metric decoding

Fast correction of rank erasures and random rank errors was presented in [119]. Several other algorithms for correcting rank errors are also defined [116 - 119]. In this section, we present the algorithm defined by Gabidulin and known as the modified Berlekamp-Massey algorithm [117]. This is an effective technique for decoding rank metric errors. The mains steps of construction are explained as follows. We consider a MRD (v, k, d) code $\mathcal{X}$. The transmitted signal is $\mathbf{x}$ and received signal can be depicted as $\mathbf{y} = \mathbf{x} + \mathbf{e}$, such as $\mathbf{e}$ is a random error with $\mathcal{R}$k t. We evaluate the syndrome $s = S_0, S_1, S_2, \ldots, S_{d-2}$ as follows

$$s = r \cdot P^T = (x + e)P^T \tag{4.21}$$

Let us expressed a $(t \times v)$ matrix H of $\mathcal{R}$k t, whose entries are constituents of the base field $\mathbb{F}_q$. Hence, we express

$$e = (E_0, E_1, E_2, \ldots, E_{t-1})H \tag{4.22}$$

such as $E_0, E_1, E_2, \ldots, E_{t-1} \in \mathbb{F}_q^v$ are linearly independent over $\mathbb{F}_q$. We now define $\mathbf{Z}$, the matrix expressed as follows

$$Z^T = HP^T \begin{pmatrix} z_0 & z_1 & \cdots & z_{t-1} \\ z_0^q & z_1^q & \cdots & z_{t-1}^q \\ z_0^{q^2} & z_1^{q^2} & \cdots & z_{t-1}^{q^2} \\ \vdots & \vdots & \ddots & \vdots \\ z_0^{q^{d-2}} & z_1^{q^{d-2}} & \cdots & z_{t-1}^{q^{d-2}} \end{pmatrix} \tag{4.23}$$

It can be demonstrated that the constituents $z_0, z_1, \ldots, z_{t-1} \in \mathbb{F}_q^v$ are linearly independent over $\mathbb{F}_q$. Thus,

$$(S_0, S_1, S_2, \ldots, S_{d-2}) = (E_0, E_1, E_2, \ldots, E_{t-1}) \cdot Z^T \tag{4.24}$$

Therefore, we get a structure composed of $d-1$ equations with $2 \cdot t$ unknown elements which are linear in $z_0, z_1, \ldots, z_{t-1}$. We also consider that the $\mathcal{R}$k t of e is unknown. It is enough to determine one solution of the system thanks to every solution of $E_0, E_1, E_2, \ldots, E_{t-1}$ and $z_0, z_1, \ldots, z_{t-1}$ derives in the same error vector e [117].

We now define $\wedge(\alpha) = \sum_{j=0}^{t} \wedge_j \alpha^{q^j}$, the row error polynomial and $S(\alpha) = \sum_{j=0}^{d-2} S_j \alpha^{q^j}$ be the linearized syndrome polynomial. We now expressed the key equation by

$$\wedge(\alpha) \otimes S(\alpha) = F(\alpha) \mod \alpha^{q^{d-1}} \tag{4.25}$$

where $F(\alpha)$ denotes ad auxiliary linearized polynomial. Assuming that $\wedge_0 = 1$ and $\wedge_i = 0$ for $i > t$. Hence,

$$S \begin{bmatrix} \wedge_t \\ \wedge_{t-1} \\ \vdots \\ \wedge_1 \end{bmatrix} = \begin{bmatrix} -S_t \\ -S_{t+1} \\ \vdots \\ -S_{2t-1} \end{bmatrix} \quad S = \begin{bmatrix} S_0^{q^t} & \cdots & S_{t-1}^{q^1} \\ S_1^{q^t} & \cdots & S_t^{q^1} \\ S_2^{q^t} & \cdots & S_{t+1}^{q^1} \\ \vdots & \vdots & \ddots \\ S_{t-1}^{q^t} & \cdots & S_{2t-2}^{q^1} \end{bmatrix} \tag{4.26}$$

It can be shown that S is non singular matrix leading to a unique solution for the system of equations. This solution can be effectively obtained utilizing the modified Berlekamp-Massey algorithm as depicted in Fig. 4.2 and summarized as follows.

1. Evaluate the syndrome with equation (4.21).
2. Resolve the key equation with the modified Berlekamp-Massey algorithm to get $\wedge(\alpha)$.
3. Estimate the elements $E_0, E_1, E_2, \ldots, E_{t-1}$ of $\wedge(\alpha)$.
4. Solve the linear system of equations for the unspecified elements$z_0, z_1, \ldots, z_{t-1}$.
5. Determine the matrix $\mathbf{H}$ utilizing (4.23).
6. Calculate e using (4.22) and the decoded codeword $\hat{x} = y - e$

4.2.3.6 Low Rank Parity Check Codes

Low Rank Parity Check code (LRPC) [120]: this kind of code is a derivation of Gabidulin codes. They exhibit a lower complexity decoding algorithm.

Definition 3 *A Low Rank Parity Check code is a code of $\mathcal{R}$k d, length n, and dimension k over $\mathbb{F}_{q^m}$. Its parity check matrix $\boldsymbol{P} = (p_{ij})$, a $((n-k) \times n)$ matrix exhibits the following property: the sub-vector space of $\mathbb{F}_{q^m}$ generated by its coefficients p_{ij} has a dimension at most d. We call this dimension the weight of $\boldsymbol{P}$.*

LRPC code has a specific construction for its parity check matrix $\mathbf{P}(p_{ij})$. The generator matrix $\mathbf{G}$ is derived from $\mathbf{P}$ in systematic form. This method leads to find a low rank matrix [121]. We present the steps of the construction below:

- We generate a matrix called $\omega_d(d, q^d)$ formed by all vectors over the space vector $\mathbb{F}_{q^d}$. This matrix has a $\mathcal{R}$k d.

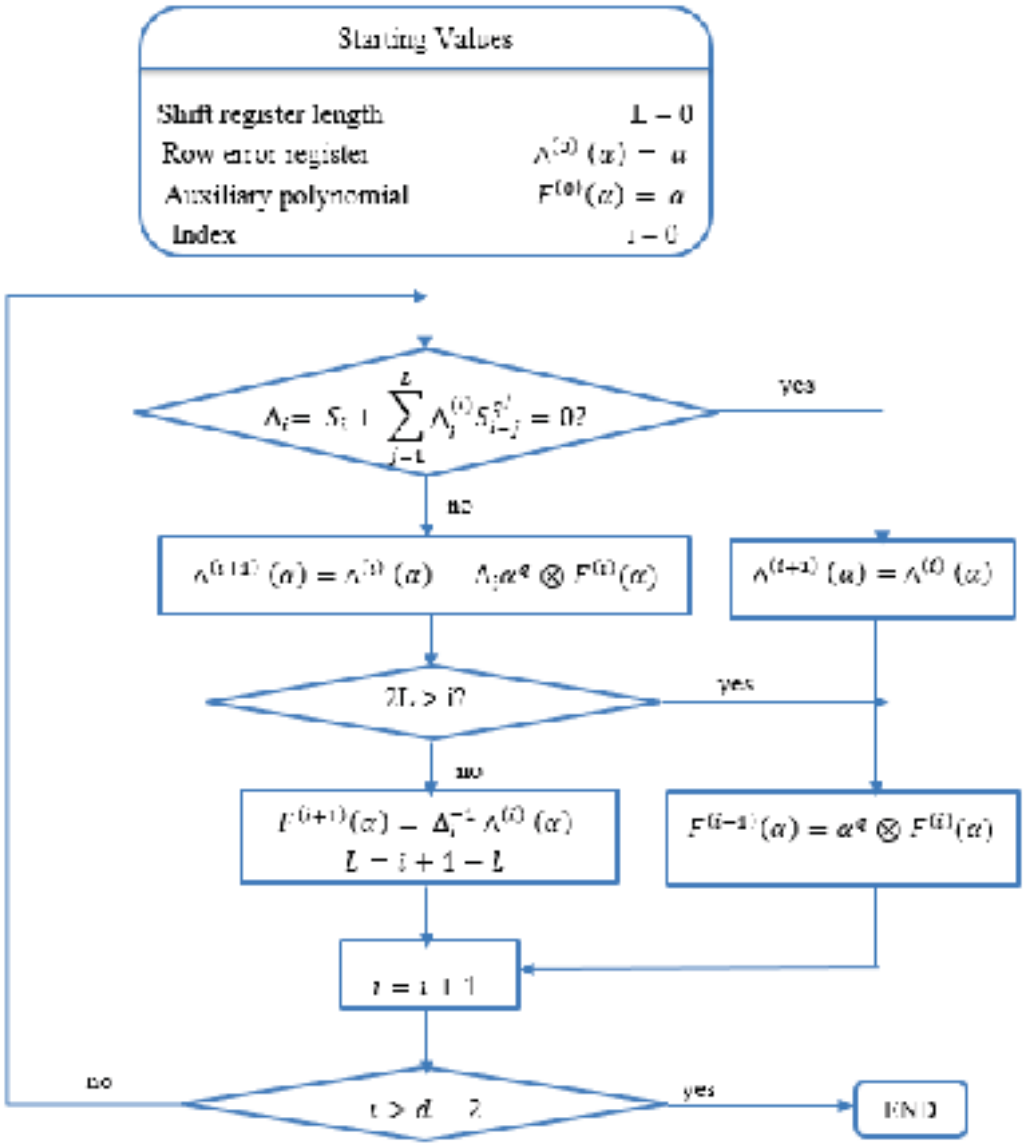

Figure 4.2: Berlekamp-Massey algorithm for Rank Metric decoding.

- To obtain a $\omega_m(m, q^d)$ matrix with m rows over $\mathbb{F}_{q^m}$, we expand the ω_d matrix by adding $(m-d)$ rows $(\alpha, \cdots, \alpha)$ / $\alpha \in \mathbb{F}_q$. We obtain a $\omega_m(m, q^d)$ matrix with m rows.
  Remark: $\mathcal{R}\mathrm{k}(\omega_m)$=$\mathcal{R}\mathrm{k}(\omega_d) = d$.

- We write the columns of ω_m (length m) over $\mathbb{F}_{q^m}$. We denote $\mathbf{D}$ the set of these elements as: $\mathbf{D} = \{\alpha_1, \cdots, \alpha_{q^d}\} \subset \mathbb{F}_{q^m}$.

- From $\mathbf{D}$ the low rank parity check matrix $\mathbf{P}$ is generated as $\mathbf{P} = (p_{ij})$ for $1 \leq i \leq n-k, 1 \leq j \leq n \ / \ h_{ij} \in \mathbf{D}$.
  Remark: $\mathbf{P}$ is called the parity check matrix with low rank d.

4.3 Synthesis of Impulsive Noise Reduction Techniques

In this section, we have investigated several impulsive noise reduction techniques proposed in the literature. They can be split into three categories. The first category concerns the modulation scheme. It is particularly shown that MCM schemes are inherently more robust to impulsive noise compared to single carrier schemes. Moreover, some iterative algorithms that are performed both in time and frequency can help to reduce the impact of impulsive noise over transmissions significantly. However, these algorithms may sometime be very complicated to implement. The second category of impulsive noise countering strategies consists of signal processing-based solutions. Some simple methods such as amplitude clipping or blanking are widely used, and they usually enable a significant performance gain compared to when no treatment is applied. However, the optimal threshold is only obtained by either empirical or very complex approaches. The last category is the error correction solution. Several FEC schemes have been proposed in the literature as described in the section above. However, every code has advantages and inconveniences according to the application or the considered environment. Code RS or LDPC is the most desired when the environment is disrupted by impulsive noise. Gabidulin code is also useful for these types of errors. Depending on the particular application, selecting a code or decoding algorithm can be a complex task; the choice depends on many of the overall design parameters of the system. To determine whether an error control coding scheme is warranted for an application, the following factors should be considered:

- Channels requirements and constraints,
- Decoding performance,
- Cost and complexity ,
- Coding efficiency,
- Coding delay, ...

From the system design, the most critical factor is the decoding performance, delay, and complexity. Our comparison is more going to concern to the codes RS, LDPC, and Gabidulin. LDPC codes are also useful but are greedy in calculation time. This is the reason why it does not allow its use at the level of the sensors considering the energy constraint. Codes with fixed efficiency as codes RS or LDPC could be used on channels with the disappearance. The inconvenience of RS codes is a complexity of decoding. The reason for this complexity is that every coded symbol RS depend on all the symbols of information. Besides, the efficiency of these codes must be calculated and calibrated for

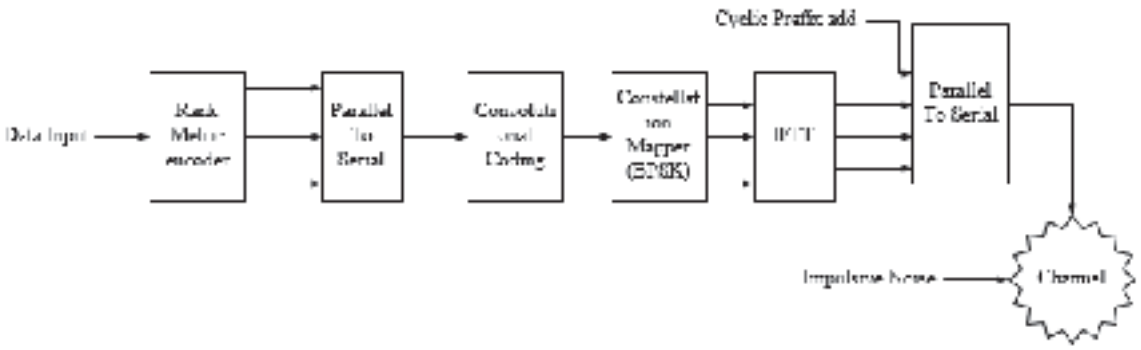

Figure 4.3: The Physical Layer Overview.

the characteristics of a channel given before any transmission. For better exploitation of the codes, RS or LDPC codes are concatenated with a CC scheme. In this case, the use of an interleaver is essential; what makes more complicated the transmission chain. As an alternative to RS codes, Gabidulin or RC codes are used to cancel the impulsive noise occurring environments. The main advantage of RC codes is its low complexity (decoding with modified Berlekamp-Massey). Contrary to RS or LDPC, RC codes do not need an interleaver which further favors the low complexity. Another problem solved by the RC concerns erasure and propagation errors for random linear network coding.

4.4 Proposed Coded-OFDM for Impulsive Noise Mitigation

4.4.1 The Proposed Scheme

The proposed physical layer consists of a coded-OFDM based RC concatenated with a CC scheme as depicted in Fig. 4.3. The RC coding scheme is mostly studied in coding theory but used now in communication systems to mitigate impulsive noise. Since the noise present in power substations appears as burst errors, this kind of scheme is well suited for cancellation. However, it has been demonstrated that the background noise considered as Gaussian noise is also present in this environment. In order to cancel the isolated noise, the use of CC becomes essential.

4.4.1.1 Mapping Description

In a multi-carrier transmission system, the signals can be "naturally" represented in a matrix structure, where each column is used to generate an OFDM symbol. Let us define a vector B of elements in Finite Field $]\cdot[_{q^v}$, $B = (b_1, b_2, \ldots, b_v)$ the signal to be sent. $]\cdot[_{q^v}$ can be considered as a vector over the space $]\cdot[_q$. Let us call A a base of $]\cdot[_{q^v}$ over $]\cdot[_q$. We

can represent the vector B as a matrix B with entries in Finite Field $\mathbb{F}_q$ by decomposing the elements b_i of B following the base $\mathcal{A}$.

$$B = \begin{bmatrix} \begin{bmatrix} b_{11} \\ b_{21} \\ \vdots \\ b_{v1} \end{bmatrix} \begin{bmatrix} b_{12} \\ b_{22} \\ \vdots \\ b_{v2} \end{bmatrix} \dots \begin{bmatrix} b_{1v} \\ b_{2v} \\ \vdots \\ b_{vv} \end{bmatrix} \end{bmatrix} \tag{4.27}$$

Since a binary modulation will be used, $q = 2$. By using a rank metric code defined on $\mathbb{F}_{2^v}$, a code vector can be denoted as follows

$$c = x \times G = (c_1, c_2, \dots, c_v) \tag{4.28}$$

where x is the message to send, and G is the generator matrix. Thus, c can be represented as a matrix in the Finite Field $\mathbb{F}_2$ as follows

$$\mathbf{C} = \begin{pmatrix} c_{1,1} & c_{1,2} & \cdots & c_{1,v} \\ c_{2,1} & c_{2,2} & \cdots & c_{2,v} \\ \vdots & \vdots & \vdots & \vdots \\ c_{v,1} & v_{v,2} & \cdots & v_{v,v} \end{pmatrix} \tag{4.29}$$

Using $v = 16$, we obtain a 16×16 matrix with entries on 32 information bits. The elements of the matrix $\mathbf{C}$ are then transposed into a serial format in order to prepare them for the convolutional encoding. A BPSK is applied to ensure transmission of the coded sequence with an effective bandwidth.

4.4.1.2 OFDM Mapping

OFDM is a multi-carrier modulation employed mainly in wired systems, power-line communications (PLC) [122-123] and standard wireless systems (i.e., (Digital Video Broadcasting-Terrestrial (DVB-T) [124], WiMAX, IEEE 802.11 a/g/n/ac [123]). The high data rates and robustness in reducing the effect of a multi-path fading make OFDM an obvious candidate for thoughtful industrial environ- ments[19]. Instead of transmitting a high-speed data stream over a single carrier, OFDM utilizes a vast number of orthogonal sub-carriers conveyed in parallel. In our case, the number of sub-carriers is $S_c = 512$. Each sub-carrier is modulated with a BPSK encoded matrix. An "OFDM symbol" is formed by each column of this matrix. The output noted F is as follows

$$F = \begin{pmatrix} f_{1,1} & f_{1,2} & \cdots & f_{1,t} \\ f_{2,1} & f_{2,2} & \cdots & f_{2,t} \\ \vdots & \vdots & \vdots & \vdots \\ f_{s,1} & f_{s,2} & \cdots & f_{s,t} \end{pmatrix} \tag{4.30}$$

where

Table 4.1: OFDM Parameters

Parameters	Values
Bandwidth	20 MHz
Chip Duration	50 ns
Number of FFT Points	512
FFT Symbol Period	25.6 μs
Number of Cyclic Prefix	48

- f_{ij} represents the tone of frequency i and time slot j,
- s corresponds to the number of used sub-carriers,
- t is the number of OFDM symbols sent on the channel.

4.4.2 Performance Evaluation

4.4.2.1 Performance Analysis in AWGN and Impulsive Noise Channel

This part discusses the results obtained from the designed transceiver over AWGN and impulsive noise channel. We compare the results of the Gabidulin code RC $(16, 8)$ and LRPC $(16, 8)$ over $\mathbb{F}_{q^u} = 16$. These coding schemes are concatenated with a CC with a coding rate R = 1/2, and generator polynomials in octal form: $P_1 = 171$ and $P_2 = 133$. The simulations are performed by considering an OFDM block size of 512 carriers with BPSK modulation. During a symbol transmission, the impulsive noise obtained from the measurements is added to the symbol stream. RC decoding uses the modified Berlekamp-Massey algorithm and for LRPC decoding, we use the algorithm from [120]. The convolutional decoder uses the soft-input Viterbi algorithm. In Fig. 4.4, the system performance is illustrated. It underlines the results obtained for RC and LRPC compared to an uncoded one in the presence of impulsive noise. Referring to Fig. 4.4, by comparing the two resultant BERs for the concatenated coding schemes, we can note a significant gain compared to the uncoded case. The BER target of 10^{-5} is achieved at EbNo of 3.3 dB and 4 dB for RC and LRPC, respectively. The RC scheme outperforms LRPC scheme by 0.7 dB at BER 10^{-5}. This is due to the probabilistic decoding algorithm of LRPC codes that decode with a given probability of failure [120]. We compare our results to those obtained in [126] which uses a Turbo Code. According to these curves, the RC scheme outperforms those results in the case of a turbo coded and L_c filtering and where no treatment is applied.

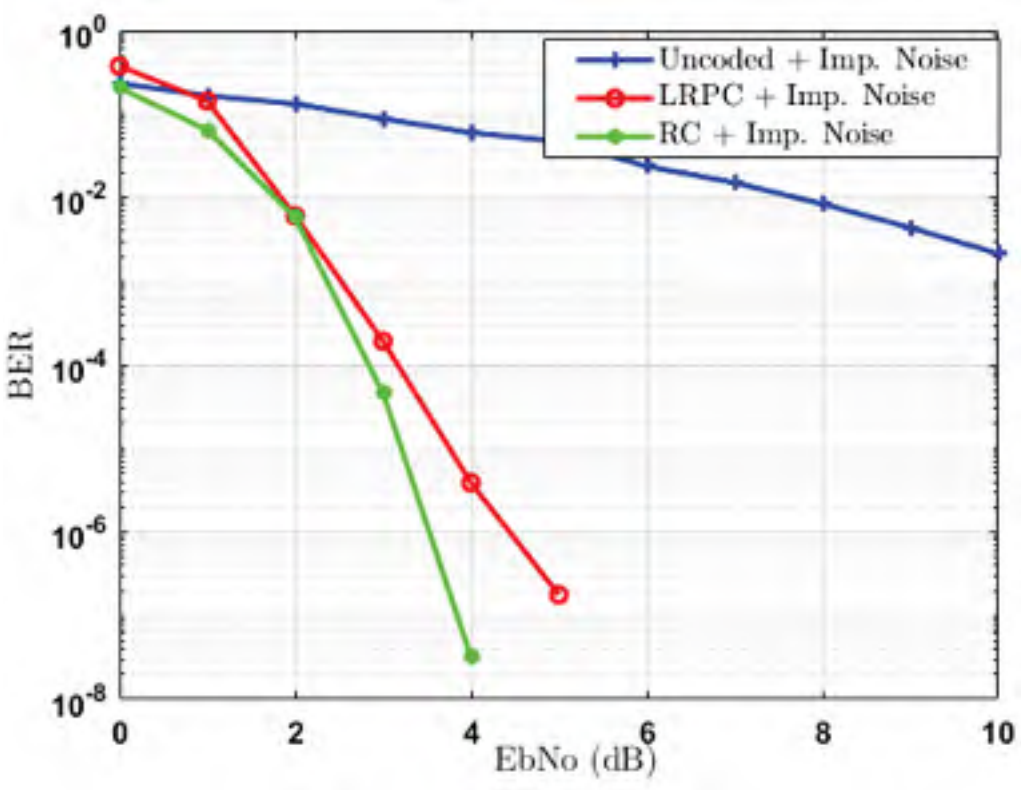

Figure 4.4: BER performance for RC, LRPC, and uncoded system in the presence of impulsive noise over an AWGN channel.

4.4.2.2 Application to a Realistic Channel

In this section, we consider a multi-path environment. For this purpose, we use a channel modeling approach based on deterministic rays tracing which takes into account the characteristics of the transmission environment. The software tool used is RaPSor and the realistic environment chosen for the simulation is the Laurentides which is an essential electric substation located in Quebec (Canada).

4.4.2.2.1 $3D$ Description

The realistic environment corresponds to the Laurentides HV power substation in Québec (Canada) with an area dimension of 1300 m $\times$ 800 m. Equipment and devices present in the substation are among other transformers, circuit-breakers, disconnect switches. Buildings, walls, and pylons are additional structures located there. In the considered transmission scenario, a Data Gathering Node (DGN) is positioned on a tower in the environment as depicted in Fig. 4.5. One receiver node is positioned on a transformer. It is placed on a 60 m high-lighting pole as represented in Fig. 4.5 In this figure, we can note that there are multiple paths due to the interactions between the signal and the objects present in the substation. The direct path has a power of -6.5 dBm associated with a delay of 699 ns.

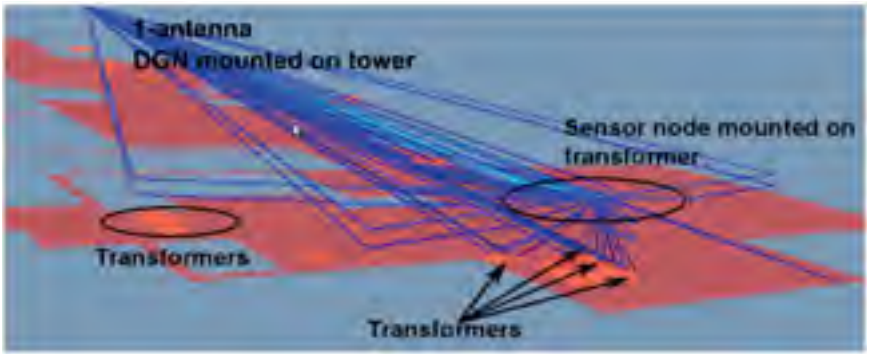

Figure 4.5: Rays interactions with objects in power station with the positions of the sensor and the DGN

Table 4.2: Example of the CIR characteristics from RaPSor.

Nature	**Received Power** (dBm)	**Delay (ns)**
R_2	- 14.06	708
R_8, D_8	- 11.42	735
R_{20}, D_{20}	-37.9	2014

The characteristics of the significant secondary paths due to the combination of interactions between reflections and diffractions are presented in Table 4.2. We use R_i for reflections and D_i for diffractions where i is the number of the path. However, to be able to use these kinds of CIR in a communication system simulator, we need to process the data.

- Extraction of data from the CIR (attenuation, delay, phase)
- Calculation of the vectorial Field
- Sampling
  - Recovering of index
  - Calculation of the vectorial sum
- Normalization of power

In Fig. 4.6, the first path at 699 ns is composed of a LOS path and several NLOS paths. The second path is thus made up of several NLOS paths and so on. The resulting channel model is frequency selective. The max delay and the coherence bandwidth associated are 733 ns and 1.3 MHz, respectively. After obtaining the normalized attenuation, we proceed

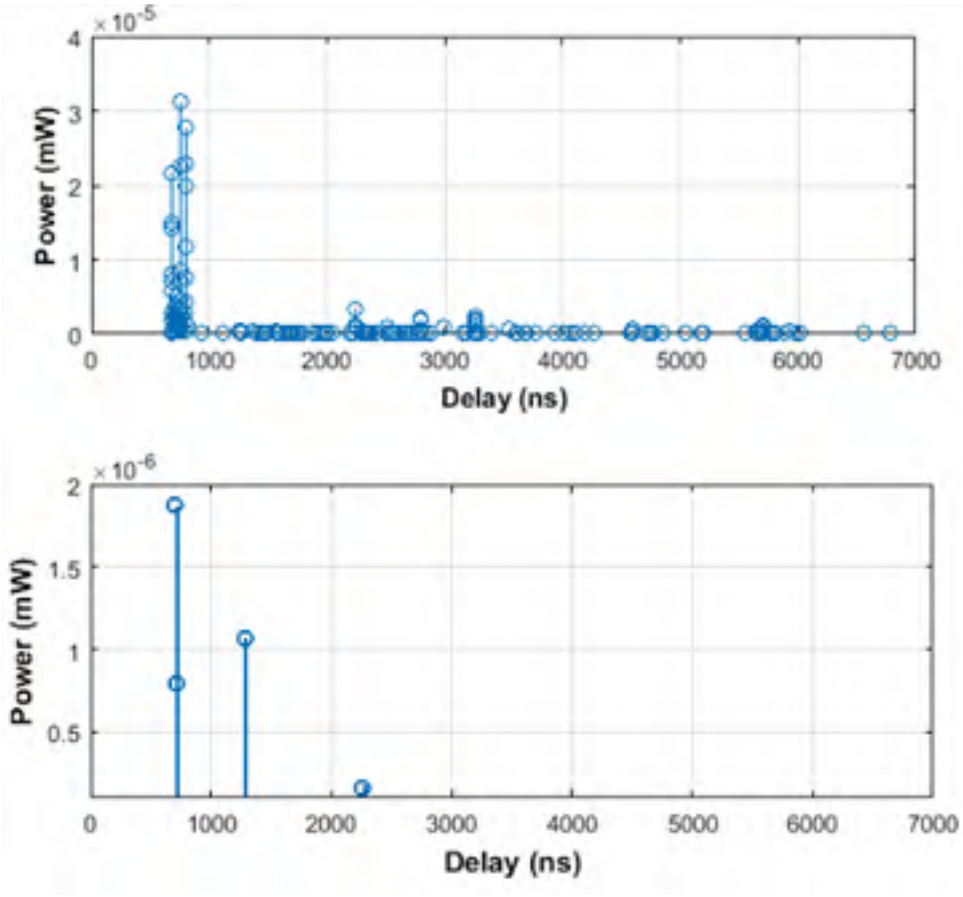

Figure 4.6: Channel Impulse Response (CIR) from RaPSor before and after sampling.

to find the coefficients of this multi-path channel by down-sampling to the transmission symbol rate of transmission. We finally obtain an equivalent CIR

$$C = \sum_{k} \sqrt{P_k} e^{j\phi_k} \delta(t - kT) \tag{4.31}$$

where P_k is the power associated with the k^{th} equivalent multi-path component and ϕ_k its phase. T is the period of the transmitted symbols. For the simulation results part, we will consider two data rates: 54 Mbps and 100 Mbps.

4.4.2.2.2 Simulation Results

In this section, we present numerical simulation results which illustrate the performance of the transmission chain including the proposed coding scheme and OFDM modulation in multi-path and impulsive noise channel. The BER and Packet Error Rate (PER) as a function of EbNo in different configurations are calculated.

Table 4.3: Coefficients of the CIR for 54 Mbps

C_1	C_2	C_3
0.5+0.5i	0.32-0.38i	0.43+0.25i

Table 4.4: Coefficients of CIR for 100 Mbps

C_1	C_2	C_3	C_4	C_5	C_6
0.6+0.41i	0.24-0.27i	0.23+0.26i	0.2-0.25i	0.19-0.2i	0.18+0.09i

First Data Rate

The data payload is 150 bytes. We obtain an equivalent channel impulse response with three coefficients (Table 4.3). In our simulation, we choose an FFT of size equal to 512. Taking into account the delay of the first multi-path component, we obtain the equivalent final CIR as

$$V_{512} = [\underbrace{0 \cdots 0 \cdots 0}_{86} \quad C_1 \quad C_2 \quad C_3 \quad \underbrace{0 \cdots 0 \cdots 0 \cdots 0}_{423}] \tag{4.32}$$

Then, an FFT is applied to V_{512} to obtain H_k which represents the channel frequency response at tone k. For each carrier k we obtain the received Y_k as shown below

$$Y_k = H_k X_k + noise \tag{4.33}$$

This signal is then equalized by the multiplication of the conjugate of H_k: $H_k^* Y_k$.

Second Data Rate

we consider here a target bit rate of 100 Mbps. Now considering the same CIR, we obtain the equivalent channel impulse response in Table 4.4. To compare these results with a powerful channel coding scheme, we use as a benchmark, a polar code of rate 1/2 with a packet size of 1500 bytes.

In Fig. 4.7, we compare BER of different schemes namely RC, LRPC, polar code, and the uncoded data. These different coding schemes are examined in the realistic multi-path channel in the presence of impulsive noise. As expected, we note a degradation of the performance when compared with the results obtained in Fig. 4.5. In contrast, we obtain a substantial gain for the three codes compared to the uncoded case. These gains are at least equal to 10 dB at BER 10^{-5}. The BER of RC at 10^{-5} is achieved when EbNo is equal to 5.5 dB. Meanwhile, for LRPC and polar codes, EbNo is equal to 6 dB and 9.5 dB, respectively. By comparing the three coding schemes, it can be easily seen that the RC and LRPC codes are more efficient than the polar code in this multi-path channel. The RC code has a gain of 4 dB compared to the polar code when a target BER of 10^{-5} is considered. We can conclude that polar codes are not designed to tackle impulsive noise. However, we also compare our results to those obtained in [14]. They used a time domain interleaving

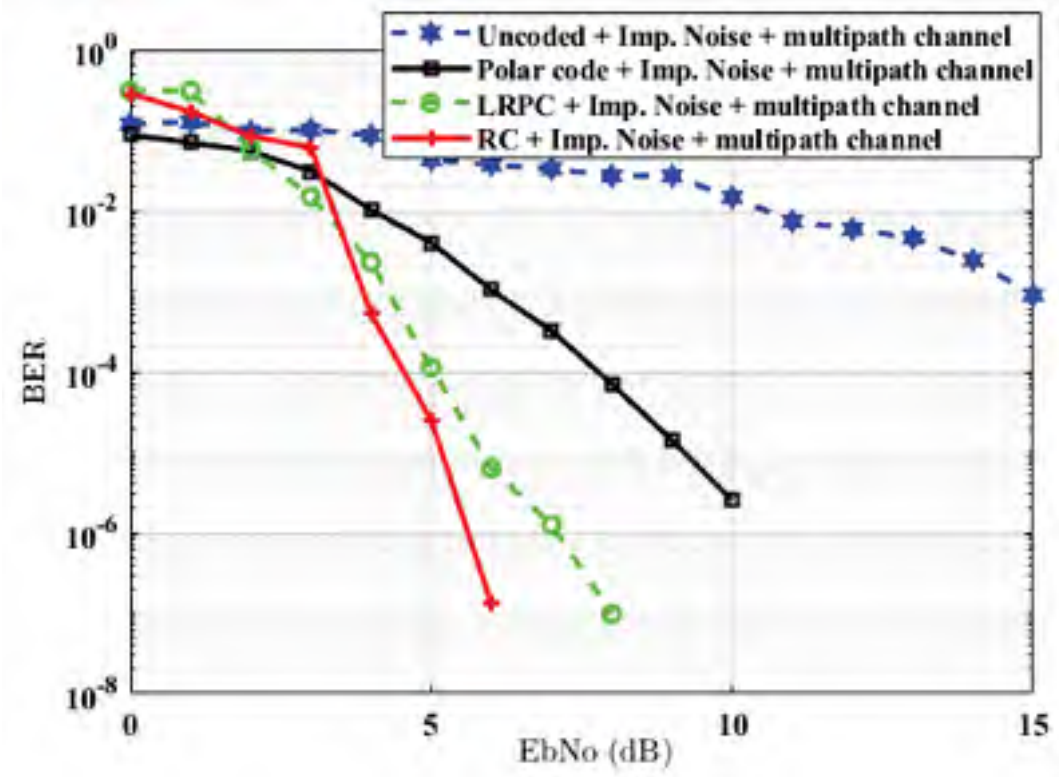

Figure 4.7: BER performance for RC, LRPC, polar code, and uncoded system in the presence of impulsive noise in realistic multi-path channel (1^{st} Data Rate).

associated with an MMSE equalizer in the presence of impulsive noise over a Rayleigh multi-path channel. The gain is about 20 dB for a target BER = 10^{-5}. Afterwards, we considered a data rate of 100 Mbps. Here, we evaluate the considered scenario in a more frequency selective multi-path channel. The coherence bandwidth of the channel (1.3 MHz) is smaller than the bandwidth of the signal.
It can be seen in Fig. 4.8 that the BER for the uncoded data is constant and equal to 10^{-1}. Compared to Fig. 4.7, for the three proposed schemes, the gap with the uncoded case is increased significantly by more than 3 dB at BER of 10^{-5}.

PER is also a very important parameter to characterize QoS. To test the performance of access terminal receivers, PERs are simulated and the results are depicted in Fig. 4.9 and 4.10 for the two data rates.
Fig. 4.9 shows that the PER of RC at 10^{-2} is achieved when EbNo is equal to 10.5 dB. In the case of LRPC and polar code, for the same BER target, EbNo is equal to 11 dB and 13 dB, respectively.

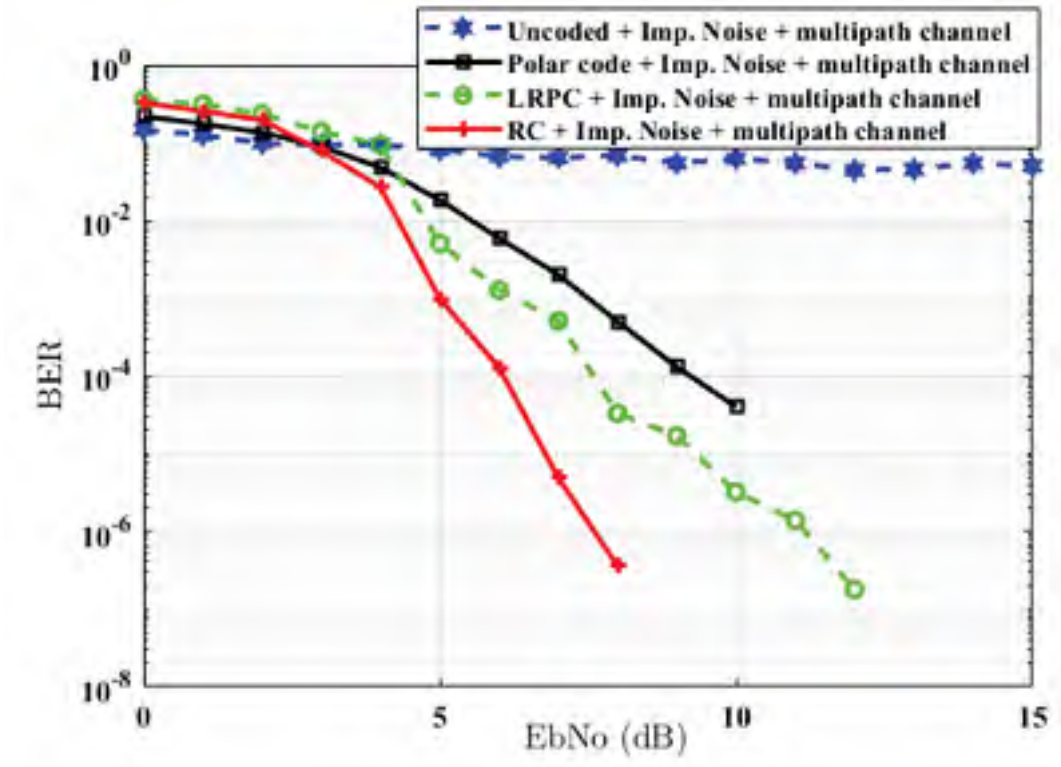

Figure 4.8: BER performance for RC, LRPC, polar code, and uncoded system in the presence of impulsive noise in realistic multi-path channel (2^{nd} Data Rate).

Furthermore, the PER for 100 Mbps is shown in Fig. 4.10. EbNo for the three proposed schemes are between 11 dB and 14 dB at PER equal 10^{-2}. To summarize, the two RC codes are more efficient than the polar code.

4.4.2.3 Conclusion

In this section, we have proposed a physical layer based on coded-OFDM to mitigate impulsive noise from electricity substations. We have investigated the performance improvements brought about by the use of the RC coding, LRPC, polar code, and OFDM modulation for transmissions impaired by partial discharge signal issued from measurements. The performance of the proposed physical layer has shown that it is possible to cancel all the impulsive noise which can disrupt the transmission. The concatenation of the RC and the CC schemes allows us to have significant BER and PER improvements in the presence of impulsive noise compared to a polar code and an uncoded system. Indeed, we note that the results obtained for the data transfer rate of 54 Mbps are better than the 100 Mbps case because, in this latter, the channel is more frequency selective.
This study will encourage the material implementation of these codes in sensors for Smart Grid applications in order to optimize the performance of these systems which is presented in the next section.

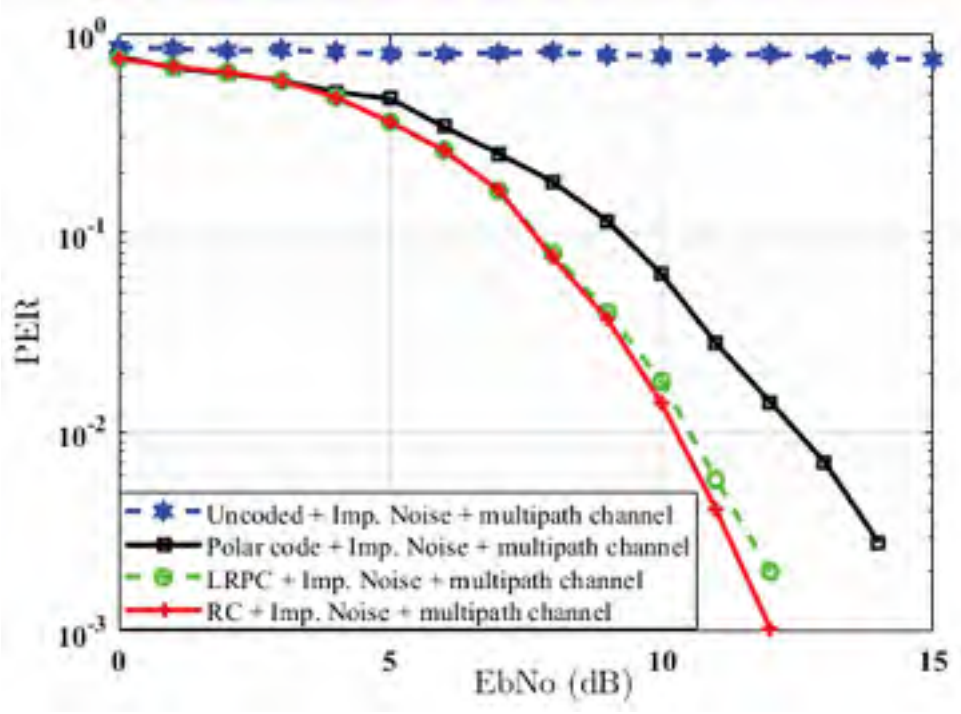

Figure 4.9: PER performance for RC, LRPC, polar code, and uncoded system in the presence of impulsive noise in realistic multi-path channel (1^{st} Data Rate).

4.5 Implementation of the Proposed Approach using GNU Radio SDR-USRP

4.5.1 Introduction

In the section above, we proposed a resistant physical layer based on the concatenation of RC and CC with OFDM. We have used this model to compare different signalling schemes on this channel [130]. The results showed that our approach is robust and efficient compared to other systems. However, the obtained results are based solely on simulations. Moreover, in the literature, there does not exist experimental results for impulsive noise suppression that can be used as a basis for comparison. Several works have been proposed, but the results are only based on simulations. To validate the proposed physical layer, it is essential to compare the theoretical results to the experimental ones. Indeed, in recent years, Software-Defined Radios (SDRs) have drastically changed the way that research and experimental works are done in the wireless arena. Their advantages over traditional hardware-based radios are that significant aspects of the communication stack are implemented in software programs [128], while in hardware radios, the lower layers are realized in hardware, making their use extremely constrained when modifications on physical or medium access layers are required. Thus, with SDRs, most of the radio functionality and signal processing are implemented in software that runs on a computer, and

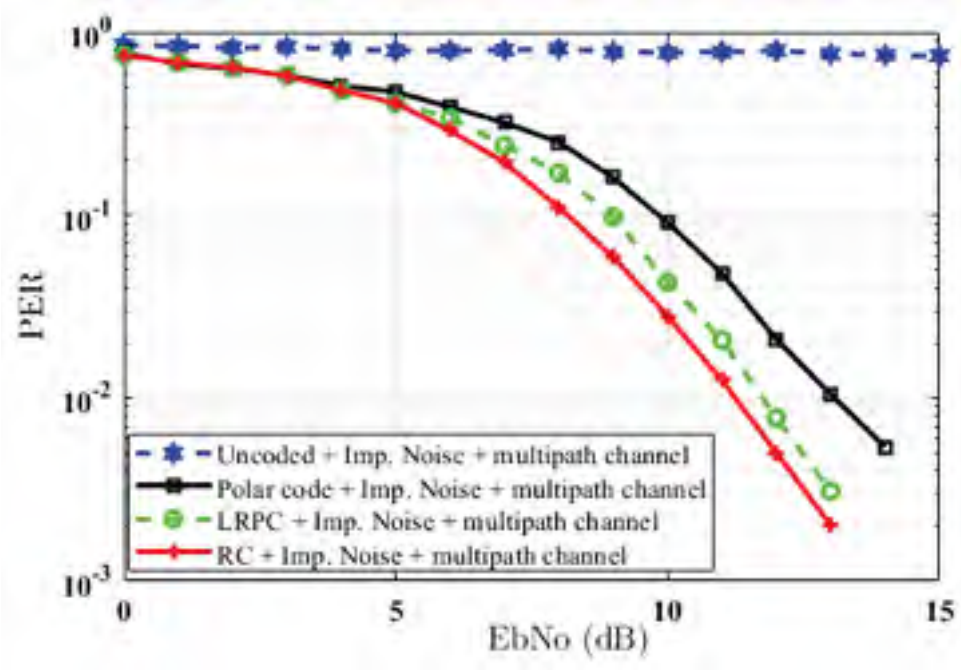

Figure 4.10: PER performance for RC, LRPC, polar code, and uncoded system in the presence of impulsive noise in realistic multi-path channel (2^{nd} Data rate).

the only task of the hardware is taking care of functions, such as transmissions and reception of the signal [130]. We now propose a combined analysis and experimental validation of the best coding schemes with an appropriate OFDM signal. The objective is to come up with an optimized overall physical layer to ensure better communication in substations. For this purpose, we use the GNU's Not Unix Radio (GNU Radio) platform, which is presently the open-source reference apparatus for academic work and wireless research allowing the researcher to implement signal processing blocks with no additional hardware requirements. We implement a new block namely "RC Encoder + WiFi Mapper" to perform error correction. It is based on the implementation of *gr-ieee* 802.11 proposed by Bloessl et al. [127,128]. The main contributions of this section are summarized as follows:

1. Implementation of a new block performing forward error correction code based on the RC code and CC encoding in GNU Radio.

2. Setup design and impulsive noise measurements in a controlled laboratory condition: this is a new method using the GNU Radio instead of an oscilloscope as proposed in other laboratory tests.

3. Over the air experiments in an impulsive noise environment in a laboratory: several scenarios are made up including Line-Of-Sight (LOS) and Non-Line-Of-Sight (NLOS) situations by also considering the impulsive noise level, the distance between the emitter, the receiver and the source.

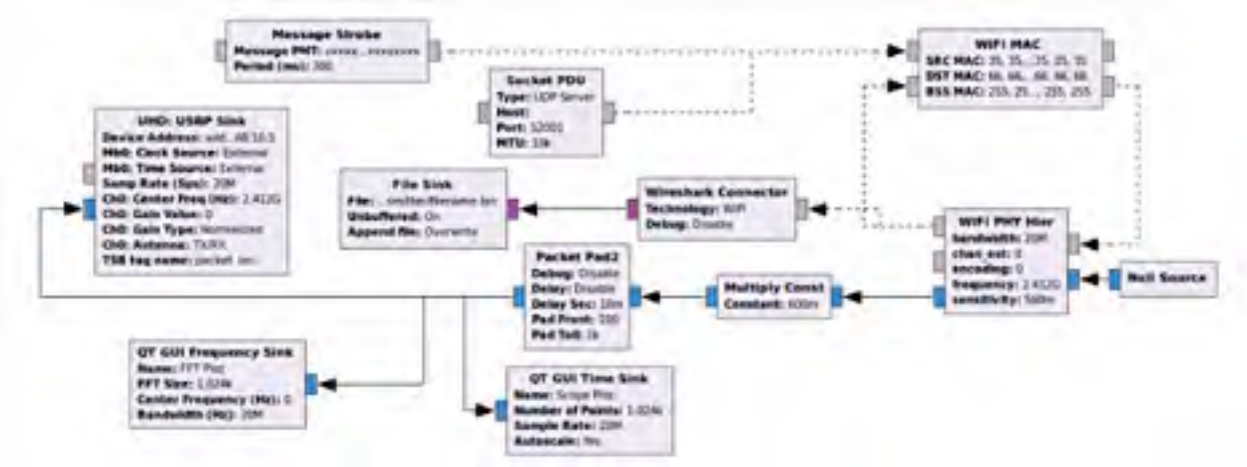

Figure 4.11: Transmitter system developed in GNU Radio using USRP.

The rest of this section is organized as follows. Section 2 presents an overview of the system. It describes the transmitter and the receiver designed in GNU Radio. Section 3 provides the specifications and the measurement scenarios. In Section 4, we present the performance analysis of the obtained results. It first details the network performance by examining the overall rate of traffic and the average delay, which shows that the LOS situation presents better performance than the NLOS configuration. After that, the Bit Error Rate (BER) performance in the presence of impulsive noise obtained by experiments is presented. The performances obtained in this section are globally satisfactory even if we can notice a little degradation in some cases. A comparison between the simulation results shown in [130] and the experimental results is also overviewed in this section, which confirms that the same performances are maintained with several impulsive noise level voltages. Finally, the conclusion and perspectives are given in the last section.

4.5.2 Implementation in GNU Radio

In this section, we describe the structure of the modified gr - ieee 802.11 transceiver implemented in GNU Radio as depicted in Figs. 4.11 and 4.13. The transmitter and the receiver are both constituent parts of the transceiver implementation developed by B. et al. [127].

4.5.2.1 The Transmitter

The structure of the transmitter is illustrated in Fig. 4.11. The difference between the previous implementation of Bloessl is the new block called “RC Encoder + Wifi Mapper” otherwise the rest of the blocks remains the same. Let us describe each block of this figure.

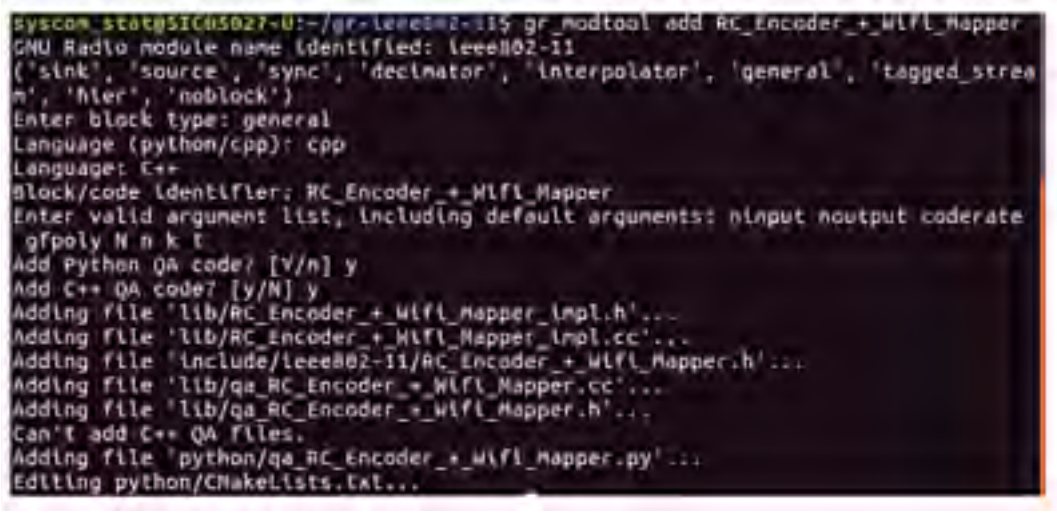

Figure 4.12: RC Encoder + Wifi Mapper block adding in gr - ieee 802.11

RC Encoder + Wifi Mapper

The novelty in this structure is the new block namely "RC encoder + Wifi Mapper" that is created for rank metric encoding and convolutional encoding. First, we recover the old implementation of gr - ieee 802.11. Following the steps of the building, which can be found in [127], we create a new block by using $gr - modtool\ add$ and the different arguments linked to the blocks as depicted in Fig. 4.12.

The different parameters associated with this block are also identified:

- *ninput* corresponds to the data from the MAC layer. They can be in message or bit format.
- *noutput* represents the encoded data after convolutional encoding.
- *coderate* is the coding rate of the convolutional encoder and = 1/2.
- $gfpoly$ corresponds to the primitive polynomial of the RC encoder. Since we use v = 16, the generator is as follows

$$p(\alpha) = \alpha^{16} + \alpha^{12} + \alpha^3 + \alpha + 1 \tag{4.34}$$

- N is the size of the Galois Field.
- t represents the power of correction.

Packet Header Generator

It generates the header of the frame, including the signal and service fields. The header is BPSK modulated by the top Chunks to Symbols block and the remaining frame is modulated by the bottom *Chunks to Symbols* block, according to the chosen modulation (BPSK in our case). Then, the header is finally joined to the remaining of the frame.

OFDM Carrier Allocation

This block is responsible for the aggregation of the pilot sub-carriers, and the FFT block is responsible for the inverse FFT, i.e., for the transition from frequency to the time domain.

OFDM Cyclic Prefixer

Since the OFDM symbols will be sent to a multi-path channel, the signal at the receiver side will be distorted. One way to combat the effect of the multi-path channel such as the Inter-symbol interference (ISI) is to add a cyclic prefix.

4.5.2.2 The Receiver

The receiver part of the IEEE 802.11 physical layer is designed to receive and demodulate OFDM signals. As described in [128], the OFDM receiver consists of a frame detection part, which exploits the short cyclic preamble repeated 10 times at the start of a frame. The frame is then aligned, equalized, and decoded into the MAC information needed for proper delivery.

NB: Since we evaluate performance over the air, the transmitter and the receiver used are interfaced with USRP radios. At the receiver side, recall that the last block was the decoding of the frame. However, this decoding is only performed by the Viterbi decoder. After that, we use Wireshark connector to save the information and performs MATLAB processing for the haul decoding of the rank metric.

4.5.3 Experimental Planning and Testbed Design

This section deals with the description of the hardware and software specifications needed in the test bed. We also overview the measurement scenarios where we conduct the experiments.

4.5.3.1 Specifications

4.5.3.1.1 Hardware

The materials necessary to perform the experimental measurements include a USRP N210 from Ettus Research, an antenna, etc. A brief description of each of these components is given below.

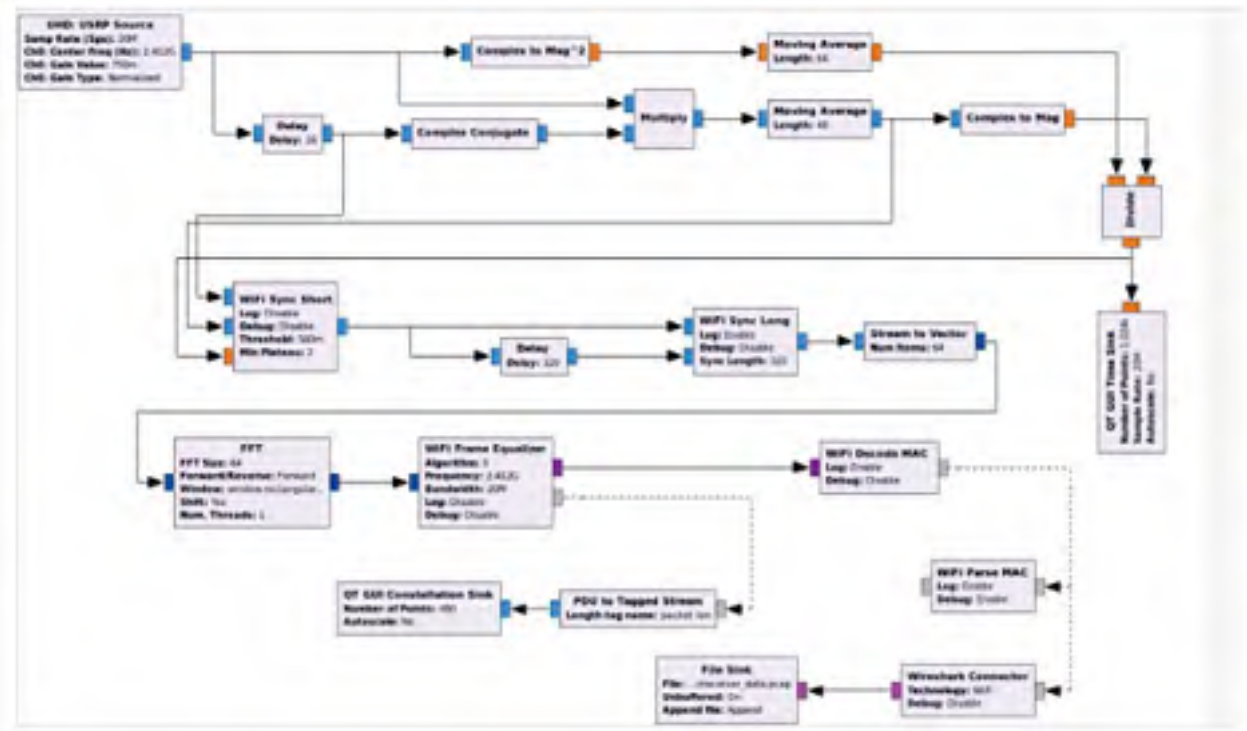

Figure 4.13: Receiver system developed in GNU Radio using USRP.

- USRP N210:It is an SDR product that enables designing and implementing software radio systems. The USRP N210 presents high-dynamic range processing capability and high bandwidth [129]. It is compatible with a wide range of Radio Frequency (RF) modules called daughter-boards. In receiving mode, the samples acquired by the daughter card are scanned by the Analogue-to-Digital Converter (ADC), then converted to the desired intermediate frequency (IF). Finally, the sequence of samples is multiplied by a sine and a cosine to obtain respectively the two components I and Q. The motherboard is connected to a daughter-board allowing the transmission and reception of analogue RF signals. On its daughter-boards, the signal is filtered, amplified and put on a baseband frequency that depends on the IF band of the board and the frequency of the local oscillator. These cards also include basic Rx/Tx cards without conversion frequency or filtering. The two daughter-boards used in this paper are RFX 2400 and SBX. These cards can operate in duplex mode, integral for simultaneous transmission and reception. They offer a bandwidth up to 50 MHz and cover the 2.4-GHz band.

- Antenna: The antenna used is the $ANT\text{-}2.4\text{-}CW\text{-}HW$ model by Linx. It belongs to the HW series 1/2-*wave* center-fed dipole antennas. It is an omnidirectional antenna in wide cover rubber. It uses a horizontal polarization and is connected to the USRP via a SubMiniature Version A (SMA) connector. The characteristics of the antenna

Table 4.5: Overview of the software used to verify the transceiver system.

Components	Types
Operating system	Ubuntu V. 16.4 LTS
CPU	Intel Core i7-2600
GNU Radio	Version 3.7.10
Matlab	R2016a
Wireshark	Version 2.4.5.

are among others a frequency range between 2300 and 2600 MHz, a gain of 3.2 dBi and a maximum power of 50 W.

- Generator bar: To generate the impulsive noise in the laboratory, we use the generator bar as described in Section 3.

4.5.3.1.2 Software

The different components are listed in the Table 4.5.

4.5.3.2 Measurements Scenarios

This section discusses the different scenarios used to perform the measurements. It is divided into two scenarios that are described in the following paragraphs.

4.5.3.2.1 Experimental Scenario 1

For the first experimental scenario, we consider an LOS situation as depicted in Fig. 4.14. We consider two configurations in this situation.

- The impulsive noise source is placed at equal distance from the emitter and the receiver, which is 1 m. The distance between the two USRPs is 2 m.
- In the second case, we place the emitter at 1.90 m from the source, and the receiver is at 1.80 m from the source.

For all the configurations, we generate four types of voltage for impulsive noise from 12 kV–18 kV. We limit the maximum to 18 kV to avoid the risk of breakdown.

4.5.3.2.2 Experimental Scenario 2

The second experimental scenario consists of NLOS situations. It is very similar to the first case except for one detail. We use a metallic reflector as depicted in Fig. 4.15 to generate multi-path phenomena.

- We consider 2 m between the two USRPs. The emitter and the receiver are at 1 m from the source.

Figure 4.14: Line of Sight configuration

Figure 4.15: Non-Line of Sight configuration

- The second scenario consists of placing the receiver at 1.80 m from the source and the emitter at 1.90 m.

As for the LOS experiments, we evaluated four types of voltage varying from 12 kV–18 kV.

4.5.4 Performance Analysis

In this section, we analyse the performance results obtained in the different scenarios. First, the parameters used are defined. Secondly, tests with the proposed implementation are performed to evaluate the performance. We measure the overall traffic rate, the Packet Delivery Ratio (PDR), the average delay and the BERs using USRPs. Finally, a comparison between the simulation results obtained in [130] and the experimental ones is made.

4.5.4.1 Parameters Setting

In this section, we define the parameters used in the experimental tests. For this purpose, we describe in the following the transmit power and the frame format.

Table 4.6: RadioType header subframe format.

Fields types	Components	Values (Bytes)
Header	Header revision	1
	Header pad	1
	Header length	2
Flag	Present flags	4
	Flags	1
Rate	Data rate	1
Channel	Channel frequency	2
	Channel flags	2
Signal	SSI signal	1
	SSI noise	1
	Antenna	1

4.5.4.1.1 Transmit Power

With the USRP, it is not possible to set the transmit power directly as a parameter. It can be configured via the usrp hardware drive, *UHD gain*. The output power depends on other parameters such as the frequency, the total harmonic distortion (THD), which corresponds to the level of unwanted harmonics in a sinusoidal waveform. To have an approximate value of the output power, it can be measured by using a spectrum analyzer. For this purpose, in [131], the authors proposed radio frequency measurements on an SBX daughter-board. In this paper, we can notice that the output power decreases with the increasing of the carrier frequency. The UHD gain is an important parameter; nonetheless, its increment has to be done carefully. Since in our test, we use a frequency of 2.4 GHz with a UHD gain of 20 dB, the corresponding output power is equal to 12.05 dBm.

4.5.4.1.2 Frame Format

The frame that we consider in our simulations is composed of three main parts and can be explained as follows:

1. RadioType header: This contains all the radio information and has a length of 17 bytes. It is composed of the fields represented in Table 4.6.

2. Frame information with a length of 28 bytes is composed of a Frame Control Field (FCF) and Logical Link Control (LLC), as presented in Table 4.7. LLC contains addressing information consisting of two fields: the Destination Service Access Point (DSAP) and the Source Service Access Point (SSAP), as well as a control field.

3. Data correspond to the useful information that will be encoded. Its length is 316 bytes.

We run simulations by considering the two scenarios mentioned above. We use the same traffic load, which corresponds to one packet sent every 300 ms. The duration time

Table 4.7: FCF and LLC sub-frame format.

Fields Types	Components	Values (Bytes)
Frame Control Field	Type/Subtype	1
	Version	1
Duration ID	Duration	2
Addresses	Destination address	6
	Source address	6
	Broadcast address	6
Sequence control	Fragment number	1
	Sequence number	1
Logical Link Control	DSAP	1
	SSAP	1
	Control field	2

of each simulation is approximately 120 s.

Notice that synchronization between the transmitter and the receiver is essential during the experiment. To do this, both USRPs are synchronized using an SMA cable.

4.5.4.2 Network Performance Analysis

In this section, we examine the overall traffic rate, the PDR and the average delay of the packets. The following annotations are used:

- $\{X\}_{LOS1}$ corresponds to the case of the LOS situation and when the emitter and the receiver are both positioned at 1 m from the noise source.
- $\{X\}_{NLOS1}$ is the case of the NLOS situation and when the transmitter and the receiver are both located at 1 m from the impulse source.
- $\{X\}_{LOS2}$ represents the case of the LOS situation and when the emitter is placed at 1.90 m from the source and the receiver at 1.80 m.
- $\{X\}_{NLOS2}$ corresponds to the case of the LOS situation and when the emitter is positioned at 1.90 m from the source and the receiver at 1.80 m.

where $\{X\}$ is either μ or PDR

4.5.4.2.1 Traffic Rate

We compute the primary Input/Output (IO) graphics from Wireshark in different situations. The IO graphs identify the overall rate of traffic seen in the capture files. The X-axis corresponds to the time in second, and the Y-axis is the packets per second.

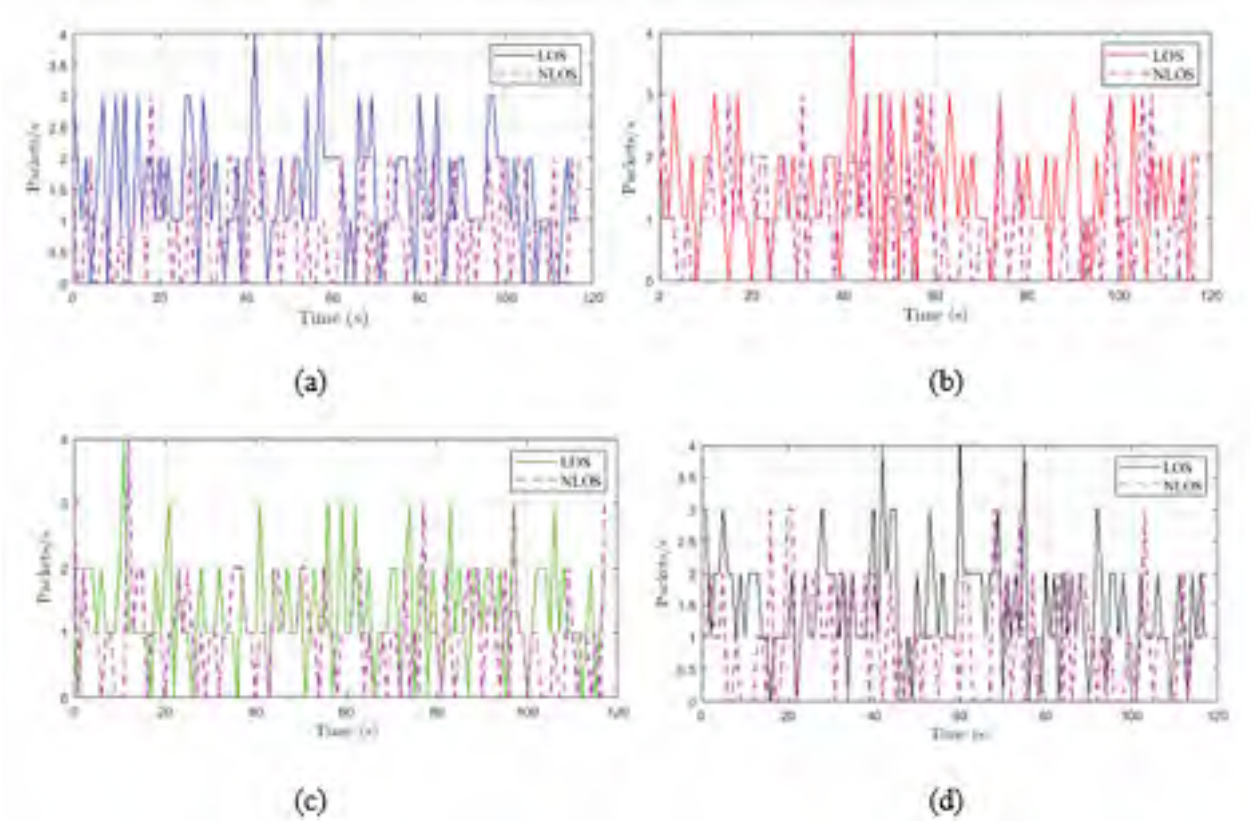

Figure 4.16: Overall rate of traffic for different voltages when the emitter and the receiver are both placed at 1 m from the source.

Examples of the results are depicted in Figs. 4.16 and 4.17. The traffic for 12 kV in the first situation is plotted in Fig. 4.16(a), while Fig. 4.16(d) represents the traffic for 18 kV. The first remark is that we receive more packets in LOS situation than NLOS for the two configurations. By analyzing the results in Fig. 4.16, we can note that we voltage does not affect the traffic of the received packets considerably. However, we have a degradation of performance when we are in a situation of NLOS. It means that the traffic of the LOS environment can be controlled and managed, whereas it is not possible for NLOS because of the events' randomness. In Table 4.8, we evaluate LOS and NLOS traffic averages for both configurations. On this table, we notice that the average μ_{LOS1} is around 1.5 regardless of the voltage level, while in NLOS, the average μ_{NLOS1} is approximately 1. We derive Δ which is the difference between the average in LOS and NLOS. This difference Δ_1 is equal to 0.5. However, for the second situation, we observe that the average traffic is roughly similar in LOS and NLOS, i.e., $\mu_{LOS2} \approx \mu_{NLOS2}$. This is well proved by the difference Δ_2, which is approximately equal to 0.1.

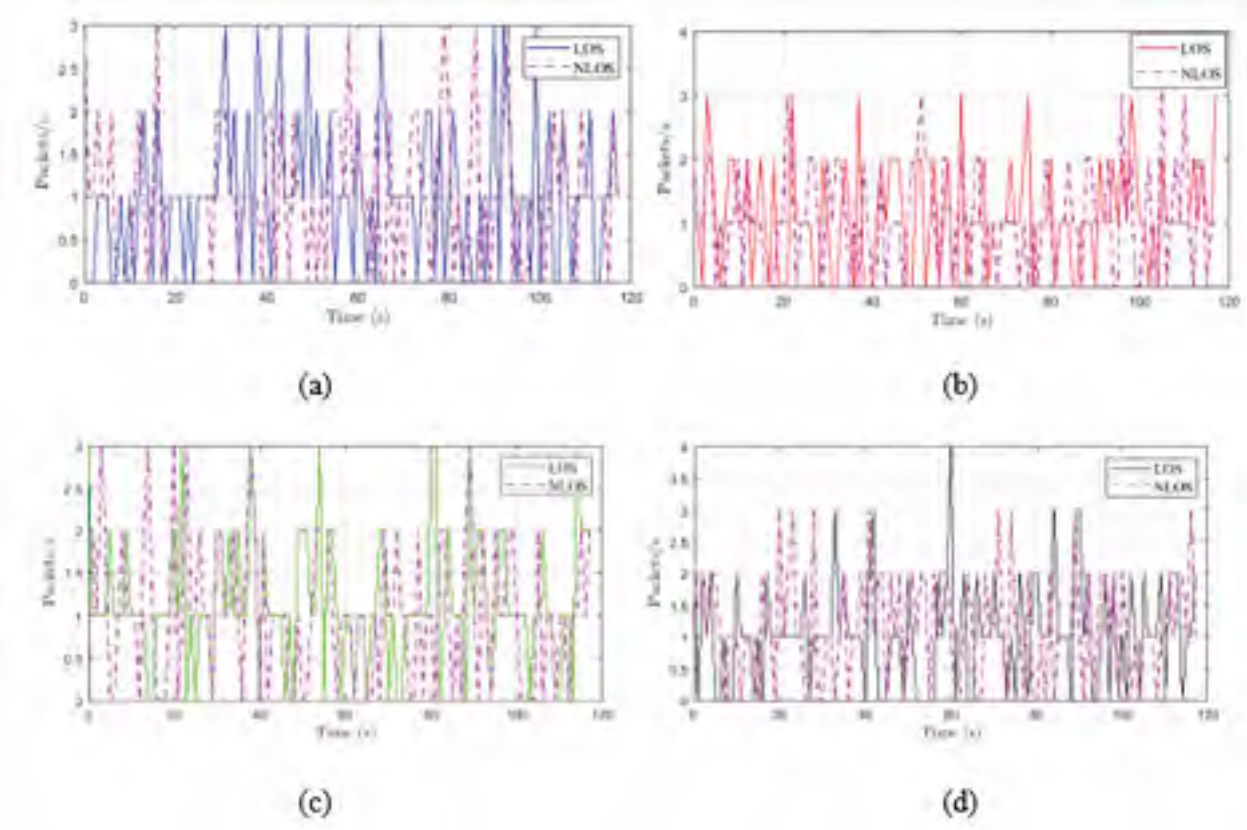

Figure 4.17: Overall rate of traffic for different voltages when the emitter is at 1.90 m from the source and the receiver at 1.80 m.

Table 4.8: Mean of the overall rate of traffic for all voltages in different configurations.

	Voltages			
Mean	**12 kV**	**14 kV**	**16 kV**	**18 kV**
μ_{LOS1}	1.5	1.42	1.31	1.48
μ_{NLOS1}	1.05	0.9	0.98	0.95
Δ_1	0.45	0.52	0.33	0.53
μ_{LOS2}	1.025	1.09	1.16	1.05
μ_{NLOS2}	0.84	1.08	1.05	1.14
Δ_2	0.18	0.01	0.11	-0.09

In order to analyze the traffic in depth, we now compute the PDR, which is the ratio between the received packets and the emitted ones. The following relation defines the PDR

Table 4.9: Packet delivery ratio for all voltages in different configurations.

	Voltages			
PDR	**12 kV**	**14 kV**	**16 kV**	**18 kV**
PDR_{LOS1}	0.45	0.43	0.39	0.44
PDR_{LOS2}	0.31	0.33	0.35	0.32
$PDR_{mean_{LOS}}$	0.38	0.38	0.37	0.38
PDR_{NLOS1}	0.25	0.3	0.29	0.28
PDR_{NLOS2}	0.32	0.32	0.31	0.34
$PDR_{mean_{NLOS}}$	0.28	0.31	0.3	0.31

$$PDR = \frac{\sum P_r}{\sum P_e} \tag{4.35}$$

where P_r and P_e are the received and the emitted packets, respectively. The obtained results are summarized in Table 4.9.

The information in Table 4.9 confirms the analysis made with the overall traffic rate. We can note that we received more packets for the LOS than the NLOS situation. Another remark is that we have approximately the same delivery ratio when considering the voltage. As can be seen, the $PDR_{mean_{LOS}}$ is ≈0.4, which means that 60% of packets are lost. However, for NLOS situation, 70% of packets are lost, which means that $PDR_{mean_{NLOS}}$ is ≈0.3. This was expected because when we use a transmission power of 12 dBm, it is demonstrated that with the SDR, the PDR is ≈0.5 in normal conditions, i.e., with a low length of packets (95 bytes) and a BPSK modulated with a rate of 1/2. To improve the PDR, we should increase the transmission power.

4.5.4.2.2 Average Delay

In this section, we compute the average delay versus the voltage for the overall situations. With Wireshark capture files, we have the information about the delta time from the previously captured frame and the time reference since the first frame. The average delay defines the average sum of the difference delay of each data packet received by the sink and the time the source sends a data packet. It is calculated as follows:

$$A_d = \frac{\sum_{i=1}^{N_P}(T_{ri} - T_{ei})}{N_P} \tag{4.36}$$

where T_{ri} is the time when a packet i is received by the sink, T_{ei} the time when a packet i is sent by the source and N_P corresponds to the total number of the received packets. In this case, we limit N_P to 100.

The obtained results are depicted in Figs. 4.18 and 4.19. The results for LOS configurations are in Fig. 4.18. As can be seen, the average delay increases with the distance. The average delay for the LOS configuration is equal to 0.4 s. We can also note that the 16

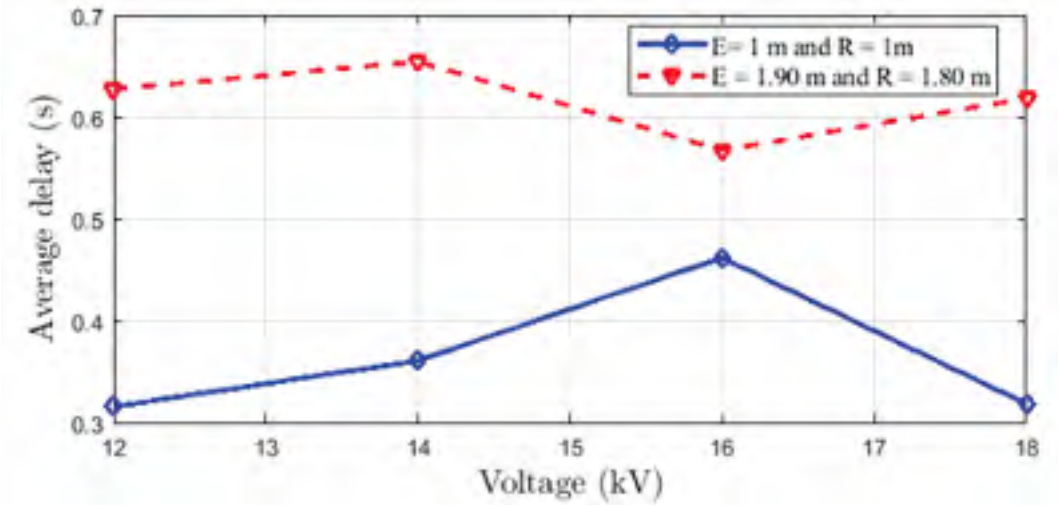

Figure 4.18: Average delay performance in LOS configuration.

kV have the most significant delay in the first case and the lowest one when we increase the distance. Another remark is that the average delay is less important for the LOS situation than the NLOS situation, as expected. This can be explained by the fact that in the NLOS situation, we have the delay due to the multi-path phenomenon.

The results for the NLOS configuration are depicted in Fig. 4.19. However, we can note that when the distance increases, the delay decreases, contrary to the LOS situation. The worst delay is obtained when the voltage is equal to 12 kV for 2 m between the transmitter and the receiver. This is expected and can be explained by the IO graphics in which the received packets are more important in LOS than those obtained in NLOS. The average delay for the NLOS situation in all configurations is equal to 0.67 s.

4.5.4.3 Bit Error Rate Computation

We now present and analyze the performance results concerning bit error rate versus the energy per bit to noise power spectral density ratio (EbNo) from the different scenarios described in Section 4.

4.5.4.3.1 Case 1: Emitter and receiver both placed at 1 m from the source

The results for this first experimental scenario are depicted in Figs. 4.20 and 4.21 for the LOS and NLOS situations, respectively. The first remark is that we note some irregularities in the curves. This can be explained by the critical aspect of the error performance of bounded distance for the RC decoder. Indeed, considering a received word, a bounded distance either procures a codeword or affirms a failure within an agreed radius of the received word. In the first case, an error of decoding appears when the codeword produced does not correspond to the sent codeword. In addition, as can be seen in Figs. 4.20 and

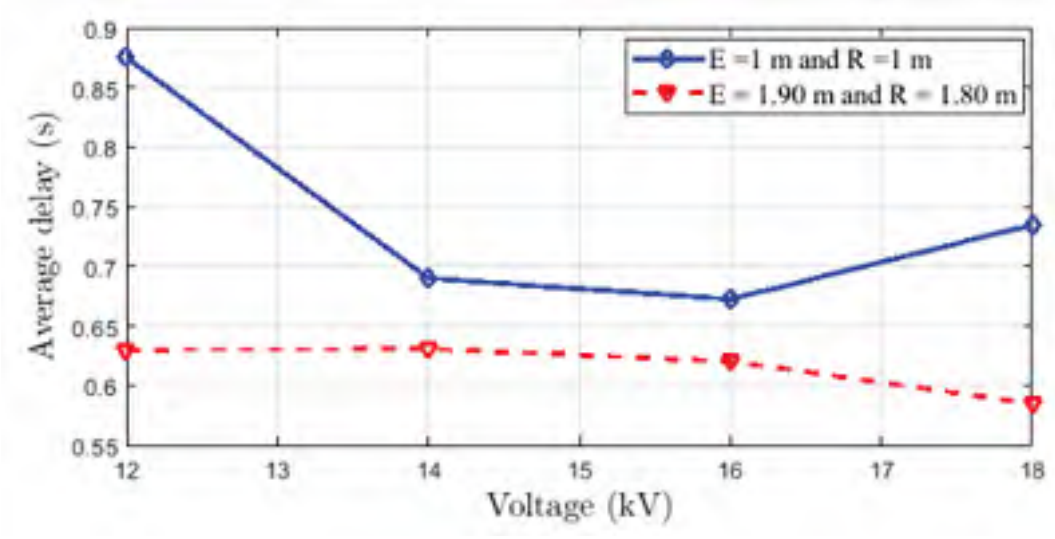

Figure 4.19: Average delay performance in NLOS configuration.

4.21, we have a degradation of performance when the impulsive noise is present whatever the voltage used. This degradation is more important in the LOS situation than the NLOS case. In Fig. 4.20, the voltage increase does not affect the BERs much. We have approximately the same performances both on 12 kV and 18 kV. A target BER of 10^{-4} is achieved at an EbNoof 3.2 dB when the channel is not affected by impulsive noise and approximately 6 dB in the presence of impulsive noise for all voltages. By comparing the results in Figs. 4.20 and 4.21, we can notice that the first case, i.e., the LOS case achieves the best performance. However, in Fig. 4.21, the performance degradation is not as remarkable without impulsive noise compared to the case of the presence of impulse samples. A target BER of 10^{-4} is achieved at an EbNo of 5.2 dB when the impulses are not affecting the channel. The worst performances are obtained by the presence of 12 kV noise. This is expected because the channel is more affected in this case, as confirmed by the PDR, which is 0.25.

4.5.4.3.2 Case 2: Emitter placed at 1.90 m from the source and the receiver at 1.80 m

We now increase the distance between the emitter and the source, as well as the receiver and the source. We have the same situations as for the first configuration, i.e., the LOS and NLOS cases. The obtained results are detailed Figs. 4.22 and 4.23. By comparing the results to those obtained in the first experimental scenario, we can notice that the increase of the distance does not affect the BERs much. This remark is also valuable for the voltage. However, we can note a degradation of performance when the impulsive noise is present whatever the voltage used compared to the absence of impulsive noise. In Figs 4.22, a target BER of 10^{-4} is achieved at an EbNo of 3.2 dB and 6 dB for the 12-kV

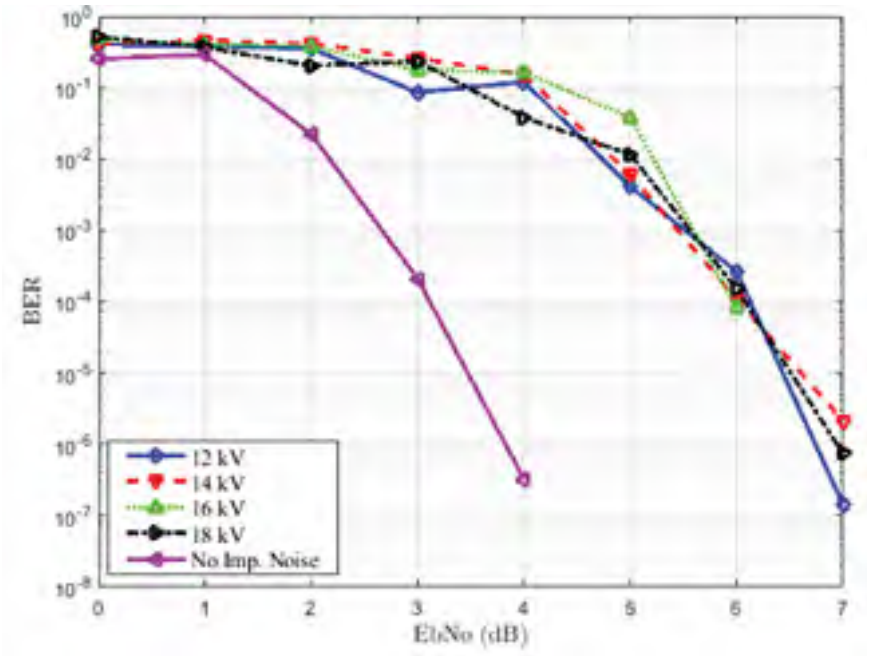

Figure 4.20: BER performance for different voltages in LOS situation.

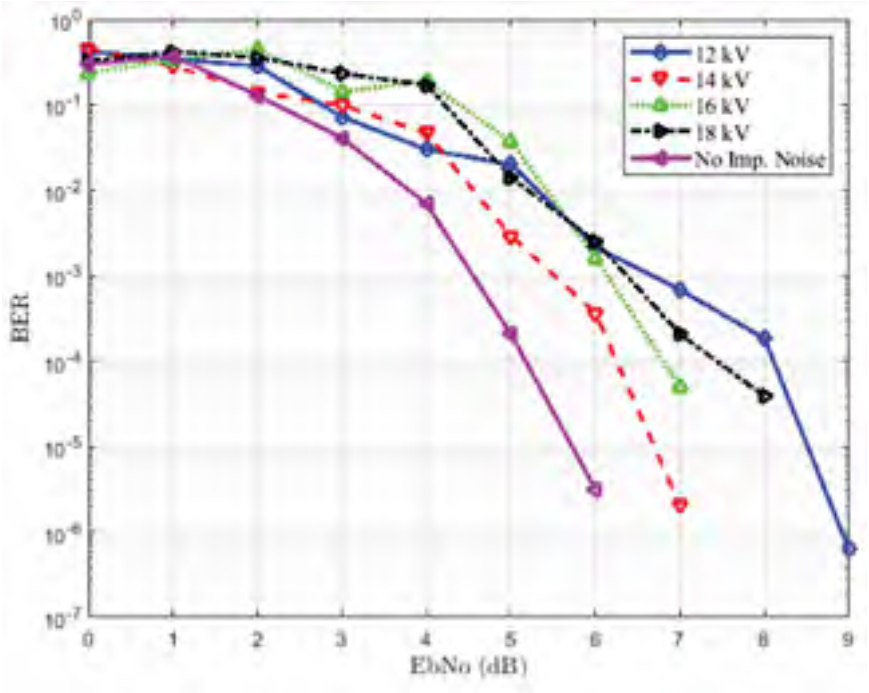

Figure 4.21: BER performance for different voltages in NLOS situation.

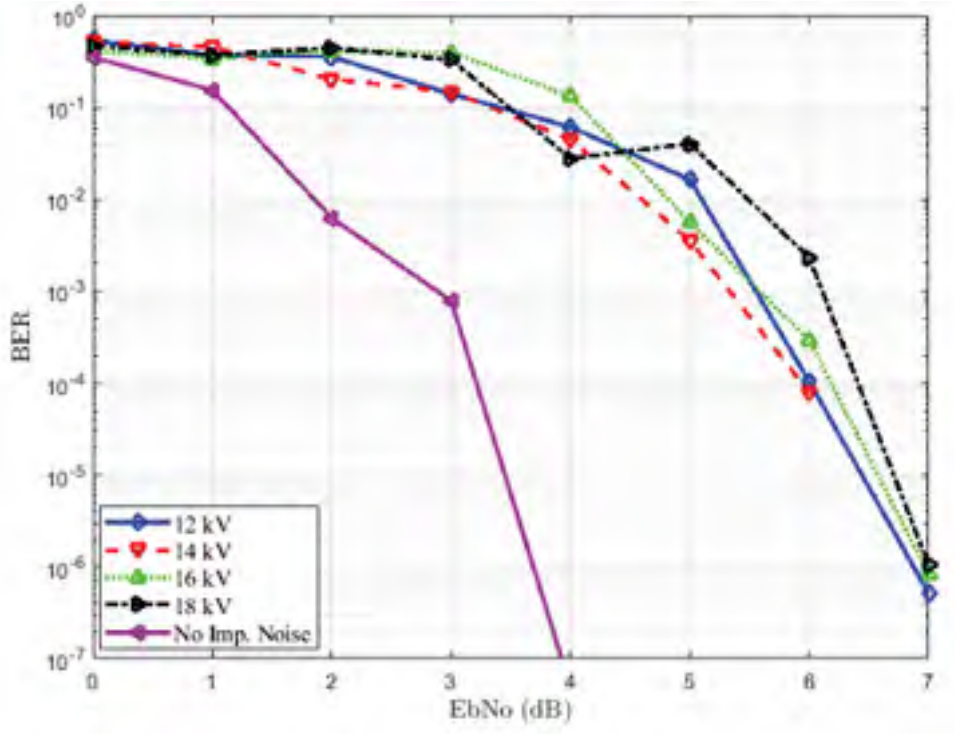

Figure 4.22: BER performance for different voltages in LOS situation.

and 14-kV noise samples, respectively. When the channel is affected by 16-kV and 18-kV noise, the target BER of 10^{-4} is approximately 6.2 and 6.5 dB, respectively. Nevertheless, without an impulsive noise, a target BER of 10^{-4} is achieved at an EbNo of 4.4 dB, as depicted in Fig. 4.23.. The degradation is approximately 2.1, 1.6, 2.1 and 3.1 dB for 12-, 14-, 16- and 18-kV impulsive noise, respectively.

4.5.5 Conclusion

In this section, we have investigated the validation of the proposed approach using GNU Radio and USRP. For this purpose, a new block namely *RC Encoder + Wifi Mapper* is entirely designed and implemented in GNU Radio. It is based on the previous implementation of $gr - ieee801.11$ made by Bloessel et al. Under different scenarios in a controlled laboratory, we have done several experiments in order to validate the proposed approach in the presence of impulsive noise. Using several metrics such as the packet delivery ratio, the average delay and the bit error rate, the performance of the system are evaluated. The obtained results are globally satisfactory and confirm the assertion made by simulations. However, based on the PDR results, we recommend using the transmission power of at least 15 dBm in order to benefit from a maximum packet delivery. As perspectives, it may be interesting to do other tests by further increasing the distance between the emitter and the source as well as the receiver and the source, and the voltage above 18 kV if possible.

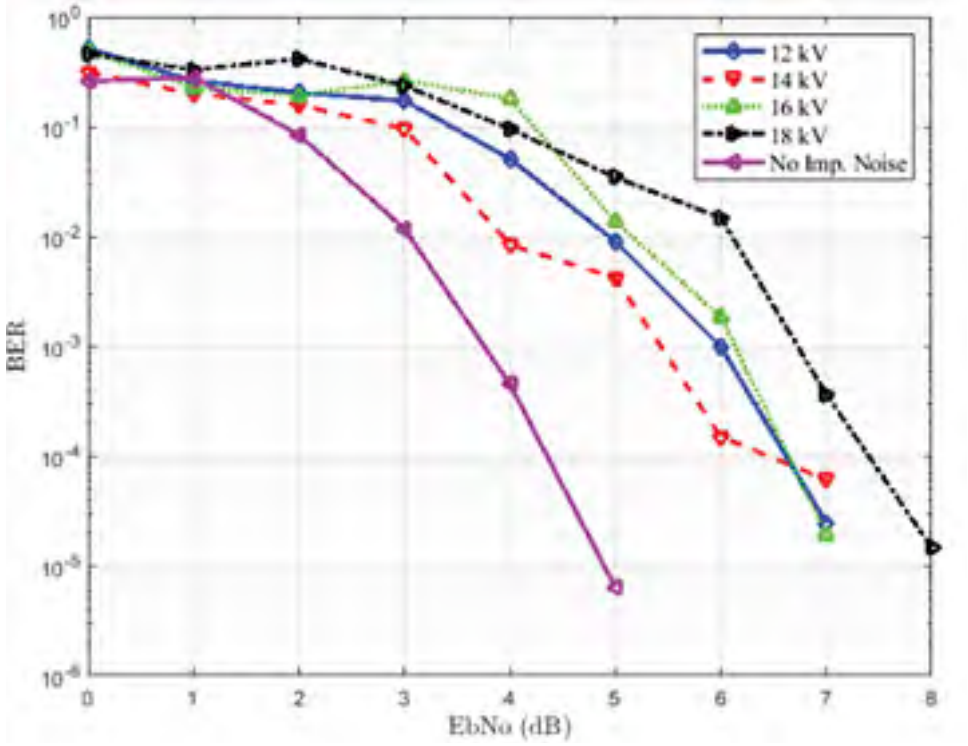

Figure 4.23: BER performance for different voltages in NLOS situation.

4.6 Comparison Between Simulations and Measurements

In this section, we examine the validity of our proposed physical layer. In the previous section, we performed simulations, and in this one, we have evaluated the performances empirically in a controlled laboratory. To validate or reject the results, we first set the difference between the simulation results and the empirical ones. Since in our experiments, we have evaluated two types of distances and four voltages, we consider the BER for LOS as the mean of all configurations, and the same procedure is applied for the NLOS situation. The results are presented in Table 4.10. After that, a Kolmogorov–Smirnov (K-S) test is done using the kstest2 function of MATLAB.The two-sample K-S test is a non-parametric hypothesis test that evaluates the difference between the distributions of the two sample data vectors over the range of x in each dataset. Mathematically, it can be written as follows

$$T_{K-S} = \sup_{x}(F_1(x) - F_2(x)) \tag{4.37}$$

where $F_1(x)$ and $F_2(x)$ correspond to the proportion of x_1 and x_2 values less than or equal to x, respectively. x_1 corresponds to a vector which contains the data of EbNo in LOS

Table 4.10: Summary of the performance for a target BER of 10^{-4}.

	LOS	**NLOS**
Simulations	5 dB	6.2 dB
Measurements	6.1 dB	6.9 dB
Δ_{SM}	1.1 dB	0.7dB

Table 4.11: K-S test between simulations and measurements.

Test	**LOS**	**NLOS**
K-S	logical 0	logical 0

situations for simulations and x_2 is also a data vector containing the values results of experiments. For the NLOS situation, the same procedure is applied during the K-S test.

In Table 4.10, we can notice that the difference between the simulation results and the experimental results for a target BER of 10^{-4} is quite small for the LOS and NLOS cases. We have a difference of 1.1 dB for the LOS situation, whereas for NLOS, it is 0.7 dB. These results validate the implementation in GNU Radio and confirm that our proposed approach is very efficient in mitigating the bursty nature of impulsive noise while having quite a low level of complexity. The K-S test is also another confirmation of this assertion. For LOS and NLOS, the return value of zero indicates that the test does not reject the null hypothesis at a 5% significance level. In other words, the results of the K-S test validate that the measurement results and the simulation results come from the same distribution at a confidence interval of 95%.

4.7 Conclusion

In this chapter, we first describe the approaches to reduce the effect of impulse noise on wireless communications. Interesting techniques are proposed in the literature. They are divided into three categories. The first method concerns the use of error-correcting codes such as RS codes, Turbo codes, and LDPC. The second is the approaches based on signal processing in the time and frequency domain like clipping, blanking, Matsuo's algorithm. The last category concerns single-carrier and multi-carrier modulations. Significant performance are achieved with these techniques. However, some techniques such as single carrier modulations are not robust on their own. The clipping or blanking is quite reliable but must be combined with others which generates a certain complexity. The best performing error-correcting codes are RS, LDPC, and Turbo codes. However, LDPC and Turbo codes are greedy regarding processing. Based on the performance of each method, we propose a straightforward and robust technique to achieve the objectives concerning BER and PER. It is a physical layer based on the concatenation of error correcting codes, in this case, the

RC and the CC with the OFDM modulation. The rank metric is well known in the field of cryptography, but its proof in the field of telecommunications by offering robustness against impulsive noise while having low complexity. OFDM modulation is well known for its performance to combat fading. Using real measurements of impulsive noise, the impact of RC, LRPC, and polar codes is evaluated regarding BER and PER in a realistic multi-path channel. Globally, the obtained results are satisfactory. We obtain an essential gain for the three codes compared to the uncoded case. These gains are at least equal to 10 dB at target BER of 10^{-5}. BER of RC is achieved when EbNo is equal to 5.5 dB. By comparing the three coding schemes, we have seen that the RC and LRPC codes are more efficient than the polar code in this multi-path channel. The RC code has a gain of 4 dB compared to the polar code when a target BER of 10^{-5} is considered. Using PER metric, we also observe that the rank metric code is more efficient than the polar code and LRPC. Globally, the results show that using this coding scheme is very efficient in mitigating the bursty nature of impulsive noise while having quite a low level of complexity. Since the first validation is made only by simulations, we design and implement a new block namely $RC\ Encoder + Wifi\ Mapper$ in GNU Radio for experimental validation. It is based on the previous implementation of $gr - ieee802.11$ made by Bloessel et al. Under different scenarios in a controlled laboratory, we have done several experiments in order to validate the proposed approach in the presence of impulsive noise. Using several metrics such as the packet delivery ratio, the average delay, and the bit error rate, the performance of the system are evaluated. After showing that using this coding scheme is very efficient in mitigating the bursty nature of impulsive noise by simulations, we then confirm that the same performance are maintained even with various impulsive voltages and experimental scenarios, which confirms the high performance of the proposed approach.
The proposed approach gives excellent performance concerning BER and makes it possible to meet the requirements of SG applications at HV substations. Even considering the large dimensions that can have some substations, this solution also remains valid. However, if the number of sensors becomes considerable, this solution becomes limited given the energy constraints that can have the sensors. It allows us to consider another solution based on a multi-antenna cooperative system which is presented in the next chapter.

Chapter 5

Cooperative Closed-loop MIMO Systems

Contents

5.1 Introduction

In Chapter 3, we have shown the limitations of existing protocols in the presence of impulse noise. A technique for improving the quality of services and performance has been proposed in Chapter 4. This technique based on the concatenation of FEC and the OFDM modulation makes it possible to have a system that is both simple and robust while ensuring the specifications required to satisfy SGs applications.
However, as discussed in Chapter 1, Hydro-Quebec's HV substations can be very large in size up to 1 km^2. The first solution proposed, therefore, becomes limited because the energetic constraints of the WSNs are always present and also by the distance, the performance can be deteriorated.

To avoid the constraints mentioned above, a solution has been studied for a few years. It is a transmission architecture based on the use of MIMO. It allows to reach at the same time very high spectral efficiencies and to fight effectively against the fading of the signal. The general idea is to take advantage of the spatial dimension of the channel and exploit multiple paths rather than delete them. MIMO systems are very efficient because they can use all the techniques of SISO transmissions, in addition to the techniques of their own. MIMO systems have several advantages. These advantages can be used to reduce the transmission energy in the WSNs for the same reliability of the transmission and for the same flow rate. However, the limited size of the sensor does not make it possible to directly apply the multi-antenna technique to the sensor networks.

To avoid the constraints mentioned above, the use of MIMO cooperative techniques [134-138] may be an obvious solution enabling nodes to be grouped in a set of virtual antennas. Closed-loop cooperative transmission ensures that the source node cooperates with the idle neighbors to provide spatial diversity. Since the distance between nodes is less than the distance between the cluster and the data gathering node (DGN), each cooperating node, then precodes the data before it transmits over the different sub-channels to the receiver where data is combined and detected.

In the impulsive noise environments, we elaborate a space-sensitive technique using MIMO, which is particularly well suited in these usually challenging situations. We assume the availability of channel state information (CSI) at the transmitter to achieve typical MIMO system gains in ad-hoc mode. In this chapter, we show that more than 10 dB gains are obtained with the most efficient system that we propose for achieving SG application requirements. On the one hand, the results illustrate that the $\max - d_{min}$ criterion associated with the RC coding scheme is especially adapted to minimize the BER when a maximum likelihood (ML) receiver is employed. On the other hand, it is shown that a node selection technique can reduce the required nodes transmission energy.

The rest of this chapter is detailed as follows. Section 2 reviews the cooperative techniques found in WSNs. Section 3 is about MIMO systems while section 4 presents the cooperative MIMO techniques. Section 5 shows our contribution and deals with cooperative coded-MIMO in a perturbed environment. It first reviews the existing approach presented in [138]. Secondly, the system model that we propose are overviewed. Finally, the

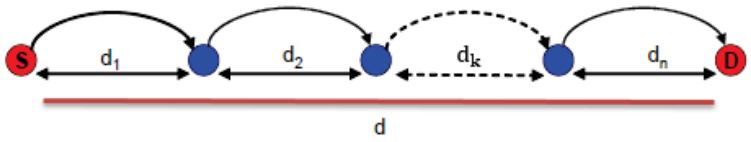

Figure 5.1: Multi-hop technique with n hops.

performance regarding BER and energy consumption are presented. Section 6 concludes this chapter.

5.2 Cooperative Techniques in WSN

The major constraint in a WSN is the power consumption. The sensors nodes are supplied by small batteries which are generally nonrefillable or replaceable for a long time. In several WSN purposes, the system seems to be functioning while some essential nodes still have energy. Consequently, improving the network lifetime by reducing power consumption is a substantial design concern for these systems. Since all layers in the protocol topology participate actively to power consumption in WSN communication, reducing energy necessitates constrained approach beyond all layers from high to low layers. Energy consumption in the physical layer has a crucial role where energy consumption for transmission is the principal part of long or medium range communication. Cooperation techniques benefit to diminish transmission energy consumption in several ways. Three kinds of cooperation techniques are studied in this section such as relaying, multi-hop, and cooperative MIMO transmissions.

5.2.1 Multi-Hop Techniques

For a multi-hop transmission, the received signal issued from the previous hop is decoded by the hop and transmitted to the next one. Fig. 5.1 depicts an example of a multi-hop system model. Rather than relaying the data over a longer distance from the node S to the destination D, the route is set into multiple single communications. Let us define the multi-hop system with n hops from the source node S to the destination D composed of $n-1$ cooperating nodes as depicted in Fig. 5.1. The distance separating the destination D and the source S is given by

$$d_{SD} = \sum_{k=1}^{N} d_k \tag{5.1}$$

where d_k corresponds to the distance between two nodes k and $k+1$.
In multi-hop transmission, the energy consumption can be significantly reduced if only the transmission energy is considered. Nevertheless, for short-range communication, a direct transfer shall be more effective if the circuit energy is taken into consideration.

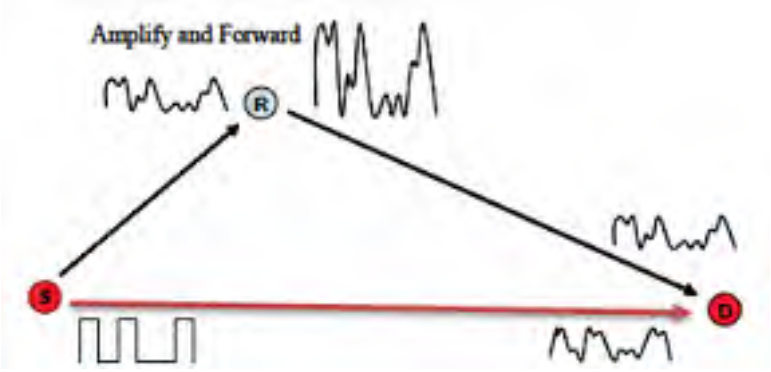

Figure 5.2: Amplify-and-Forward technique in a relay network.

5.2.2 Relay Cooperative Techniques

5.2.2.1 Amplify and Forward (AF)

Amplify and Forward (AF) [139,140] is part of the classic and most popular cooperation techniques [141] as depicted in Fig. 5.2. The source transmits the signal first, and the relay amplifies the information and transmits it to the second destination. Therefore, the destination obtains two copies of an identical signal. The signal copy sent by the relay is expressed as follows

$$X_R^{AF}[n] = \alpha Y_R^{AF}[n] \tag{5.2}$$

where $X_R^{AF}[n]$ represents the symbol sent by the relay R, $Y_R^{AF}[n]$ corresponds to the signal emitted by the source and received by the relay and α is the amplification coefficient. This strategy can be seen as communication from two different antennas. On the other hand, the relay amplifies the received signal and at the same time the contained noise. Although the AF cooperation scheme increases noise, the destination node D receives two copies of the signal x throughout the source component and relay link. There are several combination strategies to combine two signals such as the equal-gain combining (EGC), maximal ratio combining (MRC) and selection combining (SC). The MRC is an optimal technique which maximizes the global signal-to-noise ratio.

5.2.2.2 Decode and Forward (DF)

The first part of the transmission for Decode-and-Forward (DF) [142] remains identical to Amplify and Forward since the source node sends the data, the neighboring and the destination "listen." Then, the relays manage to decode the signal, re-encode it, and essay to transmit it to the destination. In this situation, the noise is not amplified as for AF, and a novel form of the signal is transmitted. The signal transmitted by R is given by the expression below

$$X_R^{DF}[n] = \hat{X}_R^{DF}[n] \tag{5.3}$$

such as $\hat{X}_R^{DF}[n]$ is the decoded and re-encoded symbol of the received signal.

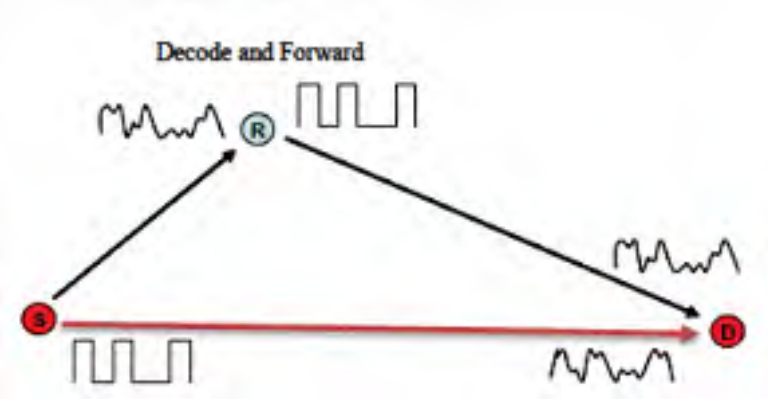

Figure 5.3: Decode-and-Forward technique in a relay network.

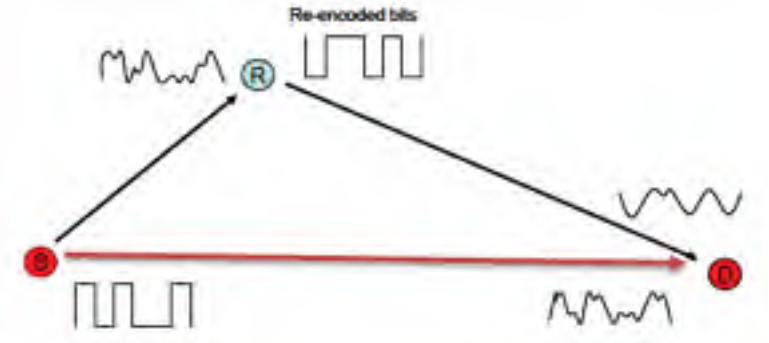

Figure 5.4: Re-Encode and Forward scheme in a relay network.

5.2.2.3 Re-Encode and Forward (RF)

Re-Encode-and-Forward (RF) is another more complex relay technique that allows both diversity and gains coding. RF [143] is a strategy which merges relay cooperation and channel encoding. The assumption is that the relay node decodes the received codewords, re-encodes and transmits the codewords over an independent fading path. This cooperation technique improves the efficiency contrary to the two preceding relay methods. However, RF expends excellent encoding and decoding complexity.

5.2.3 Parallel Relay Network

The different schemes presented above were made employing on a relay node network. In this technique, the transmission range can be spread because of the more transmission energy from relay nodes and the diversity gain. This method can be expanded to a parallel relay system in which several relay nodes are employed to accept the information and after to re-transmit to the final destination D. This structure namely "parallel relay" network in [144], [145] is depicted in Fig. 5.5. Let us define a parallel relay transmission made up with N transmitting nodes as illustrated in Fig. 5.5. Let us define a parallel relay transmission

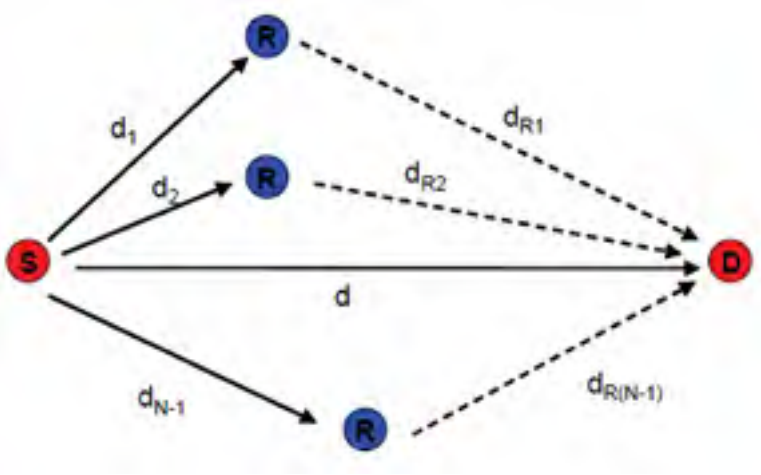

Figure 5.5: Parallel relay Network transmission technique.

made up with N transmitting nodes as illustrated in Fig. 5.5 such as $N-1$ nodes are the relays. During the first time slot, the node S sends a signal vector v to all the relays and the final node D. In the relay node k, the received signal denoted $r_{S,R}$ is expressed as follows

$$r_{S,R}^{k} = \alpha_{S,R}^{k} v + n_{S,R}^{k} \tag{5.4}$$

where $k = 1, 2, \ldots, N-1$, $\alpha_{S,R}^{k}$ corresponds to the fading coefficients between the source$S$ and the k^{th} relay node, $n_{S,R}^{k}$ represents a white Gaussian noise with zero mean μ_0 and unit variance (N_0).
Secondly, each R_k transmits its signal to the final destination D respectively. Finally, the node D receives from the $N-1$ neighboring nodes $N-1$ independent fades to transmit signals. The multiple relay system can employ the techniques mentioned above such as AF and DF for the received signal retransmission to the node D. Notice that the diversity gain increases with the number of relay nodes. In ideal circumstances, the diversity gain of a parallel relay network with N nodes can be considered as the MRC technique with N reception nodes [141].

5.3 MIMO Systems

Transmissions via the mobile radio channel are heavily penalized by signal fading due to both multi-path and inter-symbol interference. To overcome these disadvantages, a solution has been studied for a few years. These architectures, namely MIMO, allow us to reach at the same time very high spectral efficiency and to fight effectively against the fading of the signal. The general idea is to take advantage of the spatial dimension of the channel and exploit multiple paths rather than deleting them. MIMO systems are very efficient because they can use all the techniques of SISO transmissions with additional features. MIMO systems have several advantages. These advantages can be employed to decrease

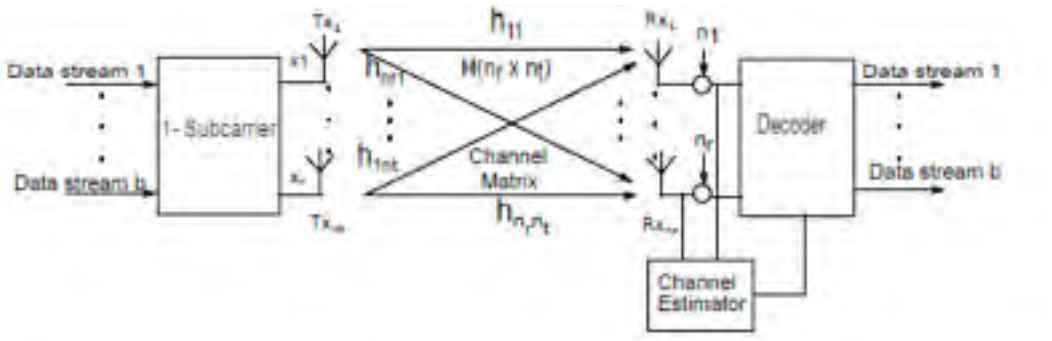

Figure 5.6: Open-loop MIMO System [55].

the transmission energy in the sensor networks for the same reliability of the transmission and the same rate. SISO systems use two diversity techniques: time diversity and frequency diversity, while MIMO systems can adopt both of these forms of diversity in addition to the spatial diversity. They can be separated according to whether the MIMO system knows the state of the channel or CSI (Channel State Information) to the transmission ($T_x - CSI$) and reception ($R_x - CSI$), or only at the reception. These two systems are respectively called the open-loop and the closed-loop MIMO systems and are detailed in the sections below.

5.3.1 Open-loop MIMO Systems

Open-loop MIMO systems refer to systems considering only the CSI on the receiver side ($R_x - CSI$) as depicted in Fig. 5.6. The principle is based on Orthogonal Space-Time Block Code (OSTBC) [146]. This coding adds redundancy to the transmitted binary data to increase spatial diversity and to avoid fading specific to the mobile radio channel. The well-known code is Alamouti code which employs two transmit antennas.

Alamouti Codes

Alamouti Code is a typical example of OSTBC. It is named as Alamouti Code, named after the person who invented this method [147]. It is a special kind of technique that is used to transmit signals through multiple antennas. In this code, the same pair of data is transmitted via two T_x antennas twice over two symbol period. It is defined by

$$\mathbf{C}_2 = \begin{pmatrix} s_1 & -s_2^* \\ s_2 & s_1^* \end{pmatrix} \tag{5.5}$$

where s_1 and s_2 are the symbols to be transmitted.

$$C_2 C_2^* = C_2^* C_2 = (|s_1|^2 + |s_2|^2) \begin{pmatrix} 1 & 0 \\ 0 & 1 \end{pmatrix} \tag{5.6}$$

For respecting the average total power stress transmitted P_0 on all the antennas during a symbol time, it is necessary to multiply the code by the constant $(\sqrt{P_0/2})$. Indeed, the input-output relationship is given in a matrix form and expressed as follows

$$\mathbf{Y} = \sqrt{\frac{P_0}{2}}\mathbf{H}C_2 + \mathbf{n} \tag{5.7}$$

where $Y[n_r \times 2]$ is the matrix of the received signal; $n[n_r \times 2]$ is the noise matrix whose components are generally modeled by the iid AWGN. The received signals are then

$$\begin{aligned} y_1^j &= \sqrt{\frac{P_0}{2}}(\tilde{h}_{1,j}s_1 + \tilde{h}_{2,j}s_2) + n_1^j \\ y_2^j &= \sqrt{\frac{P_0}{2}}(\tilde{-h}_{1,j}s_2^* + \tilde{h}_{2,j}s_1^*) + n_2^j \end{aligned} \tag{5.8}$$

where $j = 1, \ldots, n_r$, y_1^j and y_2^j are the desired signals of the receive antenna j during the first and second symbol periods respectively, $\tilde{h}_{i,j}$ is the channel complex gain between the transmit antenna i and receive antenna j, n_1^j and n_2^j are the additive noise of the receive antenna j during the first and second symbol periods respectively. The receiver estimates the elements of the channel matrix and recombines the received signals.
While developing the equation 5.8,

$$\begin{cases} \hat{y}_1 = y_1^j = \sqrt{\frac{P_0}{2}}(\sum_{j=1}^{n_r} ||\tilde{h}_{1,j}||^2 + ||\tilde{h}_{2,j}||^2)s_1 + \sum_{j=1}^{n_r} \tilde{h}_{1,j}^* n_1^j + \tilde{h}_{2,j}(n_2^j)^* \\ \hat{y}_2 = y_2^j = \sqrt{\frac{P_0}{2}}(\sum_{j=1}^{n_r} ||\tilde{h}_{1,j}||^2 + ||\tilde{h}_{2,j}||^2)s_2 + \sum_{j=1}^{n_r} \tilde{h}_{2,j}^* n_1^j - \tilde{h}_{1,j}(n_2^j)^* \end{cases} \tag{5.9}$$

where $(\sum_{j=1}^{n_r} ||\tilde{h}_{1,j}||^2 + ||\tilde{h}_{2,j}||^2) = ||\mathbf{H}||_{\mathbf{F}}^{\mathbf{2}}$ corresponds to the Frobenius of matrix $\mathbf{H}$ defined as

$$||\mathbf{H}||_{\mathbf{F}}^{\mathbf{2}} = \mathbf{trace}(\mathbf{H}\mathbf{H}^*) = \mathbf{trace}(\mathbf{H}^*\mathbf{H}) = \sum_{\mathbf{i=1}}^{\mathbf{n_t}} \sum_{\mathbf{j=1}}^{\mathbf{n_r}} |\tilde{\mathbf{h}}_{\mathbf{1,j}}|^{\mathbf{2}} \tag{5.10}$$

The two signals can be now expressed as follows

$$\begin{cases} \hat{y}_1 = \sqrt{\frac{P_0}{2}}||\mathbf{H}||_{\mathbf{F}}^{\mathbf{2}}\mathbf{s_1} + \hat{\mathbf{n}}_{\mathbf{1}} \\ \hat{y}_2 = \sqrt{\frac{P_0}{2}}||\mathbf{H}||_{\mathbf{F}}^{\mathbf{2}}\mathbf{s_2} + \hat{\mathbf{n}}_{\mathbf{2}} \end{cases} \tag{5.11}$$

where $\hat{n}_1$ and $\hat{n}_2$ are the combined noise. Notice that each signal $\hat{y}_i$ only depends on the symbol s_i and can thus employ in its evaluation. Alamouti code decouples symbols and reduces decision tests in the ML receiver $(2 \times Mtests)$. Indeed, the system can be seen as two SISO systems in parallel. Furthermore, the same gain $\sqrt{\frac{P_0}{2}}||\mathbf{H}||_{\mathbf{F}}^{\mathbf{2}}$ is ensured when

the channel is unknown. This particularity allows the code to be robust with considering the channel and also to ensure a maximum diversity order equivalent to the product of the transmit and receive antennas ($n_r \times n_t$) [148].
However, Alamouti code is only adapted to the systems with two transmit antennas. Tarokh et al. [148], [149] generalized OSTBC code whatever n_t. The principle is to consider a train of N_S symbols which the code will transmit in successive bursts on N_P symbol periods such as the transmitted vectors must be orthogonal. The generated code is a matrix whose two dimensions are space and time $[n_t \times N_P]$. Then, the receiver recombines the received samples after channel estimation and obtains the resulting signals depending only on one emitted symbol. Thus, the symbol estimates are decoupled.
There are other types of STBC codes such as lattice space-time codes or Space-Time Trellis Code (STTC) [148] and quasi-orthogonal codes (QSTBC) [150].

5.3.2 Closed-loop MIMO Systems

In these systems, the channel is known at the transmitter ($T_x - CSI$) and the reception ($R_x - CSI$). MIMO systems, according to their construction, offer many advantages. To further increase performance in regarding robustness, throughput, quality of service, precoding before transmission can be applied. The precoder optimally exploits the CSI to jointly optimize the transmitter and the receiver of a transmission system.

5.3.2.1 Linear Precoder

For a MIMO channel with no delay spread, the following linear system equation applies

$$\mathbf{y} = \mathbf{HFs} + \mathbf{n} \tag{5.12}$$

where,

$$\mathbb{E}\{\mathbf{ss}^*\} = \mathbf{I}, \mathbb{E}\{\mathbf{nn}^*\} = N_0\mathbf{I}$$

$\mathbf{y}$ is the $b \times 1$ received vector, $\mathbf{s}$ is the $b \times 1$ transmitted symbol vector, $\mathbf{n}$ is an $n_r \times 1$ additive noise vector, $\mathbf{H}$ is the channel matrix of $n_r \times n_t$, here n_r and n_t are the number of the receive and transmit antennas respectively; $\mathbf{F}$ is the precoder matrix.
The full-channel state information (FCSI) permits the precoder to diagonalize the channel into b parallel SISO channels. If E_T is the total available power, the following power constraint is applied to the transmitter:

$$\text{trace}[\mathbf{FF}^*] = E_T \tag{5.13}$$

The precoding and decoding matrices are separated into two components as $\mathbf{F} = \mathbf{F}_v\mathbf{F}_d$ and $\mathbf{G} = \mathbf{G}_v\mathbf{G}_d$, respectively. The unitary matrices, $\mathbf{G}_v$ and $\mathbf{F}_v$, derived from the singular value decomposition (SVD) of $\mathbf{H}$, diagonalize the channel and decrease the scope of 2. Hence, the received symbol in (6) becomes

$$\mathbf{y} = \mathbf{G}_d\mathbf{F}_d\mathbf{H}_v\mathbf{s} + \mathbf{G}_d\mathbf{n}_v \tag{5.14}$$

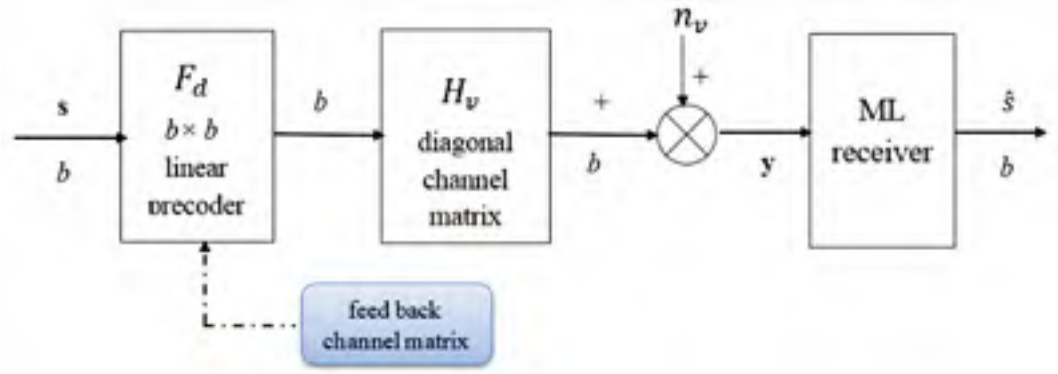

Figure 5.7: Equivalent MIMO system with a linear precoder in a virtual channel.

such as $\mathbf{H}_v = \mathbf{G}_v\mathbf{H}\mathbf{F}_v = \text{diag}(\beta_1, \ldots, \beta_b)$ is the virtual channel matrix, β_i denote the gains of the sub-channel sorted in decreasing structure, and $\mathbf{n}_v = \mathbf{G}_v\mathbf{n}$ is the $b \times 1$ channel virtual noise. Since the ML detection will be used in the following sections, the decoding matrix $\mathbf{G}_d$ does not influence the efficiency and is considered to be $\mathbf{I}_b$.
Linear precoding and decoding techniques are scalable to the number of antennas and are easier to perform compared to non-linear methods. The diagonal matrix aims to maintain parallel and independent paths structure. It can be noticed that the diagonal precoder has the advantage of reducing the ML decoding complexity by $b \times M$. This solution means to find the distribution of power thanks to the coefficients f_i^2 by optimizing a precise and relevant criterion. For this purpose, we distinguish several precoders depending on the optimized criterion:

- Water-filling (WF) precoder which maximizes the capacity;
- max $-SNR$ or beamforming precoder [151] maximizes the SNR at the reception;
- max $-\lambda_{min}$ maximizes the minimum singular value (SV) of the channel matrix;
- Minimum mean square error (MMSE) precoder [152] minimizes the mean square error;
- max $-d_{min}$ maximizes the minimum Euclidean distance. Moe detail are given in the following section.

5.3.2.1.1 Minimum Euclidean Distance Precoding: max$-d_{min}$

The precoder max$-d_{min}$ consists of the maximization of the minimum Euclidean distance d_{min} between the signal items at the receiver.
Therefore, its optimization problem entails finding the matrix $\mathbf{F}_d$ which maximizes the d_{min} criterion

$$d_{\min} = \min_{(\mathbf{s_k}-\mathbf{s_l}),\mathbf{k}\neq\mathbf{l}} \|\mathbf{H}_v\mathbf{F}_d(\mathbf{s_k} - \mathbf{s_l})\| \tag{5.15}$$

Let us define $\mathbf{e} = (\mathbf{s}_k - \mathbf{s}_l)$, the difference between possible transmitted vectors. Thus, the $d_{\min}$ criterion can be expressed as

$$d_{\min} = \min_{(\mathbf{s_k}-\mathbf{s_l})} \|\mathbf{H}_v \mathbf{F}_d \mathbf{e}\| \tag{5.16}$$

Since the ML detection will be considered, this criterion is well suited because the probability of symbol errors relies on the minimum Euclidean distance.
However, determining the solution of $\mathbf{F}_d$ is complicated due to the large solutions space and the alphabet symbols which it processes. For this purpose, we propose to simplify the technique and derive a solution for $b = 2$ virtual channels. Hence, the virtual channel matrix can be expressed as

$$\mathbf{H}_v = \begin{pmatrix} \sqrt{\beta_1} & 0 \\ 0 & \sqrt{\beta_2} \end{pmatrix} = \sqrt{2\beta} \begin{pmatrix} \cos\alpha & 0 \\ 0 & \sin\alpha \end{pmatrix} \tag{5.17}$$

where α is the channel angle, and $\alpha \in [0, \frac{\pi}{4}]$, $\beta = \frac{\beta_1+\beta_2}{2}$. Parameter β acts as a scaling factor and does not influence d_{min} optimization. This solution does not rely on the SNR but is based on the channel angle α.
The SVD applied to the matrix precoder is as follows

$$\mathbf{F}_d = \mathbf{Q}\mathbf{\Sigma}\mathbf{R}^* \tag{5.18}$$

where $\mathbf{\Sigma}$ is the diagonal matrix, $\mathbf{Q}$ and $\mathbf{R}$ are $b \times b$ unitary matrices.
Recall that the power constraint at the transmit antennas always remains, the $\mathbf{\Sigma}$ must fulfill the constraint, too, and is derived as

$$\mathbf{\Sigma} = \sqrt{E_T} \begin{pmatrix} \cos\gamma & 0 \\ 0 & \sin\gamma \end{pmatrix} \tag{5.19}$$

with $0 \leq \gamma \leq \frac{\pi}{4}$.
Since the matrix $\mathbf{R}^*$ does not influence the singular values, they can be derived from $\mathbf{H_v Q \Sigma}$. The largest singular values are obtained when $\mathbf{Q} = \mathbf{I_2}$.

Proof of $\mathbf{Q} = \mathbf{I_2}$:
Considering the form of the unitary matrix of $\mathbf{Q}$

$$\mathbf{Q} = \begin{pmatrix} (\cos\theta)e^{i\theta_1} & (\sin\theta)e^{i\theta_3} \\ -(\sin\theta)e^{i\theta_2} & (\cos\theta)e^{i\theta_4} \end{pmatrix} \tag{5.20}$$

with the constraints

$$(\theta_1 + \theta_4) = (\theta_2 + \theta_3) \mod 2\pi. \tag{5.21}$$

The angle $\theta \in 0 \leq \theta < \pi/2$.
Recall that the single values are null or (positive and real), and the determinant of a unitary

matrix = 1. We define $\mathbf{U\Lambda V}^*$ as the single value decomposition of $\mathbf{H}_v\mathbf{Q\Sigma}$ and σ_k, the diagonal components of $\mathbf{\Lambda}$. The product of SV is not based on $\mathbf{Q}$. We can note

$$\begin{aligned}\sigma_1\sigma_2 =&|\det(\mathbf{\Lambda})| = |\det(\mathbf{U\Lambda V}^*)| = |\det(\mathbf{H_vQ\Sigma})| \\ &= |\sqrt{(\beta_1\beta_2)}E_T\cos\gamma\sin\gamma\det(\mathbf{Q})| = \sqrt{(\beta_1\beta_2)}\mathbf{E_T}\cos\gamma\sin\gamma.\end{aligned} \tag{5.22}$$

Moreover, we have

$$\begin{aligned}\sigma_1^2+\sigma_2^2 &= \text{trace}(\Lambda^2) = \text{trace}(\mathbf{U\Lambda V}^*\mathbf{V\Lambda U}^*) \\ &= ||\mathbf{U\Lambda V}^*||_{\mathbf{F}}^{\mathbf{2}} = ||\mathbf{H_vQ\Sigma}||_{\mathbf{F}}^{\mathbf{2}}.\end{aligned} \tag{5.23}$$

Therefore, the phases of the constituents of $\mathbf{Q}$ do no impact on $\sigma_1^2+\sigma_2^2$. Eventually, we deduce that the single values do not rely on the phases of the constituents of $\mathbf{Q}$. Thus, we just assume real matrices $\mathbf{Q}$, whose typical structure is

$$\mathbf{Q} = \begin{pmatrix}\cos\theta & \sin\theta \\ -\sin\theta & \cos\theta\end{pmatrix} \tag{5.24}$$

where $0 \le \theta < \pi/2$.
We now examine the sum of the square single value of $\mathbf{H}_v\mathbf{Q\Sigma}$

$$\begin{aligned}\sigma_1^2+\sigma_2^2 &= ||\mathbf{H_vQ\Sigma}||_{\mathbf{F}}^{\mathbf{2}} = \text{trace}(\mathbf{H_vQ\Sigma\Sigma Q}^*\mathbf{H_v}) \\ &= E_T(\beta_1\sin^2\gamma+\beta_2\cos^2\gamma+(\beta_1-\beta_2)\cos(2\gamma)\cos^2\theta)\end{aligned} \tag{5.25}$$

As β_1 sup β_2, for every σ_1, the maximum value of σ_2 is acquired for $\theta = 0$, which denotes $\mathbf{Q} = \mathbf{I_2}$. Hence, $\mathbf{R}^*$ can be simplified as follows

$$\mathbf{R}^* = \begin{pmatrix}\cos\varpi & (\sin\varpi)e^{i\varphi} \\ -\sin\varpi & (\cos\varpi)e^{i\varphi}\end{pmatrix} \tag{5.26}$$

while developing

$$\mathbf{R}^* = \begin{pmatrix}\cos\varpi & \sin\varpi \\ -\sin\varpi & \cos\varpi\end{pmatrix}\begin{pmatrix}1 & 0 \\ 0 & e^{i\varphi}\end{pmatrix} = \mathbf{R}_\varpi\mathbf{R}_\varphi \tag{5.27}$$

with $0 \le \varphi < 2\pi$ and $0 \le \varpi \le \frac{\pi}{2}$.
Thus, the precoder can be expressed as

$$\mathbf{F}_d = \sqrt{E_T}\begin{pmatrix}\cos\gamma & 0 \\ 0 & \sin\gamma\end{pmatrix}\begin{pmatrix}\cos\varpi & \sin\varpi \\ -\sin\varpi & \cos\varpi\end{pmatrix}\begin{pmatrix}1 & 0 \\ 0 & e^{i\varphi}\end{pmatrix} \tag{5.28}$$

5.3.2.2 OSM Precoder

OSM stands for Orthogonalized Spatial Multiplexing and is a subset of closed-loop MIMO precoders. All precoding techniques presented previously are based on the diagonalization of the channel by applying the SVD. Unlike previous precoding, this one is not based on the diagonalization of the channel using the SVD. It proposes the orthogonalization of the symbols received by optimizing a criterion in the system. In [153], a technique called

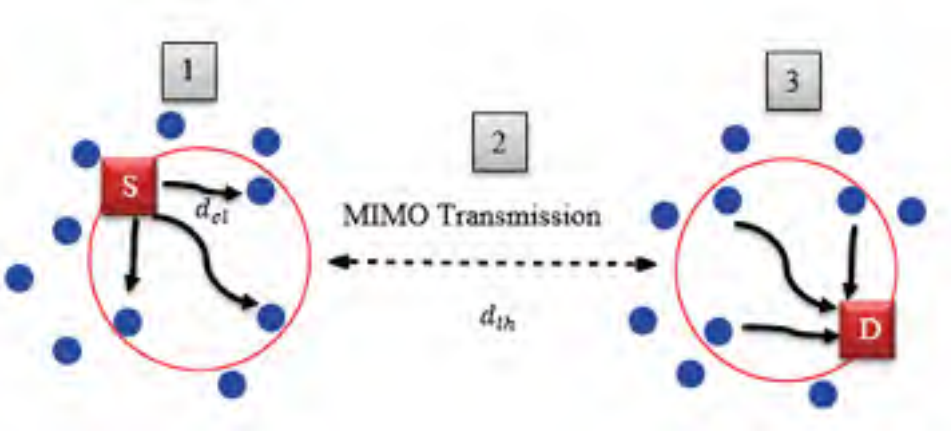

Figure 5.8: Cooperative MIMO Transmission

Orthogonalized Spatial Multiplexing (OSM) has been introduced for MIMO techniques particularly closed-loop systems. It combines symbol encoding and orthogonalization by rotation. Moreover, a precoding technique has also been proposed in [154] for the OSM system: P-OSM precoder. Similar to the max $-d_{min}$, the optimized criterion is the minimal Euclidean distance of the constellation.

5.4 Cooperative MIMO Techniques

The different transmission techniques studied in the previous sections constitute the simplest methods for reducing the transmission error rate or the transmission energy consumption. SISO system requires more transmission energy compared to MIMO techniques for an identical BER specification. However, because of the minimal size of sensors, the direct application of the MIMO technique seems to be inconvenient. For avoiding the constraints as mentioned earlier, the use of MIMO cooperative techniques [134-138] may be an obvious solution enabling nodes to be grouped in a set of virtual antennas as depicted in Fig. 5.8. As showed in Fig. 5.8, the cooperative MIMO communication from source node S to destination D through a long haul distance d_{lh} is constituted of three states:

1. Local data exchange: During the transmission, the node source S collaborates with its neighboring and interchnage its information for achieving MIMO communication in state 2. The source S can transmit the information data to the other $N-1$ cooperative nodes. Notice that the transmission distance d_{lh} is more critical than the distance between cooperating nodes d_{cl}.

2. Cooperative MIMO transmission: In this state, the received data from the source are modulated and encoded according to the constellation symbols and sent simultaneously to the node D as a traditional MIMO transmission.

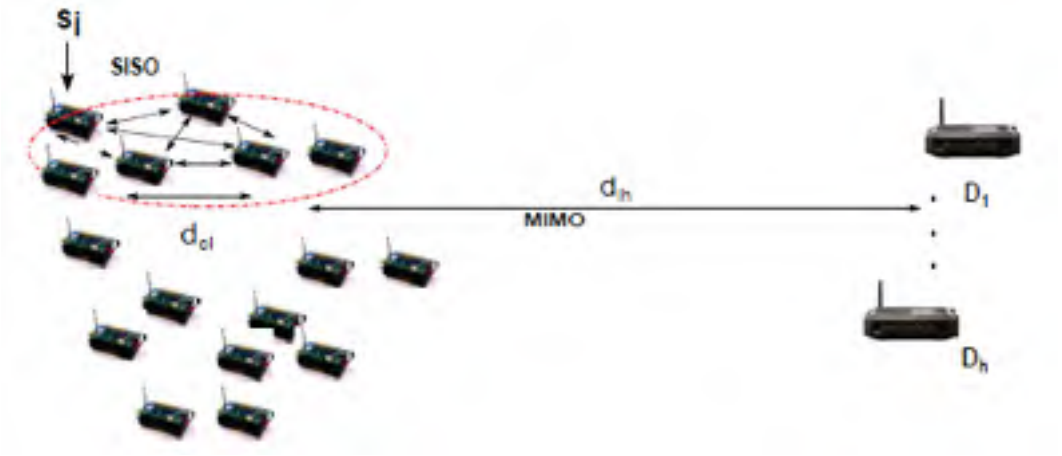

Figure 5.9: Proposed cooperative scenario [138].

3. Cooperative reception: Firstly, the cooperative nodes in the reception receive the modulated data, and after successively retransmit them to the final destination D which combines the signals and decodes the data.

The described scenario is a typical example of cooperative MIMO transmission. However, another technique in which nodes only cooperate on the transmission side exists. This scenario is studied in the next section.

5.5 Cooperative MIMO in Perturbed Environment

Cooperative transmissions are well studied for improving the error rate probability or spectral efficiency performance. It has been indicated that SISO and multi-hop approaches are less effective than the cooperative transmission in concerning energy over long-haul distance [155]. By exploiting channel state information at the transmitter (CSI-T), MIMO precoder can optimize specific criteria to increase system performance. The max$-d_{min}$ precoder optimizes the Euclidean distance for improving the performance. The work in [138] highlighted the interest of using max$-d_{min}$ by comparing the BERs and the mutual information with water filling (WF), lattice, and mercury water filling (MWF). The obtained results showed that the max$-d_{min}$ achieved the best performance.
Since our work on this chapter is a continuation and an improvement of the work proposed in [138], we will first recall the proposed system and the results obtained before detailing our contribution.

5.5.1 Review of the Existing Approach Presented in [138]

5.5.1.1 Proposed scenario and nodes selection

The system model which is considered in this section is depicted in Fig. 5.9. It is assumed

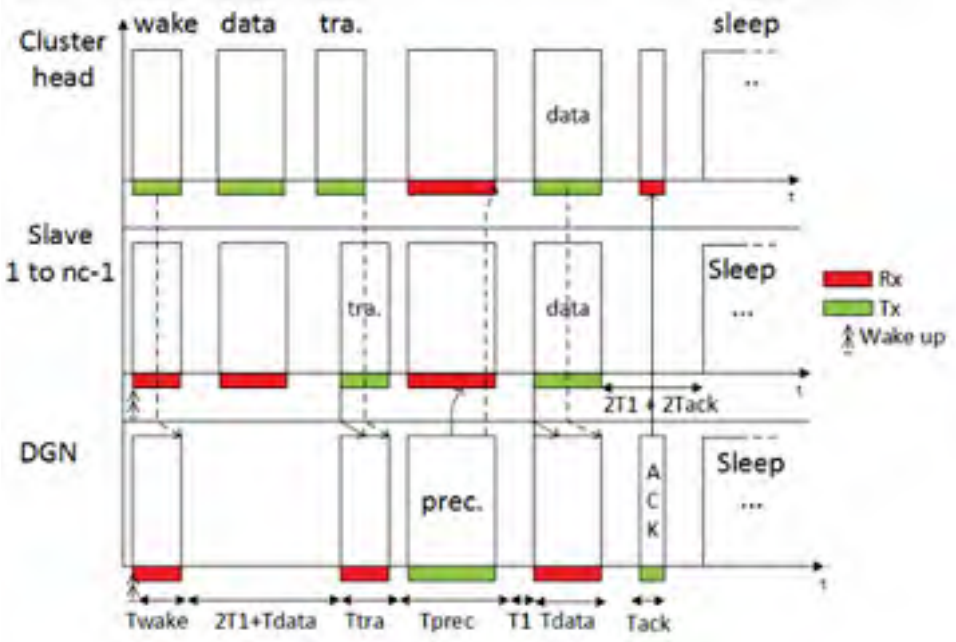

Figure 5.10: The assumed cooperative protocol.

that transmissions from a cluster of n_{cl} nodes to data gathering node (DGN) over Rayleigh fading channels and a realistic channel model obtained with the RapSor simulator. Any node i ($i = 1, 2, \ldots, n_{cl}$) in a cluster k is a single antenna node with the capability to be a slave or a cluster-head. A node acting as a cluster head synchronizes its $n_{cl}-1$ neighbors while a slave cooperates with other nodes in cluster k over a relatively short SISO communication link. The DGN is a multi-antenna receiver and equipped with relatively high processing capabilities and without energy constraints. Assuming this scenario, where substation elements and infrastructure are fitted with many of wireless sensors such as temperature, pressure, and electrical parameters (voltage, current, frequency). Such sensor nodes are required to measure and cooperatively transmit measured data wirelessly to DGN over a distance d_{lh}. Due to relatively shorter distances d_{cl} between cooperating nodes, an AWGN channel is assumed with no fading while Rayleigh fading is supposed to be fixed overall the transmission of the codeword from the cluster to the DGN over the distance d_{lh}. The communication protocol depicted in Fig. 5.10 can be described as follows.

Declaration phase: It is assumed that neighborhood discovery had been previously performed. Any source node having data to transmit forms a cluster and confirms itself as the cluster head since the first which declares is considered as the head of the cluster. All the nodes which "hear" the source node sets their "*status*" to slave ready to receive from the source. If two or more nodes perform declaration, the cluster-head with the least residual energy E_{res} wins, but nodes with data can still send to neighboring nodes after the current cluster-head.

Phase 1: The source node multicasts its data to $n_{cl}-1$ neighbors over the average distance

of d_{cl}; this is a SISO communication.
Phase 2: Next, the $n_{cl}-1$ neighbors, as potential relays, send each training frame *tra.* to the DGN which uses this to estimate the multi-path coefficients for each of its received antennas. The DGN also note the identification (ID) of the cluster-head for future acknowledgment. It then constructs the channel matrix $\mathbf{H}$ and selects the best n_t nodes, including the optimal precoding matrix index for the selected nodes.
Phase 3: The DGN selects n_t nodes that will use the precoding matrix whose index is found in the precoding message *prec.* sent by the DGN to n_t nodes. The message *prec.* also includes the ID of the selected nodes.
Phase 4: The n_t selected nodes precode with the precoding matrix, and then transmit the data frames to the DGN using MIMO transmission over a Rayleigh channel or a channel obtained with RapSor.

5.5.1.1.1 Nodes Selection

The nodes selection defined in [138] and depicted in Fig. 5.11 can be summarized as follows. Node selection is performed by the DGN to select n_t nodes from a cluster of interest by evaluating d_{min} associated with each node as

$$d_{min}(\mathbf{h}^{(j)}) = \min_{\mathbf{e}'} \|\mathbf{G}_v^{(j)}\mathbf{h}^{(j)}\mathbf{F}^{(j)}\mathbf{e}'\| \tag{5.29}$$

where $\mathbf{G}_v^{(j)}[1\times n_r]$, $\mathbf{h}^{(j)}$ is the j^{th} column of the cluster destination channel matrix $\bar{\mathbf{H}}[n_r\times n_c]$, $\mathbf{F}^{(j)}$ is the associated precoding matrix j^{th} column of $\bar{\mathbf{H}}$, and $\mathbf{e}'$ is the difference between possible transmitted vectors belonging to a set $\{1,-1\}$. Due to constraint $b \leq \min(n_r, n_t)$, $\mathbf{F}_d^{(j)}$ becomes a scalar. The unitary matrix $\mathbf{F}_v^{(j)}$ obtained by the method of dictionary construction explained previously (or by SVD for full CSI) is a scalar, i.e, $\mathbf{F}_d^{(j)} = \mathbf{F}_v^{(j)} = 1$. Sorted in descending order, the n_t indexes of the eigenvalues corresponding to the column vectors of matrix $\bar{\mathbf{H}}$ are the n_t columns of matrix $\mathbf{H}$ of selected nodes.
Nodes can be selected faster as opposed to maximizing the d_{min} of L sub-carriers for each $\bar{\mathbf{H}}$, where $L = C_{n_t}^{n_{cl}} = \frac{n_{cl}!}{n_t(n_{cl}-n_t)!}$

5.5.1.2 Obtained Performance

In this section, we present some results obtained in [138]. It allows to have an idea of the performance with the proposed approach and will serve as a basis of comparison with our new system. For this purpose, we only present two cases to observe the impact of the nodes selection when the channel is affected by impulsive noise. The system considered is an uncoded closed-loop MIMO performed with a 4-QAM modulation.

As can be seen in Figs. 5.12 and 5.13, the performance are degraded by the presence of Middleton impulsive noise. By implementing the nodes selection algorithm, it is showed that the required power of the transmitted signal of the nodes can be reduced.

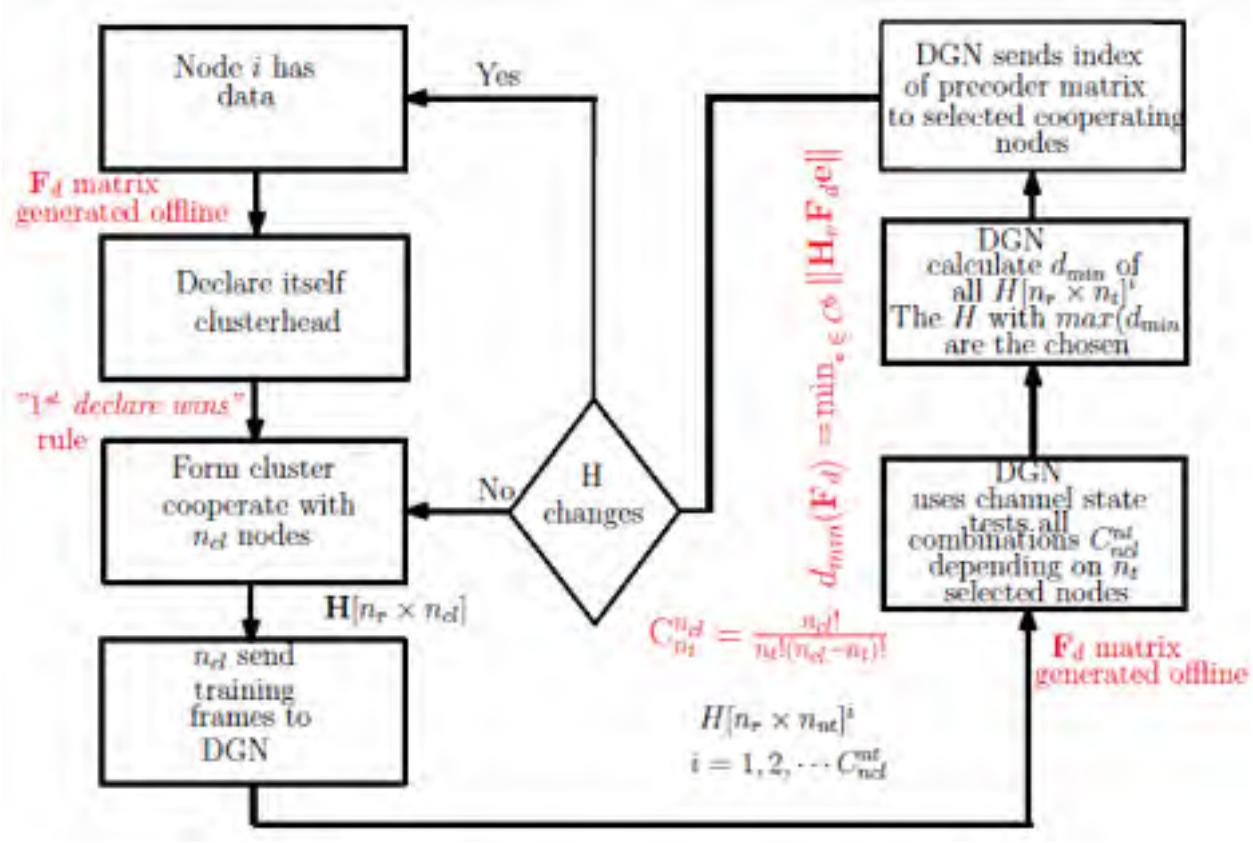

Figure 5.11: Nodes selection by cluster [138].

5.5.1.3 Conclusion

The works in [138] had proposed nodes selection technique to reduce transmission energy. The contribution involves the development of a simulation tool based on nodes selection technique for the max$-d_{min}$ distributed MIMO precoding. Globally the results are interesting but the solution relies on an uncoded system and the noise model on which the simulations are based is a model for representing narrowband impulses. It has been proposed in perspective to improve the work taking into account broadband noise modeling. To go further, we propose to integrate a channel coding given the interesting results obtained in chapter 4. For this purpose, we present in the next section, our contribution in order to provide a more reliable communication system.

5.5.2 Cooperative Coded-MIMO in Perturbed Environment

In the previous section, we noticed the interesting results obtained with the MIMO system based on the max-dmin precoder. As demonstrated in Chapter 4, FEC solutions bring more robustness to the communication system compared to uncoded techniques. In this sense, several studies have shown the importance of coded MIMO techniques. Coded-

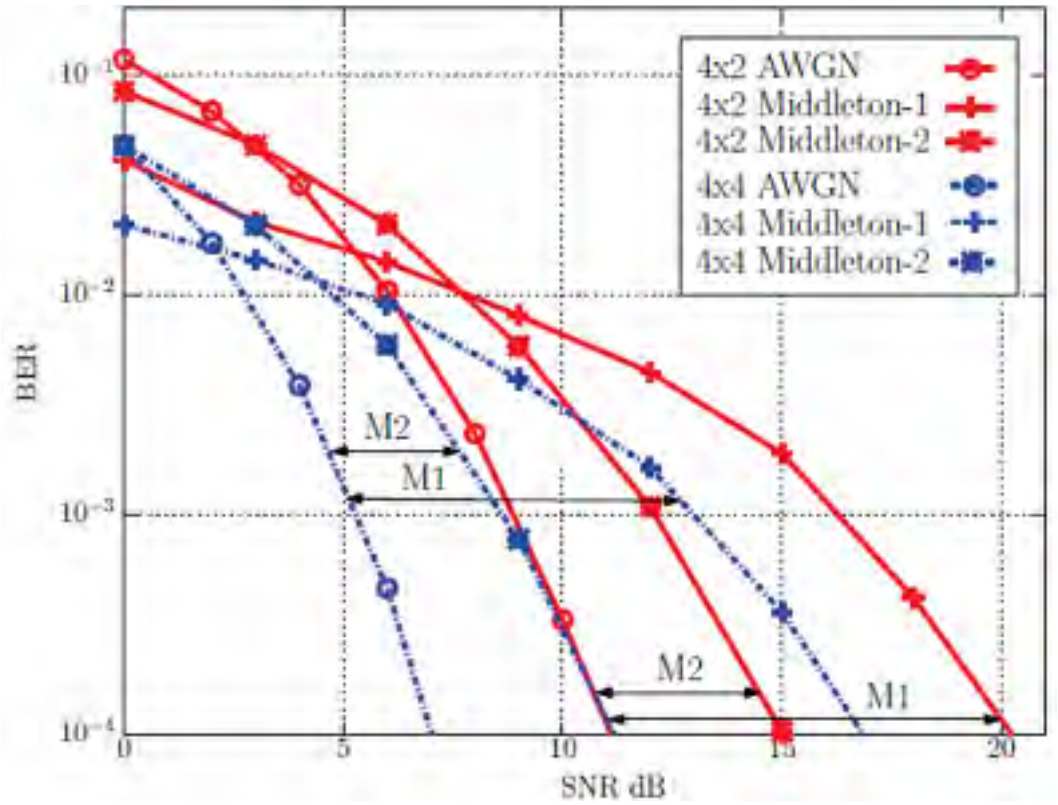

Figure 5.12: 4 nodes in cluster and 2 to 4 active nodes - without node selection [138].

MIMO ensures more efficiency and reliability in communication systems. For this purpose, it has also been primarily studied for performance improvements. In [156-157], the authors proposed a coded-MIMO based on Turbo codes and block-wise concatenated convolutional code (BCCC) respectively. The obtained results showed significant improvements. In a previous study [130], we proposed a coded-OFDM system based on RC code and CC scheme. The system approach was simple and robust for mitigating the bursty nature of impulsive noise occurring in the HV substations. We now confirm that the same order of coding gain is maintained even with a closed-loop MIMO transmission. The objective of this section is to provide a reliable and efficient communication system by combining RC/CC schemes and MIMO using max$-d_{min}$ precoder and reduce the energy transmission with a useful selection nodes technique in an impulsive noise environment. The principal contributions of this section consist of:

- The max$-d_{min}$ precoder approximation for BPSK Modulation.
- The proposition of an original study case that takes into consideration the joint solution using an outer forward error correction based RC applied to the max$-d_{min}$ MIMO precoder assuming ML detection at the receiver.
- The reduction of the complexity of nodes selection technique assuming FCSI.

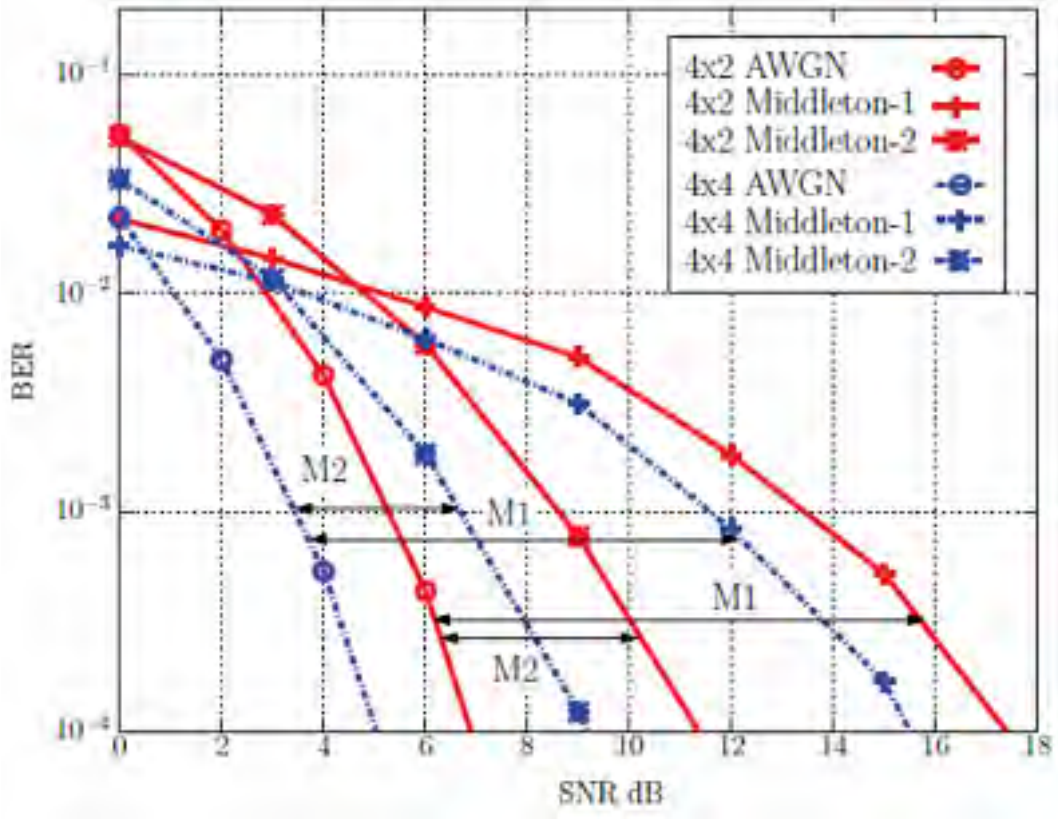

Figure 5.13: 10 nodes in cluster and 2 to 4 active nodes - with node selection [138].

- The reduction of the overall node's transmission energy in bursty impulsive interferers.

5.5.2.1 A Solution of max$-d_{min}$ for BPSK Modulation

The max-dmin solution proposed in [138] is based on M-QAM modulations. Finding the precoder $\mathbf{F}_d$ in this case requires the derivation of the forms of $\mathbf{F}_{octa}$ and $\mathbf{F}_{r1}$ [138] which is quite complex in terms of implementation and computation time. A simplification has been proposed and this solution adopts BPSK modulation. To be more consistent in our approach since all our simulations use BPSK modulation, we propose the max$-d_{min}$ precoder solution for BPSK modulation.

Considering a BPSK modulation technique, where $b = 2$, the data symbols are in $\{1, -1\}$ and the difference vectors related to $\mathbf{e} = (\mathbf{s_k} - \mathbf{s_l})$ are $\{\binom{0}{2}, \binom{0}{-2}, \binom{2}{0}, \binom{2}{2}, \binom{2}{-2}, \binom{-2}{0}, \binom{-2}{2}, \binom{-2}{-2}\}$. Since some vectors are collinear, the solution is reduced to $\mathbf{e_{BPSK}} = \{\binom{0}{2}, \binom{2}{0}, \binom{2}{2}, \binom{-2}{-2}\}$. The precoder that maximizes is obtained for $\gamma = 0°$, $\varpi = 45°$, and $\beta = 90°$. Hence, the solution for BPSK modulation is given as follows

$$\mathbf{F}_d = \mathbf{F}_{BPSK} = \sqrt{\frac{E_T}{2}} \begin{pmatrix} 1 & \sqrt{-1} \\ 0 & 0 \end{pmatrix} \tag{5.30}$$

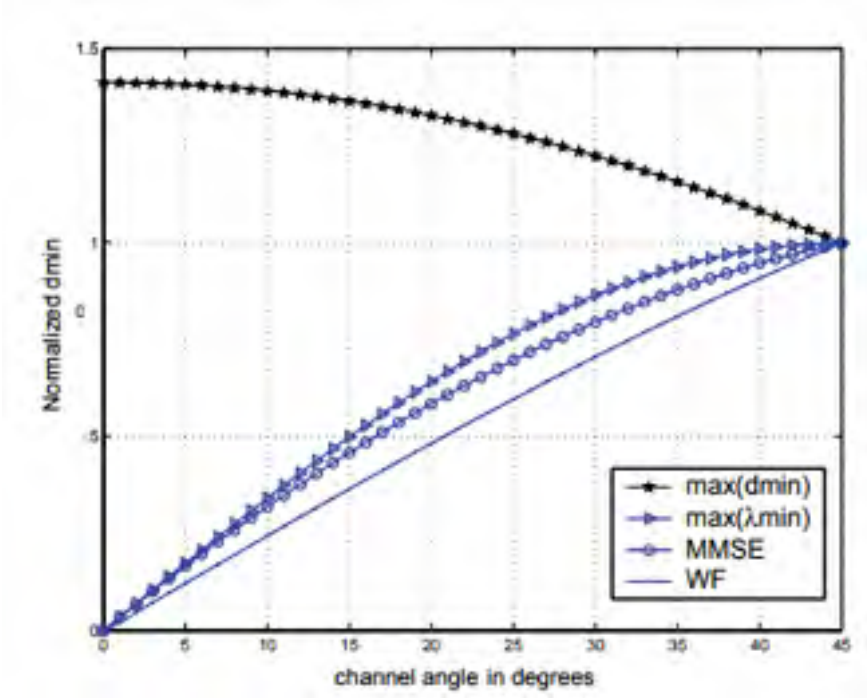

Figure 5.14: Normalized distance for BPSK modulation.

And its d_{min} namely d_{min}^{BPSK} is

$$d_{min}^{BPSK} = \|\mathbf{H}_v \mathbf{F}_{BPSK} \begin{pmatrix} 2 \\ 0 \end{pmatrix}\| = 2\sqrt{\beta E_T} \cos\alpha. \tag{5.31}$$

Notice that the second row of (5.30) is equal to 0, indicating that the signal is ultimately transmitted on the most favored sub-channel. This solution could be compared to the max-SNR that streams power just on the strongest eigen-mode of the channel [159] as can be seen in Fig. 5.14. It depicts the evolution of the normalized d_{min} for BPSK modulation compared to others precoders.

5.5.2.2 Cooperative MIMO Transmission

When the FCSI is available, $\mathbf{F}_v$ is a unitary matrix derived from SVD of the channel matrix $\mathbf{H}$. In practical applications, the hypothesis of FCSI availability at the transmitter is unrealistic, rather the channel information must be made available to the transmitter from the receiver via the rate-limited feedback control channel [160]. The channel information types that can be made available include the channel statistics, instantaneous channel and partial or quantized CSI (QCSI). The most practical of these is the QCSI because the feedback amount can be adjusted to the available rate of the feedback control channel. In the case of the limited CSI, we implement a finite codebook in which the receiver selects the optimal matrix $\mathbf{F}_d$ and $\mathbf{F}_v$ from $\mathcal{F}_v$ and $\mathcal{F}_d$ dictionaries. The optimal dictionary $\mathcal{F}_v$ containing a set $\{\mathbf{F}_{v1}, \mathbf{F}_{v2}, \ldots, \mathbf{F}_{vN}\}$ is implemented according to the algorithm in [161],

where $N = 2^{B_1}$ is the dictionary size, and B_1 is the number of quantization bits. Generally, constructing the $\mathcal{F}_d$ dictionary is required for each $\mathbf{H}$ realization in conjunction with the $\mathbf{F}_v$ dictionary, but for the BPSK modulation, the content of dictionary $\mathcal{F}_d$ will be limited to a single precoder matrix $\mathbf{F}_d$ since it is independent of the channel angle. The two dictionaries are generated offline, combined into a codebook $\mathcal{F} = \mathcal{F}_v\mathcal{F}_d = (\mathbf{F}_1, \mathbf{F}_2, \ldots, \mathbf{F}_N)$ and are made available to all nodes. The codebooks for 2, 3, and 4 transmit nodes generated with 3, 5, and 7 bits resolution, respectively, and are used for all our simulations.

5.5.3 Performance Evaluation: BER

This section introduces numerical results performed by simulations under Rayleigh and RapSor channels affected by Gaussian noise and Au impulsive noise. We assume ML detection at the DGN, indeed, the average probability of error limited to the nearest d_{min} neighbors [16] can be approximated as

$$P_e \approx \frac{\bar{N_n}}{2}\left(\sqrt{\frac{(d_{min})^2 E_T}{4\sigma^2}}\right) \tag{5.32}$$

where $\bar{N_n}$ is the mean of the nearest neighbors.
Considering a BPSK modulation, the bit error probability is given by

$$P_{bit} \approx \frac{\bar{N_n}}{2b\log_2(M)}\operatorname{erfc}\left(\sqrt{\frac{(d_{min}^{BPSK})^2 E_T}{4\sigma^2}}\right). \tag{5.33}$$

where $M = 2$ is the modulation order. To estimate the performance of the MIMO system with $\max -d_{min}$ precoder, the MATLAB software is utilized. The simulation started with uncoded MIMO system then used concatenated RC and CC in the presence of Gaussian noise and Au impulsive noise. Two configurations are also considered: a transmission without node selection and a transmission with node selection. MIMO system efficiency is investigated for both Rayleigh fading and RapSor channel. The reliability of the system is expressed by the correlation between BER versus the signal to noise ratio (SNR). Firstly, the system described with no channel coding approaches, is to demonstrate the impact of employing a coding scheme in cooperative MIMO system by utilizing BPSK modulation over AWGN and impulsive noise with Rayleigh fading and RapSor channels. We also investigated the performance of concatenated RC and CC. The size of Galois Field for the RC is $\mathbb{F}_{q^u} = 16$, while the CC employed has a coding rate $R = 1/2$, and generator polynomials in an octal form: $P_1 = 171$ and $P_2 = 133$. The decoding of RC is implemented by the modified-Berlekmap Massey, while a soft decision of the Viterbi algorithm performs CC decoding. In the following section, we present only the results for a 4×4 MIMO transmissions.

5.5.3.1 AWGN and Impulsive Noise under Rayleigh Channel

5.5.3.1.1 Transmission without Node Selection

Fig. 5.15 depicts BER performance of max$-d_{min}$ MIMO precoding with FCSI without node selection. The results demonstrate that the worst performance of MIMO system are with no channel coding for both AWGN and impulsive noise. Considering the AWGN noise, we can note that the system in the presence of channel coding does not perform well compared to the uncoded system up to a SNR of 1 dB. From this moment, we can notice an improvement of the performance. Uncoded-MIMO when the impulsive noise is present, indicates a flattening of the BER between -5 and 5 dB. Then, it is improved by adding the coding technique. Using concatenated RC/CC with max$-d_{min}$ precoding give more improvement to the system. Considering the presence of impulsive noise, the coding gain between uncoded and suggested approach is approximately 8 dB at a target BER of 10^{-4}. We now compare our results to those obtained in [162]. The authors proposed a useful technique to track the double-selected multi-path channel for MIMO-OFDM system. A Space-Time Block Coding (STBC) is applied and leads to interesting performance. However, our system is more robust and presents better performance as can be seen in Fig. 5.15. We have a gain of approximately 12 dB compared to the proposed approach described above. Furthermore, in [163] the authors presented a MIMO-OFDM system with a concatenated Reed-Solomon/convolutional codes. The system evaluated in both Rayleigh and Rician channel. The obtained results are improved compared to an uncoded system. However, our system still has the best performance.

5.5.3.1.2 Transmission with Node Selection

The first simulations we made, concerned the communication without node selection. In this paragraph, we present numerical results when optimal and suboptimal node selection are implemented combined with the knowledge of the channel (FCSI or QCSI). By assuming the full channel knowledge, the system model described previously is achieved. For the QCSI, a codebook quantized using 3, 5, and 7 bits for 2, 3, and 4 selected nodes are considered, respectively. The performance are shown in Figs. 5.16 and 5.17. Results are only shown for 4 transmit nodes. In Fig. 5.16, the results of uncoded systems are presented, and the performance between FCSI and QCSI are compared. As can be seen, FCSI outperforms QCSI for both AWGN and impulsive noise. Since FCSI yields better performance results than QCSI, we represent only results in FCSI with the node selection in Fig. 5.17, which shows simulation results with a coded system. As for the case without selection, a performance improvement can be noticed. Considering a channel impaired by impulsive noise and a concatenated RC/CC, a target BER of 10^{-4} is achieved at an SNR of approximately 1 dB. It leads to a coding gain of 4.7 dB between uncoded and coded MIMO system.

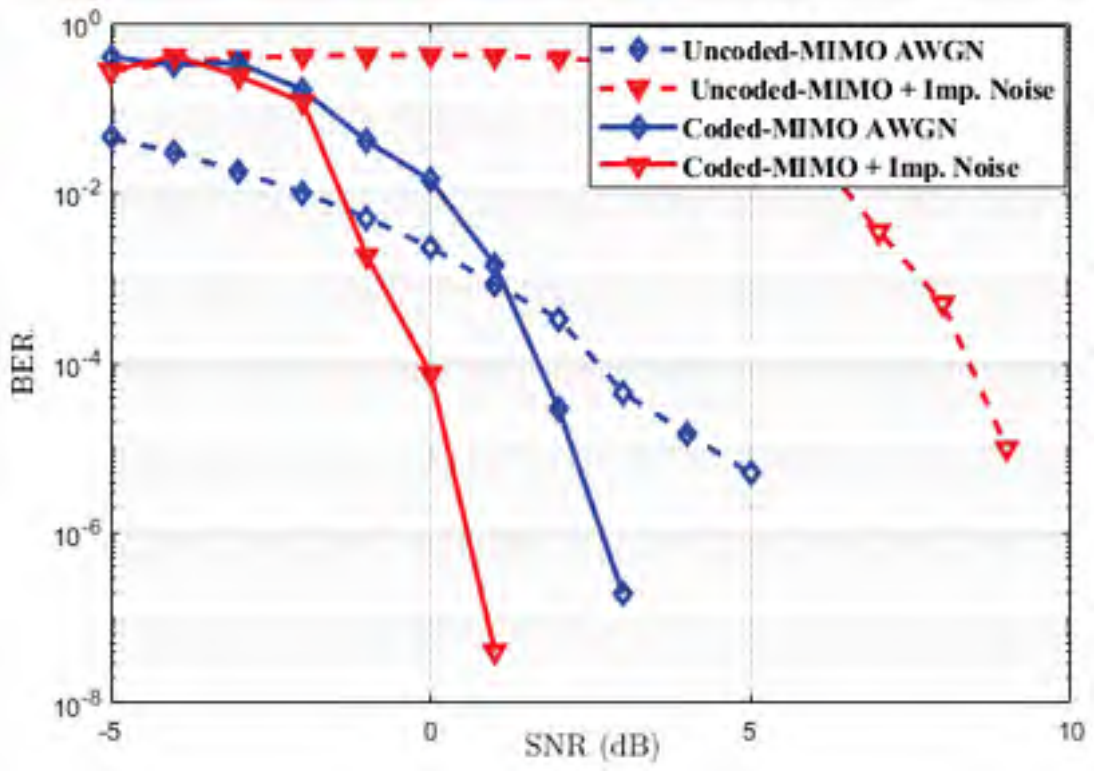

Figure 5.15: BER performance of max$-d_{min}$ MIMO precoding with FCSI under Rayleigh channel without node selection.

5.5.3.2 AWGN and Impulsive noise under RaPSor Channel

In the preceding section, we studied the impact of coded-MIMO communications under a Rayleigh fading channel affected by impulsive noise and AWGN. The results obtained showed that good performance are achieved. However, it was a simple case since an AWGN noise was consired without any multipath effects. The reality of power substations considers multi-path components due to the presence of metallic structures, equipment, and devices. To take into account the aspects mentioned above, we now consider a deterministic channel extracted from the RapSor software [23]. Our objective is to acquire the channel impulse response (CIR) of the simulated channel matrix $[n_r \times n_t]$ coefficients. For this purpose, we select a high voltage substation located in Québec (Canada) operated by the energy company Hydro-Québec. Our WSN application consists of a 6×4 virtual MIMO system made up with the DGN node as the receiver placed on a tower of 60 m and the sensors forming a 10-nodes cluster mounted on transformers serving as the emitters. The clustering distance is approximately 14 m, while the long haul distance is 1029 m.

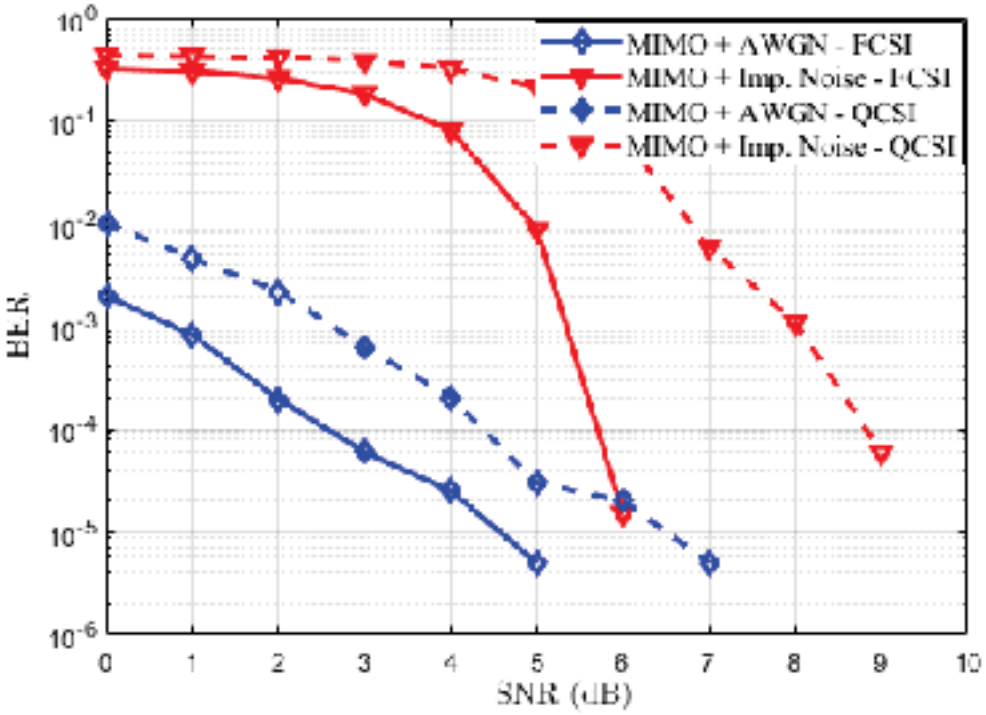

Figure 5.16: Performance comparison between FCSI and QCSI: curves with solid lines represent full CSI while dashed lines represent the QCSI.

5.5.3.2.1 Transmission without Node Selection

We consider the same situation as for the Rayleigh fading channel. However, only results for 4×4 MIMO are depicted, since they achieve the best performance. The results obtained are plotted in Fig. 5.18. For the uncoded system, we notice a performance degradation when the channel is affected by impulsive noise. As for Rayleigh channel, a flattening of the BER curve between -3 and 2 dB can be noticed in the presence of impulsive noise. However, by combining the concatenated codes and max $-d_{min}$ precoder with MIMO, we have an increase of system performance. Target BER of 10^{-4} is achieved at SNR of 0 and 8.7 dB for coded and uncoded-MIMO, respectively when the channel is affected by impulsive noise. It yields to a coding gain of 8.7 dB between uncoded and coded MIMO system.

5.5.3.2.2 Transmission with Node Selection

In this section, optimal node selection is implemented to select 2 and 4 transmit nodes from the cluster of 10. Assuming the full channel knowledge, we explore the BER results for both coded and uncoded MIMO systems. The results are depicted in Fig. 5.19. For the uncoded case, we can note the degradation of the performance. It is improved when the concatenation of codes is added. Target BER of $10^{-}4$ is achieved at SNR = -1 dB

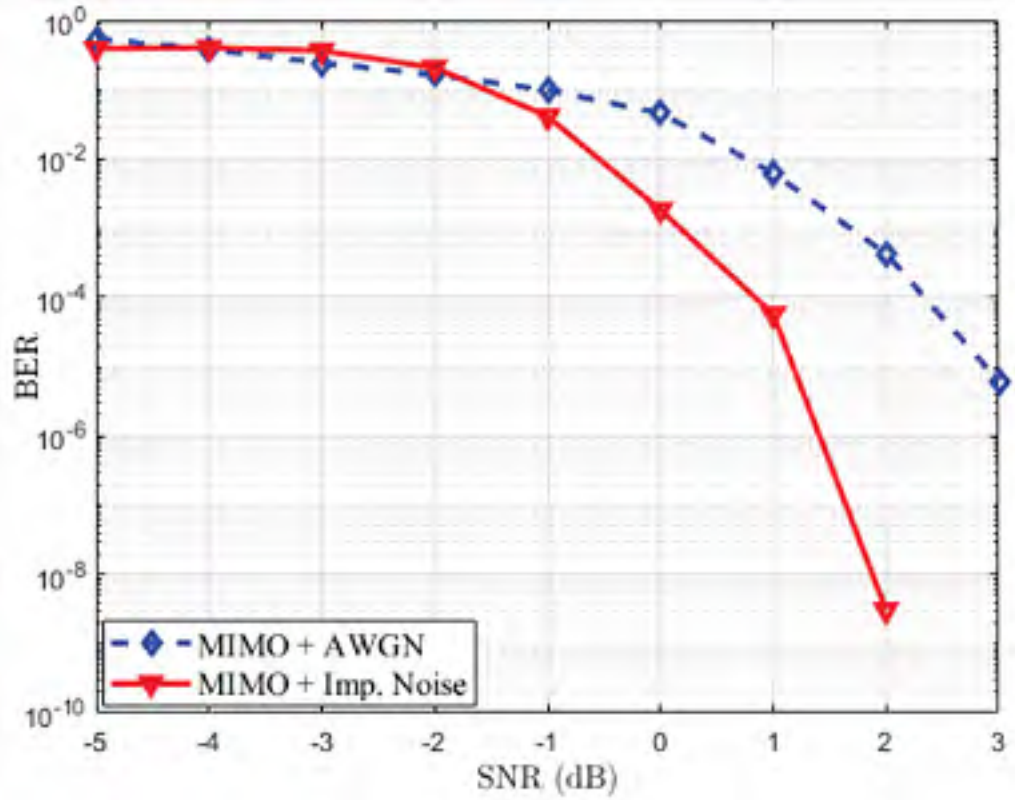

Figure 5.17: Coded-BER performance of max$-d_{min}$ precoding under Rayleigh fading channel with FCSI and node selection.

for coded-MIMO, while it is 8 dB for the uncoded system when the channel is affected by impulsive noise.

5.5.4 Energy Consumption

Wireless sensor networks contribute actively to the design of SG applications. However, these networks are different from other systems as they generally have the following specificities: high density, low throughput, low energy capacity, and they are placed in a challenging environment. These last two specificities make energy a significant constraint since the batteries of the sensors are generally nonrefillable. With the cooperative MIMO system, our challenge is the reduction of the transmission energy based on the initial exchange and nodes selection as described previously.

5.5.4.1 Energy Model

In this section, we consider the model of energy consumption developed in [164]. This model has been used in several contexts to evaluate the energy consumption of systems SISO and MIMO cooperative in sensor networks [165], [166]. The max $-d_{min}$ protocol employs

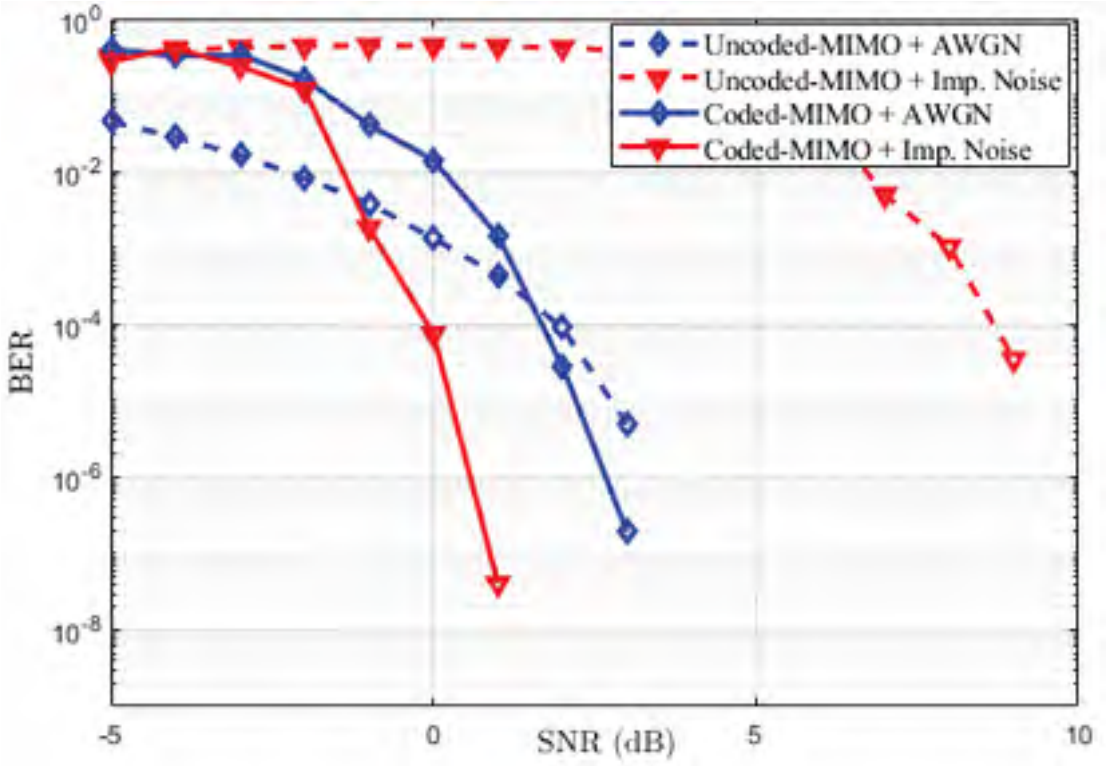

Figure 5.18: Performance comparison between coded and uncoded MIMO for max$-d_{min}$ Precoding with FCSI under RapSor channel.

cooperative MIMO with the distributed nodes serving as multiple antennas. Hence, we are involved in the total energy consumption E_{coop} of the nodes for full communication. According to the protocol description, the total energy of the cooperating nodes can now be expressed as

$$E_{\text{coop}} = E_{\text{loc}} + E_{\text{init}} + E_{\text{fbk}} + E_{MIMO} \tag{5.34}$$

where E_{loc} is the local transmission energy, i.e., the SISO communication between the nodes, E_{init} is the initialization phase, E_{fbk} is the feedback control channel energy, and E_{MIMO} is the energy of the data packet for MIMO transmission.
The average energy consumption of a radio frequency (RF) system can broadly be separated into P_{Amp} and P_{cct} which are the power consumption of power amplifiers and other circuits blocks, respectively. The model of typical RF blocks [164] representing the emitter is depicted in Fig. 5.20, while the receiver can be seen in Fig. 5.21. The P_{Amp} is expressed as

$$P_{Amp} = \frac{\varsigma}{\varepsilon} P_{out} = \frac{\varsigma}{\varepsilon} \frac{E_b}{N_0} \frac{(4\pi)^2 d^{L_0} L_m D_r}{A g_t A g_r \lambda^2} R_b \tag{5.35}$$

ς is the peak-to-average ratio (PAR), ε corresponds to the power amplifier efficiency, $\frac{E_b}{N_0}$ is the ratio energy per bit to the noise, Ag_t, and Ag_r are the emitter and the receiver antenna gains, respectively, L_m is the margin component which compensates for the variations of

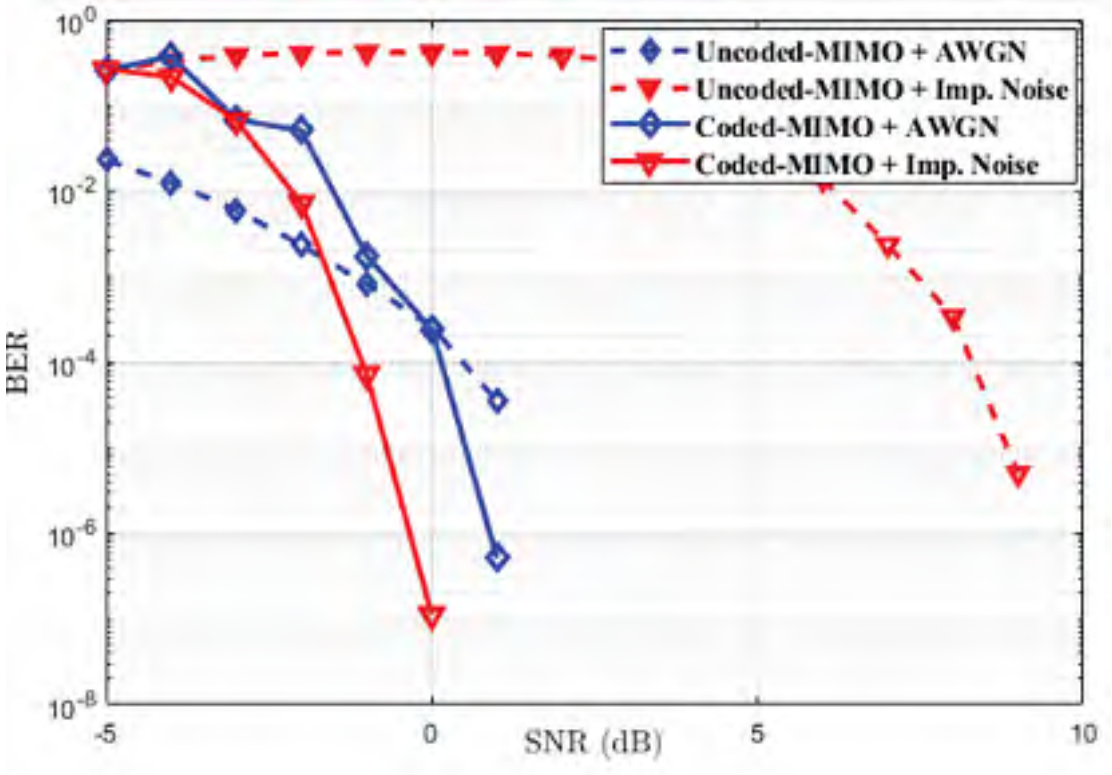

Figure 5.19: BER performance for max$-d_{min}$ MIMO precoding with FCSI under RapSor channel with node selection.

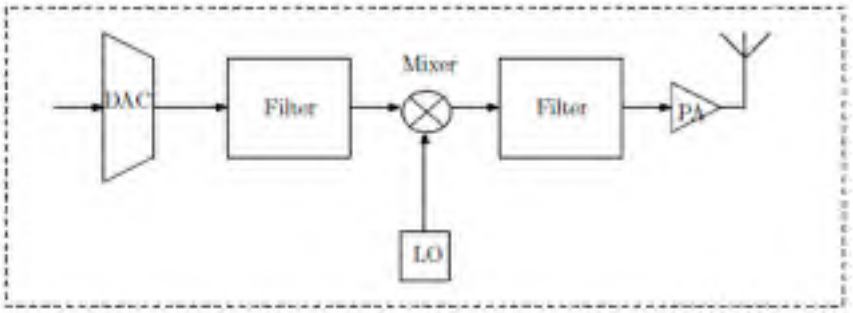

Figure 5.20: Transmitter circuit block.

the hardware process and other noises, λ is the wavelength, D_r is the power density at the receiver, d is the long-haul distance, L_0 is the path-loss component, and R_b is the bit rate. The total power dissipated in circuit, P_{cct} for n_t transmitters and n_r receivers can be approximately expressed as

$$\begin{aligned} P_{cct} &= (P_{DAC} + P_{filt} + P_{mix} + P_{synth}) + (P_{filr} + P_{LNA} + P_{mix} + P_{IFA} + P_{synth} + P_{ADC}) \\ &= n_t P_c^{Tx} + n_r P_c^{Rx} \end{aligned} \tag{5.36}$$

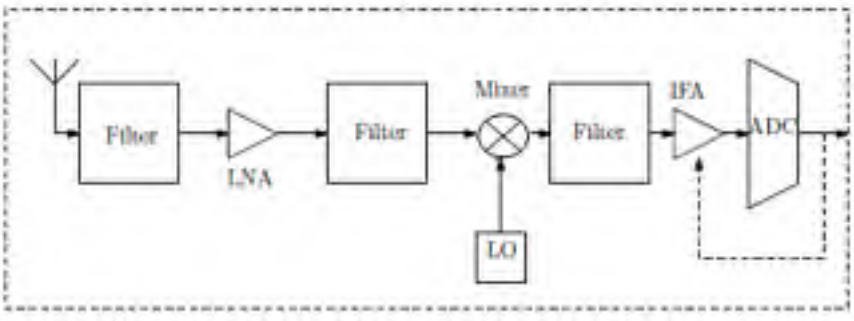

Figure 5.21: Receiver circuit block.

where P_{DAC} and P_{ADC} are consumed energy for the digital-to-analog converter (DAC) and the analog-to-digital converter (ADC), respectively. P_{filt} is the power consumed for the active filters at the transmitter, whereas P_{mix} and P_{filr} are the energy consumed for the mixer and the active filters at the receiver, respectively. P_{LNA}, P_{synth}, and P_{IFA} are power consumption for the Low-Noise Amplifier (LNA), the frequency synthesizer, and the Intermediate Frequency Amplifier, respectively. Parameter P_c^{Tx} represents power dissipated in the circuit for a single node during data transmission, and P_c^{Rx} for the reception. Total energy consumed per bit, E_{bit} for a fixed-rate system is evaluated in equation (5.37)

$$E_{bit} = \frac{P_{Amp} + P_{cct}}{R_b} \tag{5.37}$$

Assuming a packet size of D symbols is to be transmitted, and training symbols size of pn_t is inserted (each node transmits p symbols), the effective bit rate R_b^{eff} is

$$R_b^{eff} = \left(\frac{D - pn_t}{D}\right) R_b \tag{5.38}$$

Note that replacing R_b in equation (5.35) by R_b^{eff}, we obtained the energy consumption model which accounts for the additional energy due to the p training symbols.
For the max $-d_{min}$ MIMO precoding transmission, the bit rate R_b can thus be calculated as follows

$$R_b = RmB \tag{5.39}$$

where R is the MIMO transmission rate, expressed as a ratio of the number of symbols transmitted, N_S, over the number of periods, N_P, (i.e., $R = N_S/N_P$). $m = \log_2(M)$, where M is the constellation size, and B is the modulation bandwidth. The parameter, E_{loc} is the total local transmission energy expended within a cluster k that consists of n_c nodes, separated by an average distance of d_c. Each source node can transmit to $n_r = (n_c - 1)$ receivers. Thus, E_{loc} is expressed as

$$E_{loc} = N_{pkt}\left(\frac{P_{Amp} + P_{cct}}{R_b^{eff}}\right) \quad with P_{cct} = P_c^{Txk} + (n_c - 1)P_c^{Rxk} \tag{5.40}$$

Table 5.1: Nodes and PAR parameters for energy computation

Parameters	Values
Gains G_r and G_t	2.5 dBi
Frequency carrier f_c	2.5 GHz
Bandwidth	20 MHz
Power Amp. Efficiency ε	0.35
BER	$10e^{-4}$

where N_{pkt}= n_cL is the total number of bits in all sent packets, and for the random nodes cooperative transmission scenario, $n_c = n_t$. In (5.41), the training phase energy, E_{init} is given, where N_{Ts} is the number of training bits

$$E_{init} = N_{Ts}\left(\frac{P_{Amp} + P_{cct}}{R_b^{OSTBC}}\right) \quad withP_{cct} = (n_c)P_c^{Txk} \tag{5.41}$$

Only Alamouti's code yields a rate, $R = 1$ for complex modulations. The OSTBC solution for any value of n_t but with R = 1/2 is presented in [167]. Solutions for n_t = 3 and 4, but with R = 3/4 are similarly performed. To implement our training phase for 10 (n_c) cluster nodes, we consider 4 × 4 OSTBC transmissions. Then, we average rate to obtain $R_b^{OSTBC} = 2/3$, and the E_b/N_0 at the target BER. On the feedback channel, the energy E_{fbk} consumed is

$$E_{fbk} = \left(N_{fbk}\frac{n_t P_{cct}^{Rxk}}{R_b}\right) \tag{5.42}$$

where n_t sensor nodes act as receivers in this case, N_{fbk} is the number of bits sent on the feedback channel. The values of 3, 5, and 7 bits are considered for N_{fbk} when 2, 3, and 4 nodes are selected, respectively. Note that max $-d_{min}$ based selection requires $\lceil \log_2 L \rceil$ bits which have been included inN_{fbk}, where $\lceil . \rceil$ denotes the nearest higher integer. The energy needed for the transmission of the data packets by MIMO technique using the max $-d_{min}$ precoder is

$$E_{MIMO} = N_{pkt}\left(\frac{P_{Amp} + P_{cct}}{R_b^{eff-prec}}\right) \quad withP_{cct} = (n_t)P_c^{Txk} \tag{5.43}$$

$R_b^{(.)}$ is the efficiency of the MIMO technique used in transmitting the symbols over b sub-channels. Hence $R_b^{eff-prec} = 2$.

5.5.4.2 Energy Consumption Evaluation

This section analyzes simulation results for energy consumption according to the equation (5.34). The parameters used to compute the simulations are provided in Table 5.1. We calculate the total consumed energy for 4 × 4 MIMO systems. Fig. 5.22 compares the absorbed energy with and without selecting nodes for transmission. The AWGN and

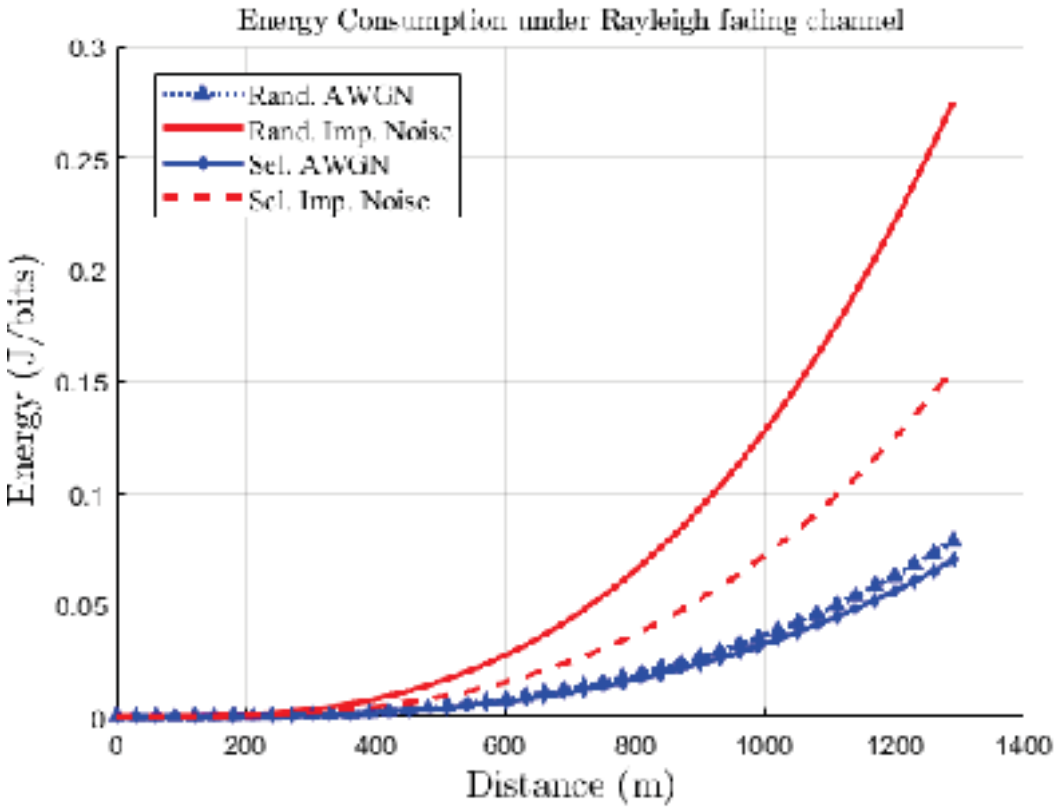

Figure 5.22: Energy consumption for max$-d_{min}$ precoding with FCSI under Rayleigh fading channel.

impulsive noise are considered in a Rayleigh fading channel. As can be seen in this figure, the node selection technique reduces the total consumed energy. The energy is reduced from 0.27 to 0.16 J/bits corresponding to about 40 % when the channel is corrupted by impulsive noise, and the node selection is applied. However, we notice that the nodes require more energy to transmit to the DGN at the target BER when the channel is affected by impulsive noise compared to the standard Gaussian noise.
Finally, Fig. 5.23 shows energy consumption per bit in a RapSor channel affected by AWGN and impulsive noise. As for the BER, only the results for 4 cooperative nodes are presented. Similarly to a Rayleigh channel, the energy is also reduced by 18 % that is from 0.29 to 0.24 J/bits.

5.6 Conclusion

In this chapter, we have overviewed the multi-hop, relay cooperative and cooperative techniques. Cooperative techniques encourage achieving the temporal diversity as well as spatial diversity gains to decrease the fading impact and to improve the system efficiency. Some MIMO techniques are also presented to exploit the advantages of a multi-antenna

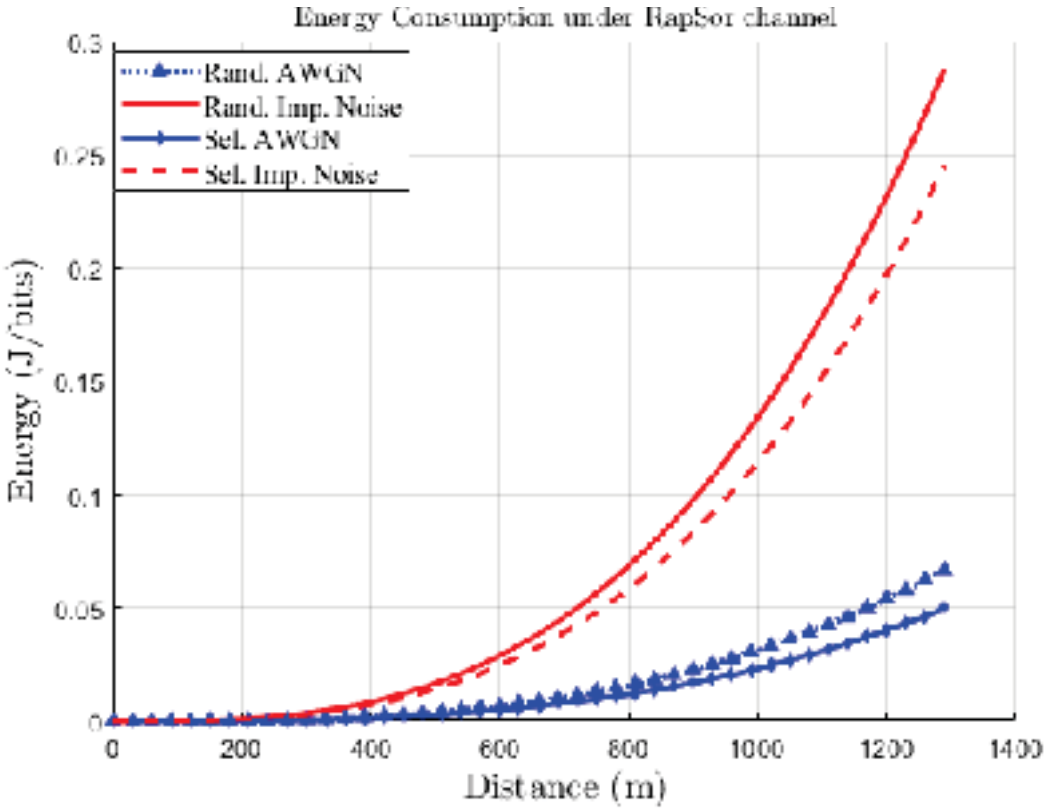

Figure 5.23: Energy consumption for max$-d_{min}$ precoding with FCSI under RapSor channel.

channel. These techniques are divided into two families whose difference relies on the knowledge or not of the channel state. On the one hand, without this information, spatio-temporal codes represent a simple solution ensuring, in particular, a maximum order of diversity ($n_t \times n_r$). On the other hand, linear precoders optimize a specific criterion using channel knowledge. They are based on the SVD to diagonalize the channel. Among these precoders, the max $-d_{min}$ precoder maximizes the minimum distance of a constellation in reception. It presents a maximal order of diversity ($n_t \times n_r$). Based on the benefits of these techniques, we have proposed a reliable and efficient communication system by combining RC scheme and MIMO using max$-d_{min}$ precoder and reduce the energy transmission with a suitable selection nodes technique in an impulsive noise environment. With BPSK modulation over Rayleigh fading channel and deterministic rays tracing RapSor channel, we have explored the performance of the suggested proposal. The concatenation of max$-d_{min}$ and RC leads to substantial performance improvement compared to the results obtained in [138]Â. SNR at the target BER reduces as the spatial diversity of MIMO system increases. Notice that the use of RC also improves the reliability of the system compared to the uncoded case. Note that FCSI is more useful than QCSI as can be observed in the results. Globally, the obtained results demonstrate that the max$-d_{min}$ with FCSI and RC code

are suitable for the impulsive noise cancellation.
We also investigate the energy efficiency for the nodes selection algorithm. Energy consumption is essential in a wireless sensor network since it affects on its lifetime. To evaluate the robustness of the nodes section algorithm technique, we use MIMO transmissions in communication channel impaired by noises. The disrupted noise was implemented using Au model validated by measurements. Results show that the node selection technique can achieve a maximum average amount of 40 % in energy saving for 4 selected nodes in Rayleigh fading channels. However, the energy saving is about 18 % in RapSor channel. In conclusion, as for the BER, this technique minimizes the energy consumption in both Rayleigh and realistic RapSor channels.

Chapter 6

Conclusion and Future Works

Contents

6.1 General Conclusion

The principal interest of this thesis is the proposition of a robust and reliable transmission protocol to ensure communication in HV substations. For this purpose in chapter 3, we present an analysis of the existing technologies. Indeed, the choice of the physical layer for a communication network is not easy. It fits to evaluate the advantages attentively, and downsides bound to the different technologies of communication. Before deploying the network, the electromagnetic environment has to be characterized, and tests have to be performed to estimate communication performances. This chapter has presented an investigation of ZigBee narrowband and wideband system performance in HV substations particularly. We have recorded data from the measurement campaign to identify the impulsive noise models. Substation noise obtained is modeled as a Middleton Class A process, Symmetric Alpha Stable and a recent model (Au). By using several statistical tests, we evaluated the several impulsive noise models. First, the results show that Middleton Class A, Symmetric Alpha Stable are not accurate for modeling partial discharges at 735 kV electricity substations. Au model is more accurate to model impulsive noise in high voltage substations. Besides, the BER performance of ZigBee are studied in a substation environment. The results show that the performance are degraded and do not allow us to meet the requirements of smart grid applications as presented in the introduction.
In Chapter 4, after a review of the literature on the improvements and the different solutions implemented to reduce the effect of impulse noise on wireless communication systems, we have proposed a first broadband approach based on concatenation of errors correcting codes: Rank metric code and convolutional code with OFDM modulation. The proposed methods in the literature include channel coding systems such as LDPC, signal processing strategies in time domains such as clipping, blanking or in frequency domains such as Zhidhov optimization. These techniques, while offering significant performance, have computational or deployment complexity; and the constraints of sensor networks are ubiquitous. Considering first an AWGN channel impaired by impulsive noise, we have performed simulations by comparing rank metric code, LRPC, and an uncoded system. The results show that a significant gain of more than 10 dB is obtained compared to the uncoded case. The rank metric code also outperforms the LRPC coding strategy. Secondly, a deterministic ray tracing RapSor channel is considered. With the same impulsive noise, we have evaluated the performance regarding BER and PER. We add the Polar coding scheme to our comparison since it allows us to achieve the limit of Shannon's capacity. As for AWGN channel, the rank metric code produces the best performance, although we note little degradation due to multi-paths. Globally, the concatenation of the rank metric code and the convolutional code allows us to have significant BER and PER improvements in the presence of impulsive noise compared to a polar code and uncoded system.
Given the significant performance obtained, we have implemented this solution on software defined radios using GNU Radio. The evaluation is performed in the laboratory generating impulsive noise for voltage levels from 12 to 18 kV. Performance are evaluated concerning average delay, packet loss, and BER. We have confirmed that the same performance are maintained even with various impulsive voltages and experimental scenarios, which estab-

lishes the high performance of the proposed approach.
In Chapter 5, another solution based on cooperative MIMO techniques is implemented. In our approach, we advocate the closed-loop cooperative MIMO solution. These systems require knowledge of the channel on the reception and transmission. To further increase performance concerning robustness, throughput, quality of service, precoding before transmission can be applied. In the literature, several types of precoders exist. We can cite the linear, diagonal and non-diagonal precoders. Several results have shown that non-diagonal precoders like the max dmin precoder offer the best performance regarding BER and mutual information. Secondly, we have evaluated a technique for selecting nodes within a cluster that transmit to the Data Gathering Node (DGN). The idea is to exploit the spatial diversity of the channel and to use the channel information with the solution of the precoder considered in our study to select the nodes. Taking into account all aspects, we have implemented a cooperative closed-loop coded MIMO system based on the Rank metric code and the max $-d_{min}$ precoder. The performance are evaluated concerning bit error rate, signal to noise ratio, and energy consumption in J/bits. For both Rayleigh fading channel and deterministic ray tracing RapSor channel, simulation results show that the required SNR at the target BER of 10^{-4} for data transmission is reduced as the number of selected nodes to transmit increases. As for the BER, this technique minimizes the energy consumption in both Rayleigh and realistic RapSor channels.

6.2 Future Works

In this thesis, significant contributions have been achieved. However, some improvements can be made. The first consists of implementing rank metric decoding on software radios instead of post-processing.

Given the results obtained, it is possible to envisage implementation of the system on real sensors for deployment at high voltage substations. However, before this phase, it is promising to carry out a feasibility study of deployment using software like Winprop in this case, the Wallman and Proman modules. Wallman is AW technology software that allows us to construct a typical database of the substation environmentas depicted in Fig. 6.1. With the Proman module, it is possible to design cell areas and define all the physical layer parameters. Two kinds of evaluations can be set up. The first concerns the propagation of the LOS, the path loss, and the power received in the substation by considering the multi-path effects such as the direct and reflected path losses, the shadowing effects, and diffraction losses.An example of propagation result can be seen in Fig. 6.2. The second is about the network planning. It gives the results of the maximum achievable data rate, the throughput taking into account the modulation, the maximum required Signal to Interference plus Noise Ratio (SINR).Fig. 6.3 represents an example of result in terms of reception probability using Proman module. This study allows us to have an economic analysis, i.e., the number of access points needed for a substation which is a determining factor of the

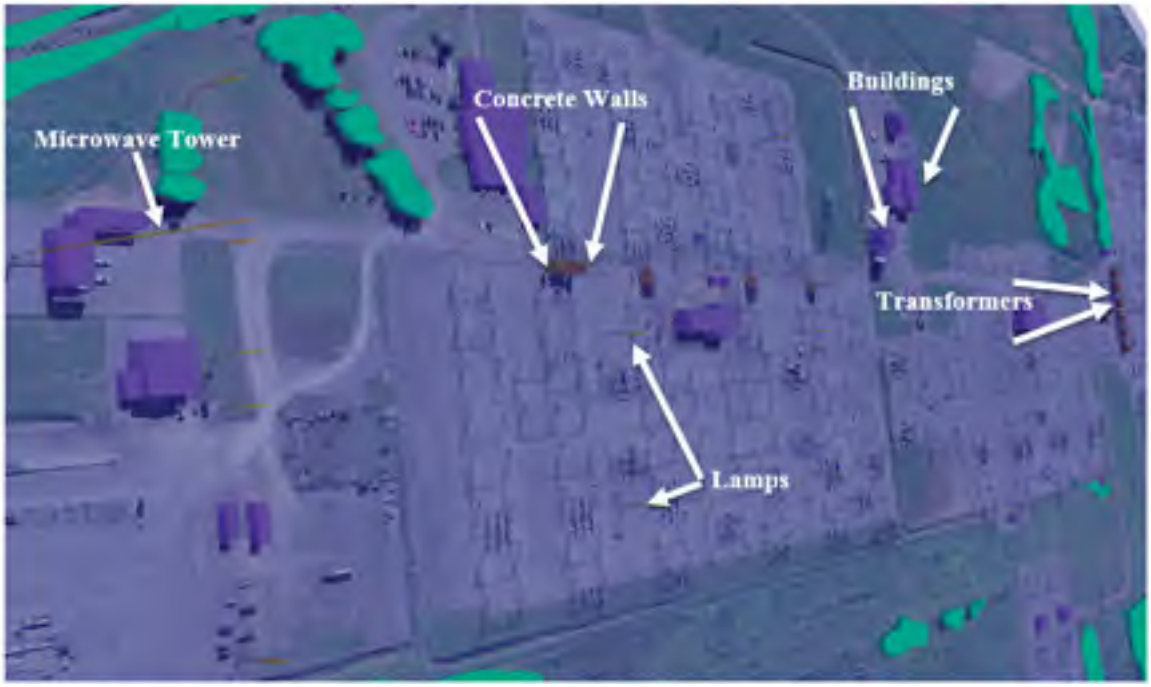

Figure 6.1: A 3D designed database of Laurentides substations using the WallMan module.

overall deployment cost.

For a deeper analysis, it will be interesting to do another study where we consider several sources of impulsive noise.

By considering cooperative closed-loop coded MIMO system, it should be interesting to design an efficient MAC protocol to have a complete communication system. However, it will be challenging because of the presence of impulsive noise in HV substations.

Another critical point in a communication system is latency. In previous chapters, the proposed methods have been robust to the detriment of latency. We know that some applications require low latency. It is, therefore, necessary to implement a strategy to reduce latency.

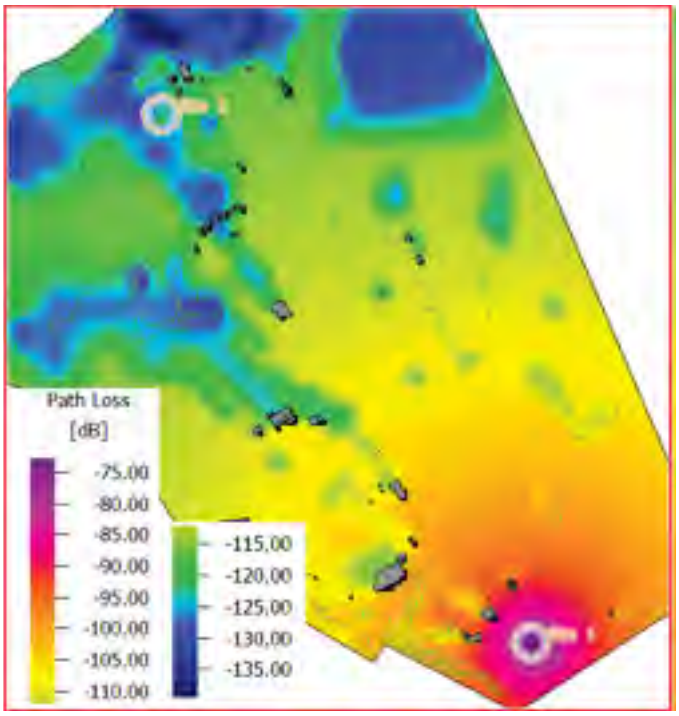

Figure 6.2: Propagation results in terms of Path Loss for one site.

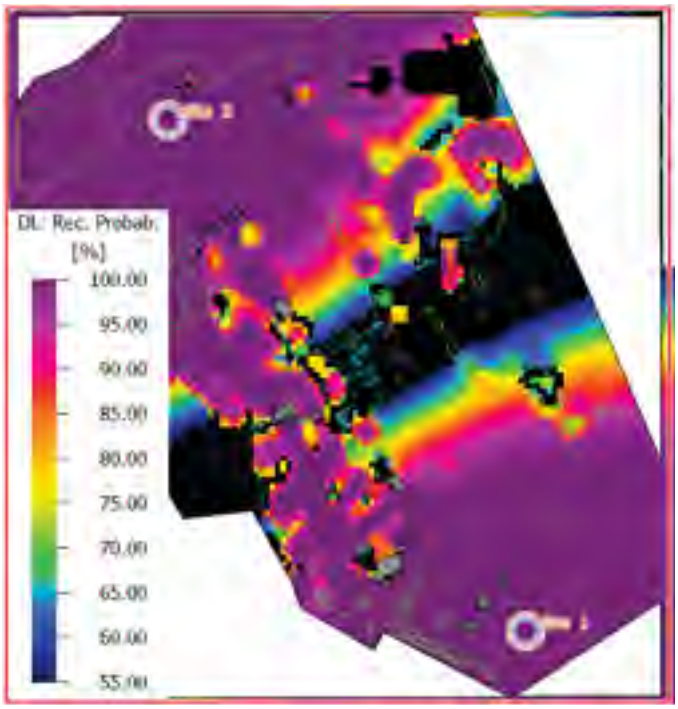

Figure 6.3: Downlink reception probability.

References

[1] IEEE Smart Grid (2014). "IEEE & Smart Grid", available at http://smartgrid.ieee.org/ieee-smart-grid.

[2] http://electrical-engineering-portal.com/smart-grid-concept-and-characteristics.

[3] NIST Framework and Roadmap for Smart Grid Interoperability Standards, Release 3.0.

[4] V. Raghunathan, C. Schurgers, S. Park, and M.B. Srivastava, "Energy-Aware Wireless Microsensor Networks," *IEEE Sig. Proc. Mag.*, Vol. 19(2), pp. 40 - 50, 2002.

[5] W.K.G. Seah, Z.A. Eu, and H.P. Tan, "Wireless Sensor Networks Powered by Ambient Energy Harvesting (WSN-HEAP)-Survey and Challenges," *Proc. Int. Conf. Wireless Commun., Vehicular Tech., Inf. Theory, Aerospace & Electronic Systems Tech., Wireless VITAE*, pp. 1 - 5, 2009.

[6] L. Wang and FG Yuan, "Vibration Energy Harvesting by Magnetostrictive Material," *Smart Materials and Structures*, 17 :045009, 2008.

[7] Q. Wang, Y. Zhu, and L. Cheng,"Reprogramming Wireless Sensor Networks: Challenges and Approaches," *IEEE Network*, 20(3), pp. 48 - 55, 2006.

[8] Mohamed AISSANI, "Optimisation de routage dans les réseaux de capteurs pour les applications temps réel," *Ph.D Thesis*, University of Paris-Est, University of USTHB, 2011.

[9] Denis DESSALES, "Conception d'un réseau de capteurs sans fil, faible consommation, dédié au diagnostic in situ des performances des batiments en exploitation," *Ph.D Thesis*, University of Poitiers, 2011.

[10] Manuel Camus, "Architecture de réception RF très faible cout et très faible puissance. Application aux réseaux de capteurs et au standard ZigBee," *Ph.D. Thesis*, University of Toulouse, 2008.

[11] Fabrice Valois, "Auto-organisation de réseaux radio multi-sauts," *HDR*, INSA de Lyon et de l'Université Claude Bernard Lyon 1, 2007.

[12] B. Sklar, "Digital Communications: Fundamentals and Applications," 2/E, Prentice Hall, 2002.

[13] T.S. Rappaport, "Wireless Communications: Principles and Practice," 2/E, Prentice Hall, 2001.

[14] Azra Kapetanovic, Mohamed A. Zohdy, Redhwan Mawari, "Fading Channels Parametric Data Simulation Supported by Real Data from Outdoor Experiments," *JSIP*, vol. 8, no.3, Aug. 2017.

[15] Gregory D. Durgin, "Theory of Stochastic Local Area Channel Modeling for Wireless Communications," *Ph.D Thesis*, Faculty of the Virginia, Polytechnic Institute and State University, Dec. 2000.

[16] A. Goldsmith, "Wireless Communications," Cambridge University Press, 2005.

[17] M. Paetzold, "Mobile fading channels," Wiley, 2002.

[18] J. D. Parsons, "The mobile radio propagation channel," Wiley, 2000.

[19] J. Gibson, "The Communications Handbook," CRC Press, 1997.

[20] M. F. Catedra, J. Perez, F. S. de Adana, and O. Gutierrez, "Effcient ray-tracing techniques for three-dimensional analyses of propagation in mobile communications, application to picocell an microcell scenarios," *IEEE Antennas Propag. Mag*, vol. 40, no. 2, pp. 15 - 28, 1998.

[21] D.A. McNamara, C.W.I. Pistorius, and J.A.G. Malherbe, "Introduction to the Uniform Geometrical Theory of Diffraction,"*Artech House*, Boston, 1990.

[22] http://rapsor.sourceforge.net/index.php.

[23] Y. Chartois, Y. Pousset, and R. Vauzelle, "Mimo radio channel characterization with 3d ray tracing propagation model in urban environment," *European Conf. propagation systems (ECPS)*, 2005.

[24] G. Madi, "Optimisation d'un réseau de capteurs par techniques MIMO coopératives. Applications possibles : Smart Grid, télédétection, ...," *Ph. D Thesis*, University of Poitiers, 2012.

[25] G. Madi, F. Sacuto, B. Vrigneau, B. L. Agba, Y. Pousset, R. Vauzelle, "Impacts of impulsive noise from partial discharges on wireless systems performance: application to MIMO precoders," *EURASIP Journal Wireless Commun. and Networking*, vol. 2011, no. 1, p. 186, Nov. 2011.

[26] A. Spaulding, D. Middleton, "Optimum reception in an impulsive interference environment-part 1: coherent detection.," *IEEE Trans. Commun.*(9), pp. 910 - 923, 1977.

[27] IEEE P802.15.4/ D18, "Low Rate Wireless Personal Area Networks draft std," pp. 27 - 52, Feb. 2003.

[28] Adrien Van Den Bossche, Thierry Val, Eric Campo, "Technologie sans fil 802.15.4 Son héritage protocolaire et ses applications", *Techniques de l'ingÃ©nieur*, Nov. 2011

[29] BA Akyol, H Kirkham, SL Clements, MD Hadley, "A survey of Wireless Communications for the Electric Power System", Jan. 2010

[30] IEEE Std 802.15.4-2006, Local And Metropolitan Area Networks-Part 15.4, Wireless MAC and PHY Specifications For LR-WPANS, pp. 27 - 66, Sept. 2006.

[31] IEEE Std 802.15.4a-2007 (Amendment to IEEE Std 802.15.4-2006), pp. 25 - 93, 31 Aug. 2007.

[32] IEEE Std 802.15.4c-2009 (Amendment to IEEE Std 802.15.4-2006), pp. 2 - 9, 19 March 2009.

[33] Part 15.4: Low-Rate Wireless Personal Area Networks (LR-WPANs), Amendment 1: MAC sublayer, 2012.

[34] Part 15.4: Low-Rate Wireless Personal Area Networks (LR-WPANs) Amendment 4: Alternative Physical Layer Extension to Support Medical Body Area Network (MBAN) Services Operating in the 2360 MHz - 2400 MHz Band, Feb. 2013.

[35] Thomas Lennvall, Stefan Svenson, Frédéric Hekland, "A Comparison of WirelessHART and ZigBee forIndustrial Applications," *IEEE Int. Workshop on Factory Commun. Systems*, 2008.

[36] C. E. Perkins, E. M. Belding-Royer, and S. Das, "Ad hoc on Demand Distance Vector (AODV) Routing," *IETF RFC 3561.*

[37] A. Wheeler, "Commercial applications of wireless sensor networks using ZigBee," *IEEE Commun. Mag.*, vol. 45, no. 4, pp. 70 - 77, Apr. 2007.

[38] ZigBee Specification-Document 053474r17. [Online]. Available: http://www.zigbee.org.

[39] http://fr.hartcomm.org/$main_article$/wirelesshart.html.

[40] Hart Communication Fundation, "Application Guide," 2005.

[41] ISA100.11a Release 1 Status. (2007, Oct.). [Online]. Available: www.isa.org/source/$ISA100.11a_Release1_Status.ppt$.

[42] Tuan Dang, Catherine Devic et al, OCARI:“ Optimization of Communication for Ad hoc Reliable Industrial networks,” *IEEE Int. Conf. Industrial Informatics (INDI)*, Korea, July 2008.

[43] Gérard Chalhoub, “MaCARI : Une méthode d’accès déterministe et économe en énergie pour les réseaux de capteurs sans fil,” *Ph.D Thesis*, Université Blaise Pascal, 2012.

[44] http://www.agence-nationale-recherche.fr/projet-anr/.

[45] Danielle Reichel, Antoine Druilhe, Tuan Dang, “An Innovative Wireless Sensor Network Protocol Implementation using a Hybrid FPGA Technology,” *World Academy of Science, Engineering and Tech.*, 53, 2011.

[46] G. Montenegro, N. Kushalnagar, J. Hui, D. Culler, Arch Rock Corp, RFC 4944, “Transmission of IPv6 Packets over IEEE 802.15.4 Networks,” Sept. 2007.

[47] Z. Chelby, S. Chakrabati, E. Nordmark, “Neighbor Discovery Optimization for Low-power and Lossy Networks draft-ietf-6lowpan-nd-12,” Aug. 2010.

[48] Nurul Halimatul Asmak Ismail, Rosilah Hassan, Khadijah W. M. Ghazali, “A Study On Protocol Stack In 6lowpan Model,” *Journal of Theoretical and Applied Inf. Tech.*, Vol. 41 No.2, pp 220- 229, 31 July 2012.

[49] Xavier Lagrange, Laurence Rouillé, “Technologie Bluetooth,” *Article Techniques de l’ingénieur : te 7410*, May 2007.

[50] Bluetooth Special Interest Group, “Specification of the Bluetooth System,” V. 4.1, Vol 2, Part A, pp. 35 - 55, Dec. 2003.

[51] Bluetooth Specification Version 2.0 + EDR [vol 0], pp. 2 - 74, Nov. 2004.

[52] https://www.wi-fi.org/

[53] L. Nuaymi, “WiMAX: Technology for Broadband Wireless Access,” Wiley, 2007.

[54] DASH7 Alliance Protocol Specification, DRAFT 0.2 Release, “An Advanced Communication System for Wide-Area Low Power Wireless Applications and Active RFID,” pp 9 - 15, 2013.

[55] J. O. Oyedapo, “ Optimisation des transmissions dans les réseaux de capteurs sans fil par technique MIMO coop‘’eratif à boucle fermée en environnement perturbé,” *Ph. D Thesis*, University of Poitiers, 2015.

[56] B. Bilgin and V. Gungor, “On the performance of multi-channel wireless sensor networks in smart grid environments,” *Proceedings of 20th Int. Conf. Computer Commun. and Networks (ICCCN)*, pp. 1 - 6, July 2011.

[57] http://statweb.stanford.edu/*aras*/jsm/NormalDensity/NormalDensity.html

[58] http://fr.mathworks.com/help/stats/normal-distribution.html

[59] F. Sacuto, "Modeling of the Impulsive Noise in the Power Substation Environment and its Application to Receiver Design," *Ph. D Thesis*, McGill University, 2015.

[60] W. E. Pakala, E. R. Taylor, and R. T. Harrold, "Radio Noise Measurements on High Voltage Lines from 2.4 to 345 kV," *IEEE Electrom. Comp. Symp. Record*, pp. 96 - 107, July 1968.

[61] W. Pakala and V. Chartier, "Radio Noise Measurements on Overhead Power Lines from 2.4 to 800 kV," *IEEE Trans. Power Apparatus and Systems*, vol. PAS- 90, pp. 1155 - 1165, May 1971.

[62] C. H. Peck and P. Moore, "A direction finding technique for wideband impulsive noise source," *IEEE Trans. Electrom. Comp.*, vol. 43, pp. 149 - 154, May 2001.

[63] Q. Shan et al., "Laboratory Assessment of WLAN Performance Degradation in the Presence of Impulsive Noise," *Wireless Commun. and Mobile Computing Conf.*, pp. 859 - 863, 2008.

[64] M. Au, F. Gagnon, and B. L. Agba, "An Experimental Characterization of Substation Impulsive Noise for a RF Channel Model," *Progress in Electromagnetics Research Symposium*, PIERS Proc., vol. 1, pp 1371 - 1376, 2013.

[65] V. L. Chartier et al, "Electromagnetic Interference Measurements at 900 MHz on 230 kV and 500 kV Transmission Lines," *IEEE Trans. Power Systems*, vol. PWRD-1, no. 2, Apr. 1986.

[66] David Middleton, "Canonical and Quasi-Canonical Probability Models of Class A Interference," *IEEE Trans. Electrom. Comp.*, vol. EMC-25, no. 2, pp. 76 - 106, May 1983

[67] Arthur D. Spaulding, David Middleton, "Optimum Reception in an Impulsive Interference Environment, Part I: Coherent Detection," *IEEE Trans. Commun.*, vol. COM-25, no. 9, pp 910 - 923, Sept. 1977.

[68] David Middleton,"Non-Gaussian Noise Models in Signal Processing for Telecommunications: New Methods and Results for Class A and Class B Noise Models," *IEEE Trans. Inf. Theory*, vol. 45, no. 4, pp 1129 - 1149, May 1999.

[69] G. Ndo, F. Labeau, and M. Kassouf. "A Markov-Middleton Model for Bursty Impulsive Noise: Modeling and Receiver Design," *IEEE Trans. Power Delivery*, pp. 2317 - 2325, 2013.

[70] M. Zimmermann and K. Dostert, "Analysis and modeling of impulsive noise in broadband powerline communications," *IEEE Trans. Electrom. Comp.*, vol. 44, pp. 249 - 258, Feb. 2002.

[71] X. Long, Y. Yuan, and X. Jiang, "A novel low-power 802.11 wireless communication system for power substation applications," *12th IEEE Int.l Conf. on Solid-State and Integrated Circuit Tech. (ICSICT)*, pp. 1 - 3, Oct. 2014.

[72] M. Au, B. L. Agba, F. Gagnon, "An analysis of transient impulsive noise in a Poisson field of interferers for wireless channel in substation environments," Summited Apr. 2015.

[73] T. Bollerslev, "Generalized autoregressive conditional heteroscedasticity," *Journal of Econometrics*, vol. 31, no. 4, 307 - 327, 1986.

[74] F. Sacuto, F. Labeau, B. L. Agba,"Wide Band Time-Correlated Model for Wireless Communications under Impulsive Noise within Power Substation," *IEEE Trans. Wireless Commun.*, vol. 13, issue: 3, Mar. 2014.

[75] Y. C. Wu et al., "Efficient communication of sensors monitoring overhead transmission lines," *IEEE Trans. Smart Grid*, vol. 3, pp. 1130 - 1136, Sept., 2012.

[76] G. Madi et al., "Impulsive Noise of Partial Discharge and its Impact on Minimum Distance-Based Precoder of MIMO System," *EUSIPCO2010*, Denmark, pp. 1602 - 1606, Aug. 2010.

[77] S. A. Bhatti et al., "Vulnerability of ZigBee to impulsive noise in electricity substations," *Proc. 2011 XXX th URSI General Assembly and Scientific Symposium*, pp. 1 - 4, Aug. 2011.

[78] S. A. Bhatti et al., "Performance Simulations of WLAN and ZigBee in Electricity Substation Impulsive Noise Environments," *IEEE SmartGridComm Workshop*, pp. 675 - 679, 2012.

[79] I. B. S. Ali, M. Au, B. L. Agba, and F. Gagnon, "Mitigation of Impulsive Interference in Power Substation with Multi-Antenna Systems," *IEEE ICUWB*, 2015.

[80] N. B. Sarr, H. Boeglen, B. L. Agba, F. Gagnon, R. Vauzelle, "Partial Discharge Impulsive Noise in 735 kV Electricity Substations and its Impacts on 2.4 GHz ZigBee Communications," *Int. Conf. Selected Topics in Mobile & Wireless Networking (MoWNeT)*, Cairo Egypt, pp. 1 - 7, Apr. 2016.

[81] B. L. Agba, S. Riendeau, H. Bertrand, J. Bélan, "The Deployment of Wireless Networks in High Voltage Substations: A Feasibility," *IEEE Electrical Power and Energy Conf. (EPEC)*, pp. 46 - 50, Oct. 2012.

[82] Y. S. Cho et al., "MIMO-OFDM Wireless Communications With Matlab," *John Wiley & Sons (Asia) Pte Ltd*, 2010.

[83] H. C. Ferreira, L. Lampe, J. Newbury and T. G. Swart, "Power Line Communications: Theory and applications for narrowband and broadband communications over power lines," *John Wiley & Sons*, 2006.

[84] H. C. Ferreira, H. M. Grove, O. Hooijen and A. J. Han Vinck, "Power line communications: an overview," *Proc. of IEEE 4th AFRICON*, vol. 2, pp. 558 - 63, Stellenborch, South Africa, Sep. 1996.

[85] H. Dai and H. V. Poor, "Advanced signal processing for power line communications," *IEEE Commun. Magazine*, vol 41, no. 5, pp. 100 - 107, May 2003.

[86] M. Gotz, M. Rapp and K. Dostert, "Power line channel characteristics and their effect on communication system design," *IEEE Commun. Magazine*, vol. 42, issue 4, pp. 78 - 86, Apr. 2004.

[87] M. Viswanathan, "Simulation of Digital Communication Systems Using Matlab," *eBook*, Second Edition, 2013

[88] A. M. Wyglinski, F. Lebeau and P. Kabal, "Bit loading with BER constraint for multicarrier systems," *IEEE Trans. Wireless Commun.*, vol. 4, no. 4, pp. 1383 - 1387, Jul. 2005.

[89] L. Goldfeld, V. Lyandres and D.Wulich, "Minimum BER power loading for OFDM in fading channel," *IEEE Trans. Commun.*, vol. 50, no. 11, pp. 1729 - 1733, Dec. 2002.

[90] A. M. Wyglinski, F. Labeau and P. Kabal, "An efficient bit allocation algorithm for multicarrier modulation", *Proc. of IEEE WCNC*, pp. 1194 - 1199, Mar. 2004.

[91] D. Hugh-Hartog, "Ensemble modem structure for imperfect transmission media," *U.S. patent Nos. 4,679,227 (Jul. 1987) 4,731,816 (Mar. 1988), and 4,833,706 (May 1989).*

[92] J. S. Chow, J. C. Tu and J. M. Cioffi, "A discrete multitone transceiver system for HDSL applications," *IEEE Journal Sel. Areas in Commun.*, vol. 9, no. 6, pp. 895 - 908, Aug. 1991.

[93] K. S. Al Mawali and Z. M. Hussain, "Adaptive power loading for OFDM-based power line communications impaired by impulsive noise," *Proc. of the IEEE Int. Symp. Power Line Commun. and its Applic.*, pp. 178 - 182, Mar. 2010.

[94] J. Proakis and M. Salehi, "Digital Communications," *5th ed, McGraw- Hill*, New York, 2008.

[95] G. Ndo, P. Siohan, M. -H. Hamon, "Adaptive noise mitigation in impulsive environment: application to power-line communications," *IEEE Trans. Power Delivery*, vol. 25, no. 2, pp. 647 - 656, Apr. 2010.

[96] H. M. Oh et al., " Mitigation of Performance Degradation by Impulsive Noise in LDPC Coded OFDM System," *IEEE ISPLC*, Orlando, FL, USA, 26 - 29, March 2006.

[97] S. Zhidkov, "Analysis and comparison of several simple impulsive noise mitigation schemes for OFDM receivers," *IEEE Trans. Commun.*, vol. 56, no. 1, pp. 5 - 9, Jan. 2008.

[98] C. R. Nokes, O. P. Haffenden, J. V. Mitchell, A. P. Robinson, J. H. Stott and A. Wiewiorka, "Detection and removal of clipping in multicarrier receivers," *European patent application EP1043874*, Oct. 2000.

[99] T. N. Zogakis, P. S. Chow, J. T. Aslanis, J. M. Cioffi, "Impulse noise mitigation strategies for multicarrier modulation," *Proc. IEEE Int. Conf. Commun. (ICC)*, Vol. 2, pp. 433 - 437, May 1993.

[100] M. Sliskovic, "Impulse noise detection algorithms for multicarrier communication systems performance analysis," *Proc. The 2nd Int. Symp. Image and Signal Processing and Analysis*, pp. 496 - 501 , Jun. 2001.

[101] S. Zhidkov, "Impulsive noise suppression in OFDM based communication systems," *IEEE Trans. Consumer Electronics*, Vol. 49, No. 4, pp. 944 - 948, Nov. 2003.

[102] J. Armstrong and H. A. Suraweera, "Impulse noise mitigation for OFDM using decision directed noise estimation," *Proc. The 8nd Int. Symp. Spread Spectrum Techniques and Applications*, pp. 174 - 178, Sep. 2004.

[103] A. Glavieux, "Codage de Canal," Lavoisier 2005.

[104] P. Elias, "Error-Free Coding," *IEEE Trans. Inf. Theory*, pp. 29 - 57, Sept. 1954.

[105] C. Berrou, A. Glavieux, and P. Thitimajshima, "Near Shannon limit Error-correcting Coding and decoding: Turbo-codes. 1," *IEEE Int. Conf. Commun (ICC)*, vol. 2, pp. 1064 - 1070, May 1993.

[106] A. Viterbi, "Error bounds for convolutional codes and an asymptotically optimum decoding algorithm," *IEEE Trans. Inf. Theory*, vol. 13, no. 2, pp. 260 - 269, Apr. 1967.

[107] G. Forney, "The Viterbi algorithm," *Proc. of the IEEE*, vol. 61, no. 3, pp. 268 - 278, Mar. 1973.

[108] L. Bahl, J. Cocke, F. Jelinek, and J. Raviv, "Optimal decoding of linear codes for minimizing symbol error rate (corresp.)," *IEEE Trans. Inf. Theory*, vol. 20, no. 2, pp. 284 - 287, Mar. 1974.

[109] M. K. Simon and M.-S. Alouini, "Digital Communication over Fading Channels," *John Wiley & Sons,*, 2005.

[110] R. Gallager, "Low-density parity-check codes," *IEEE Trans. Inf. Theory*, vol. 8, no. 1, pp. 21 - 28, Jan. 1962.

[111] D. J. C. MacKay and R. M. Neal, "Near Shannon limit performance of low density parity check codes," *IEEE Electronics Letters*, vol. 33, pp. 457 - 458, Mar. 1997.

[112] D. J. C. MacKay, "Information theory, inference and learning algorithms," *The Edinburgh Building, Cambridge CB2 2RU*, UK: Cambridge University Press, 2003.

[113] R. Tanner, "A recursive approach to low complexity codes," *IEEE Trans. Inf. Theory*, vol. 27, no. 5, pp. 533 - 547, Sep. 1981.

[114] E. Arikan, "Channel polarization: A method for constructing capacity-achieving codes," *IEEE Int. Symp. Inf. Theory*, ISIT 2008

[115] E. Arikan, "Systematic Polar Coding," *IEEE Commun. Letters*, vol. 15, no. 8, Aug. 2011.

[116] P. Delsarte, "Bilinear forms over a finite field with applications to coding theory," *Journal of combinatorial theory, Series A*, 25(4), 226 - 241, 1978.

[117] E. E. M. Gabidulin, "Theory of codes with maximum rank distance," *Problemy Peredach iInformatsii*, 21(1), pp. 3 - 16, 1985.

[118] R. M. Roth R, "Maximum-rank array codes and their application to crisscross error correction," *IEEE Trans. Inf. Theory*, 37(2), pp. 328 - 336, 1991.

[119] S. Plass et al., "Coding Schemes for Crisscross Error Patterns," *Springer Science+Business Media*, LLC. 2007.

[120] A. K. Yazbek, V. Meghdadi, and J. P. Cances, "Low Rank Parity Check Codes against Reed-Solomon Codes for Narrow-band PLC Smart Grid Networks," *Int. Conf. Computer & Commun. Engineering (ICCCE)*, 2016.

[121] Renato Pivesso Franzin et al., "A performance comparison between OFDM and FBMC in PLC applications," *IEEE Second Ecuador Technical Chapters Meeting (ETCM)*, 2017.

[122] ETSI EN 300 744 V1.6.1.

[123] Wael Abd-Alaziz et al, "Non-binary turbo-coded OFDM-PLC system in the presence of impulsive noise," *EUSIPCO*, 2017.

[124] Mohsen Maadani and Mohammad Baseri, "Performance evaluation of the OFDM modulation in IEEE 802.11-based wireless industrial networks," *2nd Int. Conf. Knowledge-Based Engineering and Innovation (KBEI)*, 2015

[125] Erik G. Strom, "On 20 MHz channel spacing for V2X communication based on 802.11 OFDM," *IEEE IECON*, 2013

[126] G. Ndo et al, "Optimization of Turbo Decoding Performance in the Presence of Impulsive Noise using Soft Limitation at the Receiver Side," *IEEE Global Telecommuni. Conf.*, Dec. 2008.

[127] https://github.com/bastibl/gr-ieee802-11

[128] GNU Radio. Available: http://gnuradio.org/redmine/projects/gnuradio/wiki

[129] https://www.ettus.com/product/details/UN210-KIT

[130] N. B. Sarr et al., "An impulsive noise resistant physical layer for smart grid communications", *IEEE Int. Conf. Commun. (ICC)*, pp. 1 - 7, May 2017.

[131] H. A. Haldren III, "Studies in Software-Defined Radio System Implementation," 2014.

[132] Palak P. Parikh et al., "Opportunities and challenges of wireless communication technologies for smart grid applications," *IEEE Power and Energy Society General Meeting,* 2010.

[133] F. Sacuto et al., "Impulsive Noise Measurement in Power Substations for Channel Modeling in ISM Band," *CIGRE Canada Conf.*, Sept. 2012.

[134] M. Vu and A. Paulraj, "Some Asymptotic Capacity Results for MIMO Wireless with and without Channel Knowledge at the Transmitter," *37th Asilomar Conf. Signals, Systems, Computers,* pp. 258 - 262, Nov. 2003,.

[135] - , "Optimal Linear Precoders for MIMO Wireless Correlated Channels with NonZero Meam in Space-Time Coded Systems," *IEEE Trans. Sig. Proc.,* vol. 54, pp. 2318 - 2332.

[136] C. Tepedelenlioglu and P. Gao, "On Diversity Reception over Fading Channels with Impulsive Noise," *IEEE Trans. Veh. Tech.*, vol. 54, no.6, pp. 2037 - 2047, Nov. 2005.

[137] S. Al-Dharrab and M. Uysal, "Cooperative Diversity in the Presence of Impulsive Noise," *IEEE Trans. Wireless Commun.*, vol. 8, no. 9, pp. 4730 - 4739, Sept. 2009

[138] O. Oyedapo, B. Vrigneau, R. Vauzelle and H. Boeglen, "Performance Analysis of Closed-Loop MIMO Precoder Based on the Probability of Minimum Distance," *IEEE Trans. Wireless Commun.*, Vol. 14, no. 4, pp. 1849 - 1857, 2015

[139] J. Laneman, D. Tse, and G. Wornell, "Cooperative diversity in wireless network: Efficient protocols and outage behavior," *IEEE Trans. Inf. Theory*, vol. 50, no. 12, pp. 3062 - 3080, Dec. 2004.

[140] S. Yang and J.-C. Belfiore, "Towards the optimal amplify-and-forward cooperative diversity scheme," *IEEE Trans. Inf. Theory*, vol. 53, no. 9, pp. 3114 - 3126, Sept. 2007.

[141] M. Dohler and Y. Li, Cooperative Communications : Hardware, Channel and PHY," *Wiley & Sons*, Feb. 2010.

[142] A. Nosratinia, T. Hunter, and A. Hedayat, "Cooperative communication in wireless networks," *IEEE Commun. Magazine*, vol. 42, no. 10, pp. 74 - 80, oct. 2004.

[143] T. E. Hunter and A. Nosratinia, "Diversity through coded cooperation," *IEEE Trans. Wireless Commun.*, vol. 5, no. 2, pp. 283 - 289, 2006.

[144] B. Schein and R. Gallager, "The Gaussian parallel relay network," *IEEE Int. Symp. Inf. Theory*, ISIT, 2000.

[145] I. Maric and R. Yates, "Forwarding strategies for Gaussian parallel-relay networks," *IEEE Int. Symp. Inf. Theory (ISIT)*, 2004.

[146] E. Larsson and P. Stoica, Space-Time Block Coding dor Wireless Communications," *Cambridge university*, 2003.

[147] S. M. Alamouti, "A simple diversity technique for wireless communications," *IEEE Journal Sel. Areas Commun*, vol. 16, pp. 1451 - 1458, Oct. 1998.

[148] V. Tarokh, N. Seshadri, and A. R. Calderbank, "Space-time codes for hight data rate wireless communication : Performance criterion and code construction," *IEEE Trans. Inform. Theory*, vol. 44, pp. 744 - 765, Mar 1998.

[149] V. Tarokh, H. Jafarkhani, and A. R. Calderbank, "Space-time codes from orthogonal designs," *IEEE Trans. Inf.. Theory*, vol. 45, no. 5, pp. 1456 - 1467, Jul. 1999.

[150] H. Jafarkhani and A. Calderbank, "A quasi-orthogonal space-time block code," *IEEE Trans. Inf. Theory*, 2001.

[151] P. Stoica and G. Ganesan, "Maximum-snr spatial-temporal for matting designs for MIMO channels," *IEEE Trans. Sig. Proc.*, vol. 50, no. 3036 - 3042, p. 12, Dec. 2002.

[152] A. Scaglione, P. Stoica, S. Barbarossa, G. Giannakis, and H. Sampath, "Optimal designs for space-time linear precoders and decoders," *IEEE Trans. Sig. Proc.*, vol. 50, no. 5, pp. 1051 - 1064, May 2002.

[153] H. Lee, S. Park, and I. Lee, "Orthogonalized spatial multiplexing for closed-loop MIMO systems," *IEEE Trans. Commun.*, vol. 55, pp. 1044 - 1052, 2007.

[154] Y. Kim, H. Lee, S. Park, and I. Lee, "Optimal precoding for orthogonalized spatial multiplexing in closed-loop MIMO systems," *IEEE Journal Selected Areas Commun*, vol. 26, no. 8, 2008.

[155] T.D. Nguyen et al., "Cooperative MIMO Schemes Optimal Selection for Wireless Sensor Networks," *65th IEEE VTC*, pp. 85 - 89, 2007.

[156] N. Mysore, "Turbo-Coded MIMO Systems: Receiver Design and Performance Analysis," *PhD. Thesis McGill University*, Feb. 2006.

[157] Y. Li and M. Salehi, "Coded MIMO Systems with Modulation Diversity for Block-Fading Channels," *46th Annual Conf. Inf. Sciences and Systems (CISS),* Sept. 2012.

[158] L. Collin et al., "Optimal minimum distance-based precoder for MIMO spatial multiplexing systems," *IEEE Trans. Sig. Proc.*, vol. 52, issue 3, pp. 617 - 627, Mar. 2004.

[159] P. Stoica, G. A. Ganesan, "Maximum-SNR spatial-temporal formatting designs for MIMO channels," *IEEE Trans. Sig. Proc.*, vol. 50, pp. 3036 - 3042, Dec. 2002.

[160] D. J. Love et al., "An overview of limited feedback in wireless communication systems," *IEEE Journal Sel. Areas in Commun.*, vol. 26, no. 8, pp. 1341 - 1356, Oct 2008.

[161] D. J. Love and J. R. W. Heath, "Limited feedback unitary precoding for spatial multiplexing," *IEEE Trans. Inf. Theory*, vol. 51, no. 8, pp. 2967 - 2976, Aug. 2005.

[162] A. Charrada, "Nonlinear complex M-SVR for LTE MIMO-OFDM channel with impulsive noise," *Int. Conf. Sciences of Electronics, Tech. of Inf. and Telecommun. (SETIT)*, 2016.

[163] Ghasan Ali Hussain et al., "Concatenated RS-Convolutional Codes for MIMO-OFDM System," *Asian Journal of Applied Sciences*, vol. 4(7), pp. 720 - 727, 2011.

[164] S. Cui, A. J. Goldsmith, and A. Bahai, "Energy-efficiency of MIMO and cooperative MIMO techniques in sensor networks," *IEEE Journal Sel. Areas in Commun.*, vol. 22, no. 6 Aug. 2004.

[165] S. K. Jayaweera, "Virtual MIMO-based cooperative communication for energyconstrained wireless sensor networks," *IEEE Trans. Wireless Commun.*, vol. 5, no. 5, pp. 984 - 989, May 2006.

[166] L. X. H. Dai and Q. Zhou, "Energy efficiency of MIMO transmission strategies in wireless sensor networks," *Int. Conf. Computing, Commun. and Control Tech. (CCCT)*, Austin, TX, USA, Aug. 2004.

[167] V. Tarokh, H. Jafarkhani, and A. R. Calderbank, "Space-time codes from orthogonal designs," *IEEE Trans. Inf. Theory*, vol. 45, no. 5, pp. 1456 - 1467, Jul. 1999.